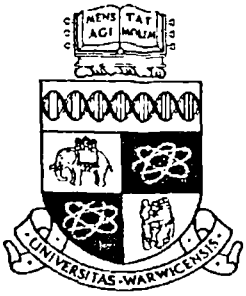

A STUDY OF TIN OXIDES IN SILICATE BASED GLASSES

by

MOHD MUSTAMAM ABD KARIM

A thesis submitted to the University of Warwick, England for admission to the degree of DOCTOR OF PHILOSOPHY

Department of Physics

March 1995

CONTENTS

LIST OF FIGURES **Page**

Chapter 2 - Glass Structure and The Role of Tin

Chapter 6 - Differential Thermal Analysis and Devitrification of $SnO-SiO_2$ Glasses

Chapter 7 - Tin-Doped Float Glass

LIST OF TABLES **Page**

Chapter 2 - Glass Structure and The Role of Tin

Chapter 3 - Theoretical Background

Chapter 4 - Experimental Materials and Techniques

Chapter 5 - The Binary $SnO\text{-}SiO_2$ Glass System

Chapter 6 - Differential Thermal Analysis and Devitrification of $SnO-SiO_2$ Glasses

Chapter 7 - Tin-doped Float Glass

LIST OF ABBREVIATIONS

DTA - Differential Thermal Analysis

JCPDS - Joint Committee For Powder Diffraction Standards

XRD - X-ray Diffraction

SEM - Scanning Electron Microscopy

XPS - X-ray Photo Electron Spectroscopy

ESCA - Electron Spectroscopy For Chemical Analysis

NMR - Nuclear Magnetic Resonance

NQR - Nuclear Quadrupole Resonance

MAS NMR - Magic Angle Spinning Nuclear Magnetic Resonance

EPMA - Electron Probe Microanalysis

EDX - Energy Dispersive X-ray Analysis

EPR - Electron Spin Resonance

TEM - Transmission Electron Microscopy

SIMS - Secondary Ion Mass Spectrometry

CEMS - Conversion Electron Mössbauer Spectroscopy

EXAFS - Extended X-ray Absorption Fine Structure

NWF - Network Former

NWM - Network Modifier

FWHM - Full Width At Half Maximum

ACKNOWLEDGEMENT

I would like to record my thanks to my supervisor, Dr. Diane Holland for her excellent guidance, interest and inspiration that made this study a rewarding experience. My special thanks go to Professor C.E. Johnson and Miss K.F.E. Williams (University of Liverpool) and Dr. J.A. Johnson (Liverpool John Moores University) for collaboration work on Mössbauer Spectroscopy. Also my thanks to B.Tilley and J.Greengrass of Pilkington Group Research for float glass samples, silica crucibles and help with the chemical analysis. I am indebted to Dr. A. Howes for helping with the NMR experiments, Dr. S. Kitchin for computer simulation of ^{29}Si NMR spectra and Professor R. Dupree for some discussion of NMR spectra.

My thanks also to the University Technology of Malaysia and The Public Services Department of Malaysia who jointly provided financial support.

Finally, my very special thanks go to my wife, Normah, for her encouragement and her care and attention to our children Hana, Nadira, Ismail and Sakinah, throughout the period of this work.

DECLARATION

The work presented here was carried out in the Department of Physics, University of Warwick from November 1991 to October 1994 under the supervision of Dr. D. Holland. The results are the outcome of my own independent research except where specifically referenced in the text and have not previously been submitted for any other degree.

Some parts of this thesis have been published or accepted for publication as follows:

(1) ' The structure of tin silicate glasses '

D. Holland & M.M. Abd Karim.

Topical Issues in Glass, Volume 1 , April 1993, Society of Glass Technology, Sheffield, England.

(2) ' Tin silicate glasses'

D. Holland, M. M. Karim, C.E. Johnson, K.Williams & J.A. Johnson.

Rivista della Stazione Sperimentale del Vetro 23, 223 (1993). European Society of Glass Science and Technology, Venice.

(3). ' Mössbauer spectra of tin in float glass'

J.A.Johnson, C.E. Johnson, K.F.E.Williams, D.Holland & M.M.Karim

Hyperfine Interactions 00 (1995) 575 - To be published.

(4) ' Physical properties of glasses in the system $SnO-SiO_2$ '

M.M.Karim & D.Holland

Physics and Chemistry of Glasses - To be published, October 1995.

It is anticipated that other parts of this thesis will be submitted for publication in the future.

M.M.A. Karim

ABSTRACT

The roles of tin in two silicate based glass systems have been investigated by NMR and Mössbauer spectroscopies and by physical property measurements of the glasses.

The first glass system investigated was *the stannous silicate (binary SnO-SiO_2)* glass. Glasses with SnO contents ranging from 17 to 72 mol.% have been made by melting pelleted powder in an alumina crucible. It was found that alumina crucibles are unsuitable for making glass with < 20 mol.% SnO because of attack on the crucible at the high melting temperature (≥1600°C). Silica crucibles will not withstand such high temperature and tin will attack a platinum crucible. The ability of this system to form glass past the orthosilicate composition has been discussed in terms of the polarizing power of Sn^{2+} and the structure of SnO. The ^{119}Sn NMR results did not give much structural information due to the high chemical shift anisotropy of Sn^{2+} site but they showed that the glass also contains trace amounts of Sn^{4+}species. The ^{29}Si MAS NMR results showed that SnO does not depolymerise the silicate network to the same extent as Na_2O or even PbO. Computer simulations of the ^{29}Si MAS NMR spectra showed that, for SnO < ~30 mol.%, the disposition of Q^n species is consistent with the binary model, which means that SnO is acting the role of modifier. For compositions > 30 mol.% SnO, the Q^n distribution follows the statistical model and this has been interpreted as SnO now acting as an intermediate. The ^{119}Sn Mössbauer results confirmed this interpretation. The Sn^{2+} isomer shift decreases with increase of SnO which is indicative of increasing covalent character of the Sn—O bonds while the larger quadrupole splitting suggests distortion of the SnO polyhedral structure in the glass. The relation of the Sn^{2+} isomer shift to the quadrupole splitting and the temperature dependence of the isomer shift of Sn^{2+} indicate the formation of Si—O—Sn linkages at high SnO contents. The decrease of the viscosity of the glass with increasing SnO is small when compared to the decrease of the viscosity in alkali metal and alkaline-earth oxides silicates when the respective modifier oxide is increased in those glasses. The variation of the density, thermal expansion and refractive index with SnO content showed discontinuities in the region of 30-45 mol.% SnO. This has been interpreted as being the point where SnO changes its role from that of modifier to intermediate.

The results of differential thermal analysis and devitrification of SnO-SiO_2 glasses showed that glass with ≥ 40 mol.% SnO can be heat treated in the temperature range of 570° to 680 °C to produce metastable $SnSiO_3$ crystals. $SnSiO_3$ decomposed to SnO + SiO_2 at temperatures above ~700°C and, at temperatures greater than 720°C, oxidation of SnO to SnO_2 and SiO_2(glass) to SiO_2 (cristobalite) took place.

The second glass system is tin-doped float glass. This is glass of the float composition remelted with tin(II) oxalate in silica crucibles under normal atmosphere conditions. In this way it has been demonstrated that we can mimic the tin oxide distribution found within the tin diffusion region in float glass. Synthesis of the glass has shown that both Sn^{2+} and Sn^{4+} can be assimilated simultaneously in the glass but there is a solubility limit for Sn^{4+}. The ^{119}Sn Mössbauer results showed that Sn^{2+} and Sn^{4+} played different structural roles in the glass. The environment of Sn^{2+} in glass is similar to that in amorphous SnO while the Sn^{4+} structure in glass does not change significantly compared to crystalline SnO_2. The Debye temperatures and recoil free fractions showed that Sn^{2+} is less rigidly bound to the network modifier site while Sn^{4+} is rigidly bound at network former sites in the glass. The different structural roles of Sn^{2+} and Sn^{4+} in the glass were reflected in the some of the physical properties of the glasses.

Chapter 1 - General

1.1 INTRODUCTION

Tin is not a common constituent of glasses. As tin oxide, it is used extensively in very small quantities in making gold, copper and selenium ruby glasses [1]. Tin oxides have also been known to be used as opacifiers and glazes for glasses [2]. Tin is 'metallophilic' ; a term suggested by Weyl [3] for elements that aid in the introduction of metal bonds into distinctly ionic bonds in glass. Because of this, tin oxide (SnO) is used to increase the adhesion of metal films to glass surfaces e.g. in making silvered mirrors and gilding of glass. In the hot end surface coating process to increase the strength of glass containers, a tin compound is applied by chemical vapour deposition or spraying on the glass surface. The diffusion of tin ions into the surface of the containers decreases the size of the damaging Griffith flaws [4] and hence strengthens the glass. Perhaps the most important use of tin in the glass industry is in the production of flat and parallel sheet glass by the float glass process, invented in 1959 by Pilkington Brothers Limited [5]. This glass is commercially known as float glass and is a silicate based glass of basic composition of $Na_2O + CaO + SiO_2$, referred to as soda-lime-silica glass. In the float glass process, the molten glass is floated on top of a bath of molten tin kept at 1050°C. The bottom glass surface is supported only by molten tin, whereas the top surface is exposed to the slightly reducing atmosphere of a mixture of hydrogen and nitrogen called forming gas. Gravity allows the glass to flow out, while its surface tension holds it back to an equilibrium thickness of ~ 7.1 mm. Sheet glass of thicknesses from 1.5 to 25 mm can be made by either stretching or compressing the glass ribbon. While in the float bath, heat is applied to both surfaces of the ribbon and this 'fire polishing' gives perfectly flat and parallel surfaces. The glass enters the bath at ~ 1150°C and with a viscosity of 10^3 Pa s and leaves it at ~ 650°C. In this way the bottom of the glass ribbon remains in direct contact with molten tin for several minutes while being drawn and it is then annealed and cut in the ordinary way.

In this condition, tin from the float bath diffuses into the float contact surface and to a lesser extent into the non-contact surface by chemical adsorption of tin vapour. It is found that the tin contact surface has a high concentration of tin in different oxidation states to a depth of 5 - 30 μm [6 - 10]. Therefore the float contact surface has chemical characteristics different in some respects from those of the bulk glass. Although this compositional modification does not extend far into the surface, it does cause the physical and chemical behaviour to differ from that of the bulk glass and the upper surface. For general uses, such as window glass, this is not critical. However, for specialized uses such as very thin glass discs used as substrates for optical and magnetic recording, this will affect the planarity of the disc. In addition, the stoichiometry of the tin oxide at the surface affects the tendency of the surface quality to deteriorate (blooming) when the glass is reheated for tempering to produce curved articles like car windscreens [6]. Past studies on the float glass were confined only to the examination of the tin profiles [6 - 10] i.e. to quantify the various tin oxidation states as a function of depth in the glass. There have not been many studies of the effect of tin concentration on the physical properties of float glass. Minko [11,12] studied the synthesis of soda-lime-silica glass containing tin of different valencies as a means of simulating the float contact side of industrial float glass and measuring its physical and chemical properties. They found that the relative amounts of Sn^{4+} and Sn^{2+} in the glass depend on the melting conditions and Sn^{4+} is assimilated in the glass melt in an amount not exceeding the alkali content of the glass, whereas this is not the limit for Sn^{2+}. The optical, thermal and chemical properties of the glass also improve significantly with the presence of tin in various valence states. The variation of these properties with tin content seems to depend on the relative amount of Sn^{4+} and Sn^{2+} in the glass. This shows that Sn^{4+} and Sn^{2+} play different roles in the glass structure. Structurally, whether these different valence states of tin occupy network-modifying or network-forming positions in the glass has yet to be examined. There is therefore an incentive to understand the structural role of tin in soda-lime-silica glass and its effect on various physical properties.

From what has been discussed above, tin constitutes only a minor component in commercially produced glasses but its role is an important one because it can improve the glasses' mechanical, optical, thermal and chemical properties. However its effect on glass properties is not well understood because of the lack of studies done on tin containing glasses. This is because the chemistry of tin in glasses is complicated by the two different valencies available to it and therefore synthesis and analysis of glass containing tin poses some problems. The tetravalent (Sn^{4+}) state is the most stable and, by extrapolation from Si and Ge (higher in Group IVA), it is expected that Sn^{4+} would act as an intermediate in silicate glasses. Past studies have shown that the solubility of SnO_2 in silicate and borate glasses is very low [13]. For example about 0.2 - 2 wt.% of SnO_2 can be dissolved in SiO_2 (quartz) in making a stannosil glass [14]. This has a low thermal expansion and transmits long ultraviolet (3000 - 4000Å) but absorbs the harmful short wave ultraviolet (2537Å). The divalent state (Sn^{2+}) is fairly readily oxidized to the tetravalent but binary glasses with high SnO content can be formed as silicates, borates and germanates. Silver et al [15] studied the SnO - GeO_2 glass system, and found that glass can form with $x > 2$ (Sn_xGeO_{2+x}) which is beyond the orthogermanate composition. The refractive indices for the glasses are very high and are of the order of those found for PbO - GeO_2 glasses and higher than those found for all other two component oxide glasses [16]. In the SnO - B_2O_3 glass system studied by Paul et al [17] glass can form with up to 58 mol% SnO which is beyond the metaborate composition. The ^{119}Sn Mössbauer spectroscopy of these glasses shows that, for glasses with high SnO content, the non-bridging oxygen ions are coordinated to Sn^{2+} ions. In the SnO - SiO_2 glass system, glass can be formed beyond the metasilicate composition. The only two important studies carried out on this system are by Carbo Nover & Williamson [18] and Ishikawa & Akagi [19]. Carbo Nover et al studied the crystallization and decomposition of glasses ranging in composition from 27 to 58 mol% SnO. Ishikawa et al studied the structures of glasses ranging from 32 to 57 mol% SnO by radial distribution studies from x-ray diffraction data.

Thus we see that glass can form with a high SnO content in stannous germanate, stannous borate and stannous silicate systems. But, why can high SnO content glasses form in these systems? Past studies have not answered this question. The structural role of tin in these glasses, particularly the stannous silicate glasses has yet to be studied. By analogy with PbO(Pb^{2+}), we might expect SnO to act in a rather complex structural manner. In PbO - SiO_2 glass, PbO acts as a modifier at low PbO content (< 30 mol%) and a combination of a modifier and an intermediate oxide at higher PbO content (> 30 mol%) [20]. In this system glasses will form with PbO contents up to 90 mol%, implying that a lead-oxygen network must exist with considerable Pb—O covalency, whereas with corresponding ionic modifiers such as SrO - SiO_2 or Na_2O - SiO_2 it is very difficult to prepare glasses beyond the metasilicate composition. Does Sn^{2+} behave like Pb^{2+} or as a modifier ?.

It is felt that there are many unanswered questions as to the role of tin in glass. Therefore this research is an exercise to seek some answers with the emphasis on silicate and soda-lime-silica glasses.

1.2 AIMS OF THE RESEARCH

It is therefore important that a systematic study of the environment of tin in silicate and soda-lime-silica glasses be carried out in order to understand the structural role of tin in these glasses. Also important is the study of the effect of tin concentration on the physical properties of these glasses in order to remedy the lack of information in the literature in these areas. Therefore the aims of the research are as follows:

(a) To study the structural role of SnO in the simple binary SnO - SiO_2 glass system by NMR and Mössbauer Spectroscopies.

(b) To study the effect of tin concentration on the viscosity, density, thermal expansion and refractive index of binary SnO - SiO_2 glass since these indirect techniques can provide some understanding of the structural features of this glass.

(c) To study the crystallization of some of the binary SnO - SiO_2 glasses.

(d) To study the structural role of the different valence states of tin in float glass by Mössbauer Spectroscopy.

(e) To study the effect of tin concentration on the viscosity, density, thermal expansion, refractive index and microhardness of tin-doped float glass.

1.3 CHOICE OF SYSTEMS

To achieve the aims of the research, two glass systems were chosen. They are:

1. Simple binary SnO - SiO_2 glass system with nominal SnO contents between 20 and 80 mol% SnO.

2. The second type of sample is a complex glass system called tin-doped float glass. This sample is made in order to simulate the tin concentration in the tin contact side of industrial float glass. Six samples of float glass composition were doped with 2.5 , 5, 7.5, 10, 12.5 and 15 wt% SnO. Because Sn^{2+} will fairly readily oxidize to Sn^{4+} we would expect, after melting, that the tin-doped float glass will contain varying amounts of tin in different valency states.

1.4 THESIS PLAN

The contents of this thesis will be divided into chapters as follows:

Chapter 2

Chapter 2 covers the definition of glass and the structure of glass with the emphasis on models of glass structure. It will continue with some reviews of tin in various glass systems and finally touches on the chemistry and structure of tin oxides.

Chapter 3

Chapter 3 is a chapter on theoretical background. It gives an account of the theory of Nuclear Magnetic Resonance and Mössbauer Spectroscopy that will be used in the structural studies. This chapter continues on the theory of viscosity of glass and some methods of its measurement.

Chapter 4

Chapter 4 describes the experimental techniques employed in the research programme. These will include preparation of glass samples and its compositional analysis, Nuclear Magnetic Resonance, Mössbauer Spectroscopy, Viscosity Measurement, Differential Thermal Analysis, Dilatometry, Refractive Index Measurement, XRD Analysis, SEM, Density Measurement and Microhardness Testing.

Chapter 5

Chapter 5 is devoted to the SnO - SiO_2 glass system. It presents the results and discussion of glass preparation and compositional analysis, the structural investigations by NMR and Mössbauer Spectroscopies, the viscosity measurement, the density and molar volume, the thermal expansion, the refractive index and molar refractivity and lastly presents the conclusions.

Chapter 6

This chapter presents the results and discussion on differential thermal analysis and devitrification of $SnO\text{-}SiO_2$ glasses. The techniques employed were Differential Thermal Analysis, X-Ray Diffraction, ^{29}Si MAS NMR , ^{119}Sn Mössbauer Spectroscopy and Scanning Electron Microscopy.

Chapter 7

Chapter 7 is a chapter on tin-doped float glass. It starts with glass preparation and compositional analysis and then presents and discusses the results of ^{119}Sn Mössbauer Spectroscopy and physical property measurements and finally the conclusions that can be derived from them.

Chapter 8

Chapter 8 summarizes the conclusions as to the structural role of tin in silicate and soda-lime-silica glasses. It also summarizes the effect of tin on the physical properties of the SnO - SiO_2 and tin-doped float glasses. Finally some suggestions for future work will be made in this chapter.

REFERENCES

1. Dodd, A.E. (1964). *Dictionary of Ceramics*, George Newnes Limited, London.
2. Rooksby, H.P. (1964). *Physics Chem. Glasses* **5**(1), 20.
3. Weyl, W.A. (1967). *Coloured Glasses*. Society of Glass Technology, England.
4. Sanyal, A.S. & Mukerji, J. (1982). *Physics Chem. Glasses* **24**(4), 79.
5. Persson, R. (1969). *Flat Glass Technology*, Butterworths, London, pg.18.
6. Pilkington,A. (1969). *Proc.R.Soc. London* **A314**,1
7. Colombin, L., Jelli, A., Riga, J., Pireaux, J.J. & Verbist, J. (1977). *J. Non-Cryst. Solids* **24**, 253-258.
8. Sieger, J.S., (1975). *J. Non-Cryst. Solids* **19**, 213-220.
9. Jie, L. & Choa, X. (1990). *J. Non-Cryst. Solids* **119**, 37-40.
10. Chappell, R.A. & Stoddart, C.T.H. (1974). *Physics. Chem. Glasses* **15**(5), 130.
11. Principi, G., Maddalena,A., Gupta, A., Geothi-Bianchini, F., Hreglich, S. & Verita, M. (1993). *Nuclear Instruments and Methods in Physics Research* **B76**, 215-217.
12. Min'ko, N.I. (1973). *Neorg. Mater.*, **9**(10) , 1816-1821.
13. Min'ko, N.I., Kislitsyn, B.F., Fabrikant, S.A. & Konik, L.T. (1973). *Steklo. i. Keram.* **4**, 19-21.
14. Volf, M. B. (1984). *Chemical Approach to Glass*, Elsevier, Oxford, pg.412.
15. Maddock, A.J. (1939). *J. Soc. Glass Tech.* **23**, 372-377.
16. Silver, J., White, E.A.D. & Donaldson, J.D. (1977). *Journal of Material Science* **12**, 827.
17. Philips, B. & Scroger, M.G. (1965). *J. Amer. Ceram. Soc.* **48**, 398.
18. Paul, A., Donaldson, M.T., Donoghue, M.T. & Thomas, M.J.K. (1977). *Physics Chem. Glasses* **18**(6), 125.
19. Carbo Nover, J. & William, J. (1967). *Physics Chem. Glasses* **8**(4), 164.
20. Ishikawa, T. & Akagi, S. (1978). *Physics Chem. Glasses* **19**(5), 108.
21. Dupree, R., Ford, N. & Holland, D. (1987). *Physics. Chem. Glasses* **28**(2), 78.

Chapter 2 - Glass structure and the role of tin

2.1 DEFINITION OF GLASS

Glass is generally defined as a product of melting that has formed a solid, amorphous material on solidification of the melt without crystallization [1]. The term 'amorphous' is a description of any condensed phase which lacks long-range order according to diffraction (x-ray , neutron and electron) criteria. Thus liquid mercury and carbon black are equally representative of the amorphous state of matter but they are not glass. Therefore the terms 'glassy' and 'vitreous' are synonymous and refer to a very restricted class of amorphous materials which are solid, hard, transparent, brittle, isotropic and which soften progressively and continuously when heated. The majority of glasses encountered, which are of high commercial value, are inorganic and are composed of certain metal oxides melted together and supercooled to a glass. Thus the American Society for Testing of Materials defines a glass as 'an inorganic product of fusion which cooled to a rigid condition without crystallizing' [2]. The emphasis on 'inorganic' matter in this definition excludes elementary glasses such as vitreous selenium or certain organic substances (glucose, glycerol, plastic etc.) which can be supercooled to a rigid condition without crystallizing and many other collections of amorphous materials prepared by techniques other than melting such as vapour deposition, chemical or electro deposition, shock treatment, sol-gel etc. Therefore a more precise definition of glass would be;

"A glass is an x-ray amorphous material that exhibits the glass transition phenomenon" [3 - 5]. The glass transition is that phenomenon in which a solid amorphous phase exhibits, with increasing temperature, a more or less sudden change in the derivative thermodynamic properties, such as heat capacity and expansion coefficient, from crystal-like to liquid-like values [3 - 5]. Having said that however, the term 'glass'

when used in this study generally refers to fused inorganic oxides of which silica is one of the principal components.

2.2 MODELS OF GLASS STRUCTURE

With the exception of quartz (SiO_2) glass, glasses that are encountered in everyday usage are multicomponent and chemically very complex. There is scarcely a glass which contains fewer than four constituent elements. Consequently the resulting structures can become extremely complicated; due to the fact that one is dealing with a disordered arrangement of atoms and molecules. Therefore elucidating the glass structure is a difficult job. Attempts to envisage the structure of these glasses has produced a variety of models. It is generally accepted that the short range order and therefore the primary building blocks (polyhedra) in a glass structure are not too dissimilar to the corresponding crystal equivalents. For oxide glasses the widely accepted model is the Random Network Model (RNM) proposed by W.H. Zachariasen [6]. This will be discussed in the following section. It must not be imagined that the basic RNM can be successfully applied to all inorganic glass forming materials, therefore its modification and other models will also be discussed.

2.2.1 RANDOM NETWORK MODEL

Historically RNM has its basis in Goldschmidt's radius ratio criterion for predicting glass formation for oxides. Goldschmidt's observation was amplified and put on a logical basis by Zachariasen in his influential 1932 paper [6]. From the observed similarity between the mechanical properties of glass and the corresponding crystal, Zachariasen deduced that the interatomic distances and interatomic forces in both must be similar. It follows that, for a glass forming oxide, the coordination number of the

cation must be closely similar in glass to that observed in crystal. This means that the basic structural units in the glass and in the crystal are identical and the ordinary rules of crystal chemistry apply to glass. In the case of oxide glass these basic units are oxygen polyhedra. For example the SiO_4 tetrahedron is the basic unit of silicate glass. Zachariasen postulated that, as in crystal, the structural units are combined to give a 3D assembly but in glass the bond angles and bond distances vary. This results in an arrangement lacking in periodicity and symmetry called a random network. Therefore the random network lacks long range atomic order and produces the diffuse, liquid-like x-ray diffraction pattern. Figure 2.1 shows the differences between the regular crystalline lattice and the random network for an oxide having the formula M_2O_3. Zachariasen then derived some empirical conditions for glass formation, as follows;

(i) No oxygen anion may be linked to more than two cations.
(ii) The number of oxygen anions surrounding the cation should be small (4 or less).
(iii) The oxygen polyhedra must share corners with each other, not edges or faces.
(iv) The structure should form a continuous three dimensional network, which requires that at least three corners in each oxygen polyhedron must be shared.

From these postulates, the dominant type of polyhedron would be the tetrahedron as the octahedron would tend to share edges and faces with neighbouring polyhedra.

In a series of papers, Warren et al [7-11] confirmed Zachariasen's model by radial distribution studies from x-ray diffraction data of a number of oxide glasses of simple composition. The systems they studied were SiO_2, Na_2O-SiO_2, Na_2O-B_2O_3 and B_2O_3-SiO_2. In 1969, with advanced experimental techniques, Mozzi & Warren [12] showed that the silicon-oxygen-silicon dihedral bond angles in fused silica glass are distributed over a broad range, from 120° to 180°, centered about 145°. This range is much broader than in crystalline cristobalite. In contrast, the silicon-oxygen and oxygen-oxygen distances are nearly as uniform in the glass as in the corresponding crystal.

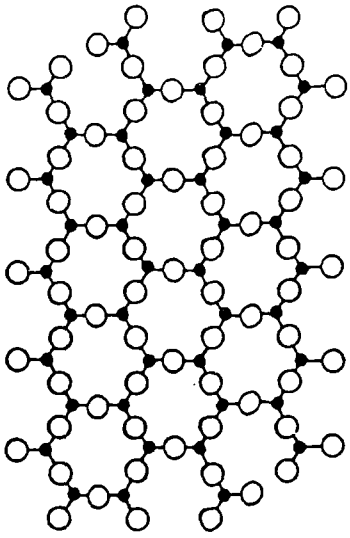

(a)

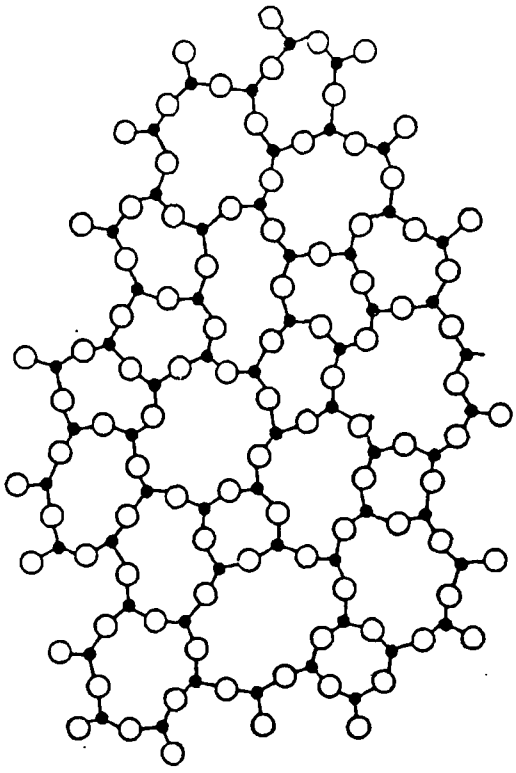

(b)

Figure 2.1 : *Schematic two-dimensional representation of the structure of (a) a hypothetical crystalline compound M_2O_3 (b) the glassy form of the same compound . Illustration taken from reference [5].*

Zachariasen also proposed a system of categorizing oxides as:

Network Formers - Oxides that readily form glasses, e.g. SiO_2, B_2O_3, GeO_2 and P_2O_5.

Intermediate - Oxides that cannot independently form glasses but can readily substitute for a network former, e.g. Al_2O_3, BeO, ZrO_2 and TiO_2.

Modifier - Oxides that disrupt the continuity of the network by breaking dihedral bonds, thus weakening the glass network, e.g. alkali-metal and alkaline-earth oxides. Na_2O is a good example and it will be used to illustrate the role of a modifier oxide.

Figure 2.2 illustrates the role of modifier oxides in the glass network. As can be seen in Figure 2.2(a), the introduction of Na_2O to silica glass causes structural changes by breaking the dihedral bonds. The addition of one molecule of Na_2O will produce two non-bridging oxygens. Thus the effect of introducing sodium oxide has been to produce a gap in the continuous network and results in changes in the properties such as reduction of viscosity and lowering of the transition temperature. The sodium ions are accommodated in the holes or interstices in the network structure (see Figure 2.2(b)). The continued addition of modifier will give rise to progressive breakdown in the dihedral bonds and hence there is a limit to the number of non-bridging oxygens that can be accommodated whilst still forming a stable glass. The glass forming limit of binary alkali silicate glasses is the metasilicate composition, where the average tetrahedron has two each of non-bridging and bridging oxygens, giving linear chains and ring structures. Further addition of alkali oxide will produce smaller units leading eventually to the formation of monomers (SiO_4^{-4} ions) at the orthosilicate composition. This results in a significant decrease in stability, making glass formation extremely difficult.

The nomenclature used to describe SiO_4 tetrahedra with varying numbers of bridging and non-bridging oxygens is as follows. The most widely accepted description employed is that proposed by Lippmaa et al [13]. The 'different' SiO_4 tetrahedra are represented by Q^n species where the superscript represents the number of bridging

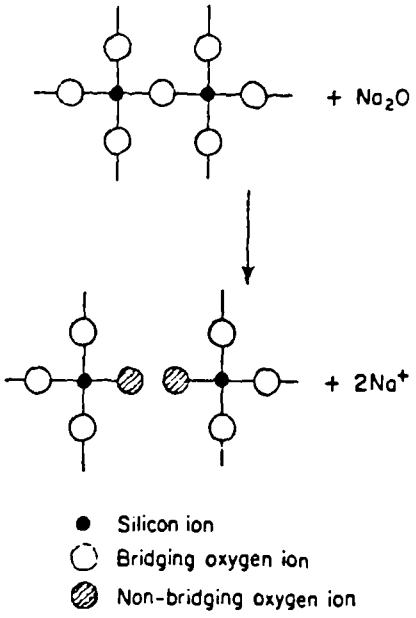

(a)

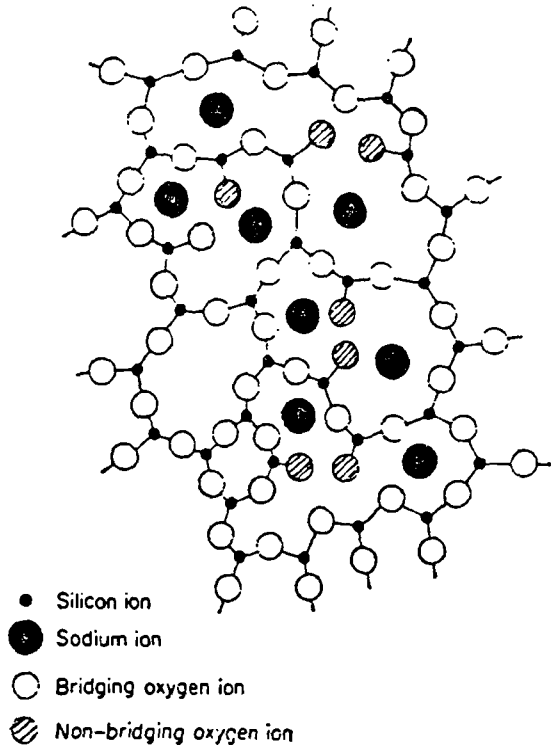

(b)

Figure 2.2 : *Two-dimensional illustration of : (a) Reaction between sodium oxide and silica tetrahedra. The addition of one molecule of sodium oxide produces two non-bridging oxygens. (b) The structure of soda-silica glass. The sodium ions are accommodated in the holes or interstices in the network structure. Illustrations taken from [2].*

oxygens to neighbouring SiO_4 tetrahedra. Therefore the value of n is between 0 and 4. Figure 2.3 schematically details the various Q^n species.

The properties of a glass depend on the exact way in which the different bond types are distributed, i.e. the quantities of different Q^n species and their distribution [14]. How the different Q^n species are distributed in the glass can be described by two models; the binary (constrained) [15] and the statistical (unconstrained random) [16] distribution models. In the binary model the non-bridging oxygens repel each other leading to maximum dilution which in turn gives successive formation of lower Q^n species and a homogeneous distribution of no more than 2 Q^n types. The statistical distribution model has no limit on the number of Q^n species present for any composition. The distribution is determined only by composition and statistics. The distribution of non-bridging oxygens has been studied for all the alkali metal silicate glasses using ^{29}Si NMR by different researchers. Grimmer et al [17-19] for Li, Na and K; Schramm et al [16] for Li; Dupree et al [15,20-21] for Na, Rb, Cs & Li and Gladden et al [22] for Li. Except for Schramm et al, who observed a statistical distribution for Li, the other researchers generally observed a binary distribution behaviour for alkali metal silicate glasses.

The structural role of intermediate oxides has the opposite effect to that of the modifying oxides because it can strengthen the network by removing the non-bridging oxygens. Al_2O_3 is a good example. In crystals, the aluminium ion can be four or six co-ordinated with oxygen giving rise to tetrahedral $(AlO_4)^-$ or octahedral $(AlO_6)^{3-}$ groups. The tetrahedral groups can replace SiO_4 tetrahedra in silicate lattices to give the arrangement shown in Figure 2.4. Because O^- ions are needed to form the polyhedral units of $(AlO_4)^-$ and $(AlO_6)^{3-}$, non-bridging oxygens are consumed and the Si—O—Al linkages repolymerise the network and produce a glass of greater stability. (It should be mentioned that Al also shows coordination of 5 in glasses and a few crystals).

It is worth noting that lead is unusual, because binary lead silicate glasses, containing very large amounts of PbO, up to ~80 mol%, readily form glasses [23].

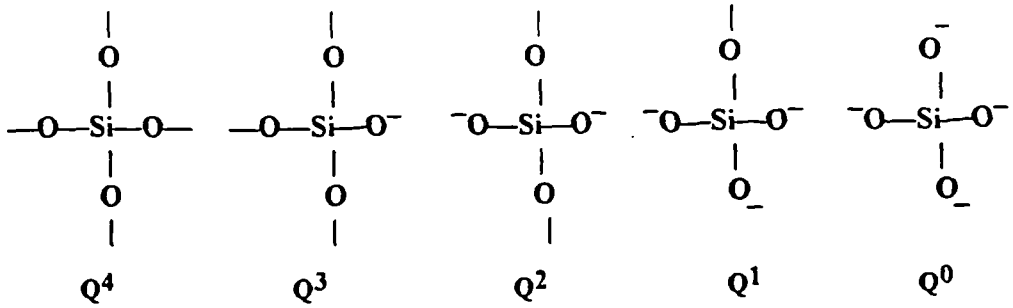

Figure 2.3 : *A schematic representation of the different Q^n SiO_4 species as defined by Lippmaa et al [13].*

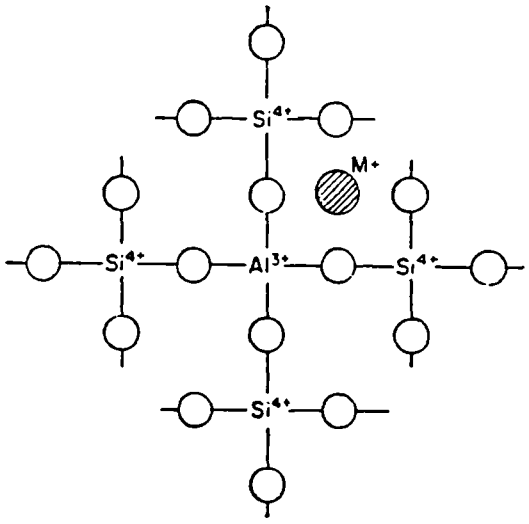

Figure 2.4 : *Al_2O_3 in silicate network. For charge neutrality purposes one alkali metal ion or half an alkaline earth ion per AlO_4 tetrahedron is located close to the AlO_4 tetrahedron, which has a delocalised single negative charge.*

Trap and Stevels suggest that there is an inversion in the structural role of the modifying ions at the metasilicate composition, hence glasses containing less than 50 mol% glass formers are called 'invert glasses' [24]. It is believed that Pb^{2+} can act as either a modifier or intermediate oxide depending on concentration [25]. Compositions higher than the orthosilicate ($2PbO.SiO_2$) can still form stable glass. This would obviously be impossible if Pb^{2+} were acting solely as modifier. Therefore it is believed that, at high PbO concentration, a lead-oxygen network must exist with considerable Pb—O covalency. Dupree et al [25] examined the ^{29}Si environment in this glass system by MAS NMR and made the following observations:

(i) Below ~30 mol% PbO - Pb^{2+} may act as a traditional modifier ion and the disposition of non-bridging oxygens is consistent with a binary Q^4/Q^3 distribution.

(ii) Between 30 and 40 mol% PbO - A Q^4 peak can still be resolved, which may reflect a change to a statistical distribution or may indicate the formation of Si—O—Pb bridging units which may be indistinguishable by NMR from Si—O—Si units because of the similarity in electronegativities.

(iii) From 40 to 65 mol% PbO - A statistical distribution of non-bridging oxygens is consistent with the observed spectra.

(iv) At 70 mol% PbO, the glass contains mainly isolated Q^0 species in a Pb—O matrix.

Another invert binary glass is stannous silicate, which forms part of the subject of this research. Complex invert glasses have also been prepared containing a mixture of at least three modifying oxides, the common conception is that mixing modifiers increases the free energy barrier for crystallization; thus hindering the diffusion of the crystal phase components [24].

Zachariasen's random network model was originally developed to describe glasses quenched from metastable melts at relatively slow cooling rates [26] and containing not less than 50 mol% glass formers [27]. Therefore its application to glasses prepared by other techniques is limited. However, Mackenzie [28] has shown that Zachariasen's rules on glass formation are applicable to all types of non-crystalline oxides prepared by routes other than melt cooling. Glass with a high proportion of

modifier oxides (> 60 mol%) has been shown to contain chains of various sizes, thus a three-dimensional network need not be a prerequisite for glass formation. In a later publication Zachariasen [29] stated that this model does not mean to imply that the vitreous network has to have three-dimensional extension. However, glasses would have the most advantageous properties if the tetrahedral or triangular network has three-dimensional cross-linking.

2.2.2 THE MODIFIED RANDOM NETWORK MODEL

In Zachariasen's Random Network Model the modifier cation occupies nearby holes within the network with an irregular and poorly defined bonding arrangement to ensure local charge neutrality. Recent neutron diffraction and EXAFS [30] evidence suggests that the network modifying cations adapt their local environment to obtain their own preferred co-ordination polyhedron as found in related crystalline materials. It is important to note here that in the crystalline state the local atomic arrangement of modifying cations (alkali or alkaline earth) can vary considerably from one mineral to the next [31]. In glass the modifying cation environments and non-bridging oxygens complement one another. The non-bridging oxygens form a well defined first coordination sphere around the modifier cation, thus adopting one of the local atomic arrangements found in crystalline minerals. Although the coordination sphere surrounding the cation is well defined, it does not imply the formation of regions of crystalline order (crystallites). By using the Zachariasen postulates, both Greaves [32] and Eckersley et al [33] state that the basic building unit of glass structure is not only the oxygen tetrahedron formed around the glass former but also the oxygen polyhedron formed around the modifier. How these two different basic building units are arranged in a complementary way is answered by the Modified Random Network hypothesis proposed by Greaves [32]. In this hypothesis the overall structure of a glass comprises two, interlacing sublattices; that of the network former and that of the

modifier. Figure 2.5 illustrates this idea in two dimensions and is best described as a Modified Random Network (MRN) model and, as such, is partly ionic and partly covalent. The structure's appearance is that of an 'archipelago' comprising peninsulas and islands of network lattice regions interspersed by modifier lattice regions that coalesce to form channels or rivers. The extent of these channels or rivers is dependent upon the concentration of modifying oxide in the glass.

The MRN model successfully describes the decrease in viscosity as the modifier oxide content is increased. The increase of modifier will increase the boundary disclinations between the ionic and covalent regions. As these boundaries are lines of easy shear, the more extensive these are within the structure, the lower the viscosity. This model also describes well the ionic conductivity of glass where the current flow is via the percolation channels as compared to conduction via jumping over energy barriers of varying height as in the Random Network Model.

2.2.3 CRYSTALLITE MODEL

According to Porai-Koshits [34] the idea that glass consisted of minute crystals was suggested by Frankenheim in 1835. He also said that the birth of the crystallite hypothesis was in 1921, authored by Lebedev. With the advancement of x-ray diffraction, the crystallite hypothesis was later developed in 1930 by Randall et al [35-38]. The x-ray diffraction patterns of glasses generally exhibit broad peaks centered in the range in which strong peaks are also observed in the diffraction patterns of the corresponding crystals. They proposed that the observed breadth of the glass diffraction pattern resulted from particle-size broadening where peak width varies inversely with particle size. Such observations led them to conclude that glasses are composed of assemblages or aggregation of very small crystals called crystallites. These crystallites consist of several polymorphs of the melt composition or compounds from the extremes of the phase diagram joined together by an amorphous zone.

Therefore the Crystallite Model of glass structure is one composed of a discrete non-continuous aggregation of extremely small crystals in an amorphous matrix as opposed to the continuous bonding of structural units in the Random Network Model.

Randall et al estimated the crystallite size of SiO_2 to be around 15-20 Å. Warren [39], using more accurate x-ray techniques revised this figure to be about 7 to 8 Å. This figure is about the size of a unit cell of cristobalite. Therefore any crystallites would be only a single unit cell in extent and such structures seem contrary to the notion of a crystalline array. According to this hypothesis, this cannot be true but no evidence has been found to indicate the discontinuity of SiO_2 species within homogeneous glasses. Phillips [40], on the basis electron microscopy and Raman spectroscopy proposed that vitreous silica is composed of crystallite clusters or granules of β-cristobalite of 66Å in diameter. This was convincingly refuted by Galeener and Wright [41] via Raman spectroscopy and neutron diffraction. Hence the crystallite hypothesis remains unsubstantiated although numerous x-ray, electron and neutron diffraction results indicate the existence of a greater degree of orderliness as discussed in the Modified Random Network Model.

2.2.4 STRAINED MIXED CLUSTER RANDOM NETWORK MODEL

The generally accepted random network model is based upon the idea that some kind of three-dimensional polymerisation occurs in the glass forming liquids as they are cooled. It does not give any clue as to how this polymer network forms, nor does it show how a glass forming liquid differs from a normal liquid which crystallises on cooling. An alternative model of glass structure that has an element of random network but also one of strained quasi crystalline cluster was put foward in 1984 by Goodman [42]. It is based thermodynamically on the variations of free energy and is independent of bonding type. It can explain glass forming ability in a wide range

of materials, where the bonding is mixed covalent-ionic, highly covalent, highly ionic or metallic.

Goodman noted that, when any liquid melt is cooled below its freezing point, the nucleation process starts with the formation of very small clusters of atoms called embryos. Embryos that grow to greater than some critical size will form a stable nucleus. On these nuclei crystal growth takes place accompanied by a decrease in free energy. Goodman added that, from empirical observation, the factor that distinguishes glass forming liquids from normally freezing liquids is that they show polymorphism in their crystallographic structures with little difference in their respective free energies. As a glass forming melt is supercooled, small clusters of atoms form with structures corresponding to the different polymorphs. Polymorphs with the lowest free energies will grow to a larger size. Therefore the supercooled liquid will contain a mixture of various types and sizes of clusters which will collide with each other due to Brownian motion. The collision will randomly mix the different clusters and in this way will minimise the possibility of 'favourable orientation' between clusters that will promote nucleation and crystal growth. Consequently, as the liquid cools, 'unfavourable orientation' between randomly-mixed, different clusters will experience a strained interface. This lack of epitaxy between clusters will increase the free energy and hence will hamper the formation of the critical size clusters required for nucleation and crystal growth. The viscosity of the liquid will increase as the concentration of agglomerated strained mixed clusters increases with further cooling. Eventually a random strained mixed cluster network will come to extend throughout the volume of the liquid as the agglomerations progressively stick together. At this point the residual liquid matrix containing the clusters cools to a space filling solid. This corresponds to the glass transition temperature (Tg). Figure 2.6(a) shows the glass structure at Tg. The variation of Tg with cooling rate can be explained by this model. Slow cooling rates will give more time for mutual adjustment of structure to minimise interfacial strains and to achieve a close fitting of mixed clusters. Rapid cooling would produce

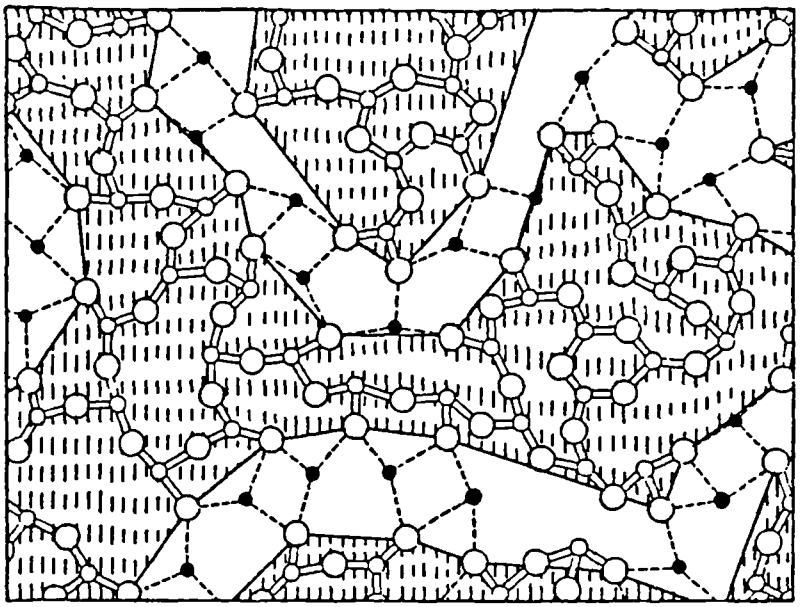

Figure 2.5: *A modified random network for a two dimensional oxide glass; $M_2O_3(G_2O_3)$, where M are modifier cations and G network forming cations. Covalent bonds are represented by solid lines, ionic bonds by dotted lines. Illustration taken from reference [32].*

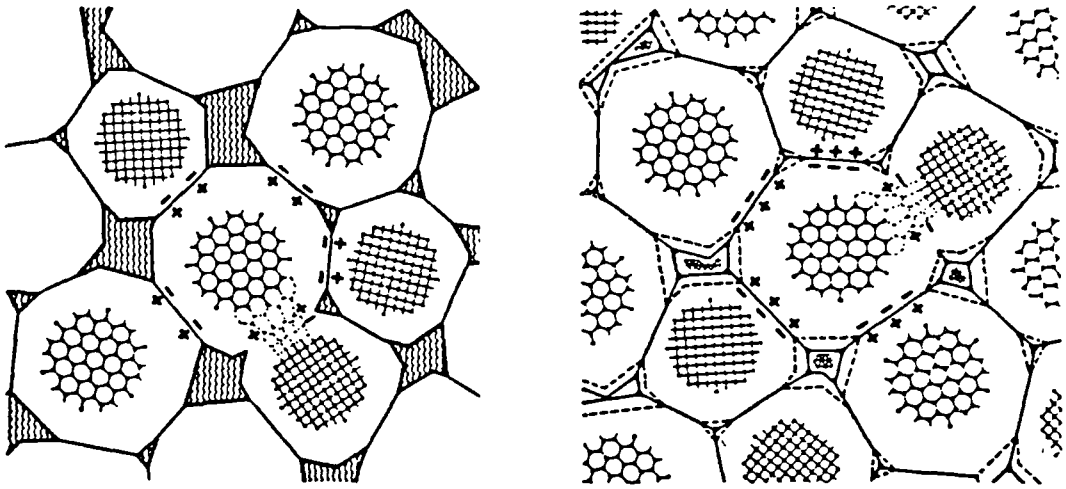

Figure 2.6 : *Goodman's illustration of a two-polymorph strained mixed cluster model. Interfacial strain is indicated by + and - symbols [42]. (a) Fully formed space-filling strained mixed cluster random network, at T_g. (b) Strained mixed cluster random network glass at a temperature below T_g when residual liquid has frozen out.*

higher interfacial strain, less efficient cluster packing, a higher content of space filling liquid and consequently a higher specific volume and therefore a higher Tg value.

On progressive cooling below Tg the residual liquid would deposit onto the surrounding cluster surfaces until all was solidified. The resulting structure is depicted in Figure 2.6(b) with each cluster surrounded by a random close packing of other clusters with half of the interfaces under tension and half under compression. Therefore the outer regions of each cluster will be significantly distorted and will not be coherent with its 'ideal' core in terms of x-ray or other diffraction. The estimated cluster size is 3 nm or more across. There is also further strain due to thermal expansion mismatches between the clusters and this will contribute to the overall increase in free energy.

2.2.5 CONCLUSION

At present an all encompassing model for glass structure does not exist. What has been presented is not an extensive classification of glass structure. Other models have also been proposed such as Krogh-Moe's [43] molecular theory for borate glasses and Bernal's [44] sphere packing for amorphous metal. An important one is the Stereo-Chemically Defined Model proposed by Gaskell [45] to explain the finding that there is a significant correlation between neutron diffraction data for calcium silicate glasses and their crystalline counterparts in respect of the local and medium range environment surrounding the calcium atoms [46-47]. This model proposed that there is a medium range order of atoms in glass. In other words this model states that the extent of similarity of a well ordered arrangement of atoms in amorphous materials with its corresponding crystalline state is beyond the first coordination sphere.

From the models presented above we can conclude that glass structures are very complex and may contain different types of bonding and the order of atomic

arrangement may be similar to the corresponding crystalline structure up to the second coordination sphere.

2.3 REVIEW OF TIN IN VARIOUS GLASS SYSTEMS

This section gives a review of some of the work that has been done to study the role of tin in the borate, germanate, phosphate and silicate glass systems.

2.3.1 BORATE GLASS

2.3.1.1 BINARY $SnO-B_2O_3$ GLASS

Paul et al [48] studied binary $SnO-B_2O_3$ glasses with SnO contents ranging from 12 to 58 mol% by infrared and ^{119}Sn Mössbauer spectroscopies. Glasses were prepared by melting tin(II) oxalate with boric oxide in silica crucibles at melting temperatures between 900°C and 1000°C. The disproportionation of SnO to SnO_2 and Sn metal was minimised by controlling the oxygen partial pressure of the furnace between 10^{-10} and 10^{-18} atm. As noted in chapter 1, the solubility of SnO_2 in borate is very low. A maximum of 0.2 wt.%(0.1 mol%) SnO_2 dissolved in some of the glasses and such a small SnO_2 contamination was neglected. The changes in infrared results showed that, like the alkali borate glasses, a small amount of SnO (less than 20 mol%) produces tetrahedral boron while large amounts result in non-bridging oxygen in addition to tetrahedral boron. The ^{119}Sn Mössbauer spectra, taken at 80K, showed that the chemical isomer shifts and the quadrupole splittings for Sn^{2+} in all glass samples were larger than in tetragonal SnO. The isomer shift increases with SnO content up to about 20 mol% and thereafter decreases smoothly with increasing SnO,

while the quadrupole splitting does not change much with SnO content. From this study they concluded that, for SnO contents up to 20 mol%, the Sn—O bonding is mostly ionic and, at higher SnO contents, the non-bridging oxygens are coordinated to Sn^{2+} ions. In other words SnO is acting as modifier at low concentration of SnO and from SnO contents of more than 20 mol% , it starts to make cross-linkages with the glass network.

2.3.1.2 ALKALI TIN BORATE GLASS

Eissa et al [49] studied alkali borate glass containing SnO_2 in minor amounts by the Mössbauer effect. The general composition formula of the glasses is (100-X) mol% B_2O_3 + X mol% Me_2O + Y mol% SnO_2, where Me= Li, Na or K, X= 10, 20 or 30 and Y is the quantity of SnO_2 introduced. Under an oxidizing atmosphere, the amounts of SnO_2 dissolved in the glasses containing 10, 20 or 30 mol% alkali oxide were not more than 2, 4 or 5 mol% respectively, while the composition with 30 mol% Li_2O did not form glass under any condition. The room temperature isomer shifts of ^{119}Sn Mössbauer spectra of the glasses were considerably different from that of the crystalline SnO_2. This shows that tin in small amounts can effect the glass structure and the γ resonance of ^{119}Sn was sensitive to structural changes of the glass. This conclusion is in agreement with an earlier study of Mitrofanov and Sidorov [50] who investigated the same series of glasses. Both studies found that the difference in the values of the isomer shift between the SnO_2 in glasses and crystalline SnO_2 indicates that the ionic nature of the Sn—O bond is stronger in the glasses than in SnO_2 crystal. The increase of the absolute value of the isomer shift with the increase of the alkali content was interpreted as being due to the increase of ionicity of the Sn—O bond in the glass. The absolute value of isomer shift decreases on going along the Li-Na-K series, which indicates that the ionicity of the Sn—O bond decreases with increasing ionic radius of the alkali ion. The quadrupole splitting and line width decrease with the

increase of alkali content and on going along the Li-Na-K series but the line width in glasses is only slightly greater than the line width in crystalline SnO_2. The general conclusion of both studies is that tin in the glass is in the quadrivalent state having a structure in which oxygen forms a highly distorted octahedron around the tin atom.

2.3.2 GERMANATE GLASS

2.3.2.1 BINARY SnO-GeO_2 GLASS

The binary SnO-GeO_2 glasses were studied by Silver et al [51], motivated by the fact that the binary PbO-GeO_2 glasses were reported [52-54] to have two interesting features. Namely; that the $Pb_5Ge_3O_{11}$ glass ceramic is an important new ferroelectric material and PbO-GeO_2 glasses have extremely high refractive indices. They studied three glass compositions: (i) Opaque yellow glass of composition $Sn_5Ge_3O_{11}$ melted in open carbon crucibles under oxidising conditions at 800°C, resulted in some metallic Sn and SnO_2 from the disproportionation of SnO in the glass and on its surface respectively. (ii & iii) Glasses of composition $SnGeO_3$ and $Sn_6Ge_7O_{20}$ melted between 700 and 800°C in vacuum out-gassed sealed silica ampoules, giving yellow-green $SnGeO_3$ glass and orange-yellow $Sn_6Ge_7O_{20}$ glass. The Mössbauer spectra of these glasses showed only a Sn^{2+} peak, indicating that the specimens were free from Sn^{4+}. The chemical shifts and the quadrupole splittings are higher than those of the tetragonal SnO. This shows that the Sn—O bond in the glass is more ionic and distorted than in crystalline SnO. The refractive indices of the glasses are very high and are of the order of those found for the PbO-GeO_2 glasses [55].

2.3.3 PHOSPHATE GLASS

2.3.3.1 BINARY SnF_2-P_2O_5 GLASS

Binary SnF_2-P_2O_5 glass was studied by Shaw & Shelby [56], motivated by the quest of finding glasses with properties of low melting temperature, high chemical durability and high thermal expansion. These properties are desirable for many applications which include the moulding of optical elements using standard equipment normally used for plastics, low temperature glass to metal seals and the incorporation of optically active organic molecules into inorganic glass matrix used in dye lasers. They succeeded in making stannous fluorophosphate glass with glass formation extending over a relatively large (0-80 mol% SnF_2) composition region and melting temperatures between 400 to 500°C. But only glasses with SnF_2 contents between 55-77 mol% were durable enough to moisture attack and they exhibited a very high thermal expansion. A structural model was proposed by Tick [57] for these glasses, suggesting a basic structural unit of Sn—O—P—O bonds. The divalent tin plays the role of a network former, in tetrahedral coordination, bonding with phosphorus via oxygen (Sn—O—P), shown in Figure 2.7. The network is extended in three dimensions by corner sharing of tin and phosphorus polyhedra, assuming no P—F bonding. The density composition relationship of this glass shows a sharp change at approximately 60 mol% SnF_2, the composition at which the glass exhibits the best resistance to water attack. This suggests that a structural change in the glass network occurs at this composition. As SnF_2 (Sn^{2+}) content increase, there is an increase in the linkage of the glass network as the formation of Sn—O—P—O bridges decreases the number of weak P—O—P bonds. At around 60 to 65 mol% SnF_2, the number of Sn—O—P—O bonds is at a maximum. Further increase of SnF_2 content eventually results in the formation of Sn—F—Sn bonds, which are weak to water attack.

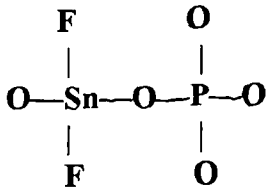

Figure 2.7: *Structural model of the binary SnF_2-P_2O_5 glass.*

2.3.3.2 TERNARY SnO-SnF_2-P_2O_5 GLASS

Shaw & Shelby [58] extended their studies to the tenary SnO-SnF_2-P_2O_5 glass system as a logical extension to the binary SnF_2-P_2O_5 glass. The addition of SnO to binary stannous fluorophosphate glasses resulted in a decrease in the volatility of the melt and dramatic improvements in the chemical durability of the glass. In binary SnF_2-P_2O_5, glasses with 60 to 65 mol% SnF_2 exhibited the best durabilities but these glasses were still susceptible to water attack. The substitution of SnO for SnF_2 dramatically reduced the dissolution rates and glass samples containing 30 mol% SnO showed dissolution rates comparable to soda-lime-silica glasses. Thus glasses with 30 mol% SnO and containing less than 50 mol% P_2O_5 are chemically very durable. According to Zachariasen's model , glass formation would be impossible for a P_2O_5 content less than 50 mol% and if the Sn^{2+} only act as network modifiers. It is evident from these studies that some fraction of Sn^{2+}act as network forming cations. Later Xu & Day [59] studied the same system and made the same finding as Shaw & Shelby. They concluded that the decrease in either the P_2O_5 contents or F/O ratio causes the major improvement in the chemical durability. In glasses containing 30 to 50 mol% P_2O_5, the infrared studies showed that Sn cations act as network formers, thereby forming an orthophosphate like structure. The infrared spectra of these glasses also showed that Tick's assumption that no P—F bonds are present in these glasses is incorrect. Therefore, Xu & Day proposed a different structural unit shown in Figure 2.8.

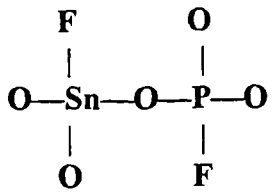

Figure 2.8: *Structural model of the ternary SnO-SnF_2-P_2O_5 glass*

The increase in chemical durability through the increase of SnO content is due to the fact that the weaker linkages of Sn—F—Sn, Sn—F—P and P—F—P are gradually replaced by stronger Sn—O—Sn, Sn—O—P and P—O—P linkages.

2.3.4 SILICATE GLASS

2.3.4.1 BINARY SnO-SiO_2 GLASS

Early studies on the binary SnO-SiO_2 glass system were focussed on the preparation of glass in order to establish the phase relations in the system. Keysselitz & Kohlmeyer [60] first reported the preparation of glass in this system by heating compressed pellets of mixtures of stannous oxalate and silica. On heating the pellet, the oxalate decomposed to give Sn, SnO, CO and CO_2. The evolution of CO and CO_2 gases expelled the air from the crucible and the low oxygen partial pressure of the gas mixture minimised oxidation of the melt. Spandau & Kohlmeyer [61] melted mixtures of SnO + SiO_2 , and obtained a yellow glass. Slonimskii & Tseidler [62] improved this technique by heating mixtures of SnO + SiO_2 in hermetically sealed alumina crucibles. The resulting glass showed that up to 3 wt% Al_2O_3 had dissolved in the melt. They also found that the glasses decomposed to metallic Sn, SnO_2 and quartz on heat treatment. Chizhikov et al [63] prepared this glass by reducing mixtures of SnO_2 + SiO_2 with carbon in a nitrogen filled Tammann furnace. All the above

researchers concluded that there are no binary compounds, stable or metastable in the phase relations of SnO-SiO_2 glass system.

Carbo Nover & Williamson [64] studied the crystallisation and decomposition of SnO-SiO_2 glasses ranging in composition from 28 to 59 mol% SnO. Their method of glass preparation was based on that used by Keysselitz & Kohlmeyer where compressed pellets of mixtures of stannous oxalate and quartz were melted in alumina crucibles. Glasses containing 42 mol% SnO or more crystallised to give a new metastable compound, designated stannous metasilicate ($SnSiO_3$). This phase grows at subsolidus temperatures as polycrystalline spherulites. The ease with which these crystalline spherulites grow depends on the composition of the glass. They grew most readily from glass compositions on either side of the 1:1 composition. This phase decomposes at 700°C to give SnO + silica and to SnO_2, Sn + silica at higher temperatures. They conclude that the structure of $SnSiO_3$ is thought to be related to that of SnO. Ishikawa & Akagi [65] studied the structures of SnO-SiO_2 glasses with SnO contents ranging from 32 to 57 mol% SnO. Glass samples were prepared from mixtures of stannous oxalate and silicon dioxide melted in alumina crucibles. The information they obtained both from infrared spectra and radial distribution studies of x-ray diffraction data of the glasses, supports the suggestion of Carbo Nover & Williamson that the structures of the glasses resembles that of the crystalline metastable $SnSiO_3$. From radial distribution studies, they also found that there is a structural contraction in the glasses with SnO contents greater than 35 mol%. Neither paper proposed atomic models of the glass structure since the structure of $SnSiO_3$ crystals has yet to be determined. Itoh & Mori [66] studied the electrical resistance as a function of temperature of SnO-SiO_2 glass containing 47.42 mol% SnO and found that the electrical resistance began to decrease at 450°C; corresponding to the glass transition temperature.

2.3.4.2 SODIUM TIN SILICATE GLASS

The solubility of SnO_2 in silicate glass is very low. A maximum of 0.8 mol% SnO_2 can be dissolved in SiO_2 (quartz) in making the stannosil glass [67], mentioned in chapter 1. However, the presence of alkali oxide, can increase the solubility of SnO_2 in a silicate melt. Zorina & Vakhrammev [68] studied the incorporation of SnO_2 in the following ternary system of sodium tin silicate glasses;

$15Na_2O.xSnO_2.(85-x)SiO_2$; $20Na_2O.xSnO_2.(80-x)SiO_2$; $25Na_2O.xSnO_2.(75-x)SiO_2$; $30Na_2O.xSnO_2.(70-x)SiO_2$. Where x = 0 ; 2.5; 5; 7.5; 10 mol% Their attempt to prepare transparent glass with SnO_2 content greater than 15 mol% failed owing to the sharp increase in the viscosity of the melt. Infrared spectra of the glasses showed that some of the octahedral coordination of tin began to change to tetrahedral coordination for SnO_2 contents greater than 5 mol% but the octahedral coordination of tin predominated. Dannheim et al [69] studied the Mössbauer effect of tin in the glass system Na_2O-SiO_2. By adding varying amounts of SnO_2 or SnO to the system and melting the glass in oxidizing or reducing atmosphere, they were able to vary the tin valence ratio (Sn^{4+}/Sn^{2+}) over a wide range in the glass. By comparing the values of the isomeric shift with that of known crystalline tin compounds, the coordination numbers of the Sn^{4+} and Sn^{2+} ions were determined and, depending on the glass composition and the valence ratio, both ions can undergo a transition from 4 to 6 coordination or vice versa. For both ions a change from 6 to 4 coordination indicates that the ion is changing from modifier to network former. Dannheim et al concluded their studies by saying that tin in the glass is in a distorted lattice. Mitrofanov & Sidorov [70] studied the Mössbauer effect of tin in the ternary system of Me_2O-SnO_2-SiO_2, where Me = Li, Na, K and found that the tin chemical shift for each alkali tin silicate glass did not change with composition and the spectral line width was only slightly greater than the line width of crystalline SnO_2. They added that in this glass systems tin atoms were surrounded by oxygen atoms and had six-fold coordination in the form of a group,

$$(Si—O)_i—Sn^{2-}_{2Me^+}—(O^-...Me^+)_{6-i}$$

whose structure remained constant when quantitative changes were made in the composition of the glass. They concluded that the glass structure was not in agreement with the Zachariasen's disordered lattice hypothesis and indicated the existence of definite chemical compounds in glasses.

2.3.4.3 TIN IN SODA-LIME-SILICA (FLOAT) GLASS

About 85% of the flat sheet soda-lime-silica glass produced in the world is made by the float process in which a ribbon of molten glass flows out of the melting furnace and solidifies while floating on a bath of molten tin enclosed in a float chamber filled with an inert gas mixture of nitrogen and hydrogen. Some tin diffuses into the lower surface that is in contact with the molten tin. A smaller amount diffuses into the upper surface by chemical adsorption from tin vapour in the float chamber. Figure 2.9 shows the typical tin diffusion profiles in the underside of float glass taken from Pantano et al [77]. It shows that the depth of tin penetration is to about 16μm and the tin oxide concentration at the surface is about 15 wt% (~ 4mol%).

There have been a few studies done on float glass, concentrating on the determination of tin oxidation states and quantifying these oxidation states as a function of depth in the glass. Chappell & Stoddart [71] studied the underside, top and air fracture surfaces of an unweathered float glass by Auger electron spectroscopy to compare compositions of the exterior surfaces with that of the bulk. Calcium, magnesium, potassium, silicon and oxygen were detected in all surfaces in qualitatively similar amounts to that in the bulk but contaminants (carbon, nitrogen and sulphur) were also found on exterior surfaces. On the underside, tin and iron were present but, on the top, tin was found at about only one tenth of the underside concentration. Sodium could not be detected because of its rapid migration from the surface along the

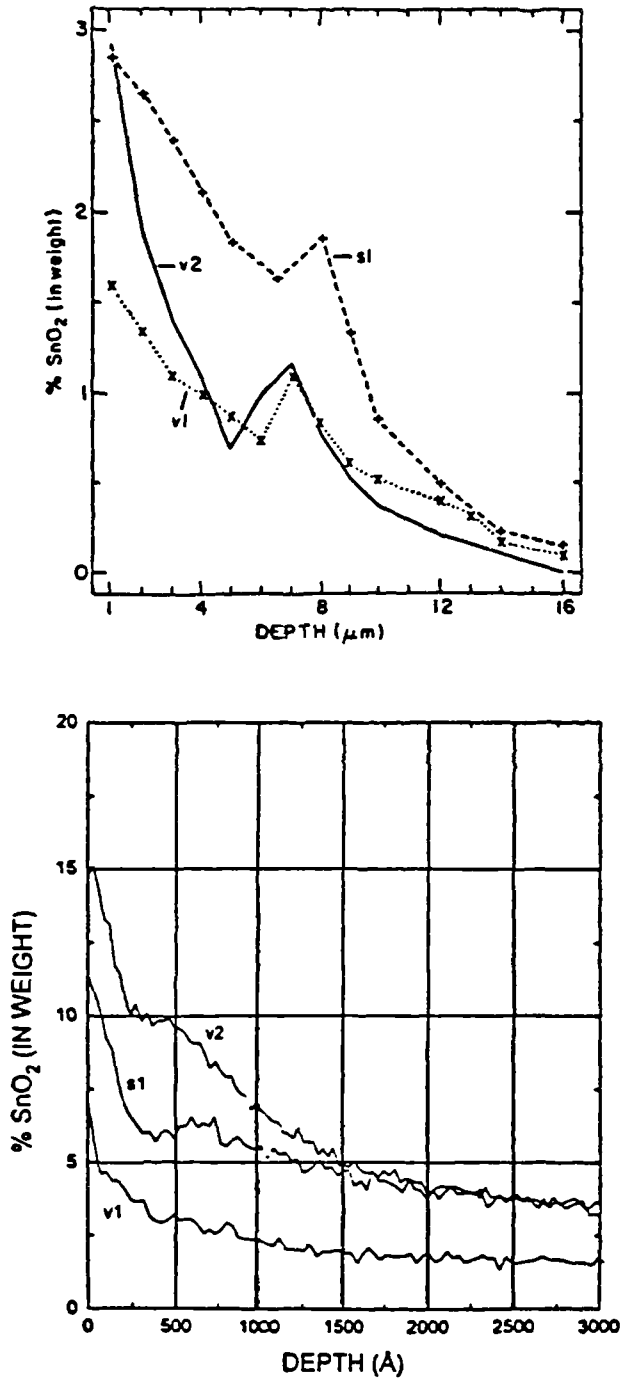

Figure 2.9 : *Typical tin diffusion profiles in the underside of float glass specimens taken from reference [77]. The in-depth and near-surface tin profiles for three different 6 mm clear float glasses; by EPMA (upper) and by SIMS (below). For simplicity the tin oxide concentration is expressed in wt.% SnO_2 even though it has been shown that tin in both valence states of +2 and +4 coexist in the glass. All the three specimens exhibit what Sieger [72] described as an anomalous 'hump' or satellite peak at about half the effective depth of penetration.*

field gradient induced by the electron beam. Sieger [72] studied the tin profiles of float glass surfaces by a method that involved electron-microprobe analysis of the edges of the samples and etching of a layer from the surface and chemically analyzing it for stannous or stannic tin. The depth of tin penetration through the underside varies with glass thickness and cleanliness of the tin bath. Glass near equilbrium thickness (6mm) shows deeper tin penetration than either 3 or 12 mm. Stannous and stannic tin are present near the bottom surface with the former predominating. The tin penetration profile also exhibits a 'hump' located at about half the effective depth of tin penetration. Colombin et al [73] measured the penetration depth of tin in float glass using ESCA [Electron spectroscopy for chemical analysis (=XPS)], photo emission induced by ion bombardment and ellipsometry. Their studies concluded that the concentration of tin in the first 100nm of the underside of float glass decreases very rapidly as a function of depth and the concentration of tin at the surface (10nm) of the underside is very high. Jie & Chao [74] studied the underside of float glass by XPS (X-ray photoelectron spectrometry) to determine the oxidation states of tin. A detailed scan for tin was made on the underside of the float glass sample, measured in the as-received state and after argon ion etching. The depth of tin scanning was about 10nm. XPS spectra of pure Sn, SnO and SnO_2 were fitted to the spectra of the glass samples. The fit in all cases was excellent and they concluded that,

(i) In the underside of float glass, tin is present in Sn^{4+}, Sn^{2+} and Sn^{0}, with Sn^{4+} having the largest fraction.

(ii) Deeper into the glass, the fraction of Sn^{4+} decreases gradually, while Sn^{2+} and Sn^{0} increases.

Principi et al [75] studied the oxidation state of surface tin in float glass using conversion electron Mössbauer spectroscopy (CEMS). The room temperature CEMS spectra show that the surface contains a mixture of Sn^{2+} and Sn^{4+} oxides. This result excludes the presence of metallic tin, contrary to the results reported by Jie & Chao. By taking into account the fact that the room temperature *f* factor of Sn^{4+} is approximately twice that of Sn^{2+}, they concluded that Sn^{2+} is the predominant oxide

species at the surface of float glass. The isomer shift and quadrupole splitting are higher than those of the corresponding crystalline phases. By heating the glass for 10 minutes at 730°C, thus simulating the industrial process which produces blooming (deterioration of glass surface quality), the Sn^{2+}/Sn^{4+} area ratio of the CEMS spectra was found to decrease. Therefore from this experiment they have shown that the blooming is caused by the oxidation of some of the Sn^{2+} tin species to Sn^{4+} when the glass is reheated for tempering or to produce curved glass. These findings supported in some way the mechanism for bloom suggested by Deubener et al [76] whereby an oxidation of Sn^{2+} in the outer layers alters both their viscosity and expansion coefficients by changing the chemical make up of the surface. Pantano et al [77] compared the tin profiles at the bottom surface of float glass due to heat treatment with that of untreated float glass. The concentration profiles of tin in the near surface (0 to 0.5 μm) were obtained using secondary ion mass spectroscopy (SIMS), while the depth profiles (0.5 to 30 μm) were determined with electron probe microanalysis (EPMA). The heat treatment schedule simulated the industrial process which produces blooming. Their results showed that after heat treatment there was a large tin concentration build-up near the surface and tin concentration depletion at greater depth. In another words there was a pronounced out-diffusion of tin to the surface due to heat treatment and this process changed the tin profiles as compared to the unheat treated float glass. Their findings supplement the mechanism for the process of blooming forwarded by Deubener et al above. The studies concluded that surface enrichment of Sn^{4+} species due to heat treatment can only exaggerate those physical and chemical property changes, while the abruptness of the decrease of tin concentration profiles magnifies their effect upon the surface wrinkling.

The above mentioned studies have concentrated on quantitative characterization of profiles of tin species that have diffused into the surfaces of float glass and try to account for the blooming of the glass due to heat treatment. There have been few studies carried out to try to make glass having the same chemical composition as the bottom part of float glass that has been in contact with the molten

tin and studying the effect of tin upon the physical and structural properties of the glass. Studies by Minko et al [78-79] mentioned in chapter 1, have concentrated on the synthesis of glass of float glass composition with varying amounts of Sn^{2+} and Sn^{4+}. Depending on the synthesis conditions, the equilbrium $Sn^{4+} \Leftrightarrow Sn^{2+}$ is established in the glass. This can be displaced almost completely to the left, but only 70 % to the right. Minko et al added that the improvement in the physicochemical properties of glasses synthesized under oxidizing compared with those under reducing conditions is due to the differing valence state of the tin in the glass structure. Owing to the different roles played in the glass by the different valence of tin, Sn^{4+} is assimilated by the soda-lime-silica melt only in an amount not exceeding the alkali content of the glass, whereas this is not the limit for Sn^{2+}.

2.3.5 CONCLUSION

Tin in the divalent state can be a major component in many glass system. Divalent tin in the form of SnO has been shown to fulfill various structural roles as either modifier or intermediate, depending on the type of glass system and composition. SnO contents of more than 50 mol% can form glasses in the binary $SnO-B_2O_3$, $SnO-P_2O_5$, and $SnO-SiO_2$ glasses. For example, in the binary $SnO-B_2O_3$ glasses the SnO role changed from modifier to intermediate at 20 mol% SnO. In the form of SnF_2 , divalent tin can be incorporated in the $SnF_2-P_2O_5$ glass system up to 80 mol% SnF_2. While glass in this system is not chemically durable, a major addition of SnO to form the ternary $SnO-SnF_2-P_2O_5$ glass system, has dramatically improves the chemical durability of the glass. With the presence of SnO, it is evident that some fraction of Sn^{2+} are acting as network forming cations in the ternary $SnO-SnF_2-P_2O_5$ glass system. Contrary to divalent tin, tetravalent tin in the form of SnO_2 is only a minor component in any glass system. This is because of its low solubility rate especially in alkali free glass. Only 0.1 mol% dissolved in stannous borate and 0.8 mol% dissolved in stannic silicate (stannosil) glasses. The solubility of

SnO_2 can be increased by the presence of alkali oxide in the glass melt but the amount that can be dissolved does not exceed the alkali content of the glass. Studies of tin in float glass have also shown that $SnO(Sn^{2+})$ is the predominating species compared to $SnO_2(Sn^{4+})$.

Based on the fact that divalent tin is a major component while tetravalent tin is minor in any glass system, the two valence states of tin must play a different role in the structure of the glass. The difference must be due to the structural difference between SnO and SnO_2 as seen in the next section.

2.4 THE STRUCTURE OF THE OXIDES OF TIN

Tin, as a p-element with atomic number 50, belongs to group IVA of the periodic table. This group comprises C, Si, Ge, Sn, and Pb. An atom of any of these elements has four electrons in its valence level. The oxides of Si and Ge are glass formers, while lead(II) oxide in silicate, germanate and borate glasses behaves as modifier or intermediate depending on its concentration in the respective glasses. The ground state electronic configuration of tin is,

	K	L	M	N	O
Sn:	$1s^2$	$2s^2$ $2p^6$	$3s^2$ $3p^6$ $3d^{10}$	$4s^2$ $4p^6$ $4d^{10}$	$5s^2$ $5p^2$

The oxidation states of tin are +2 and +4. The tetravalent state is the most stable and the formation of the lower oxidation state of +2 is referred to as the inert pair effect, since the $5s^2$ electron pair shows a reluctance or inability to ionize or to act as bonding electrons [80]. Table 1.1 gives the ionic radius, coordination number with respect to oxygen, field strength, ionic potential and ionic refraction of tin as well as silicon, lead, and sodium [1] for comparison purposes.

Table 1.1

Ion	*Ionic radius, r (Å)*	*Coordination number with respect to oxygen*	*Dietzel's field strength = z/a^2 ($Å^{-2}$) z = valency, a = interionic distance*	*Ionic potential = z/r ($Å^{-1}$)*	*Ionic refraction, R_i*
Si^{4+}	0.39	4	1.56	10.26	7.52
Sn^{2+}	-	4	0.46*	-	17.2
Sn^{2+}	0.93	6	0.41*	2.15	-
Sn^{4+}	-	4	1.13*	-	-
Sn^{4+}	0.69	6	1.01*	5.80	-
Pb^{2+}	1.18	6	0.31	1.69	27.4
Na^{+}	1.02	6	0.18	0.98	4.75

* *Taken from reference [69]*

According to Volf [1], the field strength (bond strength) of network former elements is high, exceeding 1.3 and the modifiers have low field strength below 0.36 and the intermediate elements field strength values are between these two. Volf also states that network formers have high ionic potentials, exceeding 10, modifiers have low values up to 2 and the intermediate ionic potential values are between these two. Based on these criteria tin can be classified empirically as an intermediate element along with lead. The value of ionic refraction give a measure of deformation (polarizability) of an ion [81]. The ionic refraction of Sn^{2+} is much higher than Si^{4+} and Na^{+} and comparable to Pb^{2+}. This indicates that Sn^{2+} is strongly deformable or polarizable.

Now let us look at the structure of SnO and SnO_2. The nature of the bonding of SnO and SnO_2 is classified as iono-covalent, the same as PbO and unlike the polymeric, more covalent bonding of SiO_2 and GeO_2 [80]. According to Pye [82], the fraction of ionic character of the Sn—O bond is ~ 0.6 and thus classified into the intermediate group.

2.4.1 THE STRUCTURE OF SnO_2.

Tin(IV) oxide (SnO_2) crystallizes with the rutile structure and can be regarded as essentially an ionic crystal [83]. The rutile crystal structure is a body-centered tetragonal with Sn^{4+} ions at the corners and centre of the cell and oxygen ions located at nonregular interstitial sites, causing distortion of the cell from cubic to tetragonal. The unit cell of SnO_2 crystal is depicted in figure 2.10, where the environment of tin is an octahedron of oxygen ions, and the electron density distribution close to the tin nucleus can be regarded as approximately spherical [84].

The poor solubility of SnO_2 in silicate melts can be explain by its bond strength (field strength) and structure. Oxides with bond strength values that exceed 0.8 and coordination number exceeding 4 have been classified by Volf [1] as oxides that show poor solubility in glass. In this case the bond strength of Sn^{4+} is 1.01 and its coordination number is 6. Owing to these factors, Sn^{4+} poses strong competition for silicon in polymerization. The Sn^{4+} ion can form its own strong six coordinated oxygen polyhedra differing from the SiO_4 group and, as a consequence of its high bond strength and different geometry, it is more difficult to link to the polyionic netwok of silicon tetrahedra. This results in poor solubility in silicate glasses.

2.4.2 THE STRUCTURE OF SnO

Tin(II) oxide (SnO) is amphoteric. Cole [85] classified an amphoteric oxide as generally belonging to the intermediate group, acidic oxides such as SiO_2 and B_2O_3 are network formers and basic oxides such as Na_2O and K_2O are modifiers. SnO has a complex tetragonal crystal structure, similar to PbO. The SnO crystal, unlike CaO or MgO, contains asymmetrical units. In CaO and MgO each cation is symmetrically surrounded by six oxygen ions, therefore the valence force of each ion extends equally into space. In the SnO crystal, however, the valence forces extend more to one

direction, so that the asymmetrical building units consists of a Sn atom located at the top of a square pyramid bonded with its four oxygen neighbours placed at the corners of the base of the pyramid as shown in Fig. 2.11(a). The inert pair of 5s electrons that do not take part in the bonding is situated at the apex of the tetragonal pyramid and occupies a mixed ($s\text{-}p_z$) orbital [83]. These asymmetrical building units of $(SnO_4)^{6-}$ are arranged forming a layered structure, where each tin atom has four oxygen near neighbours, all lying to one side, and all of the oxygen atoms lie between every other pair of tin layers as shown in Figure 2.11(b). The layered structure allows an electronic through-space interaction between tin atoms.

Therefore the resulting tetragonal structure of SnO consists of a prism with O^{2-} ions in each of the eight corners and Sn^{2+} placed inside not at the centre but much closer to four of the corners than to the other four. The simplest interpretation of this structure is that the four near O^{2-} ions repel the easily polarisable shell of the Sn^{2+}, especially its two outermost (inert $5s^2$) electrons. The electronic structure of the Sn^{2+} ion consists of an inner core of 18 electrons in the N-shell, and two 5s electrons in the O-shell. The two 5s electrons are easily repelled in the field of the negative ion O^{2-}. As a result the Sn^{2+} loses its spherical symmetry, and its electron distribution is such that towards the four near O^{2-} ions it extends only its 18 electrons of N-shell. Therefore towards the four near O^{2-} ions, the Sn^{2+} ion assumes the electron distribution of a much smaller and highly charged Sn^{4+} ion while the opposite side of the Sn^{2+} is characterized by a higher electron density, much resembling the Sn atom. In this way according to Weyl [86] Sn^{2+} ion possesses, what he term as 'metallophilic' character.

From the fact that the SnO crystal structure is complex and it can be a major component in many glass system, one can see that its structural role in glass must be complex and dependent on composition.

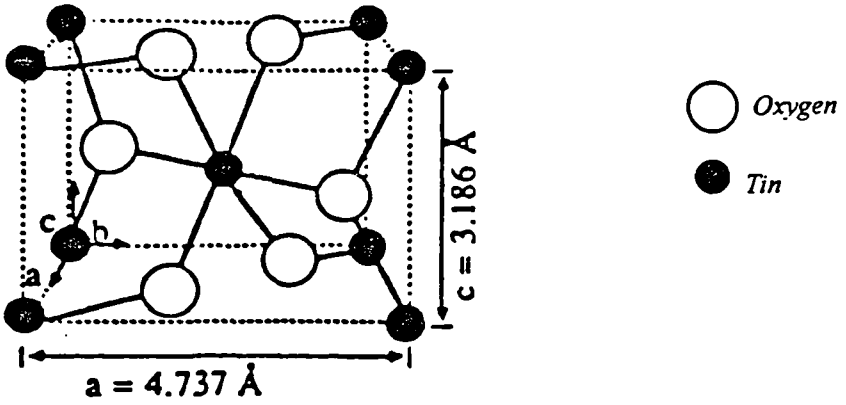

Figure 2.10 : *Rutile crystal structure of SnO_2, showing the unit cell [84].*

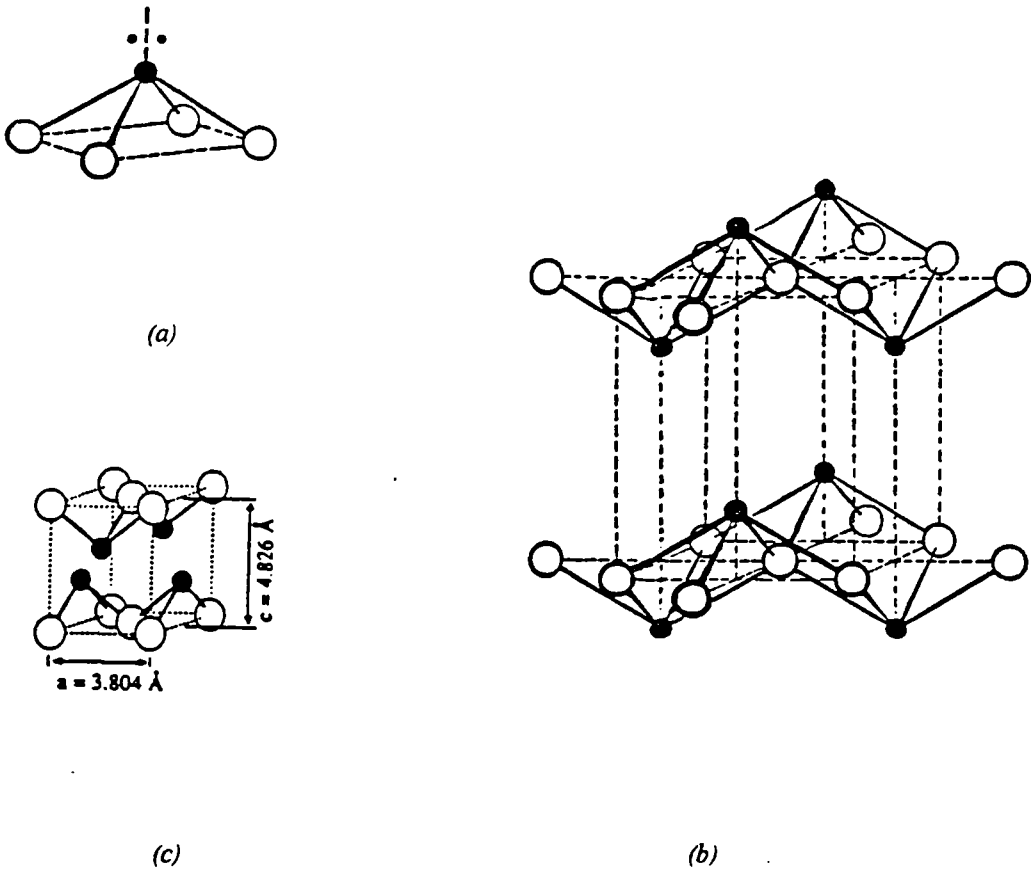

Figure 2.11 : *The crystal structure of SnO [83-84]: (a) The arrangement of bonds from a tin atom to oxygen atoms, where the two dots represent the 'inert pair' of electrons. (b) The tetragonal layered structure. (c) Unit cell of SnO.*

REFERENCES

1. Volf, M.B. (1984). *Chemical Approach to Glass,* Glass Science and Technology 7, Elsevier, Amsterdam.
2. McMillan.P.W. (1964). *Glass Ceramics*, Academic Press, London.
3. Wong, J & Angell, C.A. (1967). *Glass Structure by Spectroscopy,* Marcell Dekker, Inc. New York, p.2.
4. Paul, A. (1982). *Chemistry of Glasses*, Chapman and Hall, London, p. 2-5.
5. Rawson, H.(1980). *Properties and Application of Glass*, Elsevier, Amsterdam, p.1.
6. Zachariasen, W.H. (1932). *J. Am. Ceram. Soc.* **54**, 3841.
7. Krutter, H., Morningstar, O. & Warren, B.E. (1936). *J. Am. Ceram. Soc.* **19**, 202.
8. Warren, B.E. & Biscoe, J. (1938). *J. Am. Ceram. Soc.* **21**, 49.
9. Biscoe, J. & Warren, B.E. (1938). *J. Am. Ceram. Soc.* **21**, 259.
10. Biscoe, J. & Waren. B.E. (1938). *J. Am. Ceram. Soc.* **21**, 287.
11. Warren, B.E., Robinson, B.S. & Biscoe, J. (1939). *J. Am. Ceram. Soc.* **22**, 180.
12. Mozzi, R.L. & Warren, B.E. (1969). *J. Appl. Cryst.* **2**, 164.
13. Lippmaa, E., Magi, M., Samoson, A., Engelhardt, G. & Grimmer, A.R. (1980). *J. Am. Chem. Soc.* **102**, 4889.
14. Dupree, R. & Holland, D. (1989). ed. Lewis, M.H. *Glasses and Glass-Ceramics*, Chapman and Hall, London, p.8.
15. Dupree, R., Holland, D., McMillan, P.W. & Pettifer, R.F. (1984). *J. Non-Cryst. Solids* **68**, 399.
16. Schramm, C.M., de Jong, B.H.W.S. & Parziale, V.E. (1984). *J. Am. Chem. Soc.* **106**, 4396.
17. Grimmer, A.R., Magi, M., Hähnert, M., Stade, H., Samosan, A., Wieker, A. & Lippmaa, E. (1984). *Phys. Chem. Glasses* **25**, 105.
18. Grimmer, A.R. & Radeglia, R. (1984). *Chem. Phys. Lett.* **106**, 263.
19. Grimmer, A.R. & Muller, W. (1986). *Monatsh. Chem.* **117**, 799.
20. Dupree, R., Holland, D. & Williams, D.S. (1986). *J. Non-Cryst. Solids* **81**, 185.
21. Dupree, R., Holland,D. & Williams, D.S. (1990). *J. Non-Cryst. Solids* **116**, 148.
22. Gladden, L.F., Carpenter, T.A., Klinowski, J. & Elliot, S.R. (1986). *J. Magn. Reson.* **66**, 93.
23. Holloway, D.G. (1973). *The Physical Properties of Glass,* Wykeham, London, p.17.
24. Rawson, H. (1967). *Inorganic Glass-Forming Systems,* Academic Press, London, p. 92.
25. Dupree, R., Ford, N. & Holland, D. (1987). *Phys. Chem. Glasses* **28(2)**, 78.
26. Wright, A.C. (1990). *J. Non-Cryst. Solids* **123**, 129.
27. Mackenzie, J.D. (1960) *Modern Aspects of the Vitreous State*, Butterworths, London, p 4.
28. Mackenzie, J.D. (1987). *J. Non-Cryst. Solids* **95 & 96**, 441.
29. Zachariasen, W.H. (1935). *J. Chem. Phys.* **3**. 162.
30. Greaves, G.N.,. Fontaine, A., Lagarde, P., Raoux, D. & Gurman, S.J. (1981). *Nature* **293**, 611.
31. Wells, A.F. (1975). *Structural Inorganic Chemistry*, Clarendon, Oxford .
32. Greaves, G.N. (1985). *J. Non-Cryst. Solids* **71**, 203.
33. Eckersley, M.C., Gaskell, P.H., Barnes, A.C. & Chieux, P. (1988). *Nature* **335**, 525.
34. Porai Koshits, E.A., (1990). *J. Non-Cryst. Solids* **123**, 1.

35. Randall, J.T., Rooksby, H.P. & Cooper, B.S. (1930). *J. Soc. Glass Tech.* **14,** 219.
36. Randall, J.T., Rooksby, H.P. & Cooper, B.S. (1930). *Z. Krist.* **75,** 196.
37. Randall, J.T., Rooksby, H.P. & Cooper, B.S. (1931). *J. Soc. Glass Tech.* **15,** 54.
38. Randall, J.T., Rooksby, H.P. & Cooper, B.S. (1933). *J. Soc. Glass Tech.* **17,** 287.
39. Warren, B.E. (1937). *J. Appl. Physics* **8,** 645.
40. Phillips, J.C. (1982). *Physics Today* **35(2),** 27.
41. Galeener, F.L. & Wright, A.C. (1986). *Solid State Comm.* **57,** 677.
42. Goodman, C.H.L. (1985). *Phys. Chem. Glasses* **26,** 1.
43. Krogh-Moe, J. (1960). *Phys. Chem. Glasses* **1,** 26.
44. Bernal, J.D. & Mason, J. (1960). *Nature* **188,** 910.
45. Gaskell, P.H. (1992). *Bol. Soc. Esp. Ceram. Vid.* **31-C1,** 25.
46. Eckersley, P.H., Gaskell, P.H., Barnes, A.C. & Chieux, P. (1988). *J. Non-Cryst. Solids* **106,** 132.
47. Cahn, R.W. (1988). *Nature* **335,** 493.
48. Paul, A., Donaldson, J.D., Donoghue, M.T., & Thomas, M.J.K. (1977). *Phys. Chem. Glasses* **18(6),** 125.
49. Eissa, N.A., Shaisha, E.E., & Hussiun, A.L. (1974). *J. Non-Cryst. Solids* **16,** 206.
50. Mitrofanov, K.P. & Sidorov, T.A. (1967). *Soviet Physics- Solid State* **9(3),** *693.*
51. Silver, J., White, E.A.D. & Donaldson, J.D. (1977). *J. Material Science* **12,** *828.*
52. Phillip, B. & Scorger, M.G. (1965). *J. Amer. Ceram. Soc.* **48,** *98.*
53. Topping, J.A., Harrover,I.T. & Murthy, M.K.(1974). *J.Amer. Ceram. Soc.* **57,***209.*
54. Topping, J.A. & Murthy, M.K. (1974). *J.Amer. Ceram. Soc.* **57,** 281.
55. Bansal, N.P. & Doremus, R.H. (1986). *Handbook of Glass Properties,* Academic Press, New York.
56. Shaw, C.M. & Shelby, J.E. (1988). *Phys. Chem. Glasses* **29(2),** 49.
57. Tick. P.A. (1984). *Phys. Chem. Glasses* **25(6),** 149.
58. Shaw, C.M. & Shelby, J.E. (1988). *Phys. Chem. Glasses* **29(3),** 87.
59. Xu, X.J. & Day, D.E. (1990). *Phys. Chem. Glasses* **31(5),** 183.
60. Keysselitz, B. & Kohlmeyer, E.J. (1933). *Metall Erz.* **30,** 172.
61. Spandau, H. & Kohlmeyer, E.J. (1947). *Z. Anorg. Allg.* **254,** 65.
62. Slonimskii, B.I. & Tseidler, A.A. (1959). *Sb. Trund. Gos. Non.. Issled. Inst. Tsvet Metal.* **15,** 173.
63. Chizhikov, D.M., Volkova, N.E. & Tsvetkov, V. (1962). *Akad . Nauk. SSSR, Metal, Gorn. Delo.* **3,** 82.
64. Carbo Nover, J. & Williamson, J. (1967). *Phys. Chem. Glasses* **8(4),** 164.
65. Ishikawa, T. & Akagi, S. (1978). *Phys. Chem. Glasses* **19(5),** 108.
66. Itoh, H. & Mori, S. (1977). *Fukuoka Daigaku Kogaku Shuho* **19,** 13, Japan.
67. Maddock, A.J. (1939). *J. Soc. Glass Tech.* **23,** 372.
68. Zorina, M.L. & Vakhrameev, V.I. (1969). *Neorg. Mat.* **5(10),** 1834.
69. Danheim, V.H., Oel, H.J. & Erlangen, G.T. (1976). *Glastechn. Ber.* **49,** 170.
70. Mitrofanov, K.P. & Sidorov, T.A. (1967). *Soviet Physics - Solid State* **9(3),** 693.
71. Chappell, R.A. & Stoddart, C.T.H. (1974). *Phys. Chem. Glasses* **15(5),** 130.
72. Sieger, J.S. (1975). *J.Non. Cryst. Solids* **19,** 213.
73. Colombin, L., Jelli, A., Riga, J., Pireaux, J.J. & Verbist, J. (1977). *J. Non. Cryst. Solids* **24,** 253.
74. Lie, L. & Chao, X. (1990). *J. Non. Cryst. Solids* **119,** 37.
75. Principi, G., Maddalena, A. & Gupta, A. (1993). *Nuclear. Instr. and Methods in Phys. Research* **B76,** 215.

76. Duebener, J., Brückner, R. & Hessenkemper, H. (1992). *Glastech. Ber.* **65**, 256.
77. Pantano, C.G., Bojan, V., Verita, M., Geotti-Bianchini, F. & Hreglich, S. (1993). *Rivista della Stazione Sperimentale del Vetro* **Vol. XX111**, 285.
78. Min'ko, N.I., Kislitsyn, B.F., Fabrikant, S.A. & Konik, L.T. (1973). *Steklo i Keramika* **4,** 19.
79. Min'ko, N.I. (1973). Izv. Akad. Nauk SSSR, *Neorg. Mater.* **9(10),** 1816.
80. Puddenphatt, R.J. & Monaghan, P.K. (1986). *The Periodic Table of the Elements,* Oxford Science Publications, p.48.
81. Fanderlik, I. (1983). *Optical Properties of Glass,* Glass Science & Tech. 5, Elsevier, Amsterdam, p.93.
82. Pye, L.D., Stevens, H.J. & LaCourse, W.C. (1972). *Introduction to Glass Science,* Plenum, New York, p.25.
83. Wells, A.F. (1962). *Structural Inorganic Chemistry*, Clarendon Press, Oxford.
84. Cossement, C., Darville, J., Gilles, J-M., Nagy, J.B., Fernandez, C. & Amoureux, J-P. (1992). *Magnetic Resonance in Chemistry* **30**, 263.
85. Cole, H. (1947). *J. Soc. Glass Tech.* **41**, 142.
86. Weyl, W.A. (1967). *Coloured Glass,* Society of Glass Technology, Sheffield, p.342.

Chapter 3 - Theoretical Background

This chapter presents the theoretical backgrounds to the three main experimental techniques used in the studies. ^{29}Si and ^{119}Sn NMR were used in the structural investigations of the binary $SnO\text{-}SiO_2$ glasses. ^{119}Sn Mössbauer spectroscopy was used to investigate the role of tin oxides in the binary $SnO\text{-}SiO_2$ and in tin-doped float glasses. Viscosity measurements were made on both the binary $SnO\text{-}SiO_2$ and tin-doped float glasses.

Other physical properties were measured which can indirectly provide evidence for a better understanding of the structural features of both glasses. These were thermal expansion, refractive index, density and microhardness. They are not discussed here but will be briefly touched in chapter 4 (Experimental Materials and Techniques).

3.1 NUCLEAR MAGNETIC RESONANCE

Nuclear magnetic resonance (NMR) is the spectroscopy of nuclei of certain elements that possess non-zero spin angular momemtum and an associated magnetic moment. It is concerned with the absorption of electromagnetic radiation, at a certain precise frequency by a nucleus in an external static magnetic field, that induces a quantum transition from lower spin to higher spin nuclear energy states. As the separation of these nuclear levels is small , about 0.1 J per mole, NMR is a low energy (low frequency) spectroscopic experiment with the inducing electromagnetic radiation in the radio frequency band.

The NMR effect was first observed in protons (^{1}H) independently by Purcell et al [1] and Bloch et al [2] in 1945. One important discovery soon after this is that, for a given nucleus in a given magnetic field, the frequency of energy that causes the nuclear transition between spins states shifts slightly depending on the electronic environment of that nucleus. This was first measured in metals in 1949 [3] and was called the 'Knight' shift. This study was soon followed by a major contribution by

Arnold et al [4] who reported the first spectra that showed separate lines for the chemically different protons in a number of alcohols. The observation of this frequency difference in non-metals (termed the chemical shift) was initially limited to liquid-state matter, where the random motion of the surrounding molecules averaged away the anisotropic interactions present, to give narrow NMR spectral lines producing sufficient resolution of different environments. NMR became an important spectrosopic technique for chemists in studies of the local environments of protons (^{1}H) and carbon (^{13}C) in liquid organic matter. The extension of NMR to the solid-state was slow and complicated. In solids the neighbouring molecules are relatively fixed in position and their mutual interactions result in anisotropic distortions of the applied field which broaden the spectral lines and mask the small differences in the isotropic chemical shifts. The mechanisms of the line broadening of the NMR spectra include the magnetic dipolar interaction, the anisotropic chemical shift interaction and, for nuclei with spin $I > ½$, the quadrupolar interaction. These will be discussed in a later section.

The use of NMR spectroscopy in the study of inorganic amorphous solids, particularly glasses, was first reported in 1958 by Silver and Bray [5]. Using a continuous wave and broad line technique, they succeeded in observing the quadrupolar nuclei of ^{11}B and determining the relative amounts of 3 and 4 fold co-ordinated boron in alkali borate glasses. At that time the application of this technique to the Si nucleus in silicate based glasses was less favourable. This is because of the absence of a nuclear quadrupole moment in ^{29}Si ($I = ½$, dipolar moment), which causes the time for the experiment to be extremely long, and also because of its low sensitivity due to the low natural abundance (4.7 %) of magnetically active ^{29}Si nuclei. The advent of high-field superconducting magnets, improvement in spectrometer hardware coupled with other techniques such as magic-angle spinning (MAS) NMR [6,7], decoupling [8,9] and cross polarization (CP) [10], have extended the area of applicability of NMR spectroscopy methods from the structure determination of ^{1}H and ^{13}C in organic liquids and solids, to structural studies of

many NMR active nuclei in inorganic solids. Following the first systematic study of the ^{29}Si NMR behaviour of inorganic solids by Lippmaa et al [11], several studies of alkali silicate glasses and crystals have been carried out. Dupree and Holland [12] gave a review encompassing the structural determination for several glass systems and ceramics by MAS NMR. Structural studies on minerals and glasses using NMR have also been reviewed by Stebbins [13] and Kirkpatrick [14]. A more comprehensive review of MAS NMR of glasses has been given by Eckert [15].

NMR is a powerful probe of the static structure and dynamic behaviour of the condensed phase. It has many advantages over diffraction methods and vibrational spectroscopy because it is atom-type specific, sensitive to symmetry and coordination, site selective and sensitive to dilute components [16].

3.1.1 BASIC PRINCIPLES OF NMR

The phenomenon of nuclear magnetic resonance is based on the fact that nuclei of certain elements possess a spin angular momentum $\mathbf{p} = (h/2\pi)\mathbf{I}$ and an associated magnetic moment μ which are parallel and can be written as

$$\mu = \gamma \mathbf{p} = \gamma (h/2\pi) \mathbf{I} \qquad 3.1$$

where γ is the gyromagnetic ratio which is characteristic of the nucleus and I is the nuclear spin number. Quantum theory demands that the allowable nuclear spin states are quantized; and its z component, described by the quantum number m_z takes up one of a set of discrete values specified by the series,

$$m_z = I, I-1, I-2, \ldots\ldots\ldots\ldots, -I \qquad 3.2$$

Therefore each nuclide has 2I + 1 energy levels. In the absence of a magnetic field, these energy levels are degenerate but in an intense magnetic field the interaction between them and the field (the Zeeman interaction) lifts the degeneracy. Therefore if an isolated nucleus of such an element is now placed in a static magnetic field $\mathbf{B_0}$, applied in the z direction , the magnetic moment interacts with the field such that

$$H = -\mu \cdot \mathbf{B_0} = -\gamma (h/2\pi) B_0 I_z \qquad 3.3$$

and the energy of a m state is given by

$$E_m = - \gamma (h/2\pi) B_0 m_z \qquad 3.4$$

The energy levels are not identical but separated by an energy gap $\Delta E = \gamma (h/2\pi) B_0$. Thus the Zeeman splitting of the energy level has lifted the degeneracy of the nuclear spin states. Figure 3.1 shows an example of the Zeeman splitting for $I = \frac{1}{2}$ and $I = 1$.

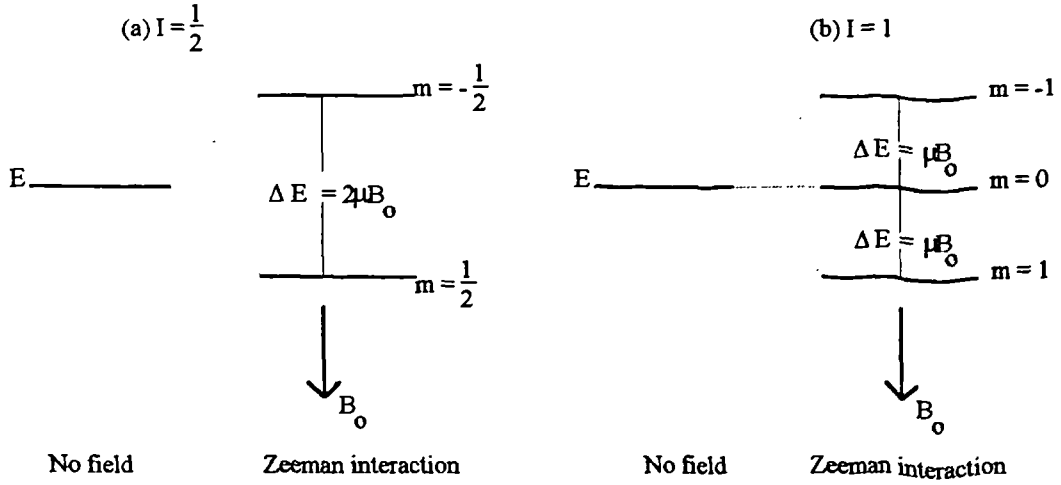

Figure 3.1 : *Zeeman splitting of nuclear energy levels* (a) I = ½ (b) I = 1 , *the quadrupole splitting is not shown.*

The fundamental principle governing the NMR technique is the induction of transitions between the different nuclear Zeeman levels of a particular nucleus. These transitions can be stimulated by radiating an energy equivalent to the energy gap, that is when they are in 'resonance'. In practice this is done by applying an oscillating magnetic field $\mathbf{B_1}$ of frequency ν_0 perpendicular to the static field B_0, such that

$$h\nu_0 = \Delta E$$

and

$$h\nu_0 = -\gamma (h/2\pi) B_0 \qquad 3.5$$

hence

$$\nu_0 = \frac{-\gamma B_0}{2\pi} \qquad 3.6$$

since $\omega = 2\pi\nu$

therefore

$$\omega_0 = -\gamma B_0 \qquad 3.7$$

where ν_0 is the resonant frequency in hertz and ω_0 is the resonant frequency in radians/second.

The resonant frequency is also known as the Larmor frequency. It is this frequency, which is in the radio-frequency range, that is measured in an NMR experiment. The classical picture of this happening is shown in Figure 3.2.

In samples consisting of a large number (N) of nuclei of a two level system (I = ½), in thermal equilibrium, in a field B_0, the relative populations of the higher energy state, m_z = -½ and lower energy state m_z = ½ are given by the Boltzman distribution,

$$N_{-½} = N_{½}\, e^{-\Delta E / kT} \qquad 3.8$$

Because of the small energy difference, the populations in the two levels are nearly the same. Only a very few nuclei are present in excess in the lower energy state, for

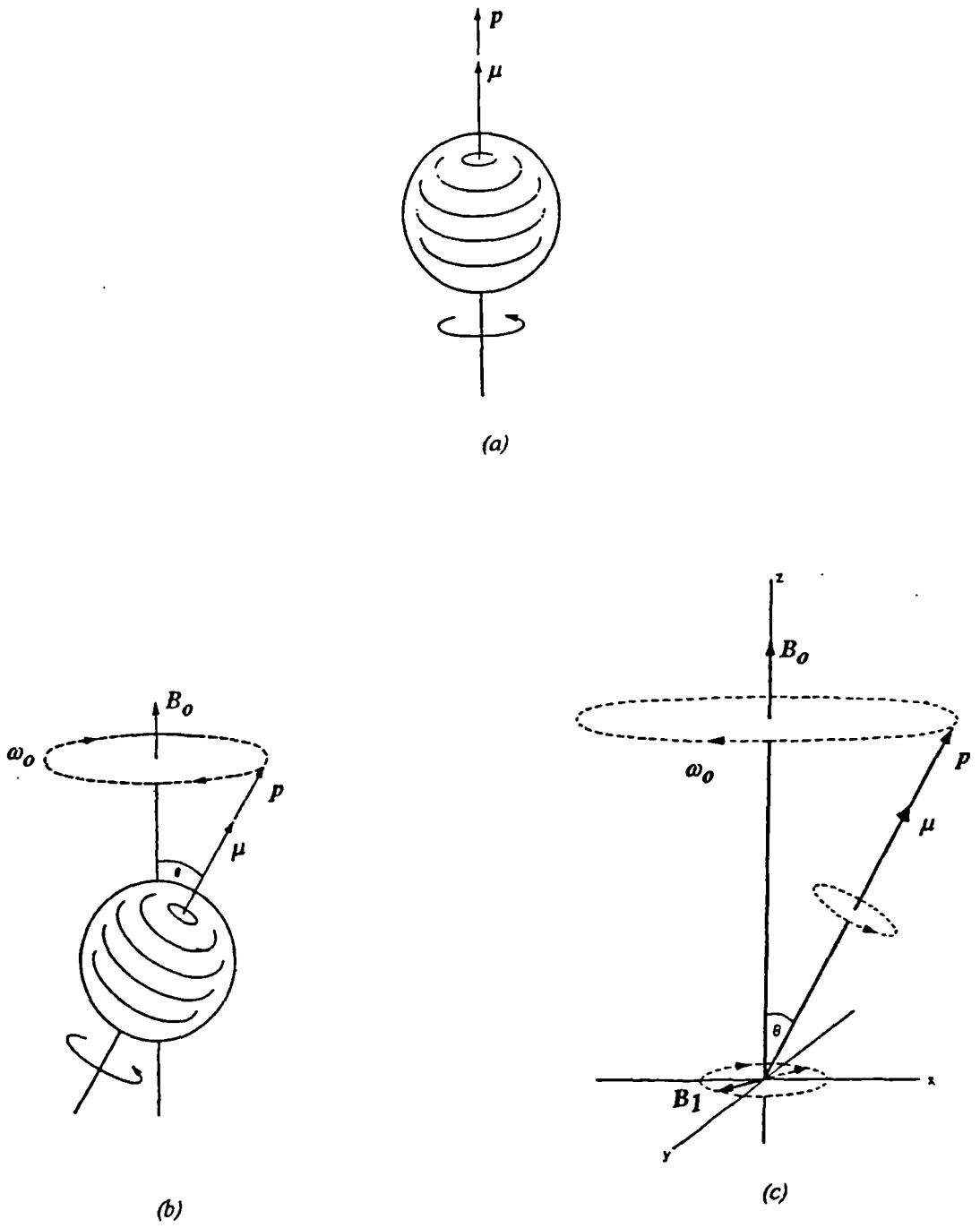

Figure 3.2 : *(a) The spinning positively charged nucleus produces spin angular momentum* $\mathbf{p}$ *and an associated magnetic moment* μ. *(b) The Larmor precession of the nuclear spin axis about the direction of the static magnetic field* $\mathbf{B_0}$. *(c) If a magnetic field (* $\mathbf{B_1}$ *) of frequency equal to the Larmor frequency (* ω_0 *) is placed at right angle to* $\mathbf{B_0}$ *; resonance is triggered by the absorption of energy into the nuclear spin system.*

example about 1 in 10^5 for ^{29}Si in a magnetic field of 8.45T at room temperature, so that the nuclear paramagnetism is weak and sensitivity low. Despite this, NMR has become an important spectroscopic technique because, in addition to the Zeeman interaction, some localised interactions are also present which perturb the Zeeman splittings, resulting in a more informative spectrum. These are the chemical shift, dipolar and, for $I > ½$, the quadrupole interactions. The feature of these interactions is that they are anisotropic in the solid due to the relatively fixed orientations of the molecules, whereas in solution average values are obtained due to the fast and isotropic motion of the molecules. In a solid these interactions are responsible for the line broadening of the NMR spectra and their relative importance will depend on the nucleus being observed and the system under study. These will be discussed briefly in the next section. Theoretical details of NMR can be found in Abragam [17], Harris [18], Derome [19], Slichter [20], Farrar and Becker [21] etc.

3.1.2 CHEMICAL SHIFT INTERACTION

In the last section we saw that the fequency (ω_o) at which a particular magnetically active nucleus will resonate when placed into a magnetic field B_o, is given by equation 3.7:

$$\omega_o = -\gamma B_o$$

This equation was obtained by ignoring the presence of electrons around the nucleus. In reality this is not the case. An isolated atom experiences a local magnetic field different from the applied field because of the shielding caused by the electrons surrounding the nucleus. Thus a nucleus experiences not the magnetic field (B_o) that is applied to the sample, but rather the field that has been altered by the interaction with the enveloping electron cloud This interaction, called the chemical shift interaction, is experienced by

nuclei of all spin number. This interaction can either reduce $\mathbf{B_0}$ (diamagnetic shielding) or enhance $\mathbf{B_0}$ (generate a paramagnetic effect). Hence the local field actually experienced by a nucleus is

$$\mathbf{B_i} = \mathbf{B_0}\,(1 - \sigma_i) \qquad 3.9$$

where $\mathbf{B_i}$ is the field local to the i nucleus and σ_i is the shielding factor. Thus the magnetic shielding factor depends on the electron density around the nucleus which in turn is sensitive to its local environment. In the field $\mathbf{B_i}$, the resonance frequency of the i nuclei is given by

$$\omega_i = 2\pi \nu_i = \gamma B_i = \gamma B_0(1 - \sigma_i) \qquad 3.10$$

Thus the resonance frequency has now shifted from ω_0 to ω_i . Each crystallographically distinct site will undergo a different amount of shift from the Larmor frequency depending on the environment. The position of various resonance signals are usually compared with the resonance of a standard substance (reference frequency, υ_{ref}) and the chemical shift is defined as

$$\delta_i = \sigma_{ref} - \sigma_i = \frac{B_i - B_{ref}}{B_0} = \frac{\nu_i - \nu_{ref}}{\nu_0} \qquad 3.11$$

The δ_i is a dimensionless parameter expressed in units of 10^{-6} (ppm). Any influence which reduces the electron density will reduce the shielding effect and the nucleus is said to be deshielded; deshielding leads to an increase in the precessional frequency. Therefore, for a particular nucleus, those nuclei in the least shielded environment resonate at the highest frequency and by convention have the most positive chemical shifts.

Generally, the electron distribution around a nucleus will not be spherical or cubic but will have a definite directional character. Therefore the shielding factor (σ) is a 3 x 3 matrix or a second rank tensor. By a suitable choice of coordinate system, the diagonal of the matrix gives the three principle components σ_{11}, σ_{22}, and σ_{33} which serve to characterize the spatial electronic distribution around a nucleus and are chosen so that $\sigma_{33} \geq \sigma_{22} \geq \sigma_{11}$. Hence σ is anisotropic and its magnitude will depend on the orientation of the molecule relative to the applied field. In chemical shift terms the shielding anisotropy is called chemical shift anisotropy. The shielding anisotropy $\Delta\sigma$ and the shielding asymmetry factor η are defined in equations 3.12 and 3.13 below,

$$\Delta\sigma = \sigma_{33} - \tfrac{1}{2}(\sigma_{11} + \sigma_{22}) \qquad 3.12$$

$$\eta = \frac{\sigma_{22} - \sigma_{11}}{\sigma_{33} - \sigma_{iso}} \qquad 3.13$$

In liquid or solution , the isotropic motion of the molecules average out the anisotropic part of σ and give the shift isotropic value given by,

$$\sigma_{iso} = \frac{\sigma_{11} + \sigma_{22} + \sigma_{33}}{3} \qquad 3.14$$

Thus, in a liquid, well resolved NMR spectral resonances lines are observed from which the isotropic value of the chemical shift is obtained. In solids the relatively static nature of the structure does not permit the natural mechanism of line narrowing that occurs in the liquid. For a single crystal in a fixed orientation to the field $\mathbf{B_0}$, a single sharp resonance line will be observed for each magnetically unique orientation of a particular nucleus to the field direction. The positions of these lines will change as the orientation of the crystal is changed. For powdered polycrystalline materials the molecules are orientated in all possible direction with respect to $\mathbf{B_0}$, resulting in an

envelope of many resonance lines called a powder pattern shown in Figure 3.3. With the additional variation of short range order and environments found in glassy materials, the spread of chemical shifts is worsened and, when convoluted with the powder pattern, can mask the detailed structural information of a spectrum. Mathematical analysis has shown that chemical shift anisotropy in solids is proportional to the term (1 - 3 $\cos^2\theta$) [22], where the angle θ determines the orientation of the molecule with respect to $\mathbf{B_0}$.

It has been said earlier that the screening factor, and therefore the chemical shift, is sensitive to the local environment. Some of the variables which determine the local environment and thus influence the chemical shift are given as follows [12]:

The coordination number

The shift range of ^{29}Si is ~ -60ppm to -128ppm when tetrahedrally coordinated to oxygen compared with -142ppm to -221ppm when octahedrally coordinated to oxygen.

The type of nearest neighbour

The ^{29}Si shift in quartz is -107.1ppm when tetrahedrally coordinated to four oxygens compared to -48.5ppm when tetrahedrally coordinated to nitrogen in β-Si_3N_4.

Bond angles and length

The value of the Si-O-Si bond angle in $(Si_2O_7)^{4-}$ units has a strong effect on the chemical shift which ranges from ~ -72ppm for 136° to ~ -95ppm for 180°. And a change in shift of ~1ppm occurs for a bond length change of 0.0001nm in Si—O.

Connectivity of the structural unit

The connectivity of SiO_4 tetrahedra units is described by Q^n units where $0 \leq n \leq 4$ is the number of bridging oxygens to other units. The ranges of ^{29}Si chemical shifts in minerals and glasses are shown in Figure 3.4 [28].

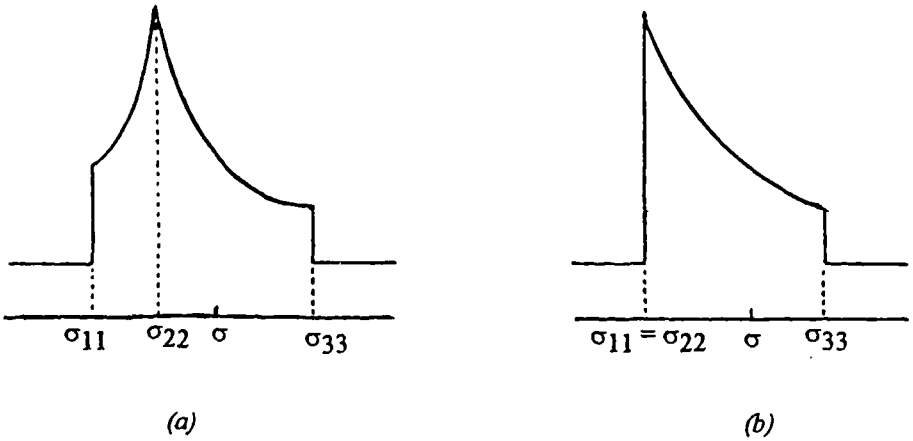

Figure 3.3 : *Powder pattern lineshapes showing principal elements of the shielding tensor for (a) lower site symmetry, (b) axial site symmetry.*

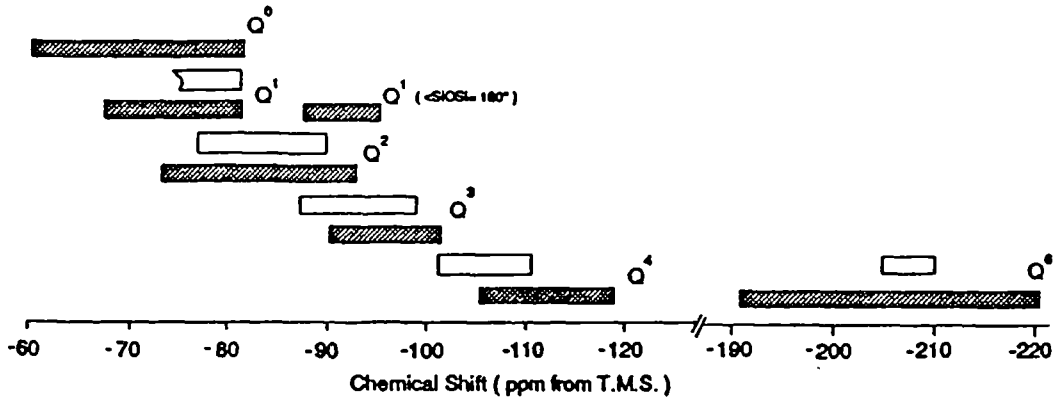

Figure 3.4 : *The reported shift ranges for ^{29}Si in minerals and glasses. White ranges are for glasses [12] and dark ranges are for 'solid' silicates [24-25].*

Second coordination sphere

The replacement of a silicon in the next nearest neighbour shell by an aluminium shifts the ^{29}Si chemical shift by 5ppm.

Thus the chemical shift can give information about the local structure of a nucleus.

3.1.3 MAGNETIC DIPOLAR INTERACTION

Besides the electronic diamagnetic effect, a nucleus i may experience the fields associated with the presence of neighbouring spins. This is a coupling between two neighbouring spins and is called magnetic dipolar or dipole-dipole interaction. There are two types of interaction mechanisms; a direct coupling, through-space interaction depending on the internuclear distances and an indirect or J-coupling, transmitted through the bonding electrons [26]. The J-coupling usually observed in liquids is completely independent of the value of static field B_0 [27] and in solids the effect of it is negligible [28]. Consider direct coupling only. If two neighbouring nuclei i and j are separated by internuclear vector $\mathbf{r_{ij}}$ (Figure 3.5), then, as each moment precesses around the applied static field $\mathbf{B_0}$, it generates an additional dipolar field at the site of the other nucleus with two components; one parallel and one rotating perpendicular to $\mathbf{B_0}$.

For spins having identical resonant frequencies the rotating component of the additional dipolar field will induce mutual energy conserving 'flip-flop' transitions that serve as a mechanism for spin relaxation [29]. The parallel component of the additional dipolar field B_d , experienced at nucleus i due to the magnetic moment μ_j is given by

$$B_d = \pm \frac{\mu_0 \mu_j}{4\pi r_{ij}^3} (3 \cos^2 \theta - 1) \qquad 3.12$$

where μ_0 is the magnetic permeability of a vacuum, θ is the angle between $\mathbf{r_{ij}}$ and $\mathbf{B_0}$, and the $\pm$ sign refers to the spin alignment of the j nucleus (parallel and anti-parallel, respectively) with respect to the applied field $\mathbf{B_0}$. Thus the magnetic field that a nucleus experiences when placed in an external field is dependent not only on the magnitude B_0 of the external field but also on the summation of parallel components of dipolar fields (B_d) due to all possible pairwise interactions with the neighbouring nuclei. Hence there will be a range of values for the magnitude of the additional field from all the spins parallel to B_0 to all spins anti-parallel to B_0 which result in a spread of the resonant frequencies and cause broadening of the line shape. In a solid these additional fields are several gauss in magnitude and they can result in the broadening of the line shape by several kilohertz [30]. However in the liquid state the molecular motions are fast and the fluctuation of θ time averages $\mathbf{B_d}$ to zero. Therefore dipolar coupling effects are not observed at all in solution spectra [31].

For spin ½ nuclei the dipole-dipole interaction is the dominant term of line broadening of spectral lines and proportional to ($3\cos^2\theta - 1$) [18].

3.1.4 QUADRUPOLE INTERACTION

The distribution of nuclear charge within a nucleus with spin $I \geq 1$ is non-spherical and this non-uniformity creates a nuclear quadrupole moment (eQ) [32]. The quadrupole interaction is the interaction between the nuclear quadrupole moment (eQ) and any electrostatic field gradient that exists at the nuclear site. The electric field gradients can arise from electrons in the chemical bonds of the atom of the nucleus and from charges on nearby atoms or ions. Since these electric field gradients depend on the nature of the chemical bonds and the arrangement of ions around the atom in which the nucleus is situated, the quadrupole interaction is a sensitive measure of bonding and structure on an atomic scale [33]. For a particular nucleus where the

interaction effect is large, the effect is observable directly by nuclear quadrupole resonance (NQR) [22,34].

In the present of an external static field $\mathbf{B_0}$ this interaction will alter the nuclear spin energy levels of the Zeeman splitting. As an example, the splitting of energy levels for I = 3/2 due to Zeeman and quadrupole interactions are shown in Figure 3.6. [35]. Generally its effect is of greater magnitude than the dipolar interaction, anisotropic chemical shift and direct spin-spin coupling. Hence the quadrupole interaction dominates over other interactions and produces a fine structure of resonance lines and causes broadening [36]. The quadrupole interaction also provides a very efficient relaxation mechanism of the spin state [34]. In high resolution NMR , the applied static field $\mathbf{B_0}$ is very large and the quadrupolar interaction energy is assumed to be small compared to the interaction between the nuclear magnetic moment and $\mathbf{B_0}$. To a first approximation the other interactions such as the dipolar, anisotropic chemical shifts and scalar spin-spin couplings may be neglected in the total Hamiltonian (H) [31], such that

$$H = H_{Zeeman} + H_{quadrupole} \qquad 3.13$$

and when calculating the energy , the quadrupolar interaction is therefore considered as a perturbation on the Zeeman interaction [32]. It has been shown that for an axially symmetric field gradient, the first order frequency splitting due to quadrupole interaction is given by [17, 22,31]

$$\Delta \nu = \frac{3e(eqQ)}{4h} (3\cos^2\theta - 1) \qquad 3.14$$

where eq is the electric field gradient and θ is the angle between the principal component of the electric field gradient tensor and the static external field $\mathbf{B_0}$. Hence the first order expression contains an angular dependence of the form $(3\cos^2\theta - 1)$.

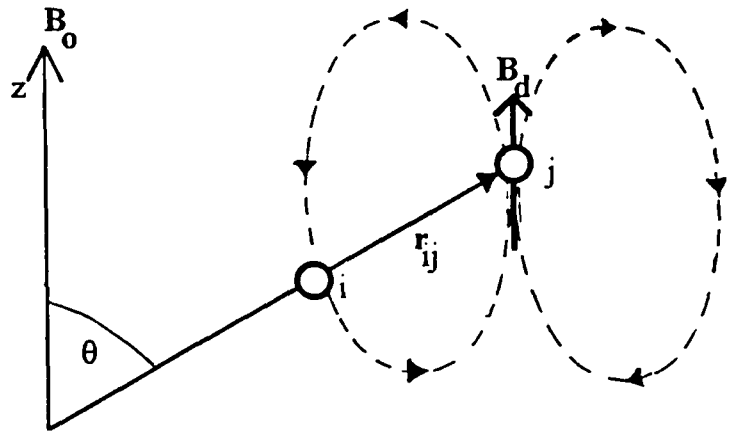

Figure 3.5 : *Two neighbouring nuclei i and j separated by internuclear vector* r_{ij} .

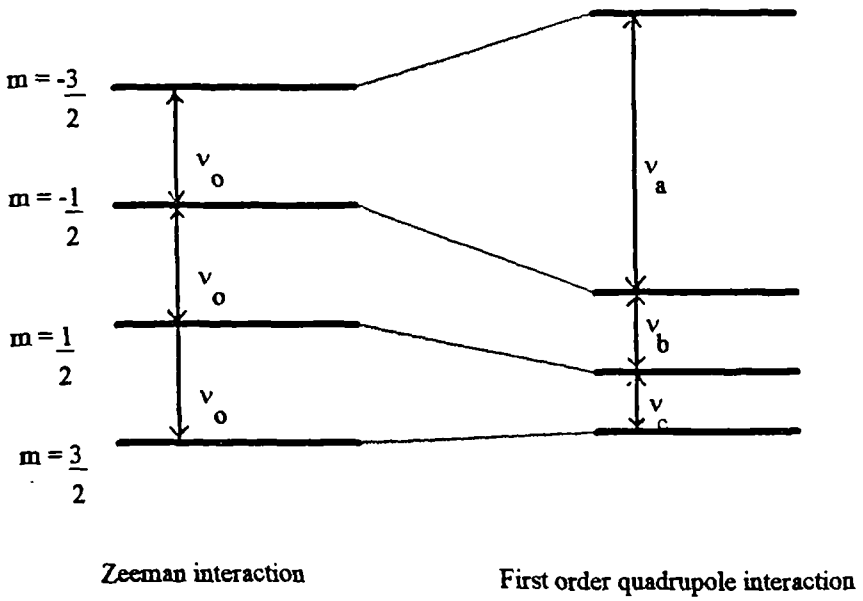

Figure 3.6: *I = 3/2 energy splitting due to quadrupole interactions.*

3.1.5 MAGIC ANGLE SPINNING (MAS) NMR IN SOLIDS

The line broadening terms from the interactions discussed above contain the term ($3\cos^2\theta - 1$), where θ is the angle between the applied field and a vector **r** which depends on the interaction. For the chemical shift and quadrupole interactions r is the z component of their principal axis system. For the dipole-dipole interaction **r** is the vector between two nuclei. For powder or polycrystalline samples all values of θ exist at random, so the lineshapes are broadened. By rapidly spinning the sample about an axis at angle β to B_0 (Figure 3.7), the term ($3\cos^2\theta - 1$) will be time averaged.

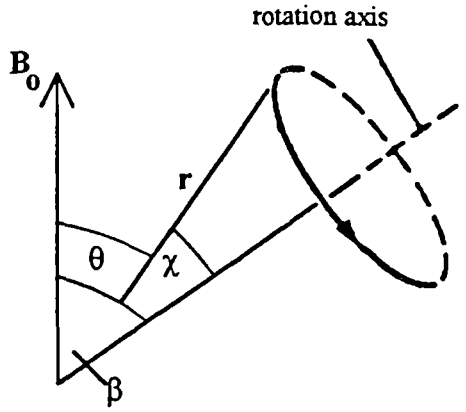

Figure 3.7 : *Macroscopic rotation of a powder sample about an axis at angle* $\beta \approx 54.7°$ *to the applied field* B_0 *, showing the geometric relationships involved.*

The time-average of ($3\cos^2\theta - 1$) about the conical path is given by [18]

$$\langle 3\cos^2\theta - 1 \rangle = \tfrac{1}{2} (3\cos^2\beta - 1) (3\cos^2\chi - 1) \qquad 3.15$$

The angle χ is fixed for a rigid solid but takes all possible values if the material is a powder. For $\beta = 54.7°$, $(3\cos^2\beta - 1) = 0$, so that $\langle 3\cos^2\theta - 1 \rangle = 0$ for all

values of χ . Hence, rapidly spinning the sample at $\beta = 54.7°$ ('magic angle spinning') will eliminate the dipolar contribution to broadening and also reduces the effect of chemical shift anisotropy and quadrupolar broadening, resulting in spectacular improvements in resolution of the spectra [37].

The rapid sample spinning effectively adds an additional time dependent Hamiltonian resulting in the formation of spinning sidebands [20] to the spectrum. However their positions are dependent on the spinning speed whereas the actual isotropic peak is not.

3.2 MÖSSBAUER SPECTROSCOPY

Mössbauer spectroscopy is the study of the recoiless emission and resonant absorption of γ radiation. This phenomenon is based on the fact that a large fraction of γ radiation emitted from radioactive isotopes bound in solids is without individual recoil. If the recoiless γ photon impinges on another identical nucleus in its ground state, the photon may be absorbed, resulting in the transfer of the nucleus to its excited state. This effect, which is possible only because the energy of the photon is exactly equal to the energy of the excited state of the second nucleus, is a case of resonant absorption.

The Mössbauer effect was discovered by R.L.Mössbauer in 1957, while investigating γ-ray absorption in ^{191}Ir [38]. The property of the Mössbauer effect which has raised it from a laboratory curiosity to a valuable and respected spectroscopic technique lies in the narrow line-width of the nuclear transition [39-41]. The typical line width of $\sim 10^{-8}$ eV is smaller than the characteristic values for the magnetic dipole and electric quadrupole interactions of nuclei with their surrounding electrons. Hence, the resonant absorption is extremely sensitive to energy variations of the incident γ radiation. For this reason small interactions between the nucleus and the

orbital electrons, which are difficult to observe by usual methods can be detected by the Mössbauer effect. It is thus the influence of the chemical environment on the γ-ray emission and absorption during nuclear transition that constitutes the basis of applications of Mössbauer spectroscopy to structural investigations in solid-state physics and chemistry.

Pollack et al [42] was the first to apply this technique in structural studies of ^{57}Fe in fused quartz and pyrex glass, followed by Bryukhanov et al on ^{119}Sn in a sodium-aluminium-borosilicate glass [43]. Many studies on glass after that were mostly confined to the nuclei of iron (^{57}Fe) and tin (^{119}Sn). Two excellent reviews of the early Mössbauer work on glass can be referred to Kurkjian [44] and Wong & Angell [45]. The resolution of this technique is extremely high, typically of the order of 1 part in 10^{12}, which makes this technique useful in studying changes in valence, bonding and coordination in glass [45]. Although similar information can be sought through NQR and NMR, an important difference lies in the possibility of studying quadrupole moments in excited, as well as ground states [44]. Thus for iron and tin, whose nuclei have no ground state quadrupole moment, this is the option. In cases where NMR and other techniques are not applicable because of reasons such as line broadening, this technique will complement the others. The important parameters measured in the study of glass by Mössbauer spectroscopy are : chemical shift, quadrupole splitting and recoil free fraction.

3.2.1 THE MÖSSBAUER EFFECT

The resonance absorption of radiation is a phenomenon encountered in many branches of physics. The tuning fork experiment is an elementary example. In the 1920 it was thought that the same phenomenon should occur by using the γ-ray emitted during a transition to a nuclear ground state to excite a second ground state nucleus of the same isotope, thus giving rise to nuclear resonant absorption and

fluorescence [46]. In 1929, Kuhn [47] tried the first experiment but failed to detect this resonant process. It was then recognized that nuclear recoil and Doppler broadening prevented detection. Continuing attempts to detect the resonance were motivated by the fact that the emitted γ-rays are an unusually good source of monochromatic radiation. This is shown by the Heisenberg uncertainty principle of energy and time. The ground state of the nucleus has an infinite lifetime, therefore there is no uncertainty in its energy. The uncertainty in time corresponds to the mean life time in the excited state, τ, and the uncertainty in energy is given by the width of the statistical energy distribution at half height, Γ. They are related by the equation,

$$\Gamma \tau \geq h / 2\pi \qquad 3.16$$

τ is related to the half life, $t_{1/2}$ by $\tau = \ln 2 \times t_{1/2}$, therefore 3.16 can be written as

$$\Gamma = \frac{0.693h}{2\pi t_{1/2}} \qquad 3.17$$

According to this formula, a typical nuclear excited state half life $t_{1/2} = 10^{-7}$ sec will result in a linewidth , $\Gamma = 4.6 \times 10^{-9}$eV. If the transition energy is 46 keV, the ratio of linewidth to the emitted γ-ray is 10^{-13}. Therefore the resolution of the γ-ray emitted is 1 part in 10^{13}. This is very high when compared to other techniques listed in Table 3.1.

Thus , the γ-ray energy is so sharply defined that Γ is smaller than some of the interactions of the nucleus with its environment, as shown in Table 3.2. Unfortunately the γ-ray emitted can be degraded by nuclear recoil and Doppler effects mentioned earlier.

Table 3.1: *Energies and linewidths of various transitions [47]*

Method	*Range of energy, E (eV)*	*I (eV) for single crystal*	*E / I*
NMR	10^{-8} *to* 10^{-6}	10^{-14} *to* 10^{-8}	10^{6} *to* 10^{2}
EPR	10^{-5} *to* 10^{-3}	10^{-9} *to* $>10^{-3}$	10^{4} *to 1*
Mössbauer	10^{2} *to* 10^{5}	10^{-10} *to* 10^{-4}	10^{12} *to* 10^{9}
Optical Absorption Bands in solid	*0.1 to 1*	*0.1 to 1*	*10 to 1*
Zero phonon lines	*0.1 to 10*	$\sim 10^{-3}$	10^{4} *to* 10^{2}

Table 3.2 : *Typical energies of nuclear and chemical interactions [46 & 48].*

Mössbauer γ-ray energies, E_γ	10^{4} - 10^{5} *eV*
Chemical bonds and lattice energies	*1 - 10 eV*
Electronic transitions	*0.5 - 5 eV*
Molecular vibrations	*0.05 - 0.5 eV*
Free atom nuclear recoil, E_R and Doppler energies, E_D	10^{-4} - 10^{-1} *eV*
Lattice vibration phonon energies	10^{-3} - 10^{-1} *eV*
Nuclear quadrupole coupling constants	$<10^{-5}$ *eV*
Nuclear Zeeman splittings	$< 10^{-5}$ *eV*
Heisenberg linewidths, I	10^{-9} - 10^{-6} *eV*

3.2.1.1 RESONANCE ABSORPTION OF RADIATION BY FREE ATOMS

The effects of nuclear recoil and thermal energy can be understood by considering the emission of γ-rays from free atoms. Consider an excited isolated nucleus of mass M, with energy E and moving with initial velocity V along the

direction of the emitted γ-ray. Before emission the total energy above the ground state is $(E + \frac{1}{2}MV^2)$. When a γ-ray of energy E_γ is emitted, the nucleus recoils backwards with velocity v. From conservation of energy

$$E + \tfrac{1}{2}MV^2 = E_\gamma + \tfrac{1}{2}M(V + v)^2 \qquad 3.18$$

Therefore the actual energy of the photon emitted is given by

$$\begin{aligned} E_\gamma &= E - \tfrac{1}{2}Mv^2 - MvV \\ &= E - E_R - E_D \end{aligned} \qquad 3.19$$

The γ-ray is deficient in energy by a recoil energy, $E_R = \frac{1}{2}Mv^2$ and a thermal or Doppler energy, $E_D = MvV$. The recoil energy is independent of V. The Doppler energy depends on V and can therefore be positive or negative. The conservation of momentum gives,

$$MV = M(V + v) + E_\gamma/c \qquad 3.20$$

where the momentum of the photon is E_γ/c and c is the velocity of light. From 3.20 the recoil momentum is $Mv = -E_\gamma/c$, hence the recoil energy is given by,

$$E_R = \frac{E_\gamma^2}{2Mc^2} \qquad 3.21$$

and depends on the mass of the nucleus and the energy of the γ-ray. The mean Doppler energy, $\overline{E_D}$ is dependent on the thermal motion of the nucleus and will have a distribution of values which is temperature dependent, given by

$$\overline{E_D} = E_\gamma \left(\frac{2\overline{E_k}}{Mc^2}\right)^{\frac{1}{2}} \qquad 3.22$$

where $\overline{E_k}$ = ½ κ T is the mean kinetic energy per translational degree of freedom and κ is the Boltzmann's constant and T is the absolute temperature.

As a result, the statistical distribution in energy of the emitted γ-ray is displaced from the true excited-state energy by $-E_R$ and broadened into a Gaussian distribution of width $2\overline{E_D}$. The absorption distribution has the same shape but is displaced by $+ E_R$. This is illustrated in Figure 3.8 and the order of the magnitude of E_R and E_D is shown in Table 3.2. Nuclear resonant emission and absorption will only happen if the energies overlap strongly. The recoil and thermal broadening prevent this. Before the Mössbauer effect was discovered, E_R was partially compensated by utilising the Doppler effect by moving the emitter towards the absorber at very high velocity ($\sim 10^2$ - 10^3 m/s) and broadening the linewidth by raising the temperature [49]. Both result in only marginal overlap but degraded the resolution of the photon to about 1 in 10^7 [46].

3.2.1.2 RESONANCE ABSORPTION OF RADIATION BY ATOMS BOUND IN A SOLID.

If the emitting atom is now in a crystal or solid, the recoiling nucleus is no longer free but instead is fixed in the lattice network. The Mössbauer effect arises from the fact that the emitting atoms are no longer able to recoil individually. From Table 3.2, we see that the recoil energy is of similar magnitude to the lattice vibration energies. If the recoil energy can be transfered directly to vibrational energy, the γ-ray energy will be degraded. However, the vibrational energy of the lattice as a whole can only change by discrete amounts of 0, ± hω, ± 2hω, ...,etc; where ω is Einstein solid vibrational frequency. Thus we can define the recoil free fraction, f ,as the fraction of γ-photons emitted without transfer of recoil energy to the vibrational states of the lattice i.e zero-phonon transitions. For many emission processes Lipkin [50] has shown that f is given by ,

$$f = 1 - E_R / h\omega \qquad 3.23$$

Only these events give rise to the Mössbauer effect. Hence the zero phonon transition or recoiless transition is often called the Mössbauer coefficient [40]. Both expressions of E_R (3.21) and $\overline{E_D}$ (3.22) contain the reiprocal mass, 1/M. In a crystal or solid containing $\sim 10^{15}$ atoms, M is large, therefore both the recoil energy and the Doppler broadening become very small and much less than Γ.

Using a more quantitative approach, f can be related to the vibrational properties of the crystal lattice [50 -52] by,

$$f = \exp \frac{-E_\gamma^2 \langle x^2 \rangle}{h^2 c^2} \qquad 3.24$$

where $\langle x^2 \rangle$ is the mean-square vibrational amplitude of the nucleus in the direction of the γ-ray. From this expression, f will only be large for a tightly bound atom with a small mean square displacement and for a small value of E_γ. To express equation 3.24 in a general and familiar quantities, a Debye model was used [40, 50-52] and gave the following expressions:

$$f = \exp \{ -\frac{6E_R}{\kappa\theta_D}[\frac{1}{4} + (\frac{T}{\theta_D})^2 \int_0^{\theta_D/T} \frac{x\,dx}{e^x - 1}]\} \qquad 3.25$$

From 3.25, it can be seen that f is large when θ_D is large (a strong lattice) and when T is small.

At low temperature where $T << \theta_D$,

$$f = \exp [\frac{-E_R}{\kappa\theta_D} \{ \frac{3}{2} + \frac{\pi^2 T^2}{\theta_D^2} \}] \qquad 3.26$$

and at absolute zero,

$$f = \exp\left[\frac{-3E_R}{2\kappa\theta_D}\right] \qquad 3.27$$

In the high temperature limit where $T >> \frac{1}{2}\theta_D$,

$$f = \exp\left[\frac{-6E_R T}{\kappa\theta_D^2}\right] \qquad 3.28$$

and where θ_D is a characteristic temperature called the Debye temperature, defined by equation,

$$h\,\omega_D = \kappa\theta_D \qquad 3.29$$

In summary, the Mössbauer effect is the recoiless resonant emission or absorption of γ-rays by nuclei in a solid matrix. The recoiless emission and absorption can be optimised for low-energy γ-rays with the nucleus strongly bound in a crystal lattice at low temperature.

3.2.2 THE MÖSSBAUER SPECTRUM

The Mössbauer experiment is commonly done in transmission geometry. It requires a suitable radioactive isotope in a solid matrix that becomes the 'source' of the γ-rays. The emission from this source is allowed to strike an 'absorber' ; a second solid matrix containing the same isotope in its ground state. A detector is used to detect the number of γ-rays transmitted through the absorber. In order to actually trace out the shape of the absorption spectrum, it is necessary to modulate the monochromatic γ-rays , so that they contain slightly different energies and the entire

absorption line-shape can be recorded. As seen in Table 3.2 the total energy range of interest, in cases where the level degeneracies are completely lifted, is of the order of 10^{-6}eV. If the source and absorber are in relative motion with velocity v, then the effective value of E_γ, seen by the absorber differs from the true energy by a small Doppler shift energy, ε , given by

$$\varepsilon = (v/c) E_\gamma \qquad 3.30$$

As an example for $\varepsilon = 10^{-6}$eV , E_γ = 14.4 keV, and c = 3 x 10^{10} cm/s (velocity of light) , v is of about 2 cm/s. Therefore modulation of the γ-ray can be achieved by moving the the source relative to the absorber with velocities of the order $\pm$ 1 cm/s. For a nucleus ('absorber') having a similar chemical environment to the 'source', if both are at the same temperature and if v is zero, the emission and absorption profiles completely overlap and the absorption is at a maximum. For other nuclei in chemical surroundings different from those of the source, the maximum absorption will be displaced from $v = 0$. Any increase or decrease in v will decrease the overlap and if the value of $\pm$ v is very large there will be no overlap and no absorption. It therefore follows that the spectrum of the Mössbauer effect is a record of the intensity of transmitted γ-ray beam as a function of the Doppler velocity v between the source and absorber. The basic setup for a Mössbauer experiment and the typical Mössbauer spectrum are shown in Figure 3.9.

The practical application of this measurement lies in the fact that the nuclear states are weakly influenced by the chemical environment. It should be stressed that it is possible to detect the extremely small pertubations in the nuclear energy level because of the high definition of the γ-ray. There are three principal interactions : the chemical isomer shift, electric quadrupole and in the case of magnetic materials, the magnetic hyperfine interactions.

Tin is diamagnetic, and therefore there are normally no intrinsic magnetic fields effective at the ^{119}Sn nuclei, hence the tin nucleus does not shows intrinsic magnetic

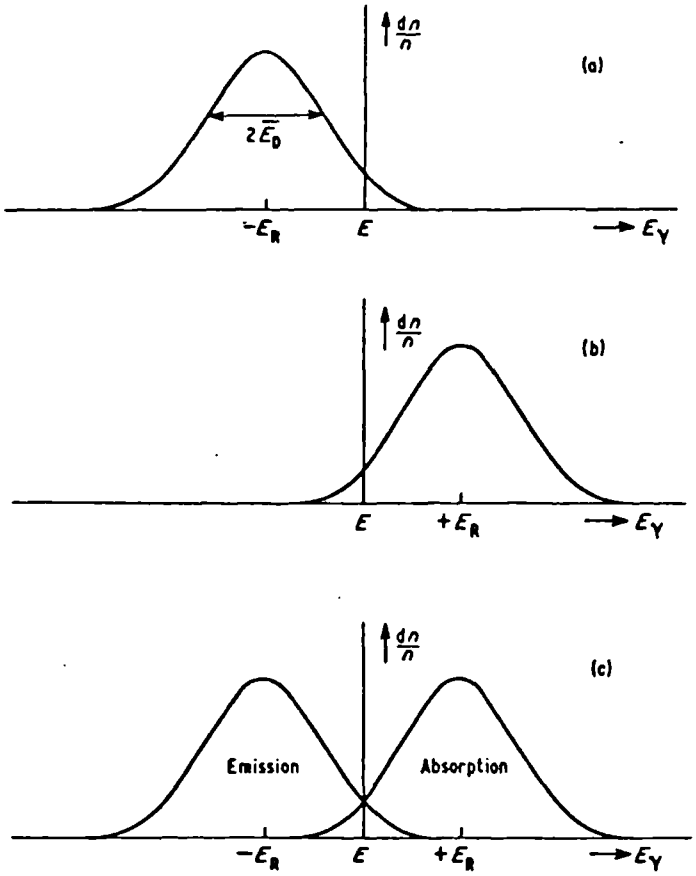

Figure 3.8 : *The statistical distribution of the γ-ray energy : (a) Emission (b) Absorption (c) The resonant overlap for successive emission and absorption. Illustration taken from [46].*

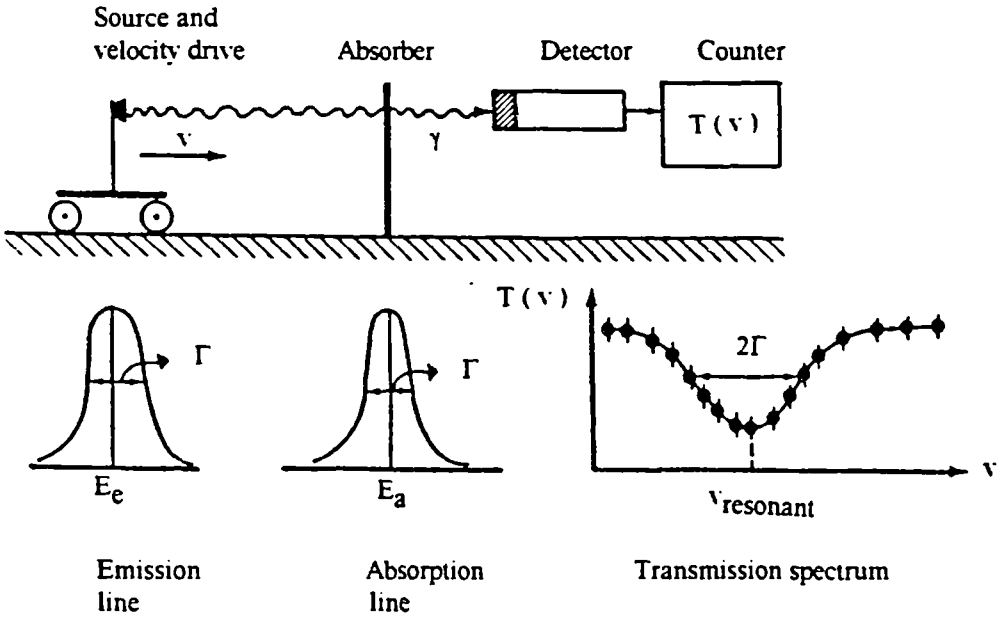

Figure 3.9 : *The basic setup for a Mössbauer experiment and a typical transmission spectrum.*

hyperfine splitting [52]. Therefore, only the chemical isomer shift and the electric quadrupole interactions are important and they will be discussed in the next sections.

3.2.2.1 THE CHEMICAL ISOMER SHIFT

The emission and absorption lines are only centered at the same energy if the corresponding nuclei are in similar environments and at the same temperature. For such cases the absorption maximum of the Mössbauer spectrum is centered at $v = 0$. This is not very often the case because nuclei in chemical surroundings different from those of the source have slight differences in transition energies. The energy difference is caused by a change in the electric monopole or coulombic interaction between the electronic and nuclear charges. This is seen as a shift of the absorption maximum away from $v = 0$ and is known as the chemical isomer shift or isomer shift. The first observation of an isomeric shift was made by Kistner and Sunyar [53] in ^{57}Fe.

The isomer shift (δ) has been shown by Walker, Wertheim & Jaccarino [54] to describe the energy difference for the same nuclear transition in two atomic nuclei as the result of changes in the s-electron density at the nucleus as shown in Figure 3.10. Therefore the isomer shift, δ , is defined as the difference in energy between the nuclear transitions in the source (E_s) and absorber (E_a) given by [54],

$$\delta = E_a - E_s = \frac{2\pi Ze^2}{5} [\, |\psi_a(0)|^2 - |\psi_s(0)|^2 \,] [\, R^2_{ex} - R^2_{gd} \,] \qquad 3.31$$

Where $-e\,|\,\psi_s(0)\,|^2$ and $-e\,|\,\psi_a(0)\,|^2$ are the electronic charge density at $r = 0$ respectively for source and absorber and R = nuclear radius of excited (ex) and ground (gd) states. If the nucleus changes its radius by a very small increment δR, $R_{ex} \approx R_{gd} = R$, 3.31 can be written as,

$$\delta = E_a - E_s = \frac{4\pi Ze^2R^2}{5}\left(\frac{\delta R}{R}\right)[\,|\psi_a(0)|^2 - |\psi_s(0)|^2\,] \qquad 3.32$$

where $\left(\frac{\delta R}{R}\right)$ is the fractional change in the nuclear charge radius between the ground and the excited states. This can be related to the measured shift in Doppler velocity units, v, by $v = (c/E_\gamma)\,\delta$. Since only a difference in source and absorber energies is measured, the measurement of the shift must specify both the source and absorber materials. Equation 3.32 is a product of a chemical term i.e the electron density at r = 0 and a nuclear term (the change in nuclear radius, δR).

The main factor affecting the magnitude of δ is the chemical term i.e the *s*-electron density at the nucleus since *p*, *d*, and *f* orbitals have zero density at their nuclei. The *p*, *d* and *f* electrons indirectly affect the *s*-electron density via interpenetration shielding of the *s*-electrons. For example a $3d^5 4s^1$ configuration will have a larger value of $|\psi_s(0)|^2$ than $3d^6 4s^1$ because in the latter case the extra *d*-electron shields the 4*s*-electron from the nucleus. The *s*-electron density is determined mainly by the valence state of the atom and on the details of the bonding of the nucleus. Thus the isomer shift can provide information on the valence state, bonding and coordination of the Mössbauer nucleus. The isomer shift is a monotonic function of the *s*-electron density at the nucleus [55]. The chemical shifts of ^{119}Sn given in Table 3.3 can serve as an example. The neutral tin atom has 14 electrons outside the krypton core; their configuration is $4d^{10}\ 5s^2\ 5p^2$, so that in the 4+ state, tin has no outer s electrons, whereas in the 2+ state, it is assumed that the higher energy $5p^2$ electrons are removed, leaving two $5s^2$ electrons. In its four-covalent bonding the configuration is $5(sp^3)$, i.e. there is only one *s* electron. The chemical shifts reflect these structures almost linearly [56] as shown in Table 3.3.

Table 3.3: *Chemical Shift of some ^{119}Sn compound [48].*

Valence state	*Electron configuration*	*Chemical shift relative to SnO_2 (mm/s)*
Sn^{4+}	$5s^0 5p^0$	*0*
α-Sn (gray)	$5sp^3$	*2.0*
Sn^{2+}	$5s^2 5p^0$	*3.7*

3.2.2.2 ELECTRIC QUADRUPOLE INTERACTION

The quadrupole splitting observed in Mössbauer spectroscopy is very similar to that observed in NMR [44] and NQR [57]. The latter are concerned with radio-frequency transitions within a hyperfine multiplet of a ground state nucleus. The former is a γ-ray transition between the hyperfine multiplets of the nucleus in its ground and excited states. Nuclei whose spin I = ½ are spherically symmetric and have a zero quadrupole moment; thus the ground state of ^{57}Fe and ^{119}Sn, with I = ½, cannot exhibit quadrupole splitting. But for such nuclei the excited state has spin I = 3/2 and therefore a quadrupole moment. The interaction of the nuclear quadrupole moment with the local electric field gradient tensor at the nucleus is quantised and splits the nuclear sub-states. The local electric field gradient is a 3 x 3 tensor. With a suitable choice of coordinate system, this can be reduced to a diagonal form so that it can be completely specified by three component : V_{xx} , V_{yy} , V_{zz} with $V_{xx}+ V_{yy} + V_{zz} = 0$. The asymmetry parameter, η, is defined by

$$\eta = \frac{V_{xx} - V_{yy}}{V_{zz}} \qquad 3.33$$

where $V_{ZZ} = eq$ is the largest component of the field gradient so that $| V_{ZZ} | > | V_{XX} | \geq | V_{yy} |$.

The interaction between the nuclear quadrupole moment and the electric field gradients is expressed by the Hamiltonian [39, 48, 52],

$$H = \frac{e^2qQ}{4I(2I-1)} [\, 3I_Z^2 - I(I+1) + \frac{\eta}{2} (I_+^2 + I_-^2)] \qquad 3.34$$

where I_+ and I_- are raising and lowering operators, eQ is the nuclear quadrupole moment and I is the total nuclear spin number. For an axially symmetric field gradient, such that $V_{XX} = V_{yy}$, the z component of the split of the energy level is given by

$$E_Q(m_Z) = \frac{e^2qQ}{4I(2I-1)} [\, 3m_Z^2 - I(I+1)\,] \qquad 3.35$$

where m_Z is the spin quantum number in z the orientation. Because of the m_Z^2 term in 3.35 the degeneracy is preserved for states having the same value of m_Z. The splitting between two sub-states is given by

$$\Delta E_Q = E_Q(3/2) - E_Q(1/2) = \tfrac{1}{2}\, e^2qQ \qquad 3.36$$

The quadrupole splitting in ^{57}Fe is shown in Figure 3.11 as an example.

The electric field gradients have their origin from two effects: they are (a) from the electrons with $l \neq 0$ that occupy the unfilled electronic orbitals , and (b) from charges on neighbouring ions [57]. Since the field gradient varies as the inverse cube of distance, the most important contribution comes from the unfilled orbitals of the atom. Thus, for example the dominant contribution to the electric field gradient of the tin(II), if in sp^3 hybridization, arises from the excess contribution of p_Z to the lone pair

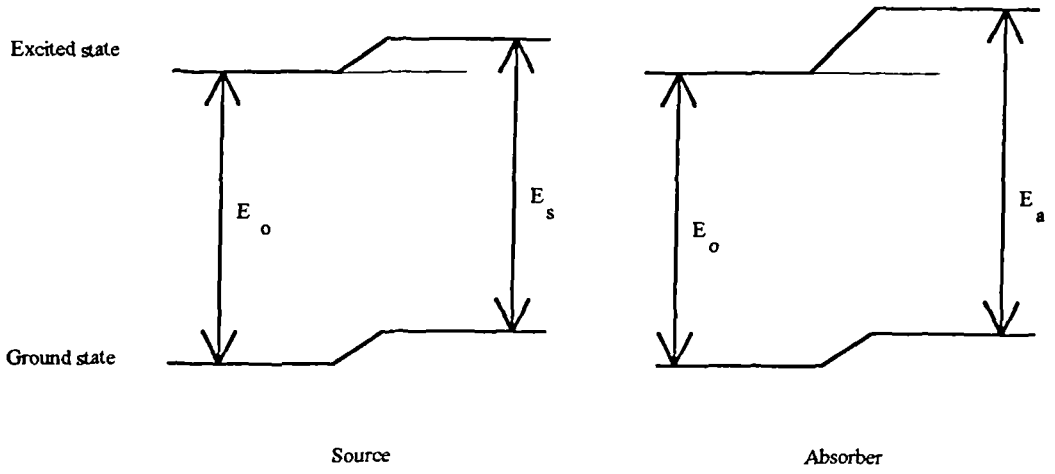

Figure 3.10 : *Origin of isomer shift; s-electron density greater in absorber.*

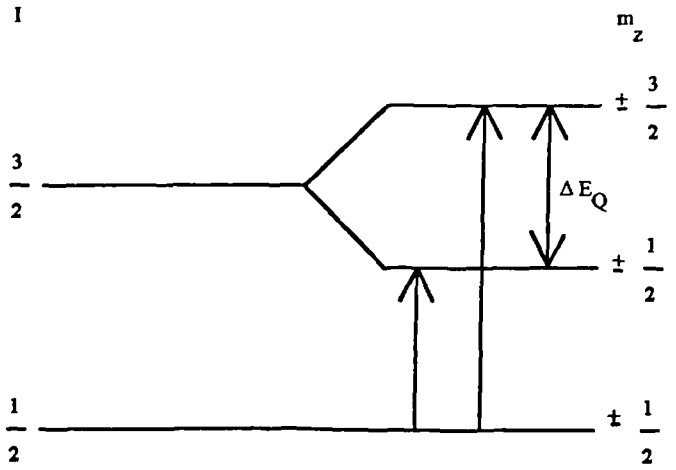

Figure 3.11 : *Quadrupole splitting in ^{57}Fe.*

over that of p_x and p_y orbitals. Therefore the quadrupole splitting can give a measure of the symmetry of the environments around a Mössbauer nucleus. In glass, together with the isomer shifts, the quadrupole splitting can be discussed in terms of bonding and the formation of non-bridging oxygens [58].

3.3 VISCOSITY

The relationship between viscosity and temperature for glasses is very important in the technology of glass making. It is the determining parameter in the course of glass fabrication processes. That is, in the course of glass melting, refining, working, shaping and annealing. In making glass-ceramics, the selection of optimum heat-treatment temperatures is partly governed by the viscosity-temperature characteristics of the glasses [59]. Other than temperature, the viscosity of glass can vary enormously with its structure and composition [60]. Hence, the viscosity of a glass depends on the bonding forces between different types of ion groups, the extent of linking and on the deformability of the ions. Thus the viscosity-temperature and viscosity-composition relationships can provide a better understanding of the structure of a glass.

3.3.1 DEFINITION OF VISCOSITY

Viscosity is a property of fluids, including glass. The viscosity , η and fluidity, f, are the reciprocal of each other:

$$\eta = \frac{1}{f} \qquad 3.37$$

Viscosity is a measure of resistance to shearing action between liquid layers. Figure 3.12 shows a liquid, confined between two parallel planes of area A and at a constant distance apart. If the lower plane remains stationary but the upper plane moves at a

constant velocity v_o; a constant transverse velocity gradient $\frac{dv}{dy}$ in the liquid is created. This is a laminar flow in which the liquid velocity is v_o at the upper plane and zero at the lower plane. To maintain this motion a force F is applied to the upper plane in the direction of its motion in order to overcome the internal friction within the liquid. By Newton's law of fluid friction, the shearing stress ($\frac{F}{A}$) at either wall is proportional to the velocity gradient ($\frac{dv}{dy}$). Therefore, the definition of viscosity may be formalised as the ratio of shear stress, $\frac{F}{A}$, to the velocity gradient of flow, $\frac{dv}{dy}$. Thus the viscosity is given by,

$$\eta = \frac{Fdy}{Adv} \qquad 3.38$$

Equation 3.38 is only valid when v_o is below a certain value. If v_o is high enough, turbulent flow may develop and the formula is no longer applicable. Fortunately , this flow is never encountered in a glass melt because of its high viscosity. The equation is valid for Newtonian fluids which is normally true for glasses above the transformation range. The S.I unit of viscosity is $Nm^{-2}s$ or Pa s (Pascal second). In cgs unit, it is dyne cm^{-2} s or P (Poise) . Therefore, 1 Pa s = 10 P.

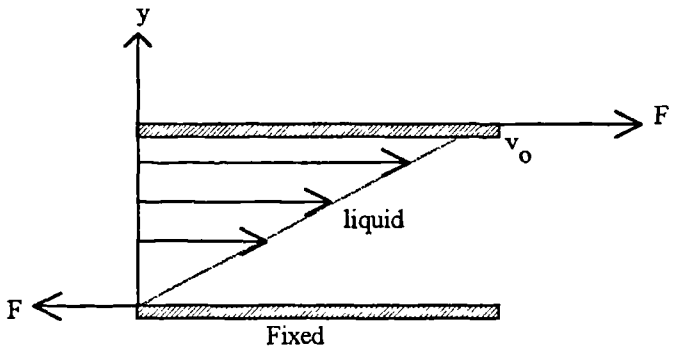

Figure 3.12 : *Viscosity. More viscous materials require a higher shear stress per unit flow rate*

3.3.2 REFERENCE POINTS VISCOSITY FOR GLASS

The viscosity of glasses which is required by many technological practices is in the range 1 to $10^{13.5}$ Pa s. During melting and refining the glass melt, the viscosity should decrease down to 10 Pa s. The glass viscosity will increase when the glass melt starts to undergo the process of making a glass article. At every stage of the process of making a glass article, the glass must maintain a certain viscosity range and, to help the technologists determine this viscosity range, international reference points viscosity have been established. [61]. This is done by defining the viscosity-temperature relationship in terms of certain characteristic temperatures at which the glass attains particular values of viscosity. This is shown in Table 3.4.

Table 3.4: *Characteristic temperatures with corresponding viscosities for glasses*

Characteristics Temperature (t)	*Viscosity (Pa s)*
Working point, t_3	10^3
Flow point, t_4	10^4
Fibre softening point, $t_{6.6}$	$10^{6.6}$
Dilatometric softening point, M_g	$10^{10} - 10^{11}$
Annealing point, $t_{12.4}$	$10^{12.4}$
Strain point, $t_{13.6}$	$10^{13.6}$
Transformation range, t_g	$10^{13.5} - 10^{10}$

The working point is the temperature at which the glass fabrication operations can be carried out. The fibre softening point is the temperature at which a uniform fibre 0.5 to 1.0 mm diameter and 22.9 cm long elongates at a rate of 1mm/min under its own weight when heated at a rate of 5°C /min. under standardized conditions. The

dilatometric softening point is the temperature at which viscous flow exactly counteracts thermal expansion during measurement. The annealing point is the temperature at which internal stress is substantially relieved in 15 minutes. The strain point, representing the lower end of the annealing range is usually taken to be the temperature at which glass can be annealed commercially in 16 hours.

3.3.3 VISCOSITY EQUATIONS

Viscosity values are temperature sensitive, decreasing exponentially with the absolute temperature, T. The viscosity η fits an Arrhenius-type equation over a wide range of temperature:

$$\eta = A \exp\left(\frac{E_\eta}{RT}\right) \qquad 3.39$$

where A is a constant, R is the gas constant and E_η is the activation energy of viscous flow. At sufficiently high temperature, deformation in glass can occur by isotropic viscous flow. Groups of atoms, such as silicate islands, rings, or ions ,move past one another in response to the stress, permitting deformation. The activation energy, E_η gives a measure of the ease with which such groups of atoms move past one another. The addition of modifiers , such as Na_2O, breaks up the network structure. This permits the atom groups to move easily, reduces E_η and reduces the viscosity and strength of the glass. Thus a knowledge of the viscosity-temperature relationship of a glass can give some information about the glass structure.

A more accurate viscosity-temperature fitting equation was introduced independently in the 1920s by Vogel, Fulcher and Tammann and Hesse [62]. It is sometimes referred as VFT (Vogel-Fulcher-Tammann) equation but most commonly as the Fulcher equation, given as

$$\eta = A \exp\left[\frac{E_\eta}{T - T_0}\right] \qquad 3.40$$

where A, E_η and T_0 are constants for a particular melt. This equation gives a very good representation of the variation of viscosity with temperature over a wide temperature range and can be very useful practically for interpolation purposes [63], if one has a good reason to believe that the equation is obeyed for a particular glass. Therefore, in principle, it only needs the viscosity to be measured at three temperatures to obtain the complete viscosity-temperature relationship.

3.3.4 METHODS OF VISCOSITY MEASUREMENT

As pointed out earlier, the range of viscosity which is of interest in the manufacture and use of glass is very wide (1 to $10^{13.5}$ Pa s). It is not possible to measure the whole range of viscosity by any one method. The viscosity measurement methods can be divided into two groups: one for measuring the low viscosities (high temperatures) and the other for measuring high viscosities.

3.3.4.1 ROTATING CYLINDER VISCOMETER

The rotating cylinder viscometer is the most widely used method for measuring viscosity of glasses at high temperatures over the range of 10 to 10^5 Pa s. The apparatus and measurement principles have been described by Dietzel & Bruckner [64]. Basically its consists of two cylinders A and B. Cylinder B is suspended co-axially in A from a torsion wire. The space between the two cylinders is filled with the glass and heated. The outer cylinder A is rotated at a constant speed of Ω radian/s, so producing a torque, T, in the inner cylinder. T is measured by measuring the angle of twist at the lower end of the torsion wire. The equation used to calculate the viscosity by this method is

$$\eta = \left(\frac{T}{4\pi\Omega L}\right)\left(\frac{r_o^2 - r_i^2}{r_o^2 r_i^2}\right) \qquad 3.41$$

where T is the torque which causes the twist in the rotating cylinders, Ω is the angular velocity, L is the effective length of the cylinder, r_o , r_i are the external and internal radii of the cylinders respectively. By slight modification to the apparatus descibed by Dietzel & Bruckner above, Napolitano et al [65] were able to measure a wider viscosity range of 1 to 10^9 Pa s.

3.3.4.2 PARALLEL PLATE VISCOMETER

This method has been described by Hay [66] and Fontana [67]. This method gives accurate results over the viscosity range 10^4 to 10^8 Pa s. It uses a sample in the form of circular glass disc which is sandwiched between metal plates. This arrangement is heated to the target temperature where the viscosity is to be measured. After some soaking time is allowed, for the temperature to equilibrate, a load is applied normal to the plate surfaces. The change in the distance between the plates is measured. The equation used to calculate the viscosity is,

$$\eta = \frac{8\pi Mg}{3V^2}\left(\frac{t}{h^{-4} - h_o^{-4}}\right) \qquad 4.42$$

where M is the applied force, g is gravity acceleration, t is time, V is the sample volume, h_o and h are the initial and final thickness of the sample respectively.

3.3.4.3 PENETRATION VISCOMETER

High viscosities (above 10^8 Pa s) are usually determined from the extension of a fibre under load, but the penetration viscometer can also be used over this range. The

indentation method is another name for this method. It was first used by Cox [68], using a sphere to penetrate a flat glass surface. Heynes & Rawson [69] used a similar method, employing a Nimonic indenter placed at the end of vertical alumina rod. The flat glass sample is heated in a furnace to the desired temperature. After thermal equilibrium has been reached, the indenter is pressed on the glass surface for a few seconds to half an hour depending on the viscosity. After cooling the sample, the diameter of the imprint is measured from which the depth of penetration, z is calculated and then the viscosity can be calculated using the formula,

$$\eta = \left(\frac{9P}{32\sqrt{D}}\right)\left(\frac{t}{\sqrt[3]{z}}\right) \qquad 3.43$$

where P is the applied load, D is the diameter of the indenter and t the time of the penetration. However, this method needs the sample to be withdrawn from the furnace and cooled down before another experiment can be done and hence limits the practical usage. Douglas et al [70] described a more practical penetration viscometer, employing an optical lever to measure the depth of penetration of the spherical indenter into the glass and succeeded in measuring viscosities around 10^{11} Pa s with ±2 % accuracy. Mekhail [71], improved the techniques by employing a Linear Voltage Displacement Transducer (LVDT) and a two channel chart recorder that simultaneously recorded the depth of penetration and time as well as temperature. Viscosities in the range of 10^{7} to 10^{12} Pa s can be measured with ±1.5 % accuracy. Whetton and Hall [72] improved the apparatus by employing a balance beam coupled to an LVDT and computer and reported that the apparatus is capable of measuring viscosities over the range of 10 to 10^{12} Pa s with about ±1 % error.

REFERENCES

1. Purcell, E.M., Torrey, H.C. & Pound, R.V. (1946). *Phys. Rev.* **69**, 37.
2. Bloch, F., Hansen, W.W. & Packard, M.E. (1946). *Phys. Rev.* **69**, 127.
3. Knight, W.D. (1949). *Phys. Rev.* **76**, 1259.
4. Arnold, J.T., Dharmati, S.S. & Packard, M.E. (1951). *J.Chem.Phys.* **19**, 507.
5. Silver, A.H. & Bray, P.J. (1958). *J.Chem.Phys.* **29**,984.
6. Andrew, E.R., Bradbury, A. & Eades, R.G. (1958). *Nature (London)* **182**, 1659.
7. Lowe, I.J. (1959). *Phys. Rev. Lett.* **2(7)**, 285.
8. Garuncy, A.N., Van der Hart, D.L. & Earl, W.L. (1981). *Phil. Trans. Royal Soc. London* **A229**, 609.
9. Pines, A., Gibby, M.G. & Waugh, J.S. (1973). *J.Chem. Phys.* **59**, 569.
10. Hartman, S.R. & Hahn, E.L. (1962). *Phys. Rev.* **128**, 2042.
11. Lippmaa, E., Magi, M., Samoson, A., Tarmak, M. & Engelhardt, G. (1980). *J.Amer. Chem. Soc.* **69**, C42-C44.
12. Dupree, R. & Holland, D. in *Glasses and Glass Ceramics*, ed. Lewis, M.H. (1990). Chapman Hall, London.
13. Stebbins, J.F. in *Spectroscopic Methods in Minerology & Geology*, ed. Hawthorne, F.C. (1988). *Reviews in Minerology* **vol. 18**, Mineral Soc. of America.
14. Kirkpatrick, R.J. in *Spectroscopic Methods in Mineralogy & Geology*, ed. Hawthorne, F.C. (1988). *Reviews in Minerology* **vol. 18**, Mineral Soc. of America.
15. Eckert, H. (1992). *Progress in NMR Spectroscopy* **24**, 159-293.
16. Elliot, S.R. (1990). *J. Non-Cryst. Solids* **123**, 149.
17. Abragam, A. (1985). *Principles of Nuclear Magnetism*, Oxford.
18. Harris, R.K. (1986). *Nuclear Magnetic Resonance Spectroscopy*, Longman Scientific and Technical, London.
19. Derome, A.E. (1987). *Modern NMR Techniques for Chemistry Research*, Oxford.
20. Slichter, C.P. (1980). *Principles of Magnetic Resonance*, 2nd Edn. Springer Verlag.
21. Farrar, T.C. & Becker, E.D. (1971). *Pulse and Fourier Transform NMR*, Academic Press, London.
22. Carrington, A. & McLachlan, A.D. (1967). *Introduction to Magnetic Resonance - with Applications to Chemistry and Chemical Physics*, Harper and Row, New York.
23. Andrew, E.R. (1958). *Magnetic Resonance*, Cambridge Press.
24. Coleman, B. (1983). in *NMR of Newly Accesible Nuclei* : **Vol. 2** , Ed. Laszlo, P., Academic Press.
25. Engelhardt, G. & Michel, D. (1987). *High Resolution Solid State NMR of Silicates and Zeolites*, Wiley.
26. Martin, M.L., Delpuech, J.-J. & Martin, G.J. (1980). *Practical NMR Spectroscopy*, Heyden & Son. Ltd. London.
27. Kemp, W. (1986). *NMR in Chemistry - A Multinuclear Introduction*, Macmillan, London.
28. Smith, M.E. (1987). *PhD. Thesis*, University of Warwick.
29. Lockyer, M.W.G. (1994). *PhD Thesis*, University of Warwick.
30. Rahman, A.U. (1986). *Nuclear Magnetic Resonance - Basic Principles*, Springer-Verlag, New York.
31. Fyfe, C.A. (1983). *Solid State NMR for Chemists*, C.F.C. Press, Guelph, Ontario.
32. Cohen, M.H. & Reif, F. (1957). *Solid State Physics*, Academic Press Inc. New York.

33. Wong, J. & Angell, C.A. (1976). *Glass Structure by Spectroscopy*, Marcell Dekker, Inc. New York.
34. Sanders, J.K.M. & Hunter, B. K. (1988). *Modern NMR Spectroscopy*, Oxford University Press.
35. Mortuza, M.G. (1989). *PhD Thesis*, University of Warwick.
36. Frende, D., Hasse, J., Klinowski, J., Carpenter, T.A., & Ronikier, G. (1985). *Chem. Phys. Lett.* **119**, 365.
37. Andrew, E.R. (1981). *Int. Rev. phys. Chem.* **1**, 195.
38. Mössbauer, R.L. (1958). *Z.Physik* **151**, 124.
39. International Atomic Energy Agency (1966). *Applications of the Mössbauer effect in Chemistry and Solid State Physics*, **Technical Reports Series no. 50.**Vienna.
40. Wertheim, G.K. (1964). *Mössbauer Effect: Principles and Applications*, Academic Press, N.York.
41. Frauenfelder, H. (1963). *The Mössbauer Effect*, W.A.Benjamin, Inc. N.York.
42. Pollack, H., DeCoster, M., & Amelinckx, S. (1963). *Proc. 2nd. Int. Conf. Mössbauer effect*, Saclay, Edited by D.M.Compton & A.H.Schoen, John Wiley.
43. Bryukhanov, V.A., Gol'danskii, V.I., Delyagin, N.N., Koryto, L.A., Makarov, E.F., Suzdaler, I.P. & Shpinel, V.S. (1963). *Soviet Physics JETP* **16**, 321.
44. Kurkjian, C.R. (1970). *J. Non-Cryst. Solids* **3**, 157.
45. Wong, J. & Angell, C.A. (1976). *Glass Structure by Spectroscopy*, Marcel Dekker, Inc. N.York.
46. Gibb. T.C. (1976). *Principles of Mössbauer Spectroscopy*, Chapman and Hall, London.
47. Pye, L.D., Stevens, H.J. & LaCourse, W.C. (1972). *Introduction to Glass Science*, Plenum , N.York.
48. Greenwood, N.N. & Gibb, T.C. (1971). *Mössbauer Spectroscopy*, Chapman & Hall Ltd, London.
49. Cranshaw, T.E., Dale, B.W., Longworth, G.O. & Johnson, C.E. (1985). *Mössbauer Spectroscopy and its applications*, Cambridge University press.
50. Lipkin, H.J. (1960). *Ann. Phys.* **9**, 332.
51. May, L. (1971). *An Introduction to Mössbauer Spectroscopy*, Adam Hilger, London.
52. Goldanskii, V.I. & Herber, R.H. (1968). *Chemical Applications of Mössbauer Spectroscopy*, Academic Press, N.York.
53. Kistner, O.C. & Sunyar, A.W. (1960). *Phys. Rev. Letters* **4**, 412.
54. Wertheim, L.R. & Wertheim, R.H. (1962). *J.Chem. Phys.* **36**, 2497.
55. Walker, L.R., Wertheim, G.K. & Jacarino, V. (1961). *Phys. Rev. Lett.* **6**, 98.
56. Banwell, C.N. (1983). *Fundamentals of Molecular Spectroscopy*, McGraw Hill, London.
57. Kubo,M. & Nakamura, D. (1960). *Adv. Inorg. Chem. and Radiochem.* **8**, 257.
58. Bahgat, A.A.,Shaisha,E.E. & Fayek,M.K.(1983). *Physics Chem .Glasses* **24(1)**, 5.
59. McMillan, P.W. (1964). *Glass Ceramics, Academic Press*, London.
60. Van Vlack, L.H. (1973). *Materials Science for Engineers*, Addison Wesley.
61. Hlavac, J. (1983). The Technology of Glass and Ceramics, Elsevier Sci. Pub. Co.
62. Rawson, H. (1980). *Properties and Applications of Glass*, Elsevier, Amsterdam.
63. Fulcher, G.S. (1992). *J.Am. Ceram. Soc.* **75(5)**, 1060.
64. Dietzel, A. & Brückner, R. (1955). *Glastech. Ber.* **28**, 455.

65. Napolitano, A. Macedo, P.B. & Hawkins, E.G. (1965). *J. Res. Natn. Bur. Stand.* **69A**, 449.
66. Hagy, H.E. (1963). *J. Am. Ceram.Soc.***46**, 93.
67. Fontana, E.H. (1970). *Bull. Am. Ceram. Soc.* **49**, 594.
68. Cox, S.M. (1943). *J. Sci. Instrum.* **20**, 113.
69. Heynes, M.S.R. & Rawson, H. (1961). *Phys. Chem. Glass* **2(1)**, 9.
70. Douglas, R.W., Armstrong, W.L., Edwards, J.P. & Hall, D. (1965). *Glass Technology* **6(2)**, 52.
71. Meikhail, M.S. (1985). *PhD Thesis,* University of Warwick.
72. Whetton, N.L. & Hall, C.R. (1987). *Glass Technology* **28(2)**, 91.

Chapter 4 - Experimental Materials and Techniques

This chapter presents the experimental materials and techniques used in this research, ranging from glass preparation and compositional analysis to techniques used for structural and physical property studies.

4.1 GLASS PREPARATION

Two types of glass systems, prepared by conventional melting, were studied in this research. They are : (1) Simple, binary SnO-SiO_2 glass and (2) Complex, tin-doped float glass.

4.1.1 BINARY SnO-SiO_2 GLASS

The starting materials for the preparation of the glass were Wacomsil quartz (99.9 % SiO_2) and Johnson Matthey's, reagent grade stannous oxalate (SnC_2O_4). The choice was based on the work of Keysselitz and Kohlmeyer [1]. Stannous oxalate, on heating to glass forming temperatures, decomposes as

$$SnC_2O_4 = SnO + CO + CO_2 \qquad 4.1$$

SnO , being metastable, disproportionates to SnO_2 and Sn (tin metal) according to

$$2SnO \rightarrow SnO_2 + Sn \qquad 4.2$$

However, in the presence of SiO_2, stannous silicates glasses can be formed. The amount of SnO in the glass depends on how successfully we can prevent reaction 4.2. The disproportionation of SnO to SnO_2 and metallic Sn has been studied by several workers [2-4]. Although little agreement exists between the available data, the

disproportionation appears to occur between 350°C and 700°C. According to Volf [5], the disproportionation of SnO follows the equation,

$$7SnO = 5SnO + SnO_2 + Sn \qquad 4.3$$

which attains a constant value at temperatures ≥ 725°C. Thus about 29% of the initial SnO content will be lost to Sn and SnO_2 and 71% retained as SnO.

Approximately 100g batch mixtures of Wacomsil quartz and stannous oxalate in the appropriate amounts were thoroughly mixed by rolling and were then compressed into cylindrical pellets. These pellets were tightly packed into an alumina crucible and melted ~ 100°C above the liquidus temperature based on the phase relations [6] shown in Figure 4.1. After approximately one hour, the crucibles were withdrawn from the electric furnace and the melt quenched to glass in the crucibles, in air. The crucibles were then transferred to an annealing furnace, maintained at 400°C for one hour and then slowly cooled to room temperature. The nominal compositions of the glasses ranged from 20 to 80 mol% SnO, but the disproportionation of SnO to SnO_2 and Sn resulted in a SnO_2 crust on the surface of the melt, globules of Sn metal at the bottom of the crucibles and glass in the middle. By cutting and grinding away the crucibles, homogenous SnO-SiO_2 glass pieces were separated. The nominal composition, melting temperature and time, the optical quality and amorphicity of the glasses prepared in this system are given in Table 4.1. In order to facilitate the ^{29}Si MAS NMR experiments, a paramagnetic impurity (0.1 mol% Fe_2O_3) was added to all samples except TS3. This is to reduce the relaxation time of the ^{29}Si nucleus, since this is typically 20-60 minutes in undoped samples.

Preparation conditions were optimised to minimise the disproportionation of SnO to SnO_2 and Sn metal and also oxidation of SnO to SnO_2 by:

(a) Melting the mixture as compressed pellets so that the volume of air in the mixtures is minimised and more mixture can be placed in the crucibles.

$SnO–SiO_2$

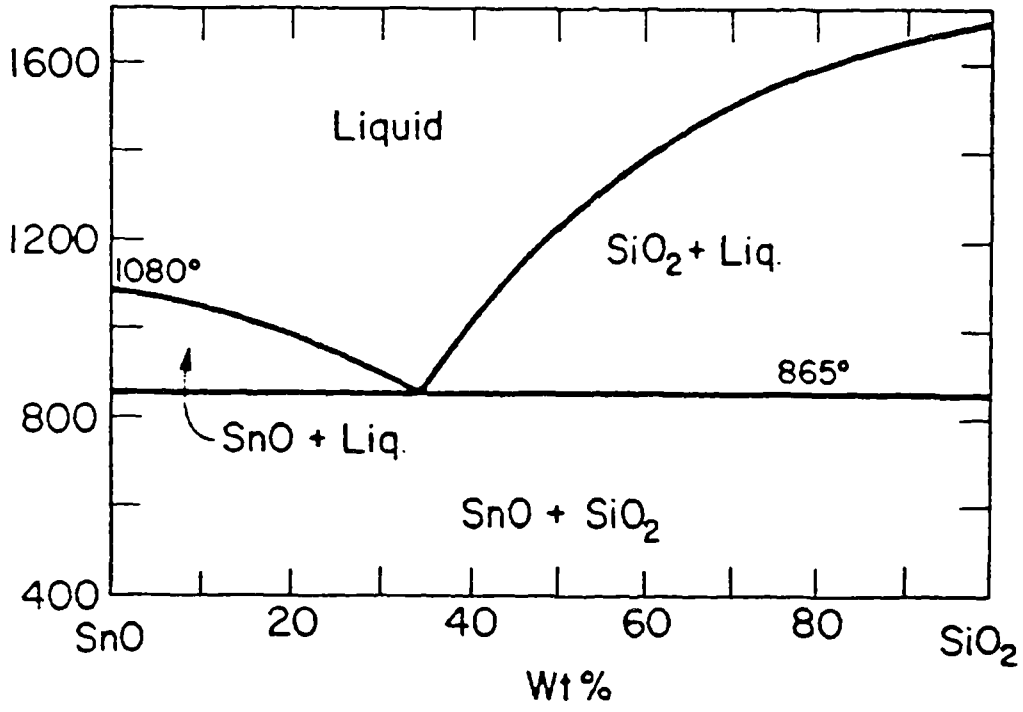

Figure 4.1 : *The phase relation for the SnO-SiO_2 glass system [6].*

(b) Covering the crucibles but leaving a very small opening so that the evolution of CO and CO_2 gases from the stannous oxalate expelled the air from the crucibles and the low oxygen partial pressure of the gas mixture minimised the oxidation of the melt.

(c) Based on the graph of the standard free energy of formation of oxides as a function of temperature compiled by Ellingham [7] and Richardson & Jeffes [8], reaction 4.2 could be minimised by heating the mixture quickly to the melting temperature.

Table 4.1: *Nominal composition , melting temperature and time, optical quality and amorphicity of SnO-SiO_2 glasses*

Sample	*Nominal composition (mol%)*		*Melting temp (°C) / time (min.)*	*Colour and optical quality*	*XRD of glass*
	SnO	SiO_2			
**TS1*	*20*	*80*	*1600 / 45*	*homogenous light yellow clear glass with murky green parts*	*amorphous*
TS2	*32*	*68*	*1350 / 45*	*yellow homogenous clear glass*	*amorphous*
TS3	*33.3*	*66.7*	*1350/ 45*	*yellow homogenous clear glass*	*amorphous*
TS4	*40*	*60*	*1350/ 50*	*deep yellow homogenous clear glass*	*amorphous*
TS5	*47.2*	*52.8*	*1200/ 50*	*very deep yellow homogenous clear glass*	*amorphous*
TS6	*50*	*50*	*1000/ 40*	*very deep yellow homogenous clear glass*	*amorphous*
TS7	*60*	*40*	*1150/ 50*	*yellowish orange homogenous clear glass*	*amorphous*
TS8	*65*	*35*	*1200/ 50*	*yellowish brown homogenous clear glass*	*amorphous*
TS9	*70*	*30*	*1200/ 50*	*brown homogenous clear glass*	*amorphous*
TS10	*75*	*25*	*1200/ 50*	*deep brown homogenous clear glass*	*amorphous*
TS11	*80*	*20*	*1200/ 50*	*reddish brown homogenous clear glass*	*amorphous*

** For glass sample TS1, the murky green parts were discarded by cutting and grinding. EDX analysis has shown that the murky green part has a very high aluminium content.*

By this method an average of 84% of the initial SnO content could be retained in the glass as given in the analyzed compositions in Table 5.1 (Chapter 5).

4.1.2 TIN-DOPED FLOAT GLASS

Tin-doped float glass samples were made with the objective of simulating the tin concentration in the tin contact side of industrial float glass. The procedures for making this glass are as follows.

The starting materials for making this glass were powdered float glass and reagent grade stannous oxalate (SnC_2O_4). The powdered float glass was made from a block of 19 mm thick float glass sheet supplied by Pilkington. To remove the tin from the float glass, about 1 mm of both surfaces were first removed and the remainder was broken into small pieces and melted in a platinum crucible for 1 hour at 1400°C. The molten glass was poured into deionized water to turn it into frit glass. The frit glass was then ball milled for 48 hours with two sizes of magnesium silicate balls and methanol as the milling medium. The resulting slurry was dried in open air for three days to obtained a fluffy white powder. The white powder was then dried at 90°C for 1 hour before being passed through 3 sieves going 180 μm → 68 μm → 38 μm. The analyzed composition of the powdered float glass is given in Table 4.2. The analysis was carried out by Pilkington Technology Centre, Lancashire England.

Appropriate amounts of powdered float glass and stannous oxalate were homogenised by rolling. Six batches were prepared, with nominal compositions of 2.5, 5, 7.5, 10, 12.5 and 15 wt.% SnO. Stannous oxalate on heating decomposes to SnO and gives out CO and CO_2 gases which kept the melt under fairly reducing conditions. Under this condition SnO will nonetheless fairly readily oxidize to SnO_2 and the presence of alkali oxide [9] will enhance the solubility of SnO_2 in the glass. As a result of this, the tin-doped float glass will contain varying amounts of tin in different valency states , thus simulating the tin contact side of the industrial float glass.

The first attempt to prepare the samples was carried out by melting in alumina crucibles at temperatures between 1500°C and 1700°C in air. However, the high viscosity of the melt when casting indicated that Al_2O_3 from the crucibles had contaminated the melt. Chemical analysis showed that the increase in Al_2O_3 content of the samples is between 600 to 1700% of the original Al_2O_3 content of the float glass composition. Therefore these samples do not correspond to the usual float glass composition and were discarded.

In the second attempt Al_2O_3 contamination was avoided by melting the glass using translucent silica crucibles of 99.6% SiO_2 purity. The glasses were melted in air at 1400°C for 1 hour. The furnace temperature was then increased to 1500°C. After refining for about 15 minutes the melt was easily poured into a mould, before being annealed at 600°C for 1 hour and subsequently cooled to room temperature. The nominal compositions, melting conditions and optical quality of the tin-doped float glass samples prepared are shown in Table 4.3.

Table 4.2 : *Analyzed composition of the powdered float glass called PK0*

Major	*Mole %*
SiO_2	73.9
Na_2O	12.1
CaO	8.1
MgO	3.9
Al_2O_3	1.1
*Minor component	0.9
Total	**100**

* - $As_2O_3 + K_2O + SO_3 + Fe_2O_3 + TiO_2 + ZrO_2$

Table 4.3. Preparation conditions and optical quality of tin-doped float glasses

Samples	*Nominal wt.% of SnO added to float glass*	*Melting conditions*	*Colour and optical quality*
PK2.5S	*2.5*	*1400°C for 1 hour and 1500°C for 15 minutes*	*Bluish, homogenous, bubble-free, clear glass*
PK5S	*5.0*	*1400°C for 1 hour and 1500°C for 15 minutes*	*Bluish, homogenous, bubble-free, clear glass*
PK7.5S	*7.5*	*1400°C for 1 hour and 1500°C for 15 minutes*	*Greenish, homogenous, bubble-free, clear glass*
PK10S	*10*	*1400°C for 1 hour and 1500°C for 15 minutes*	*Greenish, homogenous, bubble-free, clear glass*
PK12.5S	*12.5*	*1400°C for 1 hour and 1500°C for 15 minutes*	*Greenish, homogenous, bubble-free glass with some small patches of white obscuring phase of undissolved SnO_2. Parts that have this obscuring phase were discarded.*
PK15S	*15*	*1400°C for 1 hour and 1500°C for 15 minutes*	*Greenish, homogenous, bubble-free glass with some small patches of white obscuring phase of undissolved SnO_2. Parts that have this obscuring phase were discarded.*

As seen in Table 4.3, some undissolved SnO_2 had crystallised out of the glass samples PK12.5S and PK15S with the initial SnO contents of 12.5 and 15 wt.% respectively. This is an indication that both samples had the maximum amounts of SnO_2 that can be dissolved in them.

4.2 COMPOSITIONAL ANALYSIS OF GLASS

The nominal compositions of the glass samples do not remain the same after melting the glasses. This is especially true for the tin contents of the glasses because of the disproportionation and oxidation of SnO during melting. The final composition of the glass is important since it is an essential factor in the structural analysis.

4.2.1 BINARY SnO-SiO_2 GLASS

The SnO *content of the glass in this system was determined by a titration* method both at Warwick and at Pilkington Research Laboratories. Approximately 0.3 g of powdered glass was mixed with 3 g of NaOH and Na_2O_2 in a weight ratio of 1:2 and gently fused in zircosil or nickel crucibles. After cooling, the contents were extracted by 100 ml concentrated HCl acid into a conical flask. While warming the flask, the contents were reduced by 1 g of iron and 2 g aluminium powder under CO_2 gas in order to prevent Sn^{2+} from oxidizing to Sn^{4+}. This solution was cooled and then titrated with N/100 iodine solution which had been standardized against spectrographically pure tin by the above method. The Al_2O_3 contamination of the glass was determined by chemical analysis at Pilkington and by quantitative NMR at Warwick. EDX analysis to find the approximate chemical composition was also carried out at Warwick. All analyses were consistent to within 2%. The SiO_2 content of each sample was calculated by difference.

4.2.2 TIN-DOPED FLOAT GLASS

The compositional analysis on this glass were carried out by Pilkington Research Laboratories. The techniques employed were wet chemical analysis, x-ray

fluorescence analysis and atomic absorption spectrophotometry. The relative amounts of Sn^{2+} and Sn^{4+} were determined by chemical analysis at Pilkington and by ^{119}Sn Mössbauer spectroscopy at Liverpool University.

4.3 STRUCTURAL TECHNIQUES

The two main structural techniques used in this research are NMR and Mössbauer spectroscopies. For the binary $SnO\text{-}SiO_2$ system ^{29}Si NMR, ^{119}Sn NMR and ^{119}Sn Mössbauer spectroscopies were used. For tin-doped float glass only ^{119}Sn Mössbauer spectroscopy was employed.

4.3.1 NUCLEAR MAGNETIC RESONANCE

The ^{29}Si and ^{119}Sn NMR spectra were recorded at ambient temperature using a Bruker MSL 360 spectrometer (Multipurpose Solid and Liquid : proton frequency 360 MHz)[10] and the pulsed Fourier Transform method. The spectrometer operates in conjunction with an 8.45 T Oxford superconducting cryomagnet with a wide bore of 89mm [11]. This magnet achieves high field homogeneity via a set of shim coils. An Aspect-3000 computer, using the DISMSL program, control all the operations of data acquisition, data manipulation, storage and plotting. Figure 4.2 shows the block diagram of the Bruker MSL 360 spectrometer.

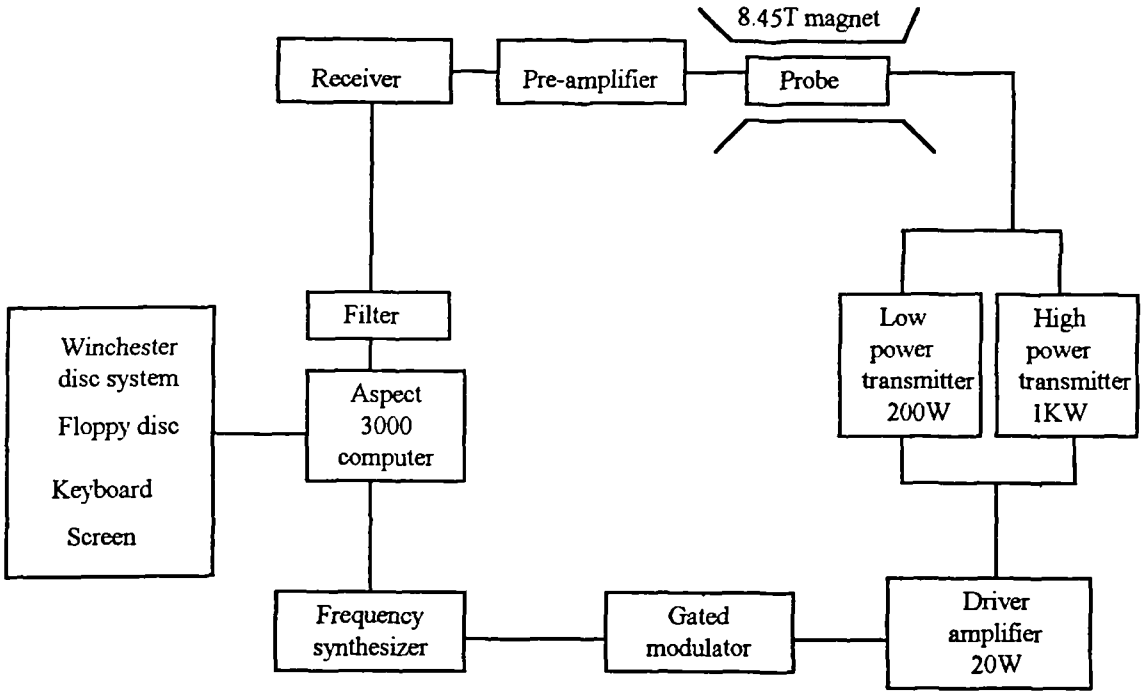

***Figure 4.2** : A schematic diagram of the main components comprising the Bruker MSL 360 spectrometer*

The spectrometer is compatible with a variety of probes; static and both single and double bearing sample spinners. The specimens were crushed into a fine powder and compacted into the sample holder which was then placed inside the coil of the Bruker NMR probe.

^{29}Si NMR

The ^{29}Si spectra were first recorded using the static probe, Bruker Z33v HP. The tuning frequency is 71.535 MHz. A short 2 μs pulse width and 5 s relaxation delay were used, resulting in an accumulation of about 1000 scans in 1 hour. The data were Fourier transformed and the resulting spectra were broad, about 40 ppm at FWHM.

To reduce the spectral broadening from anisotropic interactions and thus allow for higher resolution of the spectra, spinning the sample at the magic angle was essential. This was accomplished by spinning the sample in a Bruker cylindrical zirconia spinner of internal diameter 5.5 mm, external diameter 7 mm and length 17.7 mm. Since spinning with this spinner was very sensitive to sample imbalance, finely powdered sample and careful packing of the sample were required in order to achieve smooth fast spinning. The probe used was the Bruker Z 33.6 DR - MAS - 7DB. It was not necessary to remove this probe to change samples as this could be achieved via a separate compressed air powered insert/eject system at the top of the magnet. Spinning was powered by dry compressed air and monitored by an optical ratemeter. All samples were spun at a rate of 3.5 kHz inside the probe coil which was oriented at the magic angle (54.7°) to the magnetic field (8.54T).

Associated hardware included a low power broad band transmitter and a preamplifier box to match and tune the carrier frequency. Operation of the spectrometer required calling a reference file for the ^{29}Si nucleus, tuning the operating frequency, setting the acquisition parameters and shimming the magnet. A pulse width of 2 μs and a relaxation delay of 5 s were used and data of about 1000 scans were

accumulated. The data in the form of a FID (Free Induction Decay) was then Fourier transformed to produce the chemical shift spectrum. For further details on the spectrometer, its operation, computer control, creating a reference file and data processing the reader is referred to references [12 -16].

The ^{29}Si chemical shifts were measured relative to the ^{29}Si chemical shift of the tetramethylsilane (TMS) standard. The Si nuclei in TMS are structurally indistinguishable, with four methyl (CH_3) groups being symmetrically arranged around a central Si atom. Tetramethylsilane [$(CH_3)_4Si$] has a single resonance at the high frequency end of the ^{29}Si spectrum. Most other chemical shifts are on the low frequency side of this peak and therefore have negative values. The typical FWHM of ^{29}Si MAS NMR spectra of the glasses studied were about 20 ppm as compared to 40 ppm for the static spectra.

^{119}Sn NMR

The ^{119}Sn spectra were first recorded using the static probe, Bruker Z33v HP. The tuning frequency is 143.296 MHz. The resulting spectra were very broad (FWHM $\approx$ 900 ppm). MAS NMR of ^{119}Sn spectra were then recorded using a Doty Scientific, 360 MHz, double-bearing probe and utilising a 5 mm outer diameter silicon nitride spinner with two fluted ends. Spinning rates of 8 - 10 kHz were achieved with these spinners. The resulting spectra were still very broad but clearly showed that, there were two tin sites in the glasses. The spectra of the glasses were compared with ^{119}Sn NMR spectra of crystalline SnO and SnO_2, recorded under identical conditions.

4.3.2 MÖSSBAUER SPECTROSCOPY

The ^{119}Sn Mössbauer spectroscopy experiments were conducted in collaboration with Professor C.E. Johnson and Miss K.F.E. Williams of the Physics Department , Liverpool University. The Mössbauer spectra were recorded by Miss Williams who also carried out the peak fitting, determination of the spectral parameters and who was responsible for much of their interpretation.

The schematic diagram of the Mössbauer spectrometer is shown in Figure 4.3. The following description is a brief outline of the major principles involved in the working of the spectrometer. For more detailed account of instrumentation and experimental methods the reader is referred to Spijkerman [18], Benczer-Koller and Herber [19] and a review by Kalvius and Kankeleit [20].

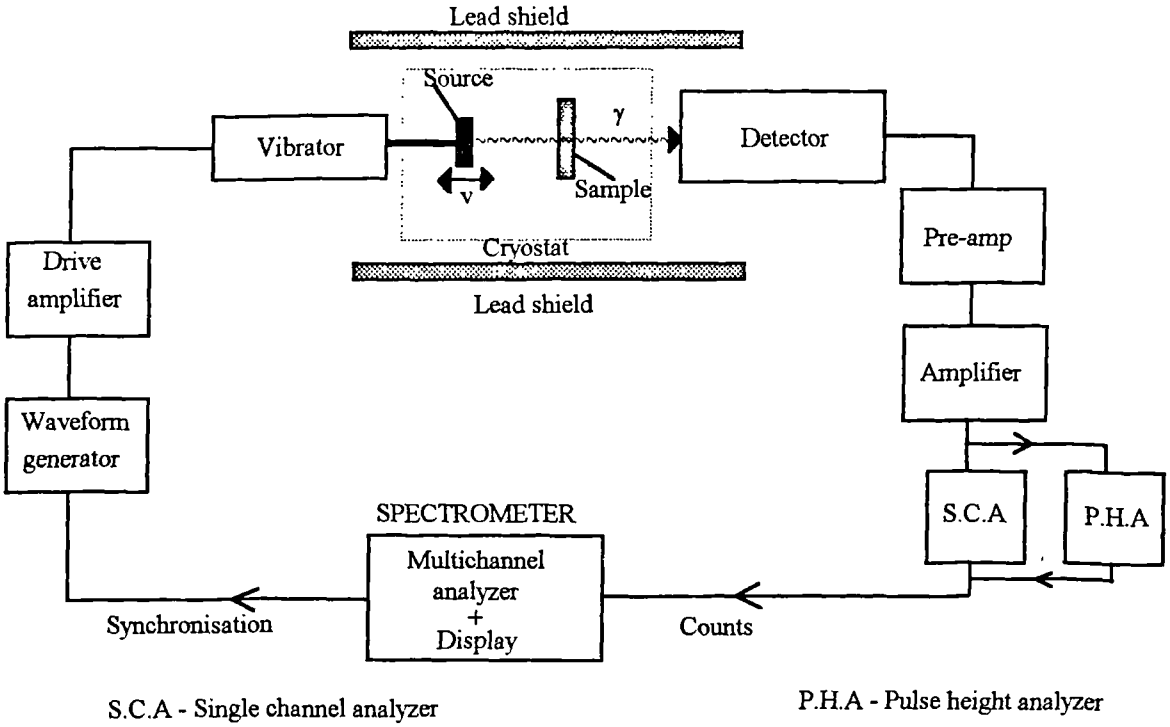

Figure 4.3 : *A Schematic diagram of the Mössbauer spectrometer*

Source motion: The source motion is by constant acceleration and deceleration modes with a double ram. This is achieved by the spectrometer relating a particular channel in the multichannel analyzer with a small range of velocities of the source motion.

The vibrator : The electromechanical vibrator has a central shaft, a drive coil, a pick-up coil and a magnet mounted on the shaft. The source is mounted on the shaft, whose position depends on the voltage applied to the drive coil. The velocity of the shaft determines the voltage coming from the pick up coil. The timing pulses from the spectrometer are used to synchronize a voltage waveform generated from the waveform generator, which is used as a command signal to drive the vibrator.

Detection system : This is designed to produce a single pulse for each γ-ray detected. A gas (90% Argon + 10% Methane) proportional counter detector is used. For samples with low tin contents an intrinsic germanium solid state detector is used in conjunction with a strong (10 mCi) ^{119m}Sn source. The high resolution of this detector (<300 V) can resolve the γ- rays from the 25.4 keV x-ray which accompanies it. A γ-ray emitted along the axis of motion of the source has a Doppler shift of $(E_\gamma v)/c$ relative to the absorber. Any other γ-ray which travels to the detector along a path at an angle θ to the axis has an effective Doppler shift of $(E_\gamma v\cos\theta)/c$. This 'cosine-effect' of solid-angle cause line broadening of the spectra [21]. The effect is reduced by maintaining an adequate separation between the source and detector and by collimation. The pulses from the detector are amplified, passed through a discriminator (S.C.A and P.H.A) which rejects most of the non-resonant background radiation and are finally counted by the multichannel analyzer for display.

Source : The source matrix of the ^{119}Sn is calcium stannate ($CaSnO_3$) in a 16mm host material of tin-palladium alloy. The source has a linewidth of 0.423 mms^{-1}. The decay scheme for the ^{119}Sn source is depicted in Figure 4.4. The isotope is a 250-day

isomer ^{119m}Sn of the parent nuclide. The 89.54 keV metastable level of the ^{119m}Sn decays by an isomeric transition directly to the 23.88 keV first excited state of ^{119}Sn. This Mössbauer level of spin $+\frac{3}{2}$ then decays by an $M1$ transition to the stable ground state with spin $+\frac{1}{2}$. The 23.88 keV γ-ray has an internal conversion coefficient of 5.2. The excited state has a half-life of 18.5 ns which corresponds to a Heisenberg width of $\Gamma_r = 0.626\ mms^{-1}$.

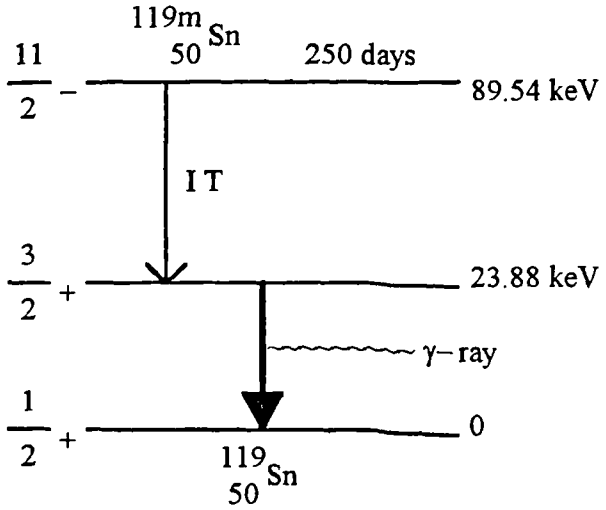

Figure 4.4 : *The decay scheme for ^{119}Sn*

Experimental : The samples were powdered and made to their 'optimum thickness' as described in ' The ideal Mössbauer Effect Absorber Thickness ' by Long et al [22]. Calibration was done with an iron source ($^{57}CoRh$) and corresponding standard absorber (α-Fe metal) at room temperature. All measurements of velocity were relative to the centroid of this 6 line reference spectrum. A $CaSnO_3$ absorber gives a shift of ~ $0.12\ mms^{-1}$. Both the binary $SnO\text{-}SiO_2$ and tin doped float glass were run at room temperature and at 77K using the liquid nitrogen cryostat. To determine the f-factor of Sn^{2+} and Sn^{4+} in tin doped float glass , a series of spectra was taken on glass sample PK15S, between 17.5K and 900K. The data collected was computer fitted.

4.4 VISCOSITY MEASUREMENTS

The importance of viscosity-temperature and viscosity-composition relationships of glass have been stressed in section 3.3. A homemade penetration viscometer which can measure viscosity in the range of 10^7 to 10^{12} Pa s with ± 1.5 % accuracy (in $Log_{10}\eta$) was used. An alumina hemi-spherical indenter of diameter D = 6.02 mm was employed. Depending on composition, the viscosities measured for the binary SnO-SiO_2 and tin-doped float glasses were in the temperature ranges of 350°C to 800°C and 550°C to 750°C respectively.

4.4.1 SAMPLE PREPARATION

In general, any reasonably flat pieces of glass can be used. In this experiment, glass pieces about 12mm square and 7 mm thick were used.

4.4.2 PENETRATION VISCOMETER

The essential parts of the viscometer are shown in Figure 4.5. The temperature of the samples was measured using an R-type Pt-Pt/13%Rh thermocouple. The thermocouple was connected to a Comark digital thermometer and the signal from the thermometer to a chart recorder where the temperature was recorded. The time (t) and penetration depth (z) of the indenter into the glass were measured by employing a Linear Voltage Displacement Transducer connected to the upper part of the indenter. The LVDT is connected to a chart recorder where the penetration displacement and time taken were simultaneously recorded.

Equation 3.44 given in chapter 3 was used to calculate the viscosity.

$$\eta = \left(\frac{9P}{32\sqrt{D}}\right)\left(\frac{t}{z^{3/2}}\right) \qquad 3.44$$

For all measurements the same weight (L) was used. Therefore this will also give the same applied load (P) to the samples via the indenter. Since P and D are constant, the first term of equation 3.44 is also a constant and 3.44 can be written as,

$$\eta = C\left(\frac{t}{z^{3/2}}\right) \qquad 4.4$$

Where C is the instrument constant. To evaluate C, a glass standard (NBS-710) from the National Bureau of Standards was used as a calibration standard.

Before making a measurement, the temperature must equilibrate. A soaking time of at least 20 minutes was taken for the temperature to reach a constant value. When this was achieved, contact between the indenter and the glass surface was carefully made by lowering the weight arm (L). The temperature, time (t) and the penetration depth (z) were noted and the viscosity calculated using equation 4.4. After one measurement, the indenter was raised and another part of the glass surface could be used for another measurement at the same temperature or higher temperature. Three measurements were taken at each temperature and the average viscosity value calculated.

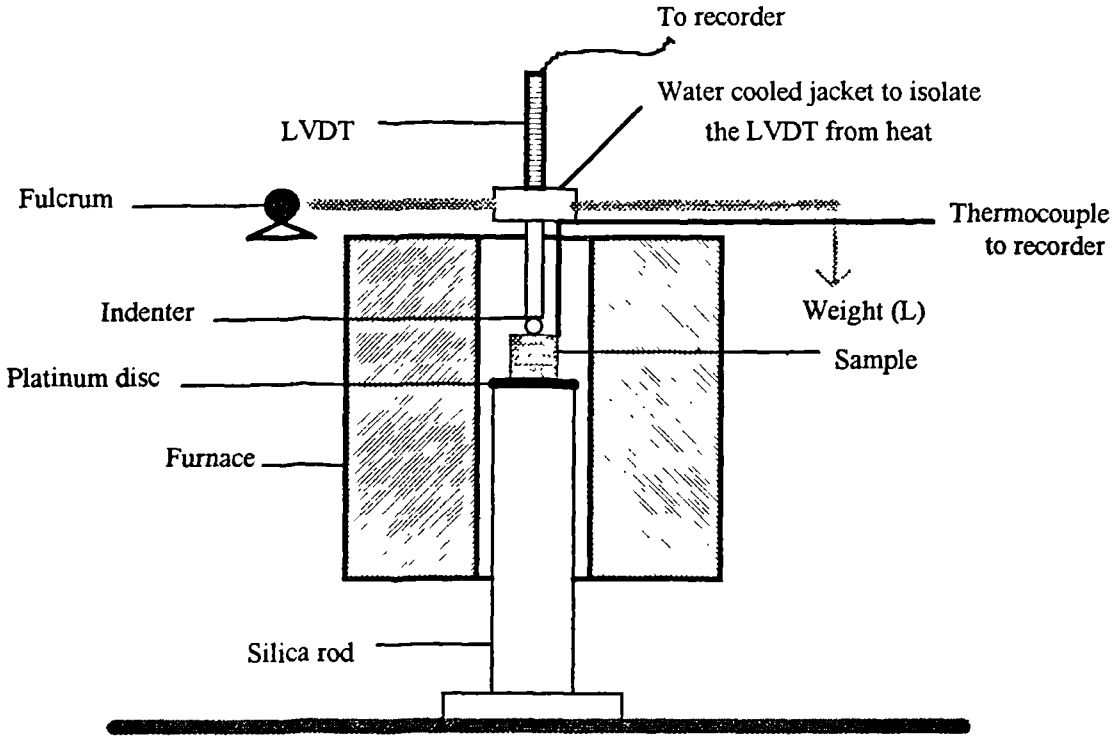

Figure 4.5 : *The essential parts of a penetration viscometer*

4.5 THERMAL TECHNIQUES

Two thermal analysis techniques were employed in this study. They were Differential Thermal Analysis (DTA), applied to the binary SnO-SiO_2 glass and dilatometry applied to both the binary SnO-SiO_2 and tin-doped float glasses.

4.5.1 DIFFERENTIAL THERMAL ANALYSIS

Differential Thermal Analysis (DTA) is the study of heat flows in a system as a function of temperature. This is a dynamic temperature technique where the difference in temperature between a sample and an inert reference material is recorded when both undergo either controlled heating or cooling. The temperature difference

can be used to determine whether the sample undergoes any chemical reaction, or structural changes (phase transformation) since these events are accompanied by the evolution or absorption of energy in the form of heat. Crystallization of a glass will show an exothermic peak since the free energy of the regular crystal lattice is less than that of the disordered glassy state. Melting will show an endothermic peak, while peaks for chemical reactions are either endothermic or exothermic. A typical DTA trace is illustrated in Figure 4.6.

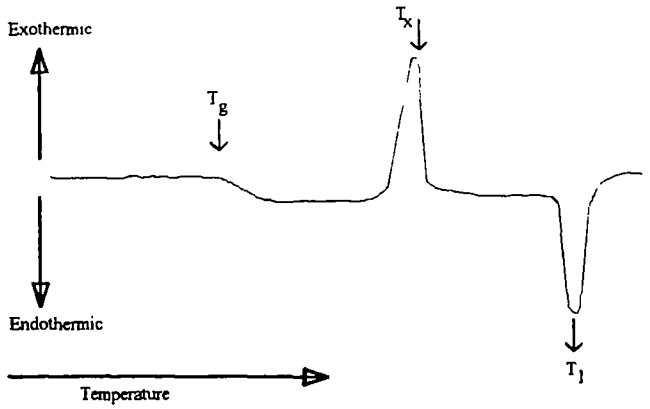

Figure 4.6 : *A typical DTA curve showing the transformation temperatures.* T_g *is the transition temperature,* T_x *is the crystallization temperature and* T_l *is the melting temperature.*

The theoretical background and practical aspects of DTA can be referred to in Pope [23]. According to Pope the main factors influencing DTA experiments are: sample weight, particle size, conditions of sample packing in DTA cell and atmospheric conditions. As DTA is a comparative method, these factors were maintained as identical as possible during the experiments on the same glass system. The reference material used in the experiments was a fine quartz powder. In cases where it was believed that the α-β quartz transition around 570°C masked transformations within

the sample, the experiments were redone using analytical grade alumina as the reference material.

The DTA experiments were carried out using a Stanton Redcroft DTA model 673-4. The heating rate was 5°C per minutes under normal atmosphere and pressure. About 0.9 g of fine ground sample and a similar mass of reference material were heated in platinum crucibles. Pt-Rh thermocouples located in recesses in the crucibles measured the sample and reference material temperatures.

4.5.2 DILATOMETRY

Dilatometry or linear thermal expansion experiments were carried out using a homemade, vertical, fused silica dilatometer [24] which was calibrated with a platinum standard. The experimental arrangement inside the furnace is shown in Figure 4.7.

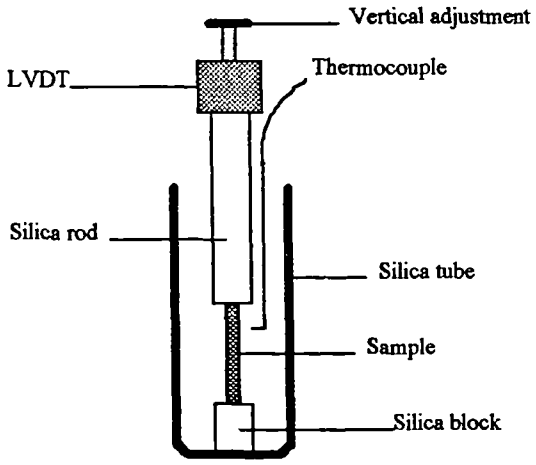

Figure 4.7 : *Cross-section of the inside of the quartz dilatometer*

Glass rods of square cross-section 3mm x 3mm were used as samples. The temperature was measured using a thermocouple in contact with the sample and connected to a pen chart recorder (x-axis). On expansion of the sample, the quartz rod was pushed upwards and its displacement was monitored by a linear variable

displacement transducer (LVDT) and recorded on chart paper (y-axis). A heating rate of 3°C/min. was used until the dilatometric softening point was reached. After taking account of the expansion of silica, the coefficient of thermal expansion, α was calculated using equation 4.5

$$\alpha = \frac{\Delta L}{\Delta T.L} \qquad 4.5$$

where L is the original length, ΔL the change in length and ΔT the change in temperature.

4.6 CRYSTALLIZATION STUDIES

The binary $SnO\text{-}SiO_2$ glasses were heat treated in ordinary atmosphere at various crystallization temperatures noted from the DTA traces of the glasses. Some selected glasses of near 1 : 1 compositions were also heat treated in inert (argon gas) atmosphere. The heat treatments are detailed in Chapter 6. The crystallized products were characterized by X-Ray Diffraction, ^{29}Si MAS NMR, ^{119}Sn Mössbauer spectroscopy and Scanning Electron Microscopy. Attempts have also been made to use Transmission electron microscopy (TEM) on some crystallized glasses but this was not successful because the samples were damaged during preparation.

4.6.1 X-RAY DIFFRACTION (XRD)

X-Ray diffraction was used to identify crystalline phases present in all devitrified samples. The technique was also used to verify the absence of crystallinity in all glass samples. The XRD patterns were obtained using a Philips Powder

Diffractometer with Cu K_α (λ = 1.54178 Å) radiation. Samples were crushed to a fine powder in an agate mortar and pestle and mounted in aluminium sample holders. The 2θ scan rate and time constant were the same for all the samples (1°/min. and 1s respectively). The phases were identified by comparing the experimental interplanar spacing and the intensity of the diffraction pattern using the standard JCPDS powder diffraction file [25].

4.6.2 SCANNING ELECTRON MICROSCOPY

Scanning electron microscopy was used to examine the general microstructure. A JEOL 6100 electron microscope was used. Conventional preparative procedures were used involving mounting the samples in bakelite resin and polishing the upper surface flat to 0.5 μm smoothness using a series of abrasive papers followed by diamond paste on a cloth wheel. When polished, the samples were mounted on standard aluminium SEM stubs using carbon paste. To prevent charging, the samples were sputter coated with a very thin carbon layer. Generally , an electron accelerating voltage of 10 kV was used. The micrographs were obtained using back-scattered imaging utilising compositional contrast rather than topographical features. Thus the regions of the material containing heavy elements appear lighter than those regions containing elements of low atomic number. The EDX (Energy dispersive X-ray analysis) spectra of some samples have also been taken to find the approximate chemical composition of the phases present. Further experimental details of analysis in electron microscopy can be referred to in Goodhew and Humphreys [26].

4.7 DENSITY AND MOLAR VOLUME

The density measurements of glass samples were made with a digital balance (Precisa 125A), using Archimedes' principle. A sample was first weighed in air. After

being weighed in air, the sample was washed in acetone, then in dilute teepol solution and finally rinsed in distilled water before placing it in a weighing pan that was permanently suspended in degassed distilled water inside an enclosed compartment below the main balance. The density was calculated using equation 4.6 below.

$$\rho = \rho_1 \frac{W_A}{W_A - W_1} \qquad 4.6$$

where W_A is the weight of sample in air, W_1 the weight in immersion fluid and ρ_1 is the density of immersion fluid. The density data were used to calculate the molar volume, V_m, given by

$$V_m = \frac{M}{\rho} \qquad 4.7$$

where M is the glass molecular weight calculated from composition.

4.8 REFRACTIVE INDEX AND MOLAR REFRACTIVITY

The refractive index of both the binary SnO-SiO_2 and tin-doped float glasses were measured using an Abbe refractometer (Bellingham and Stanley model 60/ED) which permits the measurement of refractive indices up to 1.7361 with an accuracy of 0.0002. A sodium lamp (λ = 589.6 nm) was used as the light source. Calibration of the instrument was checked using a silica standard (η = 1.45839 at 20°C for sodium light, λ = 589.6 nm).

Samples have a face polished to 0.5 μm and a face about 12 mm wide cut at right angles to it. Monobromonapthalene (MBN) was used as the contact liquid between the surface of the refractometer prism and the test samples. For η > 1.65

methylene iodide was used as the contact liquid instead of MBN. Measurements were done at room temperature and the molar refractivity (R_m) was calculated using the Lorenz & Lorentz formula,

$$R_m = V_m \frac{\eta^2 - 1}{\eta^2 + 2} \qquad 4.8$$

4.9 MICROHARDNESS TEST

The hardness of a substance can be described as a measure of its resistance to permanent deformation or damage. In practice this is taken as the resistance which the sample offers to indentation by another body, the 'indenter' (pyramid-shaped diamond) under the action of an applied load. The measure of the indentation hardness is defined as the ratio between the applied load (P) acting on the indenter and the actual surface area (M) of the pyramid-shaped permanent impression produced by this force. The greater the load the larger the indent. Large loads of the order of kg are usually expressed as *macro* hardness testing, low loads in order of g as *micro* hardness testing.

There are two different shaped diamond microindentors: the Vickers and the Knoop indenters. These shapes are shown in Figure 4.8. The hardness values are given by the following equations,

Vickers:

$$HV = \frac{1854 \times P}{d_v^2} \ kg/mm^2 \qquad 4.9$$

Knoop:

$$HK = \frac{14230 \times P}{d_k^2} \text{ kg / mm}^2 \qquad 4.10$$

where P is the applied load in g , d_V the average length of the Vickers diagonals in μm and d_K the longest Knoop diagonal in μm.

Microhardness testing was carried out on tin-doped float glasses using a M12a micro-hardness tester supplied by Vickers Instruments Limited. Samples were cut so that the two surfaces were parallel. The surface to be tested was polished to a 1μm finish and mounted on a glass slide using plasticine. A standard mounting press was used to ensure that the polished surface was parallel to the slide. The planarity of sample is important. Lack of planarity will result in an anisotropic effect where one leg of the indention diagonal is longer than the other.

A Knoop diamond indenter was employed with a load of 50 g applied for 30 seconds. The length of the longest diagonal was observed as a function of the filar divisions and converted to a hardness value using standard reference tables. Twenty readings were taken on each glass sample and the average hardness calculated.

The theory and experimental detail on hardness testing can be referred to Bousfield [27] and British Standards BS 427 and BS 5411.

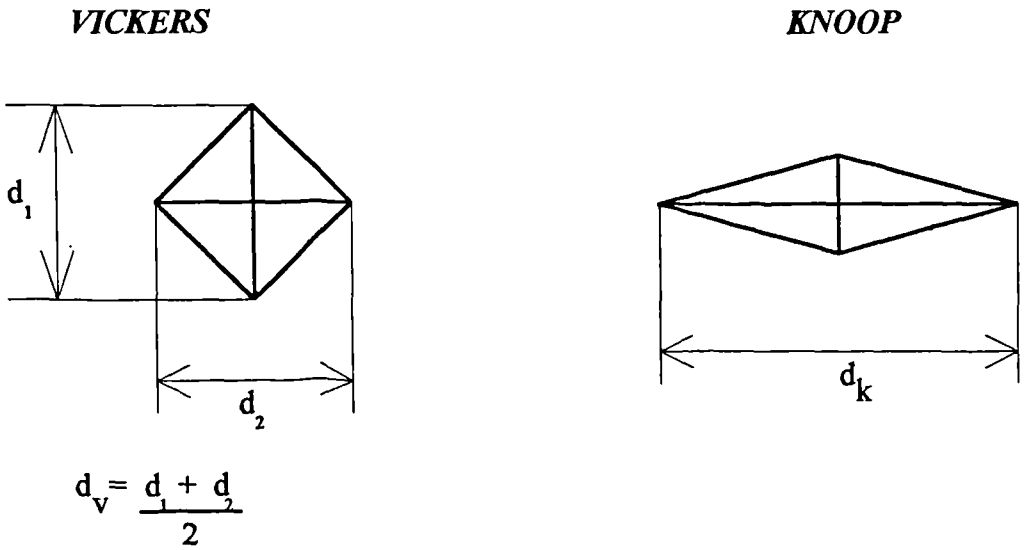

Figure 4.8 : *Hardness indentation shapes*

REFERENCES

1. Keysselitz, B. & Kohlmeyer, E.J. (1933). *Metall Erz.* **30,** 185-190.
2. Platteew, J.C. & Meyer, G. (1956). *Trans. Faraday Soci.* **5,** 32 .
3. Donaldson, J.D. & Moser, W. (1961). *J.Chem. Soc.* **7,** 835.
4. Donaldson, J.D. (1967). *Progress in Inorganic Chemistry* **8,** 287.
5.Volf, M.B. (1984). *Chemical Approach to Glass, Glass Science & Tech. 7,* Oxford.
6. Levin, E.M., Robbins, C.R. & McMurdie, H.F. (1975). *Phase Diagram for Ceramists, 1975 Supplement,* The American Ceramic Society, Inc. Columbus, Ohio.
7. Ellingham, H.J.T. (1944). *J.Soc. Chem. Ind.* **63,** 125.
8. Richardson, F.D. & Jeffes, J.H.E. (1944). *IIsl.* **160,** 3261.
9. Zorina, M.L. & Vakhrameev, V.I. (1969). *Neorg. Mat.* **5(10),** 1834.
10. *MSL Series User's Manual.* (1980). Bruker.
11. *Superconducting Magnet for NMR Operating Instructions* (1984). Oxford Instrument.
12. Smith, M.E. (1987). *PhD Thesis,* University of Warwick.
13. Mortuza, M.G. (1989). *PhD Thesis,* University of Warwick.
14. *MSL System Description,* (1986). Bruker Spectrospin Manual, Ref. no.431001.
15. *Aspect 3000 Software Manual,(1986). Bruker Spectrospin Manual.*
16. *NMR Probehead Manual: Series MAS-DB,* (1985). Bruker Spectrospin Manual.
17. *Users Manual: MSL Series,*(1985). Bruker Spectrospin.
18. Spijkerman, J.J. (1971). *'Instrumentation'* in An Introduction to Mössbauer Spectroscopy, Edited by Leopold May, Adam Hilger, London.
19. Benczer-Koller, N. & Herber, R.H. (1968). *'Experimental Methods'* in Chemical Applications of Mössbauer Spectroscopy, Edited by V.I .Goldanskii & R.H.Herber. Academic Press, N.York.
20. Kalvius, G.M. & Kankeleit, E. (1972). *'Recent Improvements in Instrumentation and Methods of Mössbauer Spectroscopy'* in Mössbauer Spectroscopy and its Applications, International Atomic Energy Agency, Vienna.
21. Riesenman, R., Steger, J. & Kostiner, E. (1969). *Nuclear Instr. Methods,* **72,** 109.
22. Long,G.J., Cranshaw,T.E. & Longworth,G.(1983).*Mössbauer Effect Ref. Data J.* **6**,42.
23. Pope,M.I. (1977). *Differential Thermal Analysis,* Heyden.
24. Bridges, D.R. (1986). *PhD Thesis,* University of Warwick.
25. *J.C.P.D.S. Powder Diffraction Files,* Alphabetical and Search Indexes. (1984).
26. Goodhew, P.J. & Humphreys, F.J. (1988). *Electron Microscopy and Analysis,* Taylor and Francis, London.
27. Bousfield, B. (1992). *Surface Preparation and Microscopy of Materials.* John Wiley and Sons , New York.

Chapter 5 - The binary $SnO-SiO_2$ glass system

5.1 INTRODUCTION

The existence of glass formation in the binary $SnO-SiO_2$ system was established during the period of 1930 to 1950, but there have been only three studies done on glasses in this system; as briefly mentioned in chapter 2. Carbo Nover & Williamson [1] studied the crystallisation and decomposition of glasses ranging in composition from 28 to 59 mol% SnO by XRD and Electron microprobe analysis. Itoh & Mori [2] measured the electrical resistance, as a function of temperature, of a glass containing 47.42 mol% SnO. The only structural studies on this glass system, covering compositions from 32 to 57 mol% SnO, was done by Ishikawa & Akagi [3] using x-ray radial distribution and infrared absorption techniques.

This chapter presents and discusses some aspects of the preparation and compositions of the glasses studied in this system, followed by results on the structural investigation using ^{29}Si and ^{119}Sn NMR and ^{119}Sn Mössbauer spectroscopies. In addition to these, physical properties measurements which include viscosity, density and molar volume, thermal expansion and refractive index will be presented and discussed.

5.2 GLASS PREPARATION AND PROBLEMS

The preparation of glasses in this glass system by modified melting techniques has been been described in chapter 4.

The lack of research done on this glass system is probably because of the difficulties in preparing good glass samples. The difficulties are due to two main problems. The first is the disproportionation of SnO to SnO_2 and Sn metal so that, during melting, the liquid $SnO-SiO_2$ glass will contain Sn metal liquid at the bottom of

the crucible and solid SnO_2 at the top of the glass melt. Because of this, the melt cannot be poured and cast properly and quenching was done with the melt in the crucibles. The glass formed in the middle of the crucibles (see Figure 5.1(a)) is removed by grinding and cutting away the crucible, resulting in odd pieces and shapes of glass. The second problem is concerned with the type of crucibles used. The first crucibles used to prepare this glass were of alumina. However, alumina reacts with the melt and contaminates the glass. Contamination is minimised by keeping the melting time to a minimum and grinding away the glass parts that are near the wall of the crucibles. Platinum crucibles cannot be used because it has been observed [4] that a platinum wire inserted into the glass melt disappeared rapidly at 1200°C forming a globule of a platinum-tin alloy. Thus, the presence of Sn metal from the disproportionation of SnO will attack the platinum if such crucible is used.

Is should also be pointed out that glass with a low SnO content is very difficult to make. The minimum nominal SnO content that has been made by this method is 20 mol%, melted at 1600°C. The resulting glass in the middle of the crucible was of a homogenous, light yellow in colour surrounded by a murky green portion extending right to the inside wall of the crucibles (see Figure 5.1 (b)). EDX analysis has shown that the murky green portion has a very high aluminium content. This highlights the difficulty in making glass samples with less than 20 mol% SnO content as a result of the high melting temperature, greater than 1600°C. Such a high melting temperature will enhance the Al_2O_3 contamination from the crucibles, causing an increase in the viscosity of the melt. Silica crucibles cannot be used because the maximum use temperature for this crucible is about 1400°C.

Experiments to make glass of low SnO contents via the sol-gel process have been attempted using di-hydrated tin (II) chloride ($SnCl_2.2H_2O$) dissolved in butan-1-tol $\{CH_3(CH_2)_3.OH\}$ and tetraethyl silicate $\{ Si(OC_2H_5)_4 \}$. The gel was succesfully prepared but $SnCl_2$ crystallised out when the gel was dried. The chlorine content of the gel could not be cured out and the attempt was abandoned.

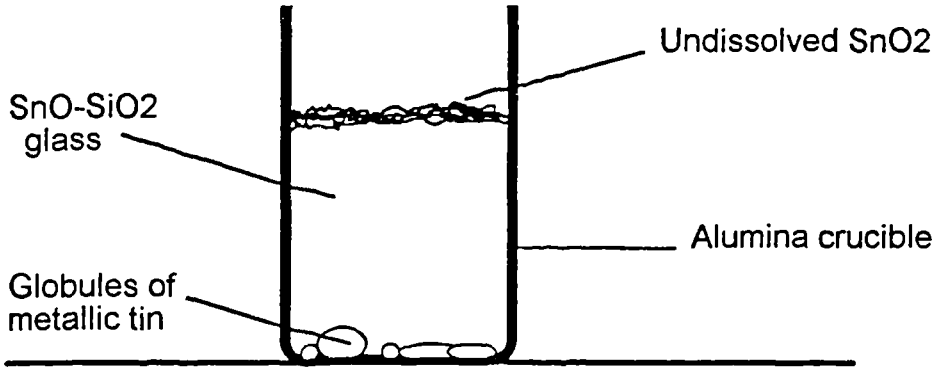

(a)

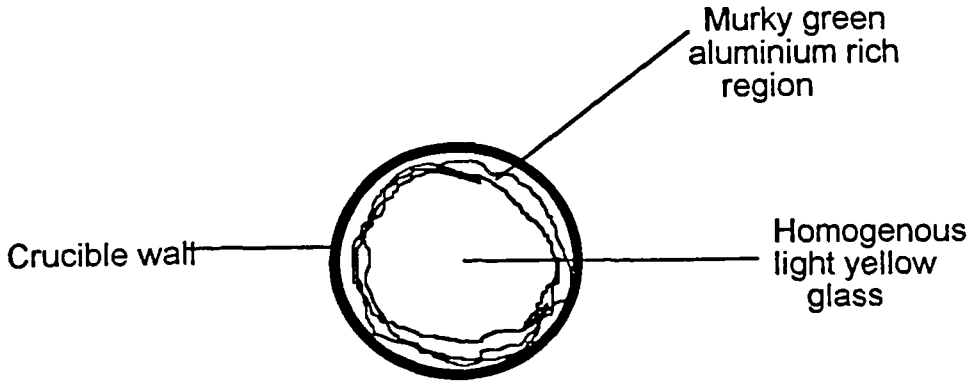

(b)

Figure 5.1 : *(a) Glass formed in the middle of the crucible, globules of tin metal at the bottom and undissolved SnO_2 at the top.*

(b) Cross section of the crucible , showing how glass with low SnO (≤20 mol.%) content formed.

5.3 COMPOSITION AND GLASS STABILITY

The nominal and analysed compositions of the glasses studied are given in Table 5.1. As seen in this table, the maximum mol% of SnO that can be incorporated in the glass by the melting of compressed, pelleted mixture in a covered alumina crucible is 71.5 mol% (nominal 80 mol% SnO). This is much higher than the 59 mol% and 57 mol% previously prepared by Carbo Nover & Williamson [1] and Ishikawa & Akagi [2] respectively. Increasing the SnO content beyond 71.5 mol% was attempted with a nominal SnO content of 85 mol%, but the melt never cooled to a glass.

Table 5.1: *The nominal and analyzed composition of SnO - SiO_2 glasses*

Glass	*Nominal SnO content (mol%)*	*Melting temperature (°C)*	*Analyzed Composition (mol%)*			*% of the nominal SnO content that goes into the glass*
			SnO (Chemical ± 1.6%)	*SiO_2 (By difference)*	*Al_2O_3 (NMR ± 0.16%)*	
TS0	*0*	-	*0*	*100*	-	-
TS1	*20*	*1600*	*16.8*	*83.0*	*0.2*	*84*
TS2	*32.0*	*1350*	*28.2*	*71.2*	*0.6*	*88*
TS3	*33.3*	*1350*	*29.6*	*70.13*	*0.27*	*89*
TS4	*40*	*1350*	*32.6*	*67.09*	*0.31*	*82*
TS5	*47.2*	*1200*	*39.7*	*60.0*	*0.3*	*84*
TS6	*50*	*1000*	*40.9*	*58.7*	*0.4*	*82*
TS7	*60*	*1150*	*49.4*	*50.4*	*0.2*	*82*
TS8	*65*	*1200*	*53.5*	*46.4*	*0.1*	*82*
TS9	*70*	*1200*	*55.4*	*43.3*	*1.3*	*79*
TS10	*75*	*1200*	*64.0*	*35.4*	*0.6*	*85*
TS11	*80*	*1200*	*71.5*	*27.4*	*1.1*	*89*

Therefore the limit of glass formation is about 70 mol% SnO, which is greater than the orthosilicate composition of 2SnO.SiO2 i.e with an O:Si ratio > 4. Figure 5.2 is the modified phase relationship for the SnO-SiO_2 glass system showing the limit of glass formation. High SnO contents can be incorporated not only in silicate glass but in

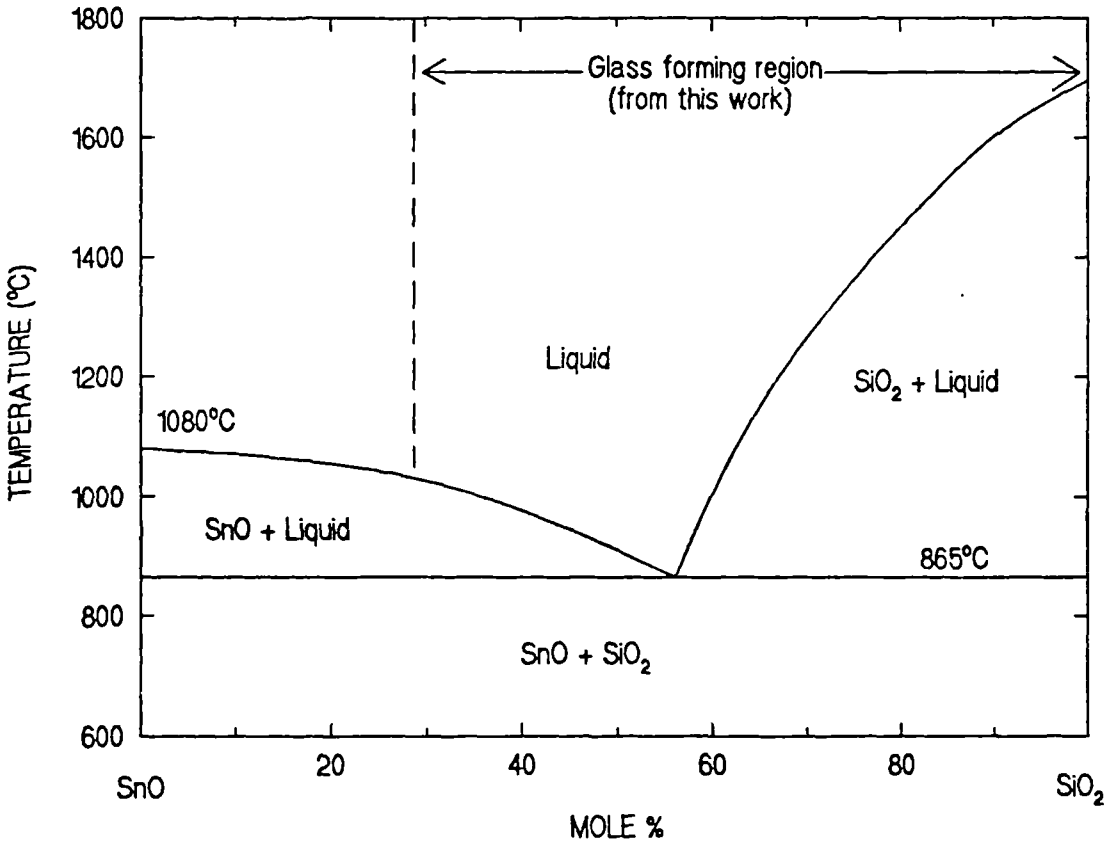

Figure 5.2: *Modified phase relationship for the SnO-SiO_2 glass system based on reference [5]*

other glass systems too. In the SnO - GeO_2 glass system, glass can form with $x > 2$ (Sn_xGeO_{2+x}) which is past the orthogermanate composition [6]. In the SnO - B_2O_3 system , glass can form with up to 58 mol% SnO [7]. One must assume that in these glasses a high proportion of isolated SiO_4 or BO_3/BO_4 or GeO_4 groups are present in the melt, a situation which we would expect to lead to crystallisation on cooling.

As SnO and PbO crystal structures are similar, we can compare the glass systems of SnO-SiO_2 with PbO-SiO_2. Fajans & Kreidl [8] and Stanworth [9] have explained the stability of PbO-SiO_2 glasses of high PbO contents in terms of the high polarizing power of Pb^{2+} ion. By analogy, the stability of these glasses can be explained by the polarizing power of the cation Sn^{2+}. The polarizing power of a cation can be approximated by the ratio of its charge (valency) to its ionic radius [10]. Comparing the polarizing power of Sn^{2+} with Pb^{2+} and Na^+ below,

Ion	**Radius,r (Å)**	**Polarizing power , z/r ($Å^{-1}$)**
Pb^{2+}	1.18	1.69
Sn^{2+}	0.93	2.15
Na^+	1.02	0.98

we can see that the polarizing power of Sn^{2+} is higher than Na^+ and of the order of the Pb^{2+} ion. This results in Sn—O bonds being more covalent and directional than Na—O bonds. Therefore, kinetic stability of the glass is enhanced because it will be more difficult to rearrange SiO_4 groups linked together via these directed bonds than would be the case if the bonds had no directional character. The covalency of the Sn—O bond is illustrated by the asymmetrical character of the bonding between a Sn^{2+} ion and the surrounding oxygen anions in the structure of SnO (Figure 2.11). It has a layer structure in which the tin atom lies at the apex of a square pyramid. The Sn^{2+} ion is considerably closer and more strongly bonded to these four oxygens than

the four in the layer above. This is a consequence of the inert pair effect where, in this instance, an electron pair in an orbital with significant p_z or d_{z^2} character takes no part in bonding ((Figure 2.11(a)).

The average % of the nominal SnO contents that go into the glasses is 84 %. The analyzed composition of the glasses also shows that the samples were contaminated by Al_2O_3 from the crucibles. The Al_2O_3 contamination ranged from a minimum of 0.1 mol% to a maximum of 1.3 mol%.

5.4 ^{119}Sn NUCLEAR MAGNETIC RESONANCE SPECTRA

The static ^{119}Sn NMR spectra for the glasses are very broad, having a typical FWHM value of ~900 ppm. Although very broad, the lineshapes have an axial site symmetry and contain two visually resolvable tin sites. To determine the tin sites in the glass, the spectrum was compared with the spectrum of tetragonal SnO and crystalline SnO_2 recorded under identical conditions. Figure 5.3 shows a spectrum of the glass, superimposed on the spectrum of SnO and SnO_2. By this way, the glasses have been shown to contain not only Sn^{2+} , but also a very small amount of dissolved Sn^{4+} species. Spinning the samples at the magic angle with typical spinning speeds of 10 kHz did not narrow the lines very much, but they clearly showed the two tin sites in the glasses. Figure 5.4 shows a typical spinning spectrum of the glass. The Mössbauer spectra of the glass (section 5.7) also indicated the presence a very small amount of dissolved Sn^{4+} but none of the glasses contained more than 1 mol.% Sn^{4+}. Therefore, tin in the glasses is mostly in Sn^{2+} state. The limited amount of Sn^{4+} dissolved in these glasses is compatible with the fact that its solubility in silica is very small.

By comparing some of the spectral features of the glasses with SnO and SnO_2 , it is possible to describe the environment of tin in the glasses as compared to its crystalline form. Cossement et al [11] studied the NMR chemical shift anisotropy of SnO_2 and SnO crystals found that the chemical shift anisotropy of SnO is very large

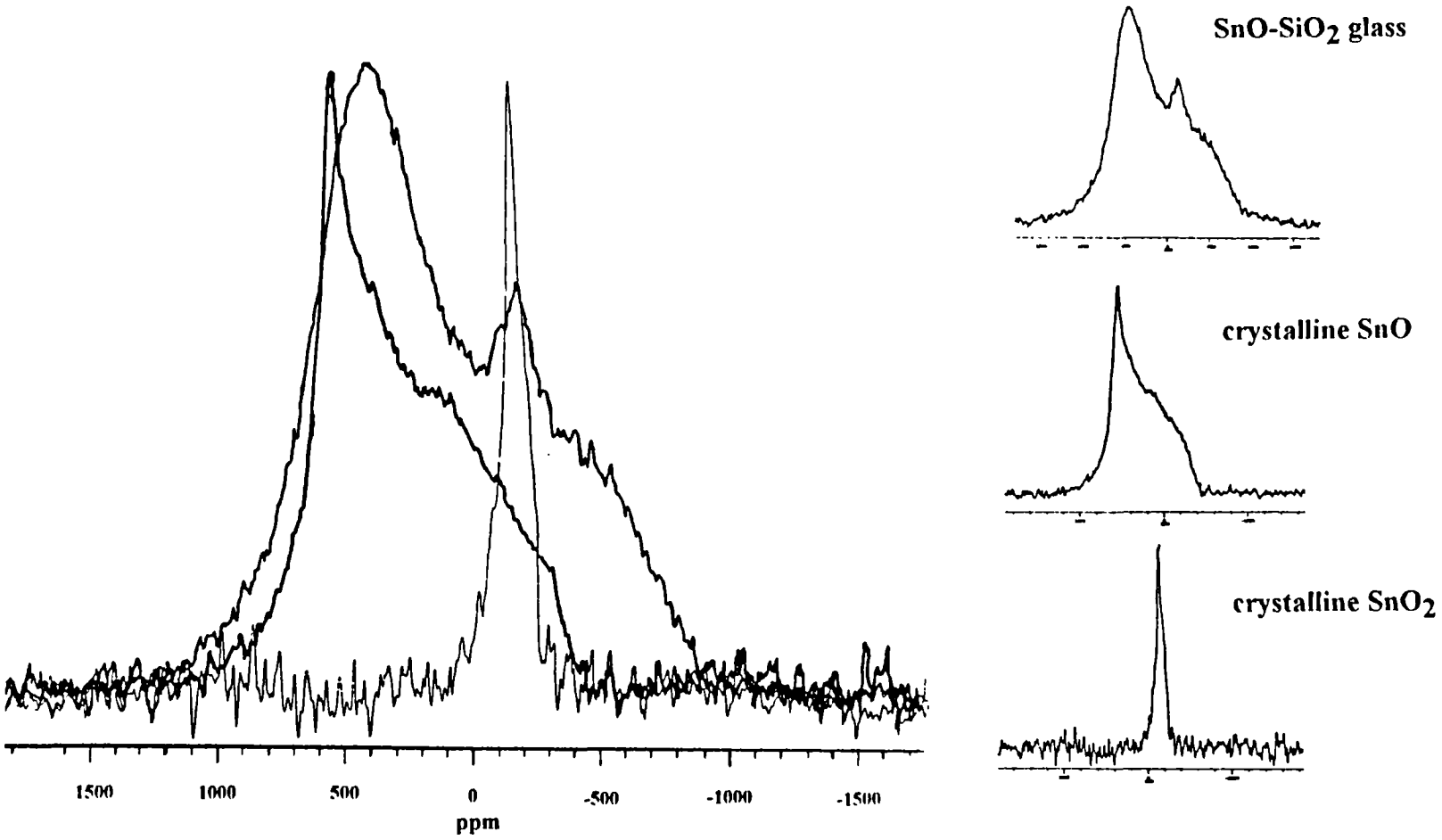

Figure 5.3: *^{119}Sn static NMR spectrum of a SnO-SiO_2 glass superimposed on the ^{119}Sn static NMR spectra of crystalline SnO and SnO_2.*

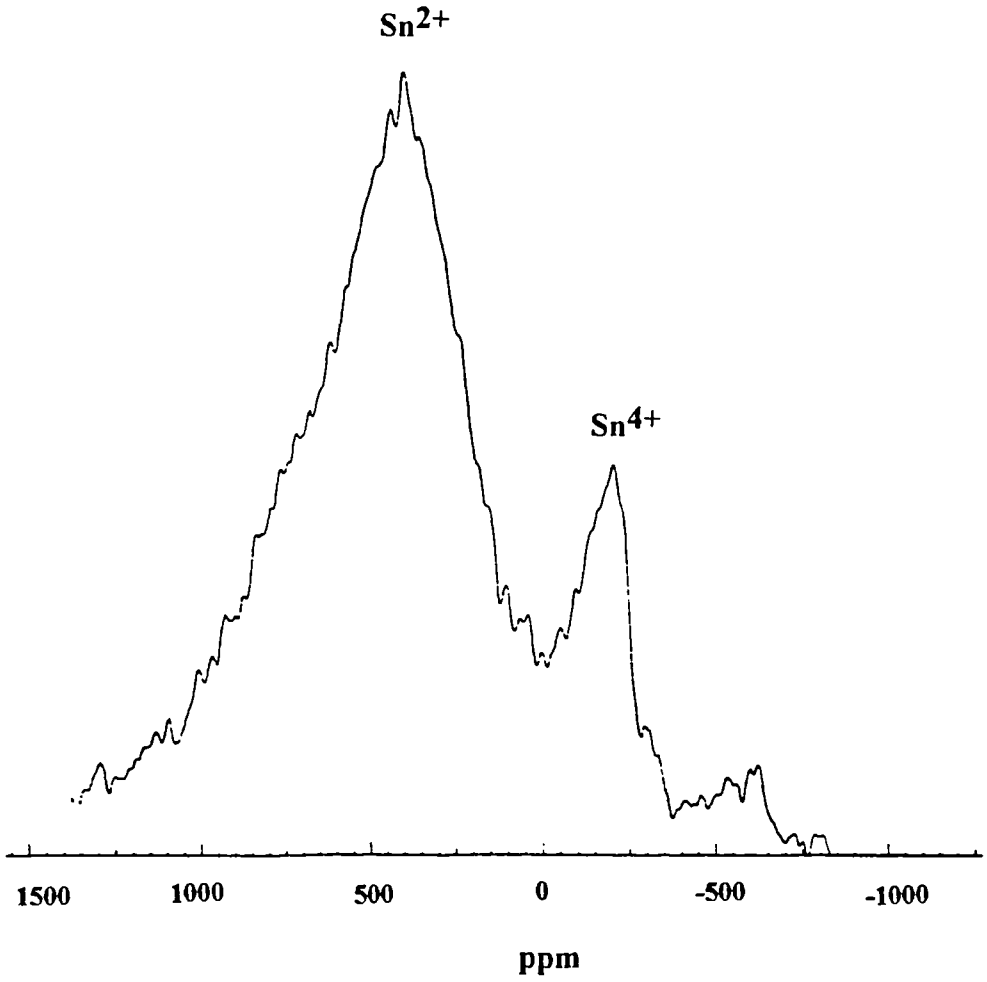

Figure 5.4: *A ^{119}Sn MAS NMR spectrum of a SnO-SiO_2 glass that clearly shows the presence of both oxidation states of Sn^{2+} and Sn^{4+} in the glass..*

and about 7 times greater than that of SnO_2. Thus the width of the lineshape from the SnO crystal is dominated by the chemical shift anisotropy. This has been ascribed as being mainly due to the asymmetry in the valence electron cloud of the tin atom in the SnO crystal structure. The tetragonal SnO powder spectral lineshape recorded in this study shows that it has an axial site symmetry and this conforms well to the Cossement et al spectrum. In the glass, the Sn^{2+} site also shows an axial site symmetry, with the width broadened and the lineshape envelope moving towards higher field positions with increasing SnO. This indicates that the ionic character of Sn^{2+} decreases with tin content, its environment is distorted but retains the features of its crystalline form. The position of the Sn^{4+} peak in the glass did not change relative to the peak of SnO_2, indicating that the environment of Sn^{4+} in the glass is the same as in the crystal.

The width of the static ^{119}Sn NMR spectrum of SnO is due to the large chemical shift anisotropy and in disordered material like glass, spinning the samples at 10 kHz did not remove the anisotropy. Indeed in crystalline SnO, Cossement et al need a speed of 12 kHz in order to remove the chemical shift anisotropy. Thus, to get a high resolution spectrum of Sn^{2+} in glass, we need to spin the sample at a very high rotation speed. Nevertheless, in this study the static ^{119}Sn NMR has shown that these glasses contain tin in both the Sn^{2+} and Sn^{4+} oxidation states, although the former is by far the dominant species.

5.5 STATIC ^{29}Si NUCLEAR MAGNETIC RESONANCE SPECTRA

Some of the static ^{29}Si NMR spectra of the stannous silicate glasses and their analyzed compositions are shown in Figure 5.5(a). The static spectra showed only a single broad peak which contained no resolvable structural features. Visually, the peak shapes do not show much resemblance to the theoretical static powder patterns that show the different Q^n species in alkali silicate glasses (see Figure 5.5(b)). For SnO

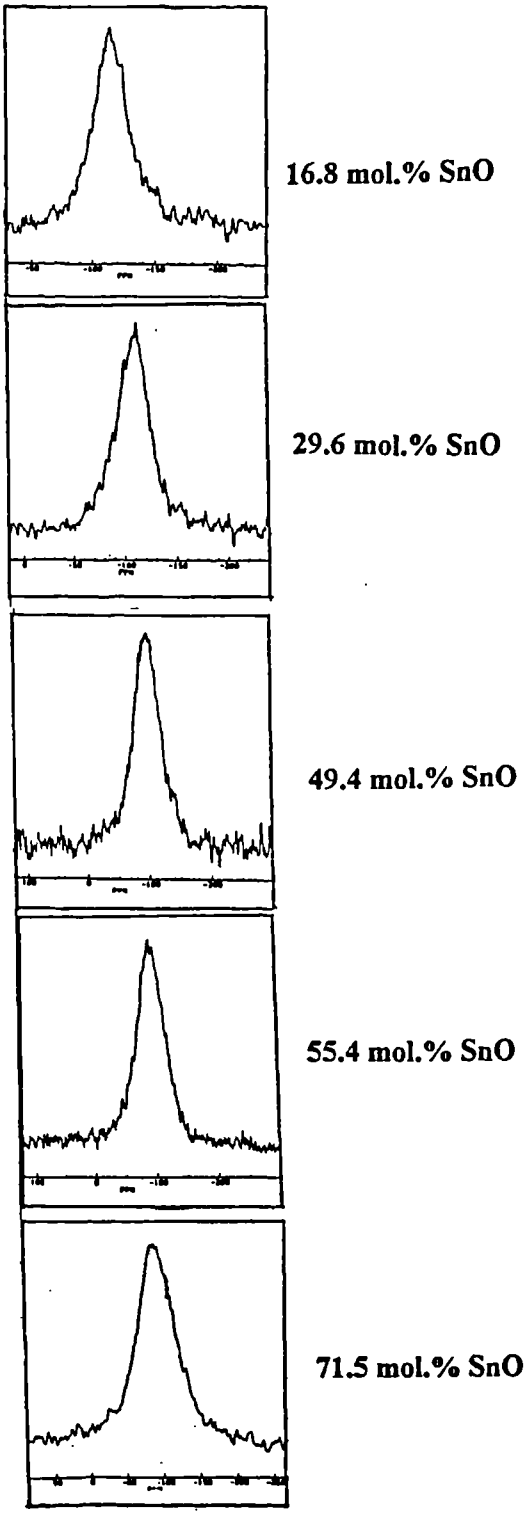

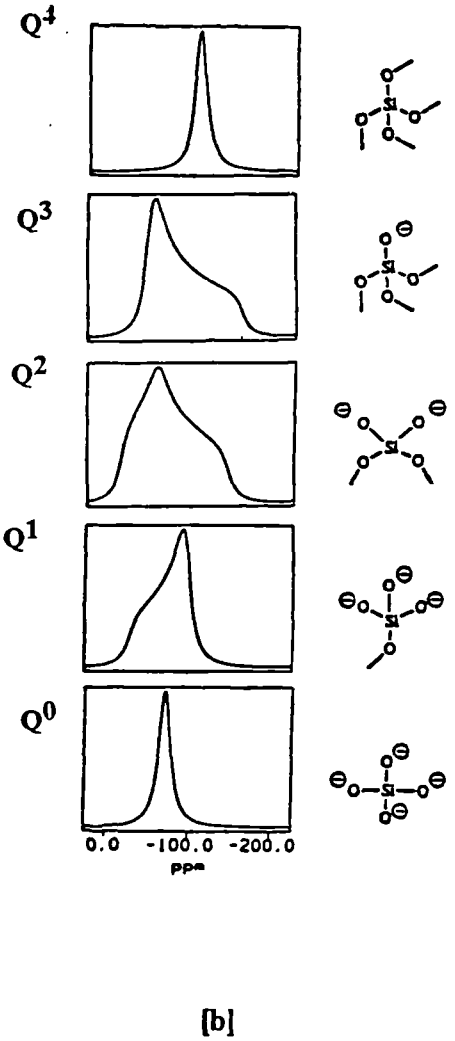

Figure 5.5 : *(a) Some static ^{29}Si NMR spectra of $SnO\text{-}SiO_2$ glasses as compared to (b) the theoretical static chemical shift powder patterns of ^{29}Si NMR of alkali silicates glasses taken from reference [14].*

contents of < 50 mol% the expected asymmetry of the peaks is not pronounced in that some are quite symmetric. This is in stark contrast to the static spectra of sodium silicate and lithium silicate [12] and lead silicate [13] which show clear asymmetrical (axially or lower symmetry) peaks that give evidence of the formation of different Q species as the modifier oxides vary in the glasses. The ^{29}Si NMR spectral parameters are summarised in Table 5.2.

As can be seen from Table 5.2 the chemical shift decreases from -110 ppm for 16.8 mol.% SnO to -89 ppm for 71.5 mol% SnO. This shows that the chemical shift range is relatively small when compared to alkali silicate glasses [14]. The peak shapes go from being quite symmetric at 16.8 mol% SnO to quite asymmetric for SnO contents of about 29 to 50 mol% and become quite symmetric again for SnO contents of greater than 50 mol%. The peak for the 71.5 mol% glass is symmetric.

Table 5.2: *^{29}Si static NMR data for $SnO\text{-}SiO_2$ glasses*

Samples	*Mol% SnO*	*Peak position of chemical shift (±2ppm)*	*FWHM (± 2ppm)*	*Visual characteristic of peak*
TS1	*16.8*	*-110*	*28*	*quite symmetric*
TS3	*29.6*	*-108*	*33*	*quite asymmetric*
TS4	*32.6*	*-104*	*35*	*quite asymmetric*
TS5	*39.7*	*-101*	*45*	*quite asymmetric*
TS7	*49.4*	*-98*	*47*	*quite asymmetric*
TS9	*55.4*	*-91*	*48*	*quite symmetric*
TS11	*71.5*	*-89*	*53*	*symmetric*

Zachariasen's random network theory predicts that, at SnO contents of greater than 50 mol%, most of the SiO_4 tetrahedra should be metasilicate (Q^2). And at 71.5 mol%

SnO, stoichiometrically, the glass should contain only spherically symmetric Q^0 (SiO_4^{4-}) units in a SnO matrix. The anisotropy associated to Q^0 is zero [15] and at this composition the static peak should be symmetric and its FWHM should decrease. However, the FWHM continues to increase with the increase of SnO. In disordered material like glass, there may be some anisotropy of Q^0 due to variation in the second coordination sphere. According to Eckert [14] this type of behavior suggests that the broadening mechanism is dominated more by dipole-dipole coupling, than chemical shift anisotropy. As Sn and Si nuclei are both spin ½ and the natural abundance of magnetically active Sn nuclei is about double that of Si, there is a reasonable probability that the dipole-dipole interaction is heteronuclear. Thus there must be some sort of Si-O-Sn linkages at high SnO contents.

It is instructive to compare these results to those from the $PbO-SiO_2$ glass system. Fujui and Ogino [13] who studied the $PbO-SiO_2$ glasses by static NMR observed that, for PbO contents of greater than 50 mol%, the peak shape is symmetric. They concluded that the three dimensional SiO_4 network remains and a certain number of PbO_2 groups interconnect with SiO_4 tetrahedra. Thus PbO_2 groups must act like glass forming polyhedra at high PbO contents.

The ^{29}Si static NMR of $SnO-SiO_2$ glasses is inadequate to explain the structure of these glasses, especially the speciation of different Q species as a function of composition. We turn to ^{29}Si MAS NMR in next section.

5.6 ^{29}Si MAGIC ANGLE SPINNING NUCLEAR MAGNETIC RESONANCE SPECTRA

Some of the ^{29}Si MAS NMR spectra of stannous silicate glass are shown in Figure 5.6. Spinning the samples at the magic angle narrowed the peaks of the ^{29}Si spectra but to a still relatively broad single line. Table 5.3 gives the parameters of the ^{29}Si MAS NMR spectra.

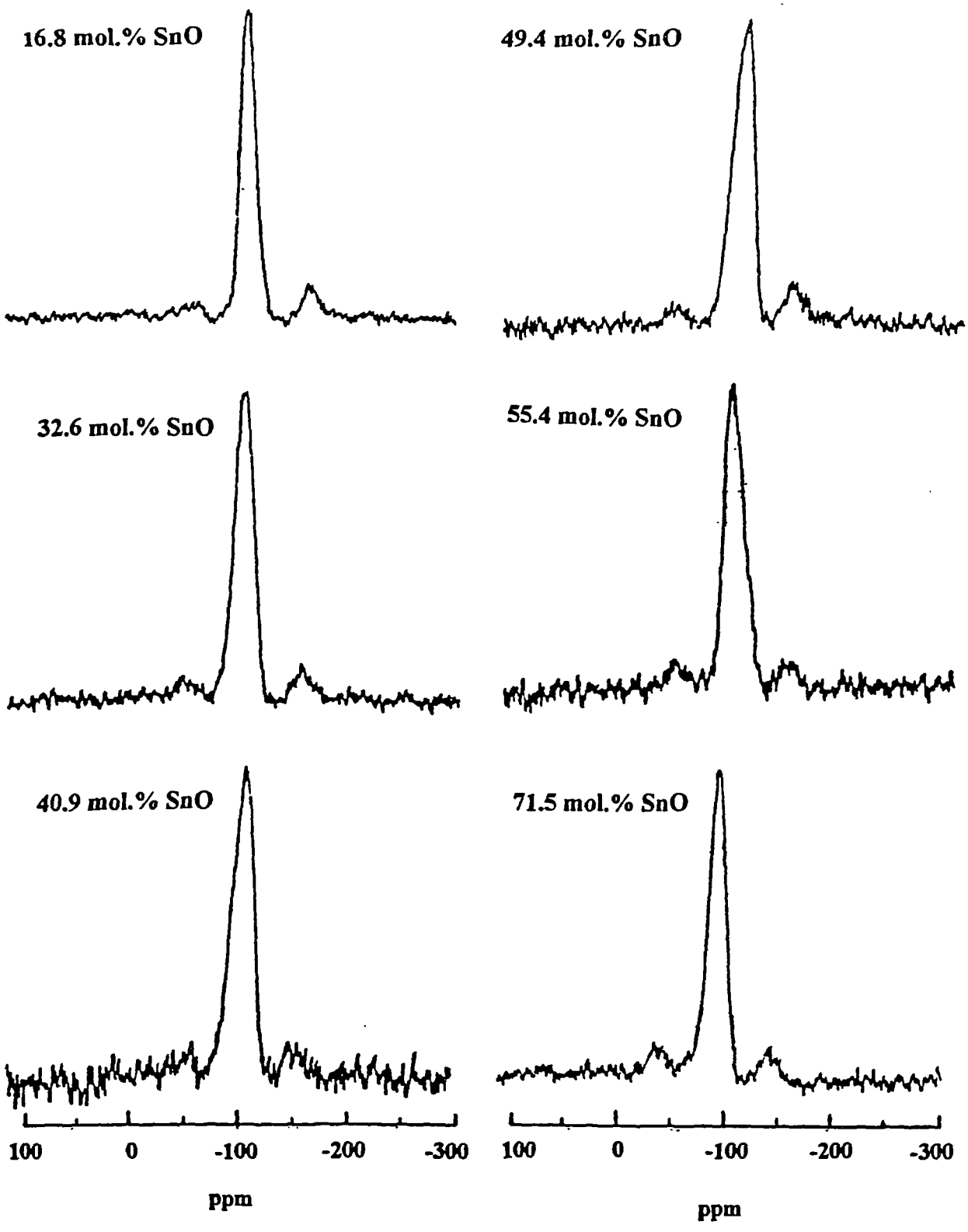

Figure 5.6 : *Some ^{29}Si MAS NMR spectra of SnO-SiO_2 glasses*

Table 5.3: *^{29}Si MAS NMR data for SnO-SiO_2 glasses*

Samples	*Mol% SnO*	*Peak position of chemical shift (±0.1 ppm)*	*FWHM (±0.1 ppm)*
*TS0**	*0*	*-112*	*11.5*
TS1	*16.8*	*-110.6*	*13.9*
TS2	*28.2*	*-109.4*	*19.4*
TS3	*29.6*	*-107.1*	*19.6*
TS4	*32.6*	*-105.6*	*20.8*
TS5	*39.7*	*-103.3*	*23.6*
TS6	*40.9*	*-100.6*	*23.2*
TS7	*49.4*	*-97.6*	*22.2*
TS8	*53.5*	*-96.2*	*20.9*
TS9	*55.4*	*-92.2*	*19.4*
TS10	*64.0*	*-89.7*	*19.2*
TS11	*71.5*	*-87.7*	*18.9*

**Taken from reference [14]*

5.6.1 CHEMICAL SHIFT

The chemical shifts, at maximum peak intensity, cover the range from -112 ppm for 0 mol% SnO to -87.7 ppm for 71.5 mol% SnO. The chemical shift range is narrower than that for the PbO-SiO_2 glasses and much narrower than that observed for alkali-silicate glasses (Table 5.3).

Table 5.4: *Comparison of ^{29}Si MAS NMR chemical shift range in SnO-SiO_2, PbO-SiO_2 and Na_2O-SiO_2 glass systems.*

Glass system	*SnO-SiO_2*	*PbO-SiO_2 [17]*	*Na_2O-SiO_2 [14]*
Modifier Oxide range (mol%)	*0 → 71.5*	*0→ 73.4*	*0 →50*
Chemical Shift range (ppm)	*-112 → 87.7*	*-112 →82.2*	*-112 →77.7*

The narrowness of the chemical shift range in $SnO-SiO_2$ glassses can be seen in Figure 5.7. which shows a plot of chemical shift versus composition of $SnO-SiO_2$ glasses as compared to the $PbO-SiO_2$ and Na_2O-SiO_2 systems. It can be seen that the chemical shift changes very slowly with composition. Two interpretations could be made:

(1) This could mean that SnO does not depolymerize the silicate network to the same extent as modifiers such as Na_2O or even PbO. At low concentrations of SiO_2 there will still be silicate polyanions which implies that segregation or clustering is occuring, with silica rich units present in an SnO matrix.

(2) Alternatively, because the electronegativity of Sn is identical to that of Si, the Si nucleus sees an only slowly varying environment as the composition changes. Thus, the electron redistribution on going from an Si-O-Si to an Si-O-Sn linkage produces very little change in the electron density seen by the Si nucleus and this is reflected in the comparatively narrow chemical shift range for Si in this glass.

It should also be pointed out that the chemical shift for the metastable $SnSiO_3$ crystal phase produced on devitrification is shifted considerably from the chemical shift values of the glasses. For example, the silicon resonance in 40.9 mol% SnO glass occurs at -100.6 ppm but in the $SnSiO_3$ crystal phase, the silicon resonance is at -111.4 ppm. This confirms that there are no "crystal like" areas in the glass structure. The fact that glasses in the composition range from ~ 40 mol% to ~50 mol% SnO, in which the metastable $SnSiO_3$ crystal phase grow, are glasses that have the widest ^{29}Si resonance half width, suggests that there is an increased range of Si-O-Si bond angles in these glasses or that there are a larger number of Q^n species species present (statistical model).

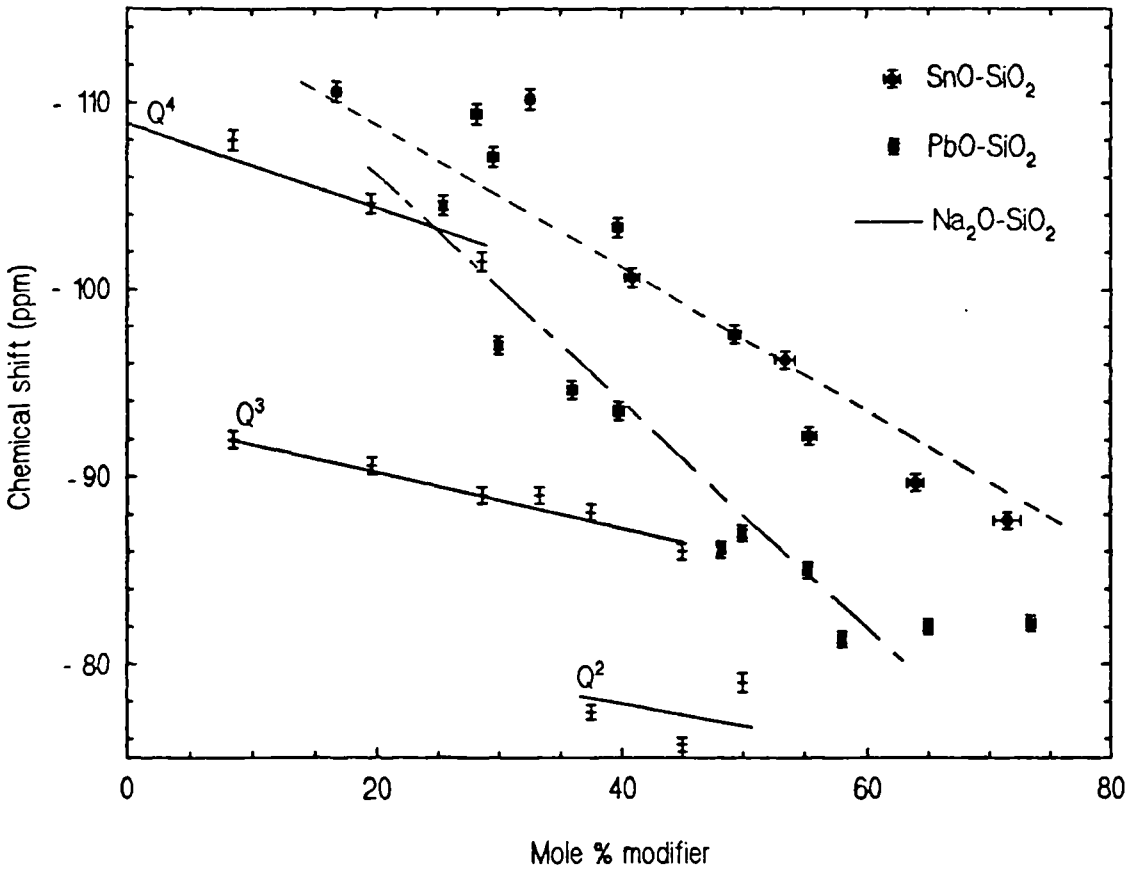

Figure 5.7: *Position of peak maxima for ^{29}Si MAS NMR spectra in various silicate glasses.*

5.6.2 FULL WIDTH AT HALF MAXIMUM (FWHM) AND PEAK SHAPE

The FWHM of the resonance increases gradually from about 14 ppm at 17 mol% SnO to a maximum value of 23 ppm at 41 mol% SnO before decreasing slowly to about 19 ppm at 70 mol% SnO. This trend is similar to that observed in the $PbO\text{-}SiO_2$ glasses (Figure 5.8). The ^{29}Si MAS NMR spectra of stannous silicate glasses shown in Figure 5.6 , consist of a single, broad and generally asymmetric peak which could contain resonances of more than one type of Q^n species. For compositions containing up to 55 mol% SnO the peaks are asymmetric. Their side bands are such that the lower frequency side is of greater intensity. This pattern of side bands is just the opposite to that observed in $Na_2O\text{-}SiO_2$, $Li_2O\text{-}SiO_2$, $Rb_2O\text{-}SiO_2$, $Cs_2O\text{-}SiO_2$ [15-17] and even in the $PbO\text{-}SiO_2$ [18]. In these systems the lower frequency side band is always of lower intensity than the high frequency side band. This is an indication that the formation of lower Q^n species with increase of SnO is slow in $SnO\text{-}SiO_2$ glass system. Which could mean that SnO does not depolymerise the silicate network as quickly as in other binary silicate glasses i.e. there are $[SnO_x]_n$ polymeric units present.

For compositions containing ~55 mol% SnO or less the observed spectra could reasonably be resolved into two lines, one narrow and one broad. The narrow Gaussian which lies in the range of chemical shift corresponding to a Q^4 resonance, predominates at high SiO_2 contents and decreases as SnO increases and may still be present at ~ 55 mol% SnO. This is not expected for a binary distribution where all Q^4 should have been replaced by Q^3 at 33.3 mol% modifier oxide, as in the $Na_2O\text{-}SiO_2$ system. The broader component may be composed of all other possible Q^n types.

In the composition range from 30 to 50 mol% SnO, where the FWHM are comparatively broader, the spectra may contain all possible Q types but are dominated by the less symmetric Q^3, Q^2 and Q^1 species. For an SnO content of 64 mol% the peak and its side bands are quite symmetric which shows that the resonance may be

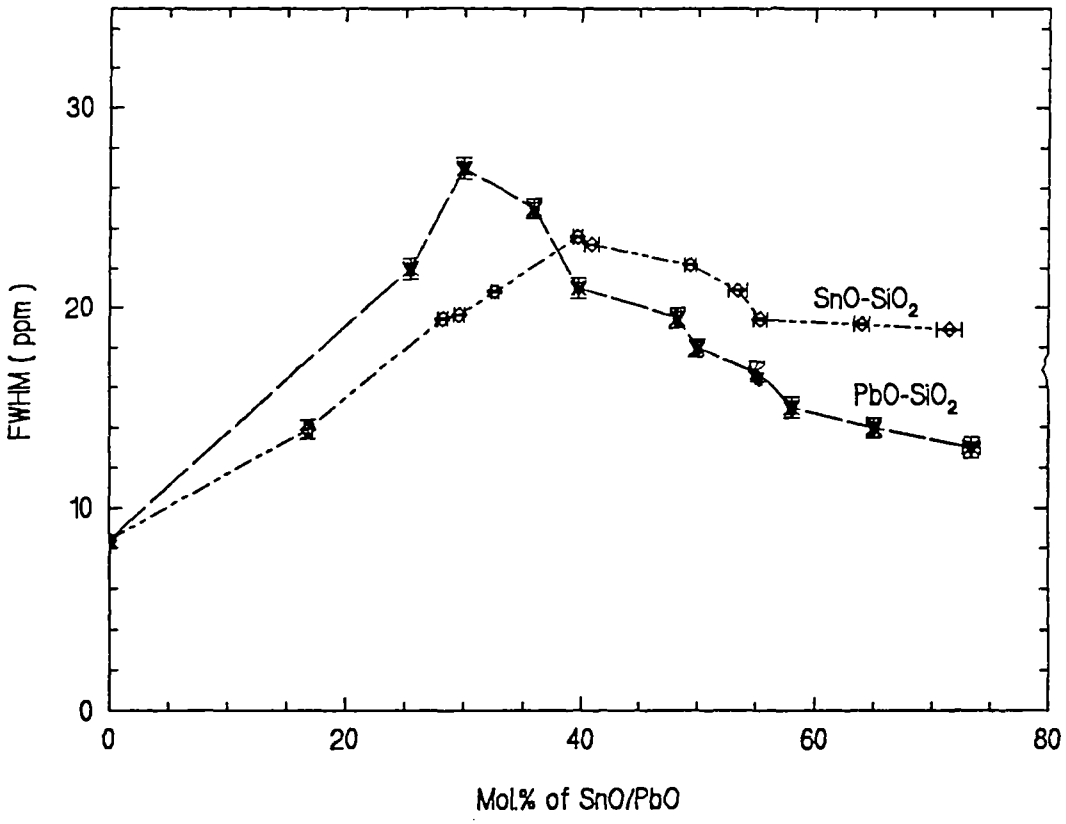

Figure 5.8: *Full width at half-maximum versus SnO/PbO contents for ^{29}Si MAS NMR spectra of $SnO\text{-}SiO_2$ and $PbO\text{-}SiO_2$ glasses.*

dominated by Q^0 species. At 71.5 mol% SnO the peak and the side band intensities are symmetric which is expected for a resonance from Q^0 species.

In order to clarify the presence of the different Q^n species and their distribution as a function of composition; the experimental peak shapes have been computer simulated using various combinations of Gaussians. The results of this exercise are discussed next.

5.6.3 DISTRIBUTION OF Q^n SPECIES

It was pointed out in Chapter 2 (section 2.2.1), that the properties of a glass depend on the quantities of different Q^n species and their distribution. Depending on the system and composition, the Q^n distribution for most glasses follows the binary or the statistical model. The binary model may be considered as arising from the 'repulsion' of non-bridging oxygens such that there are no more than two Q^n species distributed as uniformly as possible through the glass. Generally, most studies found that the alkali metal silicate glasses follow the binary distribution but the review by Eckert [14] refers to deviation from the binary distribution for high-field strength, alkali metal cations at low SiO_2 contents. The statistical distribution model was first developed by Lacy [19-20] to describe the viscosity of silicate melts. Later, Dupree et al [15-17] and Schramm et al [21] used this model in fitting MAS NMR spectra of many binary alkali metal silicate glasses in their analysis. The statistical distribution model has no limit on the number of Q^n species present for any composition and their distribution is determined by composition and statistics. The predictions for the relative proportions of the differents Q species at various compositions, according to the two models are shown in Figure 5.9.

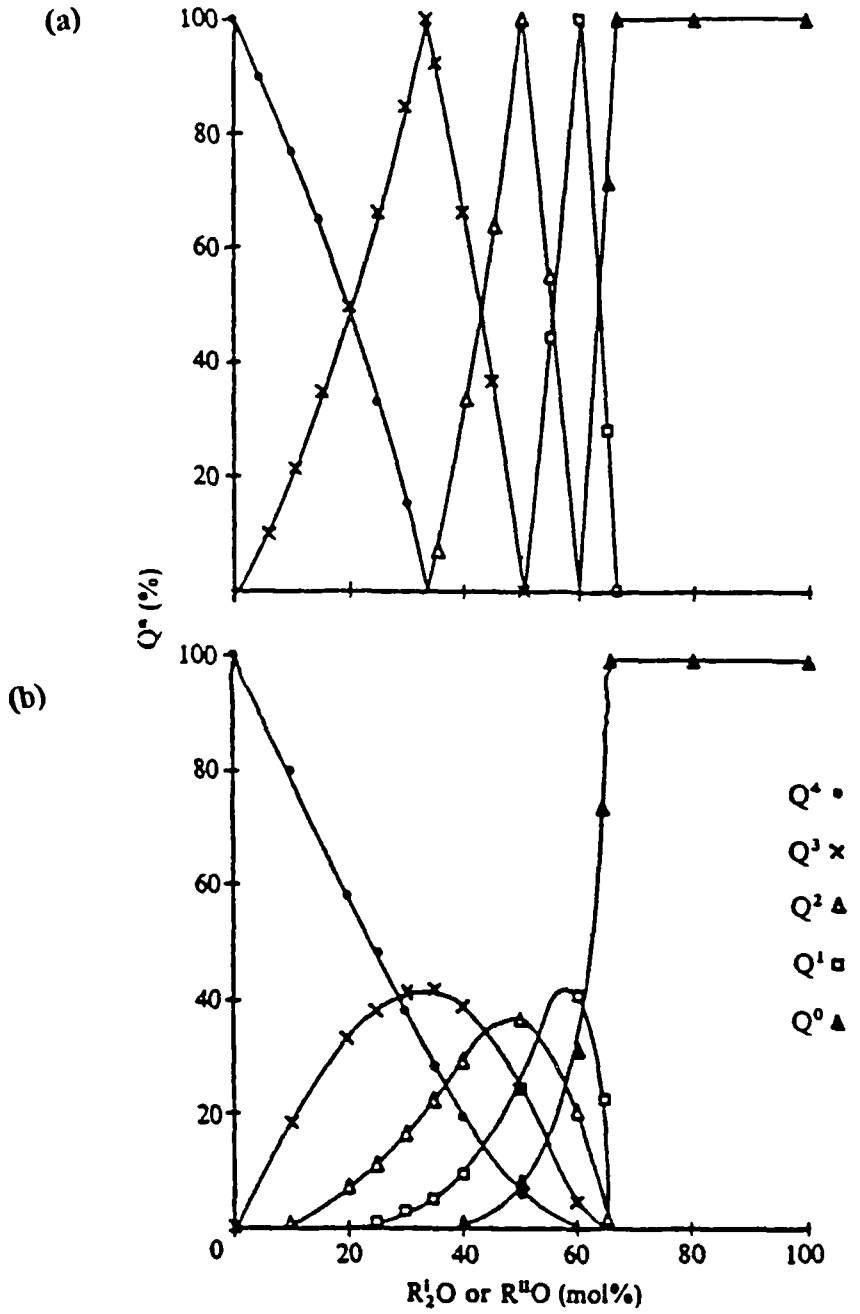

Figure 5.9: *Q^n distributions as predicted by the binary (a) and statistical (b) models taken from reference [17].*

In this fitting exercise, seven spectra were chosen that cover the glass forming range of 17 to 70 mol.%. We have assesed the quality of the fit of these spectra to the various numbers of Gaussians predicted by the binary and statistical model and compared the refined intensity of each Gaussian with the expected stoichiometry. Each spectrum was simulated by fitting the entire spectrum (i.e. the centre peak and the sidebands) to a sum of the appropriate number of Gaussians. The width of the sidebands was constrained to be equal to that of the peak about which they were symmetrically placed. Simulations using one, two, three, four or five Gaussians were attempted for some of the spectra. The positions, amplitude and widths of the resonances were varied until the best fit was obtained. However, where more than two Gaussians were involved, the number of variables was too large to allow an unconstrained fit and therefore some variables had to be fixed.

It should be noted that an assumption is made that oxygens would still be distinguished as bridging or non-bridging oxygens; i.e. ignoring any interactions between non-bridging oxygens and Sn^{2+}. The contaminations by Al_2O_3 and SnO_2 (Sn^{4+}) were also ignored because of their negligible amounts. In carrying out the simulation, the chemical shift assigned to a given Q^n type is only based on composition and intuition. This is because there are no solid state NMR data for ^{29}Si in a tin oxide environment available for reference. Peaks from the computer simulation were identified as a specific Q^n by comparison of their computed shift with the interpolated values from the observed data at 0 % SnO (Q^4), 33.3 % SnO (Q^3), 50 % SnO (Q^2), 60 % SnO (Q^1) and 66 % SnO (Q^0). It should also be noted that the quality of the fit and the refined intensities are very sensitive to the exponential line broadening and phasing of the spectrum on Fourier transforming the FID. Therefore the same exponential line broadening of 60 Hz was used prior to Fourier transformation and all spectra were phased using the same parameters.

5.6.3.1 COMPUTER FITTING OF ^{29}Si MAS NMR SPECTRA

Figure 5.10 shows some of the typical fits of the simulated ^{29}Si spectra of the $SnO\text{-}SiO_2$ glasses.

16.8 mol.% SnO

Table 5.5 gives the predicted binary and statistical Q^n distributions, followed by a two Gaussian and a three Gaussian fit. The quality of both fits, as represented by χ^2 are similar. The observed proportions of Q^4 and Q^3 for the two Gaussians fit gives a reasonable match to the predicted binary distribution. However the Q^3 FWHM is 1.7 times broader than that of Q^4 and such a difference is not generally observed for binary alkali silicate glasses. A three Gaussian fitting reproduces the observed spectrum equally well using peaks of similar FWHM and the Q^n distribution gives a reasonable match to the stoichiometry of a statistical Q^n distribution for this glass composition. In both cases more "non-bridging oxygens" are observed than predicted by the models but this overestimate is less for the binary model. Hence this composition is better described by the binary distribution.

Table 5.5 : *Q^n distributions and Gaussian fits for $SnO\text{-}SiO_2$ glass containing 16.8 mol.% SnO*

	Q^4	Q^3	Q^2	Q^1	Q^0	χ^2
Predicted distributions						
Binary (%)	60	40	-	-	-	-
Statistical (%)	65	30	5	-	-	-
Observed distributions						
1. Two Gaussian fit						1.1
Chemical shift	-111.3	-104.9	-	-	-	-
FWHM	10.6	17.7	-	-	-	-
(%)	55	45	-	-	-	-
2. Three Gaussian fit						1.2
Chemical shift	-111.5	-105.6	-96.7	-	-	-
FWHM	12.2	13.1	11.9	-	-	-
(%)	56.8	30.2	13.0	-	-	-

32.6 mol.% SnO

For this composition , the spectrum was simulated by two, three and four Gaussians (Table 5.6). The two Gaussian fit gave Q^4 and Q^2 species (judged by chemical shift) rather than the Q^4 and Q^3 predicted by the binary model and a totally inappropriate distribution of intensity. The three Gaussian fit is a good reproduction of a statistical distribution but the four Gaussian gave somewhat better reproduction of the predicted statistical Q^n distribution. The last two fittings both gave similar χ^2 values. Therefore at this composition the Q^n distributions follow the statistical model.

Table 5.6 : *Q^n distributions and Gaussian fits for $SnO\text{-}SiO_2$ glass containing 32.6 mol.% SnO*

	Q^4	Q^3	Q^2	Q^1	Q^0	χ^2
Predicted distributions						
Binary (%)	3.3	96.7	-	-	-	-
Statistical (%)	33	42	20	5	-	-
Observed distributions						
1. Two Gaussian fit						3.8
Chemical shift	-109.5	-	-100.2	-	-	-
FWHM	13.6	-	20.4	-	-	-
(%)	40.4	-	59.6	-	-	-
2. Three Gaussian fit						2.5
Chemical shift	-113.2	-104.5	-96.7	-	-	-
FWHM	12.2	13.3	11.9	-	-	-
(%)	37.1	38.6	24.3	-	-	-
3. Four Gaussian fit						2.7
Chemical shift	-111.2	-105.9	-96.7	-91.4	-	-
FWHM	13	13	13	13	-	-
(%)	31.4	36.9	21.5	10.2	-	-

39.7 mol.% SnO

Table 5.7 gives the results of two, four and five Gaussian fitting. A two Gaussian fit indicates peak positions corresponding to $Q^3 + Q^1$, and not the $Q^3 + Q^2$ predicted by the binary model. The four Gaussian fit does not indicate the presence of Q^2 species as predicted by the statistical model. But the five Gaussian simulation gives a good fit to the data and excellent reproduction of the predicted statistical distribution.

Table 5.7 : *Q^n distributions and Gaussian fits for SnO-SiO_2 glass containing 39.7 mol.% SnO*

	Q^4	Q^3	Q^2	Q^1	Q^0	χ^2
Predicted distributions						
Binary (%)	-	68	32	-	-	-
Statistical (%)	20	40	29	10	1	-
Observed distributions						
1. Two Gaussian fit						3.1
Chemical shift	-	-105.1	-	-93.5	-	-
FWHM	-	17.3	-	15.8	-	-
(%)	-	70.1	-	29.9	-	-
2. Four Gaussian fit						2.6
Chemical shift	-111.2	-102.9	-	-94.1	-84.6	-
FWHM	10.6	13.3	-	12.6	10.4	-
(%)	25.7	40.5	-	27.4	6.4	-
3. Five Gaussian fit						3.0
Chemical shift	-111.1	-104.7	-97.8	-95.4	-87.1	-
FWHM	13	13	13	13	13	-
(%)	22.9	34.2	26.8	14.6	1.5	-

49.5 mol.% SnO

The results of fitting the spectrum of 49.5 mol.% SnO are shown in Table 5.8. The spectrum can be simulated by two Gaussians but the Q^n species thus found are Q^3 and Q^1 rather than Q^3 and Q^2 as predicted by the binary model. The four Gaussian fit

does not indicate the presence of Q^1 species as predicted by the statistical model. The five Gaussian fit has the lowest χ^2 value and gave a reasonably acceptable match of Q^n to the statistical prediction.

Table 5.8 : *Q^n distributions and Gaussian fits for SnO-SiO_2 glass containing 49.5 mol.% SnO*

	Q^4	Q^3	Q^2	Q^1	Q^0	χ^2
Predicted distributions						
Binary (%)	-	4	96	-	-	-
Statistical (%)	7	26	38	24	5	-
Observed distributions						
1. Two Gaussian fit						3.6
Chemical shift	-	-105.3	-	-93.5	-	-
FWHM	-	15.7	-	17.4	-	-
(%)	-	37.5	-	62.5	-	-
2. Four Gaussian fit						2.6
Chemical shift	-113.5	-105.3	-96.4	-	-88.4	-
FWHM	12.2	14.4	14.0	-	15.3	-
(%)	3.3	30.6	45.9	-	20.1	-
3. Five Gaussian fit						2.3
Chemical shift	-109.1	-103.3	-97.2	-91.5	-86.1	-
FWHM	13	13	13	13	13	-
(%)	14.0	21.9	32.9	19.7	11.5	-

55.4 mol.% SnO

Two, three, four and five Gaussian fits were attempted on this composition (Table 5.9). The spectrum can be fitted to two and three Gaussians but does not satisfy the prediction of the binary and statistical model respectively. The four Gaussian fit does not indicate the presence of Q^0, but the relative proportions of the other species are quite close to the predicted values. The five Gaussian fit has the lowest χ^2 value and reasonably satisfies the prediction of the statistical model.

Table 5.9 : *Q^n distributions and Gaussian fits for SnO-SiO_2 glass containing 55.4 mol.% SnO*

	Q^4	Q^3	Q^2	Q^1	Q^0	χ^2
Predicted distributions						
Binary (%)	-	-	48	52	-	-
Statistical (%)	2	14	33	36	15	-
Observed distributions						
1. Two Gaussian fit						5.6
Chemical shift	-	-106.7	-	-92.3	-	-
FWHM	-	13.6	-	18.5	-	-
(%)	-	18.3	-	81.7	-	-
2. Three Gaussian fit						4.7
Chemical shift	-	-107.7	-97.1	-	-87.9	-
FWHM	-	12.3	14.4	-	13.9	-
(%)	-	17.0	40.3	-	42.7	-
3. Four Gaussian fit						4.7
Chemical shift	-109.5	-107.2	-98.5	-90.8	-	-
FWHM	14	14	14	14	-	-
(%)	1.7	23.4	28.6	46.3	-	-
4. Five Gaussian fit						3.8
Chemical shift	-108.2	-99.9	-93.7	-87.5	-85.7	-
FWHM	13	13	13	13	13	-
(%)	13.4	23.9	29.7	20.2	12.8	-

64.0 mol.% SnO

Table 5.10 shows the results of two, three and four Gaussian fit for this composition. The two Gaussian fit does not satisfy the binary model prediction. The three Gaussian gave a very good match of Q^n to the statistical prediction. The four Gaussian fit has the lowest χ^2 but does not satisfy the stoichiometry of the composition.

Table 5.10 : *Q^n distributions and Gaussian fits for SnO-SiO_2 glass containing 64.0 mol.% SnO*

	Q^4	Q^3	Q^2	Q^1	Q^0	χ^2
Predicted distributions						
Binary (%)	-	-	-	24	76	-
Statistical (%)	-	-	6	31	63	-
Observed distributions						
1. Two Gaussian fit						8.7
Chemical shift	-	-	-99.9	-	-89.3	-
FWHM	-	-	16.0	-	16.0	-
(%)	-	-	28.9	-	71.1	-
2. Three Gaussian fit						10.8
Chemical shift	-	-	-101.9	-98.0	-87.9	-
FWHM	-	-	14.0	13.7	13.0	-
(%)	-	-	6.7	33.7	59.9	-
3. Four Gaussian fit						7.8
Chemical shift	-	-105.9	-99.9	-94.8	-86.4	-
FWHM	-	13	13	13	13	-
(%)	-	7.7	12.2	34.3	46.4	-

71.5 mol.% SnO

The spectrum of this glass is symmetric and both models predict a single species , Q^0.

A one Gaussian fit gave an excellent fit as shown in Table 5.11.

Table 5.11 : *Q^n distributions and Gaussian fits for SnO-SiO_2 glass containing 71.5 mol.% SnO*

	Q^4	Q^3	Q^2	Q^1	Q^0	χ^2
Predicted distributions						
Binary (%)	-	-	-	-	100	-
Statistical (%)	-	-	-	-	100	-
Observed distributions						
1. One Gaussian fit						0.8
Chemical shift	-	-	-	-	87.9	-
FWHM	-	-	-	-	19.1	-
(%)	-	-	-	-	100	-

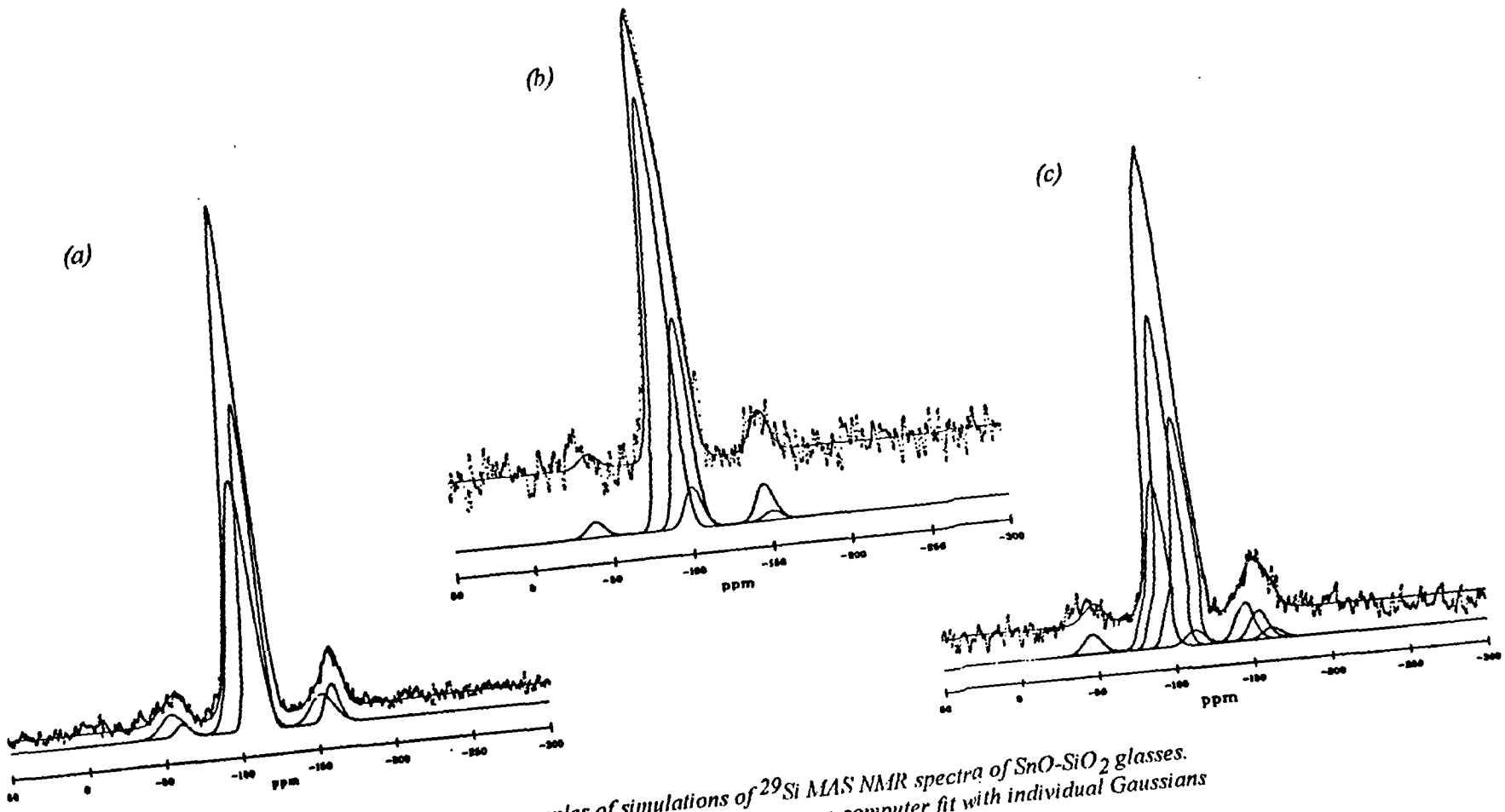

Figure 5.10 : *Some examples of simulations of ^{29}Si MAS NMR spectra of SnO-SiO_2 glasses. The dots are observed intensities and the solid lines are computer fit with individual Gaussians placed below.*
(a) Two Gaussians fit of 16.8 mol.% SnO
(b) Three Gaussians fit of 64.0 mol.% SnO
(c) Four Gaussians fit of 49.4 mol.% SnO

5.6.3.2 SUMMARY OF THE RESULTS OF COMPUTER FITTING OF ^{29}Si MAS NMR SPECTRA

The chemical shifts ranges of the different Q^n species generated from the simulated spectra are shown in Figure 5.11. The chemical shift for each different Q^n species changes very little with composition. This behaviour is unlike the case for alkali metal silicates in which the binary distribution of Q^n types results in a gradual move to less negative chemical shifts for any given Q^n type as the amount of modifier is increased over its stability region. Therefore the simulation of the ^{29}Si MAS NMR results has shown that:

(1) Below 30 mol.% SnO (Sn^{2+}) may act as a traditional modifier, in which the disposition of non-bridging oxygens is consistent with a binary $Q^4 + Q^3$ distribution.

(2) For compositions from 30 to 50 mol.% SnO the continued presence of Q^4 species in the NMR spectra indicates an unconstrained statistical distribution of non-bridging oxygens. Another view might be that some of the Si—O—Sn units are indistinguishable by nuclear magnetic resonance from Si—O—Si units because of the similarity in electronegativity. The ^{119}Sn NMR results support the latter view since the Sn^{2+} character becomes less ionic with increase of SnO content. Thus SnO now appears to exhibit a changing role , from that of modifier to intermediate as SnO content increases.

(3) From 50 to 65 mol.% the NMR spectra can be simulated on the basis of the statistical model for the distribution of non-bridging oxygens.

(4) At 70 mol.% the glass now appears to contain mainly isolated SiO_4^{4-} groups in a Sn—O matrix.

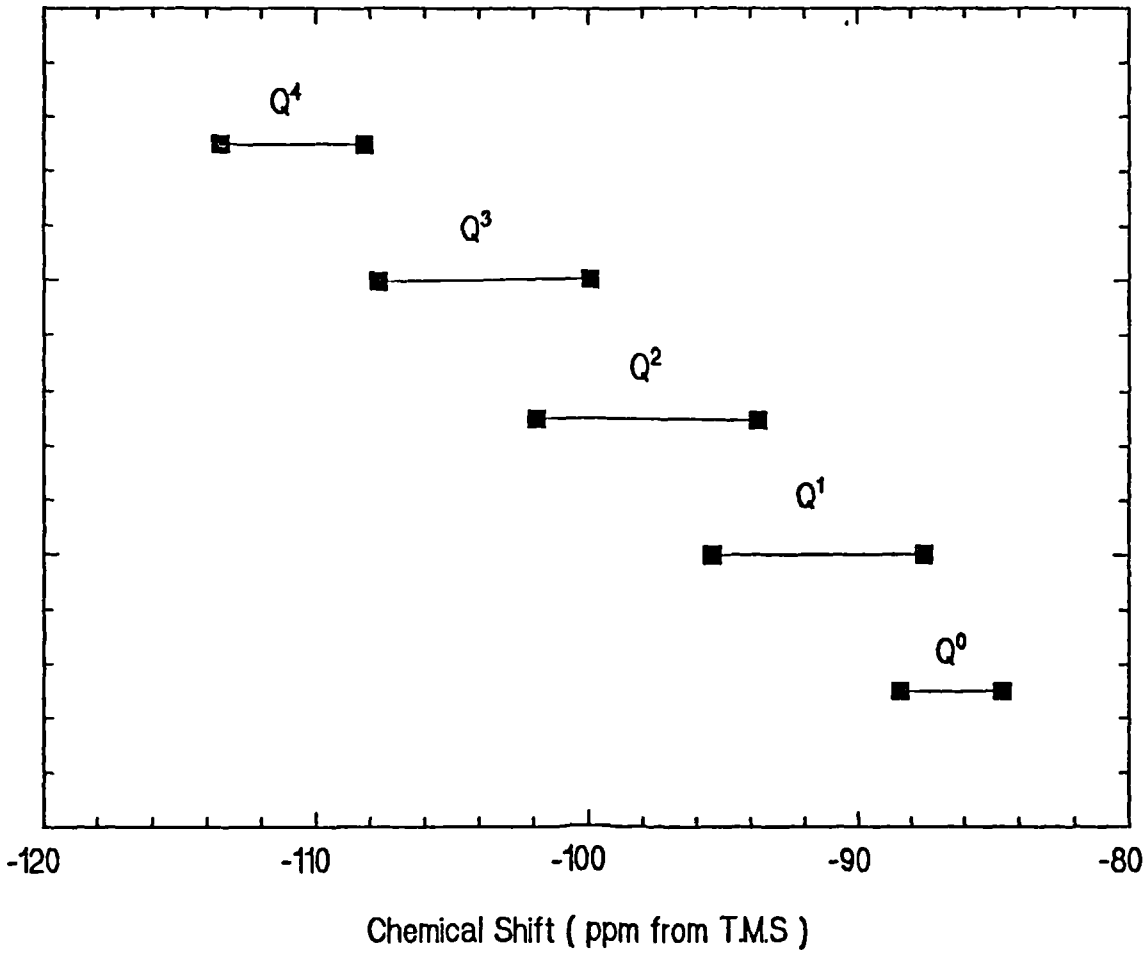

Figure 5.11 : *Chemical shift ranges of different Q^n species for $SnO\text{-}SiO_2$ glasses generated from the simulated spectra.*

5.7 ^{119}Sn MÖSSBAUER SPECTRA

Some of the Mössbauer spectra of the binary SnO-SiO_2 glasses taken at 77K are shown in Figure 5.12. The doublet absorption peak belongs to Sn^{2+}. For all the glasses these doublets are symmetric, thus showing no presence of the so-called Karyagin-Goldanskii effect [22]. The spectra also show the present of an Sn^{4+} peak but the relative areas of the Sn^{2+} and Sn^{4+} peaks indicate that most of the tin exists in the Sn^{2+} state in each case.

Table 5.12: *Composition and Mössbauer parameters of SnO-SiO_2 glasses taken at 77K.*

Samples	*Mol.% SnO*	**Isomer shift, δ (±0.005 mms^{-1})*	***Isomer shift, δ (±0.005 mms^{-1})*	*Quad. splitting, Δ (±0.005 mms^{-1})*	*Linewidth, I (±0.005 mms^{-1})*
TS1	*16.8*	*3.032*	*1.017*	*2.091*	*1.048*
TS2	*28.2*	*3.036*	*1.021*	*2.086*	*1.111*
TS3	*29.6*	*3.028*	*1.013*	*2.083*	*1.135*
TS4	*32.6*	*3.060*	*1.045*	*2.073*	*1.144*
TS5	*39.7*	*3.002*	*0.987*	*2.071*	*1.145*
TS6	*40.9*	*3.001*	*0.986*	*2.070*	*1.153*
TS7	*49.4*	*2.989*	*0.974*	*2.056*	*1.145*
TS8	*53.5*	*2.984*	*0.969*	*2.057*	*1.147*
TS9	*55.4*	*2.964*	*0.949*	*2.044*	*1.152*
TS10	*64.0*	*2.948*	*0.933*	*2.040*	*1.161*
TS11	*71.5*	*2.933*	*0.918*	*2.012*	*1.164*
+Crystalline SnO (tetragonal)			*0.67*	*1.36*	*0.917*
+Amorphous SnO			*0.857*	*1.71*	*1.23*
++$Sn_3(PO_4)_2$			*0.96*	*1.73*	-
++$Sn_3O_4SO_4$			*0.91*	*1.94*	-
+++$Sn_3(AsO_4)_2$			*1.03*	*2.01*	-
++$SnSO_4$			*1.90*	*1.00*	-
++SnC_7O_4			*1.60*	*1.45*	-

** Relative to $CaSnO_3$ source. ** Relative to α-Sn whose chemical shift from a $CaSnO_3$ source is 2.015 mm/s. + Reference [24]. Reference [22]++. +++Reference[23].*

Sample TS11, with the highest tin content of 71.5 mol.% SnO, has the highest amount of Sn^{4+} species. However, none of the glasses contained more than 1 mol.% Sn^{4+}, as estimated from the areas of the Mössbauer spectra. In calculating the molar composition from the results of chemical analysis, such small concentrations of SnO_2

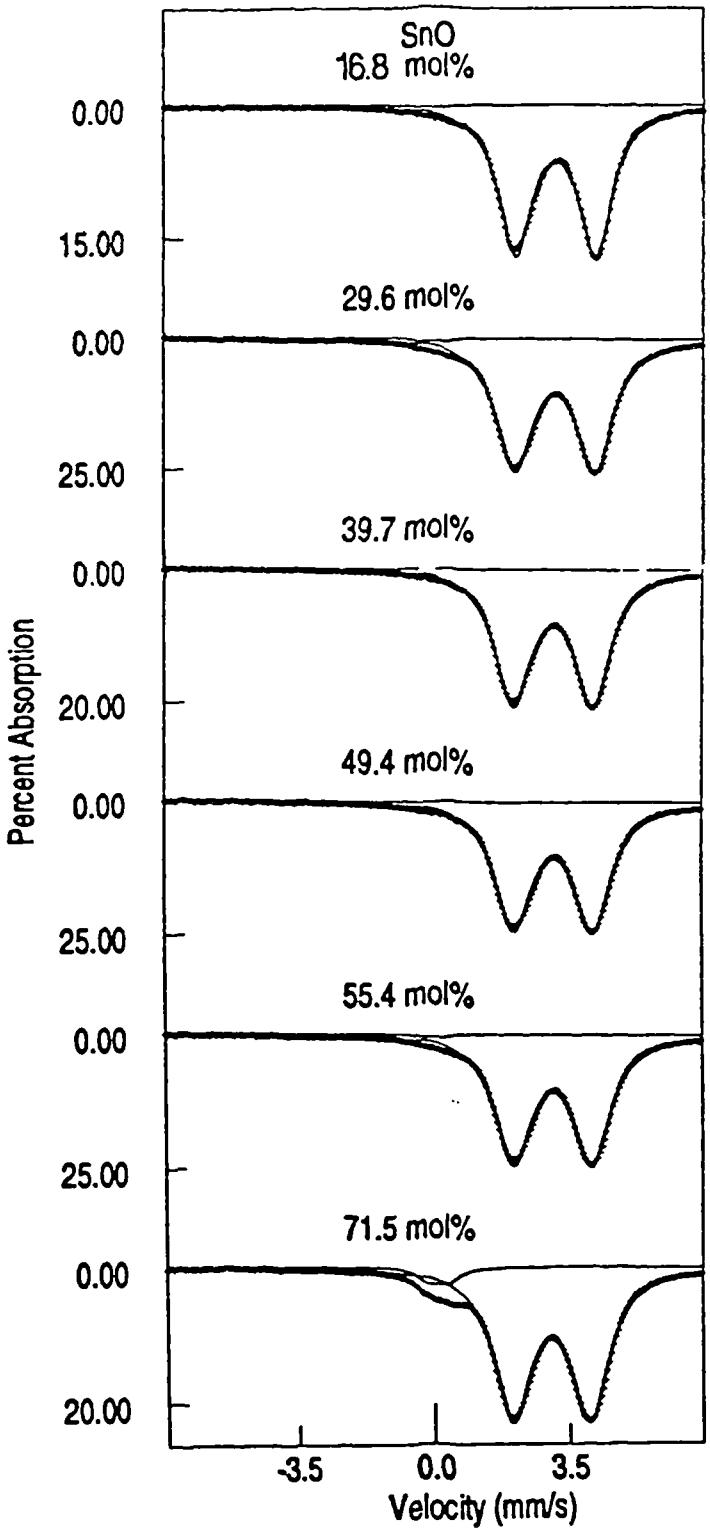

Figure 5.12 : *Some of the 77 K Mössbauer spectra of the SnO - SiO_2 glasses studied, showing the presence of small amounts of dissolved Sn^{4+} .*

were neglected. Hence the interpretation of the results does not take into account the presence of this small amount of Sn^{4+}. The Mössbauer parameters for the SnO-SiO_2 glasses are compared with the data for SnO and some salts of oxyacids with Sn^{2+} in Table 5.7.

5.7.1 THE ISOMER SHIFT OF Sn^{2+}

The chemical isomer shift depends on the *s* electron density at the tin nucleus and an increase in its value corresponds to an increase in the *s* electron density [22]. To interpret the tin isomer shift, it is instructive to look at the electronic configuration of tin. The neutral gray tin (α-Sn) has a diamond structure which is completely quadricovalent with the hybridized configuration $5(sp^3)$ [23]. Therefore α-Sn has only one electron in the *s* orbital. When compared to Sn^{2+} ($5s^25p^0$ of a free-ion configuration) and Sn^{4+} ($4d^{10}5s^05p^0$ of free-ion configuration); α-Sn should fall midway between the ionic divalent (Sn^{2+}) and ionic quadrivalent (Sn^{4+}) extremes.

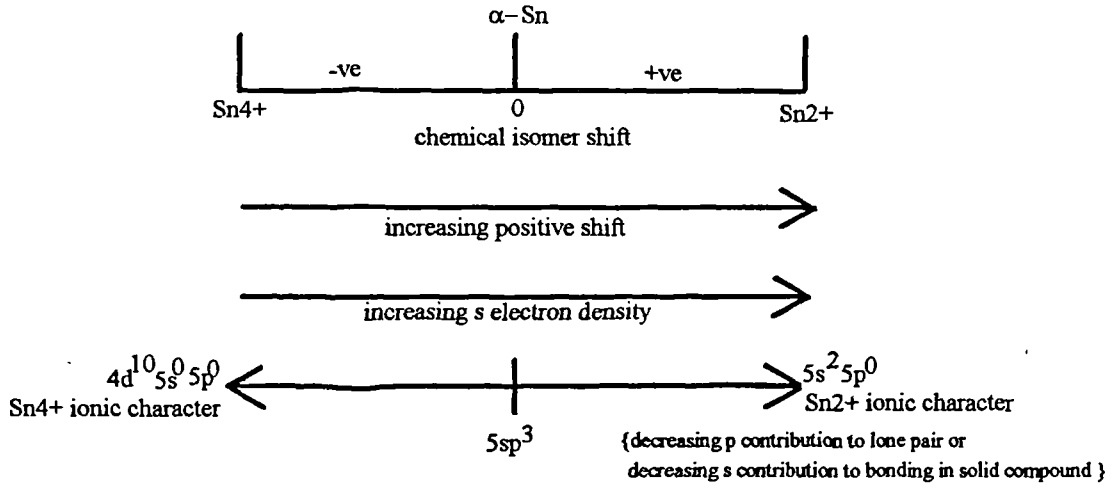

Figure 5.13. *Variation of ^{119}Sn Mössbauer chemical isomer shift with Sn 5s electron density.*

Therefore all Sn^{2+} compounds have positive shifts from α-Sn and their value increases with increasing ionicity towards the stannous free-ion, $5s^2$, configuration. Conversely, all Sn^{4+} compounds have negative shifts from α-Sn and the negative value increases with ionicity towards the stannic free-ion, $4d^{10}5s^05p^0$, configuration [23 & 25]. This is summarised schematically in Figure 5.13.

As seen in Table 5.12, the isomer shifts are positive with respect to α-Sn, confirming the presence of tin in its 2+ oxidation state in the glasses. The values of the isomer shifts of the glasses are larger than for ^{119}Sn in amorphous SnO and very much larger than in tetragonal SnO which indicates larger *s* electron densities at the tin nuclei in these glasses. These higher densities, which reflect greater electrostatic character in the Sn—O bonding, could arise from longer Sn—O bond lengths and/or from an increase in coordination number of the tin atoms. The isomer shift decreases with the increase of SnO (see Figure 5.14), indicating that the ionicity of the Sn—O bond decreases with SnO content. The decrease of the isomer shift with tin content is -0.22 ± 0.01 $mms^{-1}mol^{-1}$. Although the decrease in the isomer shift is generally linear with SnO content, the isomer shift possibly shows a maximum value at ~33 mol.% SnO, indicating some sort of discontinuity around this composition. This sort of trend was observed in the $SnO\text{-}B_2O_3$ glass system by Paul et al [7] whose isomer shift data showed a maximum at 20 mol.% SnO. They intepreted this as the point where Sn^{2+} begins to be coordinated by the non-bridging oxygens produced with the increase of SnO content. Based on these facts, and the results of ^{119}Sn NMR and ^{29}Si NMR, it appears that, at compositions greater than ~33 mol.% SnO, the non-bridging oxygen ions probably form more covalent bonds to Sn^{2+} ions. The formation of Si-O-Sn linkages has the result that the *s*-electron density at the nucleus will decrease, probably due to the increase of the shielding effect by the p_z (or d_z2) electron, and consequently there is a decrease in the isomer shift. The increase of the shielding effect of the *s*-electron by the p_z-electron could probably come from the changing hybridization resulting from formation of Si-O-Sn bonds. On the other hand, the higher values of the chemical isomer shift in the low SnO region (less than 33 mol.%)

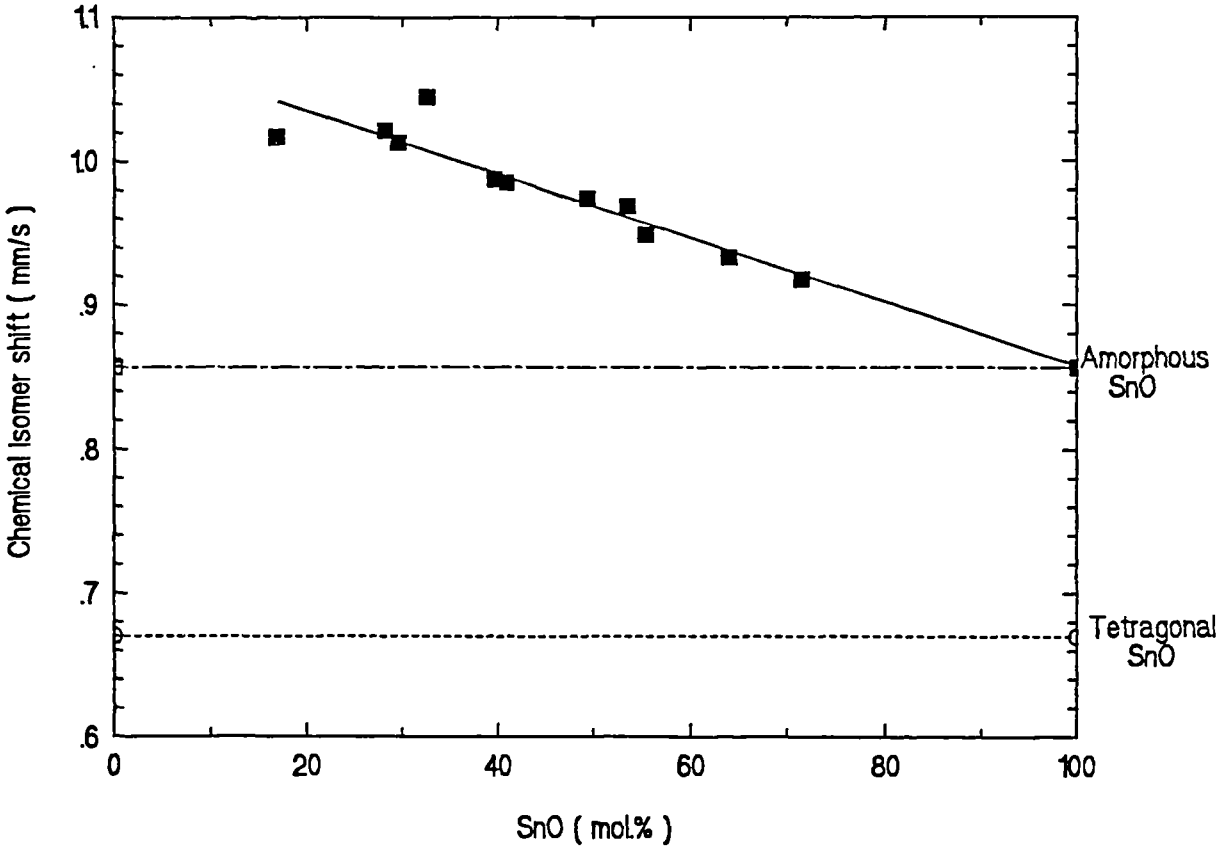

Figure 5.14 : *Variation of the isomer shift of Sn^{2+} at 77 K in $SnO\text{-}SiO_2$ glasses as a function of SnO content . The isomer shifts are relative to α- tin. (Errors are within the dimension of the symbol used).*

probably arise from larger Sn—O distances in these glasses. The larger value of Sn—O distances at low SnO content is supported by the radial distribution studies of x-ray data of SnO-SiO_2 glasses by Ishikawa and Akagi [3]. Their studies shows that, for SnO contents of less than ~33 mol.% , the Sn—O distance in these glasses is longer by 0.07- 0.11 Å than in glasses with more than ~33 mol.% SnO. Thus the changing role of SnO from modifier to intermediate is envisaged at a composition around 33 mol. % SnO.

5.7.2 THE QUADRUPOLE SPLITTING OF Sn^{2+}

The quadrupole splitting arises from the presence of an electric field gradient at the tin nucleus. Electric field gradients have their origin in two effects: (1) from any imbalance in the distribution of the tin *p* or *d* electron density and (2) from charges on neighbouring ions. Since the field gradient varies as the inverse cube of distance, the most important contribution for Sn(II) oxide comes from an excess of p_z electron density over p_x, p_y orbitals [22-25]; although other factors such as population of the bonding orbitals by the electrons and total asymmetry must also have a significant effect [26-27]. For all the glasses studied, the quadrupole splitting values are higher than those for tetragonal and amorphous SnO. This indicates that the immediate environment of Sn^{2+} is distorted compared to the axial symmetry of the square pyramidal coordination of tin in tetragonal SnO (see Figure 2.11) and even that in amorphous SnO. The decrease in the quadrupole splitting with increase of SnO is very small (see Figure 5.15 and Table 5.12). This shows that there is an absence of high order (i.e. tendency to form crystals) in the structure of the glass even at high SnO contents. The quadrupole splitting of divalent tin thus observed in the glasses is consistent with both the generally proposed Sn(II) structures, which indicates differential population of the p_x, p_y and p_z orbitals or any hybridized structure containing them.

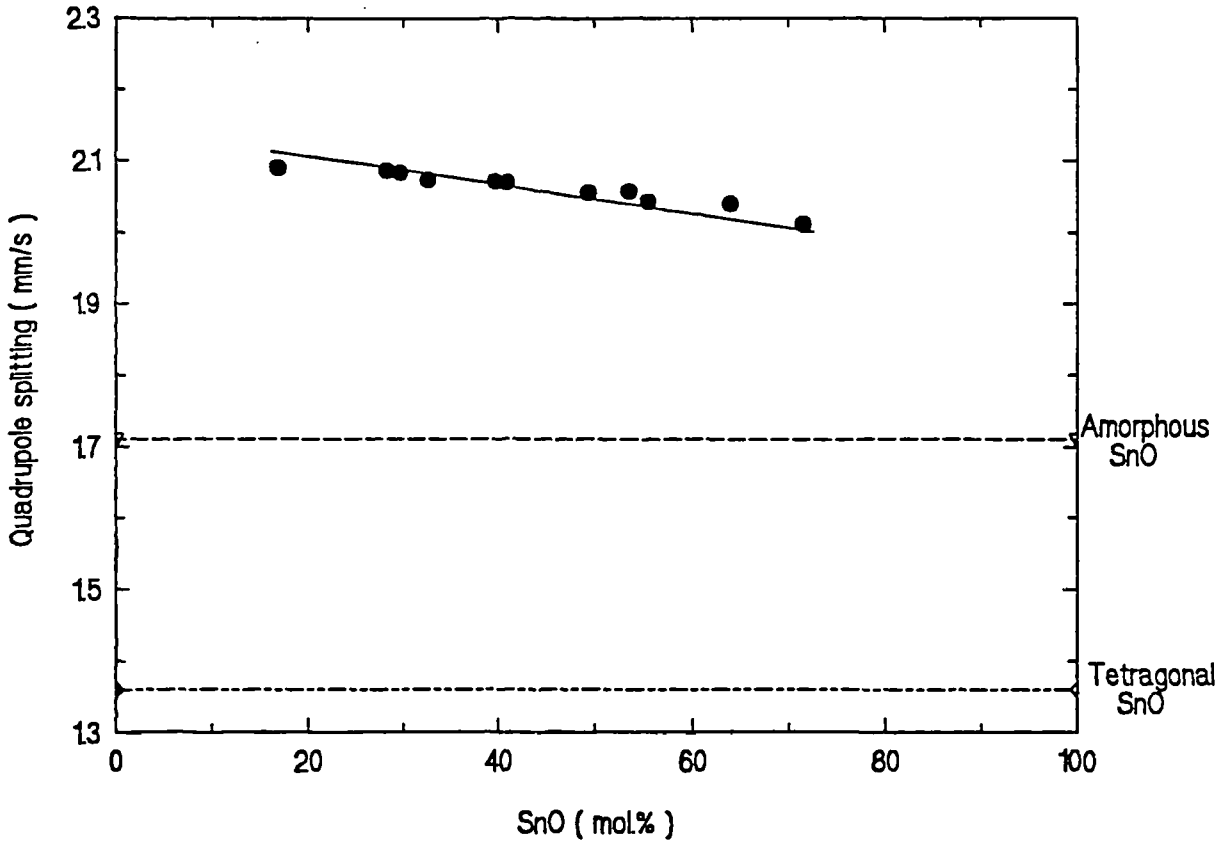

Figure 5.15 : *Variation of the quadrupole splitting of Sn^{2+} at 77 K in $SnO - SiO_2$ glasses as a function of SnO content. (Errors are within the dimension of the symbol used).*

5.7.3 RELATION BETWEEN THE ISOMER SHIFT AND QUADRUPOLE SPLITTING OF Sn^{2+}.

According to Lees and Flinn [28] there exists a correlation between the quadrupole splitting and the isomer shift data for Sn(II) compounds. Figure 5.16 shows a graph of the isomer shift against quadrupole splitting for some Sn(II) compounds taken from Lees and Flinn. From this graph, the fully ionic $5s^2$ configuration of Sn^{2+} (when the number of $5p$ electrons is zero) is attained when the quadrupole splitting value is zero, corresponding to the isomer shift value of 2.9 mm/s relative to α-Sn. Conversely, the increase in the magnitude of the quadrupole splitting as the isomer shift decreases corresponds to an increase in the $5p$ character of the bonds. For the glasses studied there is a decrease in the isomer shift with increase of SnO and from the trend it has been suggested that for compositions > 33 mol.% SnO, the SnO role changed from modifier to an intermediate through the formation of Si—O—Sn linkages. If the average isomer shift (0.96 ± 0.07 mm/s) and quadrupole splitting (2.05 ± 0.06 mm/s) of compositions > 33 mol.% is plotted in the Lees and Flinn graph (Figure 5.16), the point falls on the solid lines on the graph and gives the number of $5p$ electrons in Sn^{2+} as 0.74 ± 0.08. This shows that Sn^{2+} retains a significant p electron density in the glass and the shielding effect of the p-electron decreases the $5s$ electron density at the nucleus and consequently decreases the isomer shift. Thus the decrease in isomer shift is indicative of increasing covalent character of Sn^{2+} while the larger quadrupole splitting suggests a more distorted environment about the tin atom in the glass. Lees and Flinn also suggested that the compounds on the solid lines are those in which the covalent bond is linear, and therefore involve only the p_z orbital, while for the compounds on or near the lower line the bonding is more complicated, with the contributions from p_x and p_y orbitals also present.

The Mössbauer data of the glasses are also compared with those of oxide compounds of Sn(II) as shown in Table 5.12 and Figure 5.16. From this data it can be

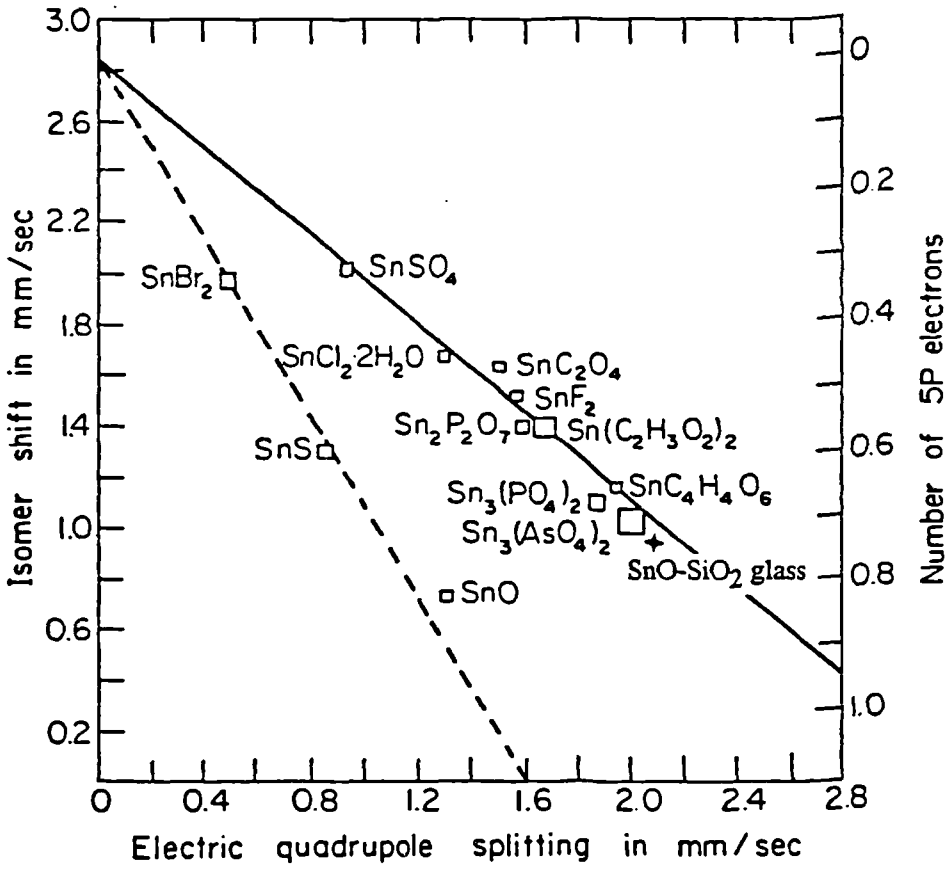

Figure 5.16 : *Isomer shifts and number of 5 p electrons against quadrupole splitting for Sn (II) compounds and SnO- SiO_2 glass. The symbol □ and + are for Sn (II) compounds and SnO-SiO_2 glass respectively. The isomer shifts are relative to α-Sn. The original graph is by Lees and Flinn [28].*

surmised that the environment of the Sn^{2+} ion in the glass could be similar to $Sn_3(AsO_4)_2$ or $Sn_3O_4SO_4$ whose structures are not yet known.

5.7.4 THE LINEWIDTH

The linewidth of Sn^{2+} as a function of SnO content is shown in Figure 5.17. The linewidth increases quite rapidly up to ~33 mol.% SnO and there afterwards increases very slowly to a near constant value with increase of SnO. The linewidths are substantially broader than that of crystalline SnO but smaller than the linewidth of amorphous SnO. The average relative broadening of the linewidth is given by

$$\frac{\Gamma_{glass} - \Gamma_{crystalline}}{\Delta} = 0.11 \pm 0.05$$

The relative broadening of Sn^{2+} in amorphous SnO is 0.18 [24] as compared to 0.11 in the glass. This suggests a narrower distribution and smaller anisotropy of electric field gradients of Sn^{2+} in the glass as compared to amorphous SnO. The broadening of the linewidth can be attributed to the irregular distribution of atoms around tin [29]. For compositions > 33 mol.%, the contant value of the linewidth suggests that the pattern of the atom distributions around tin have been established in the glasses. This probably indicates the presence of Sn—O—Si bonds involving the Sn $5p_z$ orbital and the broadness of the linewidth reflects the nonequivalence of these bonds.

5.8 DEPENDENCE OF MÖSSBAUER SPECTRA ON TEMPERATURE

The temperature dependence Mössbauer study gives some information on the behaviour of Sn^{2+} in the glass. From this data the Debye-Waller factor or recoil free fraction (f) and the Debye temperature (θ_D) of Sn^{2+} in the glass can be evaluated. The recoil free fraction and the Debye temperature reflect the bulk properties, whereas

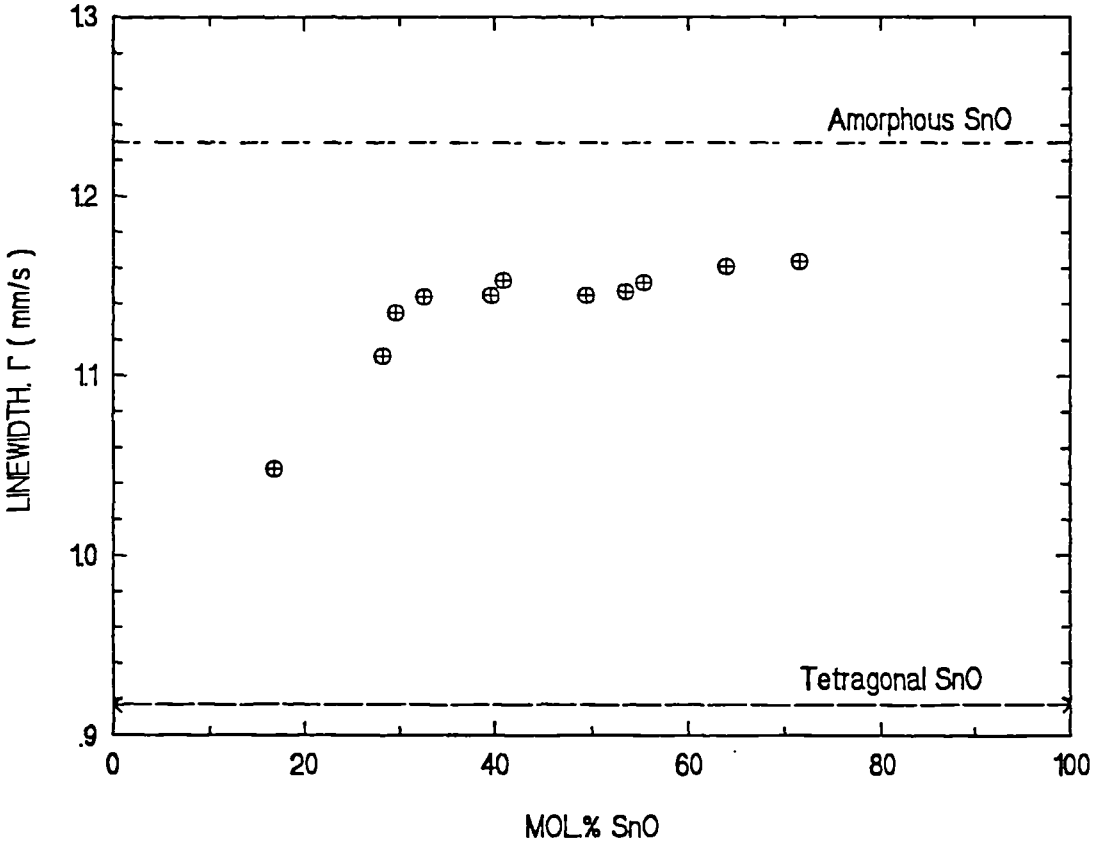

Figure 5.17: *Variation of the linewidth of Sn^{2+} Mössbauer spectra of SnO-SiO_2 glasses as a function of SnO content (Errors are within the dimension of the symbol used)*

the isomer shift and quadrupole splitting are better measures of local distortion [24]. Referring back to equation 3.25 (Chapter 3); the *f* factor is large for a large Debye temperature at low temperature (T). The Debye temperature is a characteristic of a Mössbauer nucleus and the firmer the binding of the nucleus in the lattice the higher the Debye temperature [22 & 30]. Apart from the *f* factor and the Debye temperature, the temperature dependence of the shift (total shift) could also be analysed in terms of other bulk properties of the glass.

5.8.1 THE DEBYE TEMPERATURE AND THE *f* FACTOR

The intensity of absorption (A) of a nucleus observed in a Mössbauer spectrum is proportional to the *f* factor [31]. A and *f* are related by,

$$A = \lambda c f \qquad 5.1$$

where c is the concentration of a tin state and λ is a constant which represents the fraction of the radiation which are Mössbauer γ-rays. Then,

$$\ln A = \ln f + \ln \lambda c \qquad 5.2$$

Using the Debye model for high temperature, equation 3.28 ($T > \frac{\theta_D}{2}$), we get

$$\ln f = \frac{-6E_R T}{\kappa \theta_D^2} \qquad 5.3$$

Hence a graph of lnA versus T will be a straight line with slope $m = \frac{-6E_R}{\kappa \theta_D^2}$ from which the Debye temperature is determined using

$$\theta_D = \sqrt{\frac{6E_R}{\kappa m}} \qquad 5.4$$

The recoil energy of the γ-ray , $E_R = 2.572 \times 10^{-3}$ eV for ^{119}Sn.

The Debye temperature of Sn^{2+} in the glass found by the above method is almost independent of SnO concentration, giving an average value of 193 ± 3 K. Table 5.13 gives some of the Debye temperatures of the glasses as compared to the Debye temperatures of amorphous and crystalline SnO.

***Table 5.13** : Debye temperatures of Sn^{2+} in $SnO\text{-}SiO_2$ glasses as compared to amorphous and crystalline SnO.*

Compound	*Debye temperature (K)*
Sn^{2+} for 32.6 mol.% SnO in $SnO\text{-}SiO_2$ glass	*194 ± 2*
Sn^{2+} for 40.9 mol.% SnO in $SnO\text{-}SiO_2$ glass	*193 ± 3*
+SnO amorphous	*181 ± 2*
+SnO crystalline	*203 ± 1*

+ Taken from reference [25] .

As seen in Table 5.13 the typical Debye temperature of the glass lies between the values for crystalline and amorphous SnO. The results imply that Sn^{2+} ions are more tightly bound in the glass than in amorphous SnO.

One of the main problems in structural investigation of glasses is the determination of the coordination of an atom in a material. Kurkjian [31], Parish [32] and Mitrofanov & Sidorov [33]; proposed a qualitative approach to this problem. This is done by comparing the ratio of the *f* factor at liquid-nitrogen temperature and at room temperatures ($R = f_{77}/ f_{300}$) to the known value of R of an established crystalline compound. For, silicate glasses [33], $R \approx 2.5$ when Sn^{2+} is coordinated to 4 oxygen. Therefore, the recoil free fraction, *f* of the Sn^{2+} at 77K and 300K for the

materials in Table 5.13 were calculated from their corresponding Debye temperatures using equations given in chapter 3. i.e equation 3.26 for 77K and equation 3.28 for 300K. The results of this are given in Table 5.14. which indicates that Sn in the glass is coordinated to 4 oxygens.

Table 5.14: *The* $R = f_{77}/f_{300}$ *factor*.

Compound	*f(77K)*	*f(300K)*	*R*	*Coordination number of Sn*	*Known or proposed structure*
SnO in SnO-SiO_2 glass	*0.62*	*0.24*	*2.6*	*4*	*ionic + covalent*
SnO amorphous	*0.27*	*0.19*	*3.1*	*?*	*?*
SnO crystalline	*0.65*	*0.27*	*2.4*	*4*	*ionic + covalent*

5.8.2 THE TEMPERATURE DEPENDENCE OF THE ISOMER SHIFT

The temperature dependence of the isomer shift could be analysed in terms of the molar volume and the expansivity of the glass. Glass samples 32.6 and 49.4 mol.% SnO were chosen for this purpose.

Figure 5.18 shows the variation of the total shift (δ) as a function of temperature of the glasses chosen. For both samples the shifts decrease with increase of temperature. Since $\frac{\theta_D}{2} \approx 100K$ for the glass, the high temperature limit according to the Debye model is when T > 100 K. Therefore for T > 100 K, the change of total shift with temperature for both samples are according to

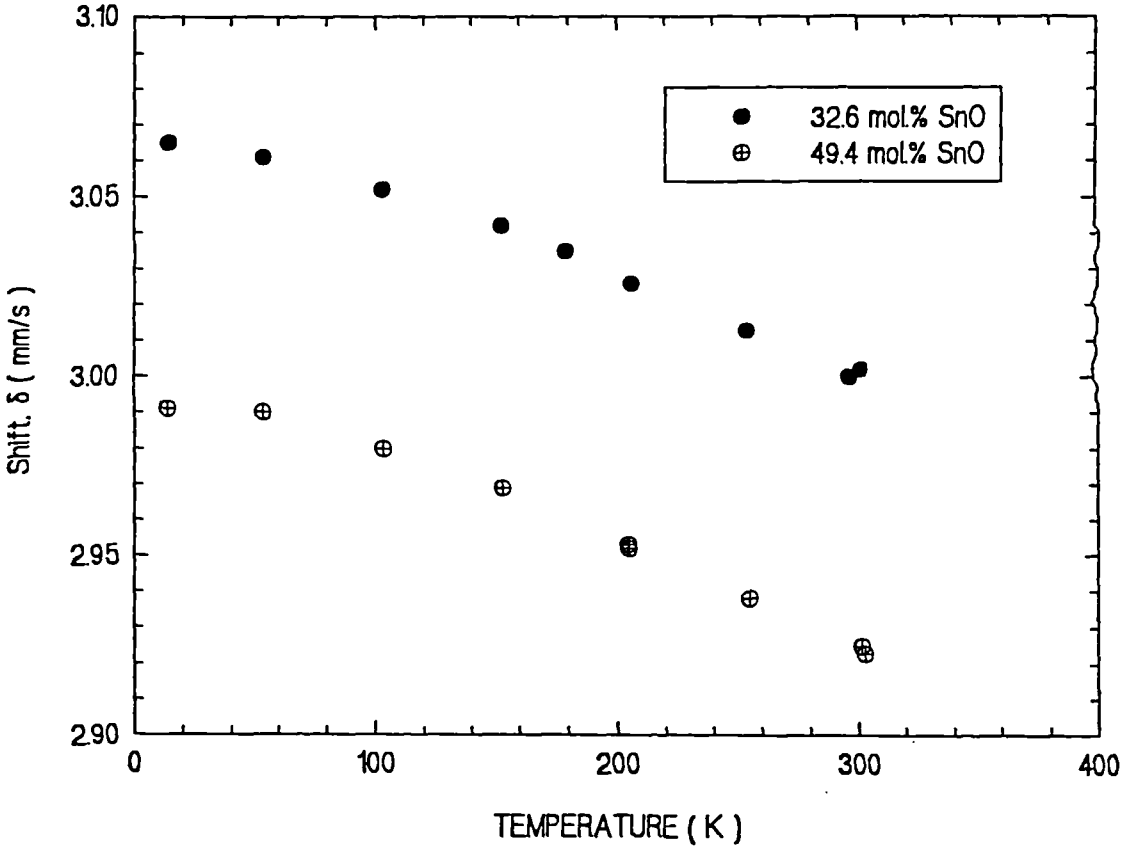

Figure 5.18 : *Variation of the total shift of Sn^{2+} Mössbauer spectra of some SnO-SiO_2 glasses as a function of temperature. The shifts are relative to SnO_2 (Errors are within the dimension of the symbol used).*

$$\partial\delta / \partial T = (-2.78 \pm 0.03) \text{ X } 10^{-4} \text{ mms}^{-1} \text{ K}^{-1} \quad \{ 32.6 \text{ mol.\% SnO } \} \qquad 5.5 \text{ (a)}$$

$$\partial\delta / \partial T = (-2.90 \pm 0.01) \text{ X } 10^{-4} \text{ mms}^{-1} \text{ K}^{-1} \quad \{ 49.4 \text{ mol.\% SnO } \} \qquad 5.5 \text{ (b)}$$

The measured shift (δ) has contributions from the isomer shift (δ^I-measured at 77K) and the second-order Doppler shift (δ^T - the classical high temperature limit), so that

$$\delta = \delta^I + \delta^T \qquad 5.6$$

The second-order Doppler shift (δ^T) is independent of temperature and is given by the expression [30]

$$\partial\delta^T / \partial T = -3R / 2Mc \qquad 5.7$$

where M is the atomic mass of the Mössbauer nuclide, R is the gas constant and c is the speed of light. For ^{119}Sn,

$$\partial\delta^T / \partial T = -3.5 \text{ X } 10^{-4} \text{ mms}^{-1}\text{K}^{-1} \qquad 5.8$$

Since $\delta = \delta^I + \delta^T$, the difference between 5.5 and 5.8 will give the experimental value of $\partial\delta^I/\partial T$. Hence, for each sample, the experimental values of $\partial\delta^I / \partial T$ are as follows,

$$\partial\delta^I / \partial T = (0.72 \pm 0.03) \text{ X } 10^{-4} \text{ mms}^{-1}\text{K}^{-1} \quad \{32.6 \text{ mol.\% SnO}\} \qquad 5.9\text{(a)}$$

$$\partial\delta^I / \partial T = (0.60 \pm 0.01) \text{ X } 10^{-4} \text{ mms}^{-1}\text{K}^{-1} \quad \{ 49.4 \text{ mol.\% SnO}\} \qquad 5.9\text{(b)}$$

The change of the isomer shift with tin concentration (C) and temperature are related by,

$$\frac{\partial\delta^I}{\partial T} = (\beta \frac{\partial\delta^I}{\partial C}) / (\frac{\partial(\ln V)}{\partial C}) \qquad 5.10$$

where β is the expansivity , C is the tin concentration and V is the molar volume. For both glasses $\frac{\partial(\ln V)}{\partial C} = -0.083 \pm 0.002$ mms^{-1}K^{-1} , $\frac{\partial \delta^I}{\partial C} = -0.22 \pm 0.01$ mms^{-1}mol^{-1} and $\beta = 3\alpha$, whose values are given in Table 5.18. Using equation 5.10, the predicted values of $\partial\delta^I/\partial T$ were calculated for both glasses. The predicted and the theoretical values of $\partial\delta^I/\partial T$ are presented in Table 5.15.

Table 5.15 : *The values of* $\partial\delta^I/\partial T$

Glass samples	*Experimental* $\partial\delta^I/\partial T$ (X 10^{-4} mms^{-1}K^{-1})	*Predicted* $\partial\delta^I/\partial T$ (X 10^{-4} mms^{-1}K^{-1})	*Molar volume contribution*
32.6 mol.% SnO	*0.72 ± 0.03*	*0.34 ± 0.02*	*47 %*
49.4 mol.% SnO	*0.60 ± 0.01*	*0.39 ± 0.01*	*65%*

Hence the change of the isomer shift with change of temperature is not 100 % contributed by the changes to the molar volume. Therefore the observed decrease in the isomer shift with increase of SnO content could be partly attributed to the increase of screening of the *s* orbital by the increasing electron density in the *p* orbital. The increase of the *p* electron density could be through the change of hybridization due to the formation of Si—O—Sn linkages that strengthen the glass network with increase of SnO.

5.9 PHYSICAL PROPERTIES OF SnO-SiO_2 GLASSES

The physical property measurements carried out on glasses in this system are viscosity, density and molar volume, thermal expansion and refractive index.

5. 9 .1 VISCOSITY MEASUREMENT

Viscosity measurements were carried out on six glass samples. Depending on the sample composition, the temperature range covered was between 380°C and 800°C and the viscosities measured ranged from $10^{6.5}$ to 10^{12} Pa s with ± 2% error in the value of $\log_{10} \eta$. Figure 5.19 shows the viscosity-temperature behaviour of the glasses. For some glasses of compositions 39.7, 49.4 and 55.4 mol.% SnO, the decrease in viscosity goes to a minimum before increasing with increase of temperature. The minima were identified, by comparing with the DTA traces (chapter 6), as the onset of crystallization of the glasses.

Figure 5.20 shows the graph of $\log_{10} \eta$ versus the reciprocal of absolute temperature of some of the glasses studied. The straight line equation

$$\log_{10} \eta = \frac{E_\eta}{2.3RT} + A \qquad 5.11$$

was used to fit the data. The slope of the line gives the activation energy for viscous flow (E_η) for the glasses. Two lines were fitted to the data from the glasses of compositions 39.7, 49.4 and 55.4 mol.% SnO. The intersection of the two straight lines will give the temperature of the onset of the crystallization event for the glasses; its values thus found are of the order of those given by the DTA traces of the glasses. Table 5.16 gives the values of E_η and the temperatures of the onset of crystallization for the glasses studied.

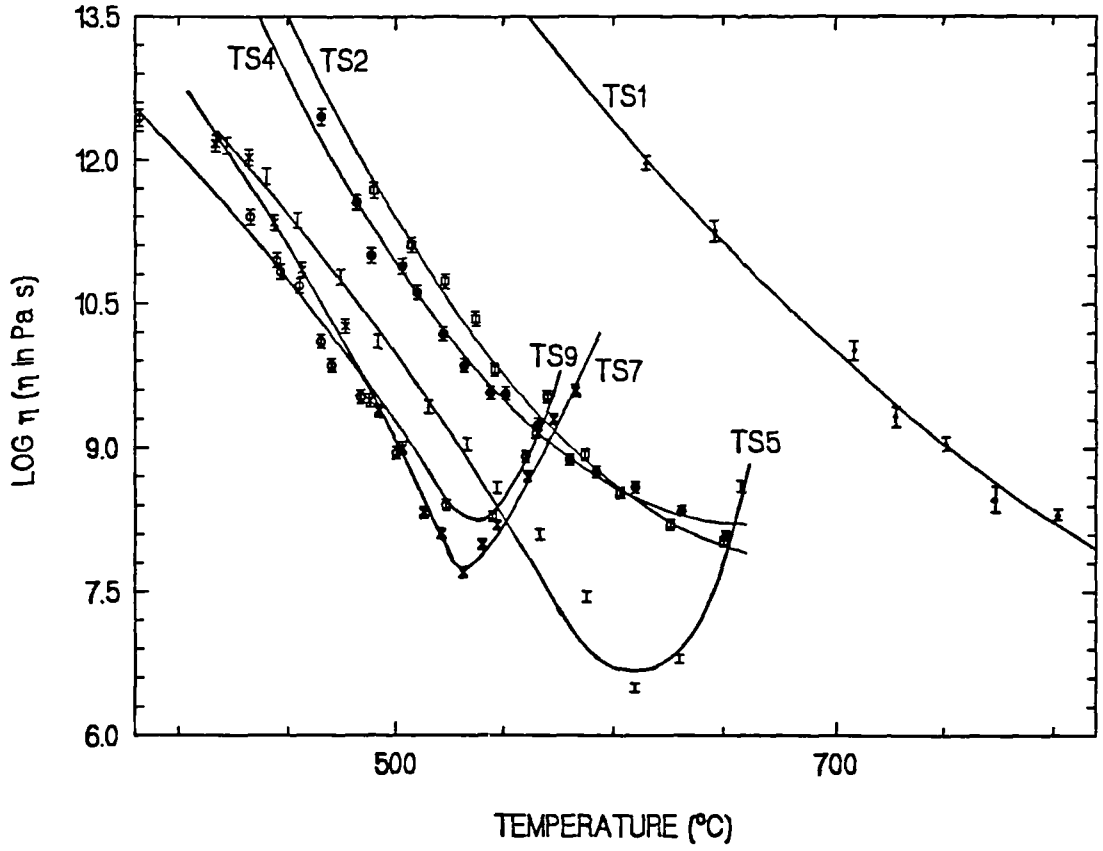

Figure 5.19 : *$Log_{10}\eta$ versus temperature of some SnO-SiO_2 glasses.*

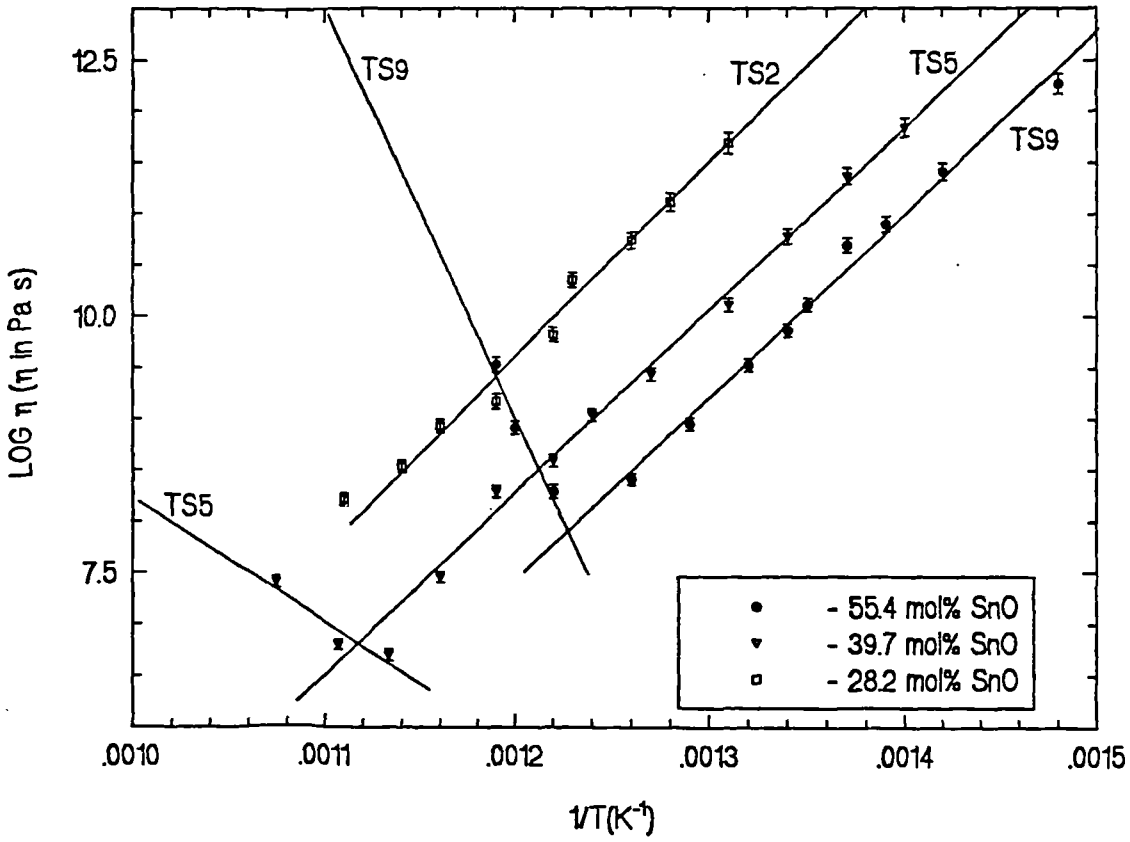

Figure 5.20 : *$Log_{10}\eta$ versus the reciprocal of absolute temperature of some SnO-SiO_2 glasses.*

Table 5.16: *Activation energy of viscous flow of $SnO\text{-}SiO_2$ glasses.*

Samples	*Mol% SnO*	*$E\eta$ (KJ/mol) Before crystallization*	*$E\eta$ (KJ/mol) After crystallization*	*Onset of crystallization from viscosity (±10°C)*	*Onset of crystallization from DTA (±5°C)*
TS0	*0*	*565**	-	-	-
TS1	*16.8*	*377 ±33*	-	-	-
TS2	*28.2*	*366 ±28*	-	-	-
TS4	*32.6*	*352 ± 37*	-	-	-
TS5	*39.7*	*341 ± 34*	*232 ±16*	*620*	*665*
TS7	*49.4*	*366 ± 45*	*492 ± 69*	*540*	*586*
TS9	*55.4*	*345 ± 41*	*764 ± 50*	*540*	*595*

** Taken from reference [34].* *{ 4.19 Joule = 1 calorie }*

Figure 5.21 is the graph that shows the variation E_η (before crystallization) as a function of SnO content. For comparison, the activation energies for viscous flow for $SnO\text{-}SiO_2$ glasses were plotted on the original graph taken from reference [34], which shows how the activation energy varies with metal oxide content in several binary silicate glasses. The activation energies of viscous flow in the temperature range of 500 to 850°C for $PbO\text{-}SiO_2$ glasses, calculated from the viscosity data taken from reference [37], were also plotted on the graph of Figure 5.21. The large decrease of activation energy of viscous flow from pure silica to about 10-20 mol% alkali metal and alkaline earth metal oxides, and the subsequent gradual decrease, indicate a rather abrupt and significant change in the structure as the metal oxides are added to silica [35]. For $SnO\text{-}SiO_2$ glasses, the decrease in the activation energy of viscous flow is not as large as in the alkali metal and alkaline earth silicates. The decrease in the activation energy of viscous flow of $SnO\text{-}SiO_2$ glasses is of the same order as the $PbO\text{-}SiO_2$ glasses. This suggest that SnO does not depolymerise the glass network in the same way as the alkali metal and alkaline earth oxides do. The behaviour of SnO in silicate is closely related to PbO and different to the modifying behaviour of the other oxides. PbO has been known to act as an intermediate in silicate glass at high PbO contents.

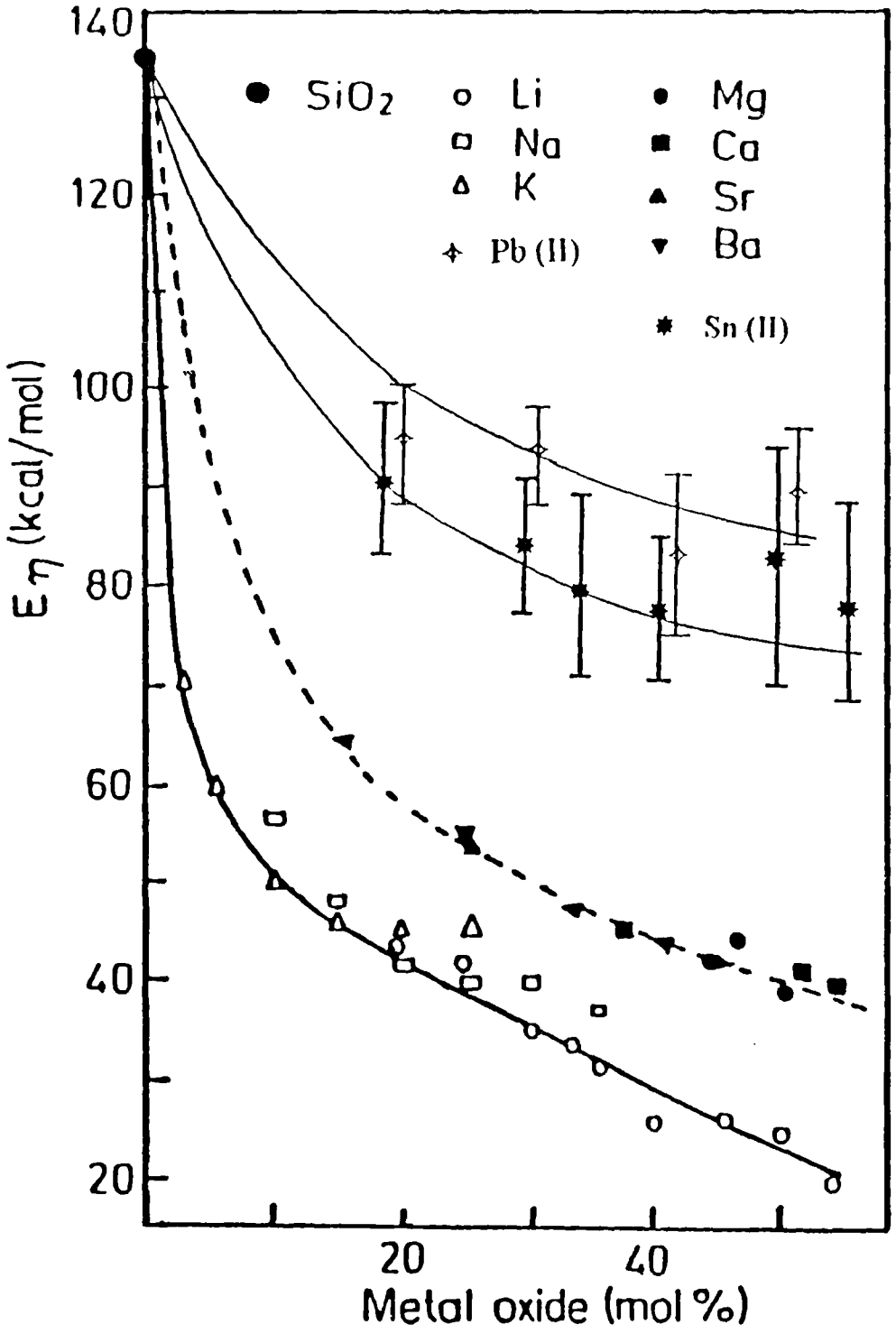

Figure 5.21 : *Activation energy of viscous flow (E_η) as a function of metal oxides content for binary silicate glasses. The original graph and the data for Pb(II) are taken from reference [34] and [37] respectively.*

5.9.2 DENSITY AND MOLAR VOLUME

The density and molar volume of the glasses are presented in Table 5.17. The variation of density and molar volume as a function of SnO content are shown in Figure 5.22. The lines represent least squares fitted straight lines for both the density and molar volume versus SnO content. As expected, the density increases and the molar volume decreases with increasing SnO content. Drake et al [36] suggested that a monotonic change in density with composition would suggest that the structure of a glass does not change with composition; a change in the structure would be reflected by a change in the slope of the density against composition plot. A closer look at the density versus composition plot shows a slight deviation from linearity at around 35 to 45 *mol% SnO and this is more pronounced in the molar volume plot.* This could suggest that SnO is changing its position from a modifier to a network forming role through some sort of structural contraction. The density versus mol% of SnO plot of Ishikawa & Akagi [3] , however does not indicate this is happening but, by radial distribution studies they showed that for SnO content greater than 35 mol% the Sn—O distances are shorter when compared to glasses with SnO content less than 35 mol% SnO. The Sn—O distances for glasses with less than 35 mol% SnO are almost the same as in crystalline SnO.

The straight line fit of density versus mol.% SnO follows the equation $\rho = 0.0341x + 2.18$, where x is the mol.% SnO. From this equation, the experimental values of SiO_2 glass and SnO are 2.18 ± 0.23 g/cm^3 and 5.59 ± 0.56 g/cm^3 respectively. These can be compared to the values of 2.20 g/cm^3 [37] for SiO2 glass and 6.45 g/cm^3 [38] for crystalline SnO. Although the discontinuities in these plots are not that pronounced, there are discontinuities in other physical properties which may be related to a change in structural role of SnO in the glass.

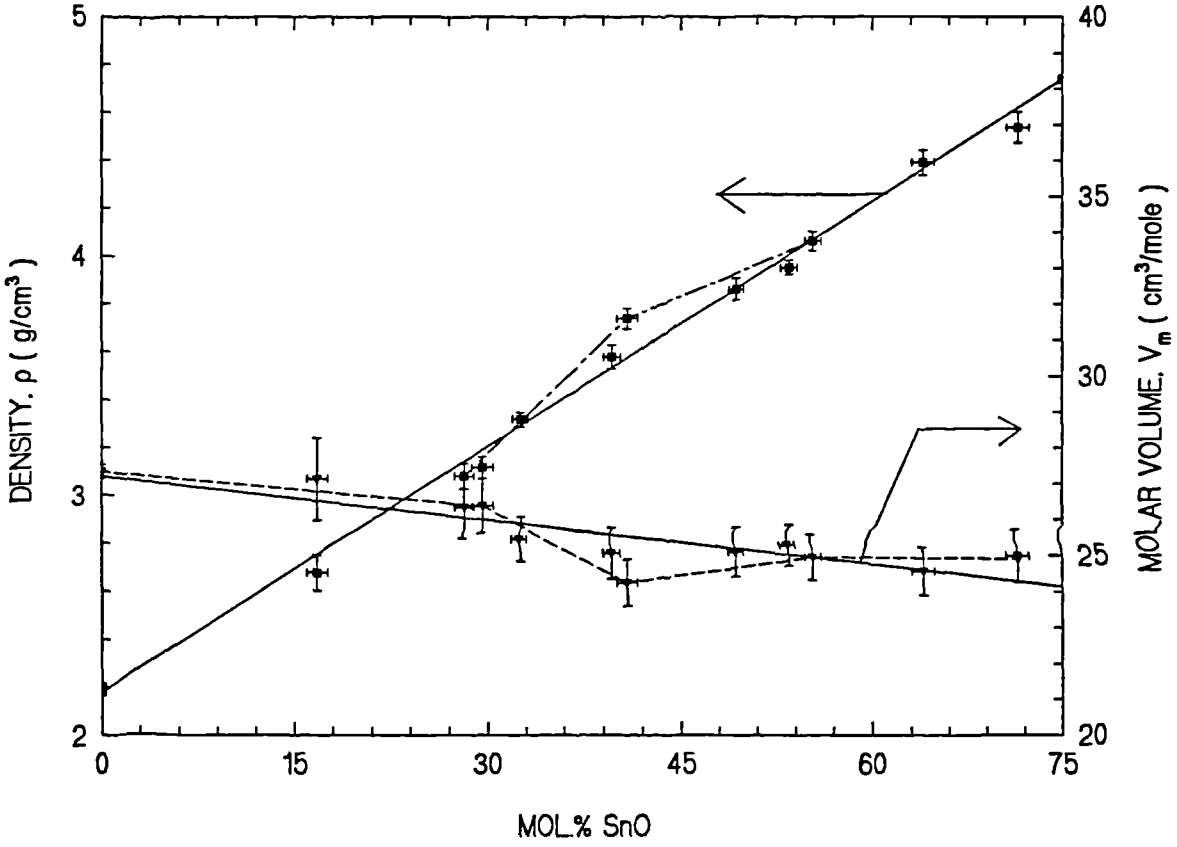

Figure 5.22 : *Variation of density (ρ) and molar volume (V_m) as a function of SnO content*

Table 5.17 . *The nominal and analyzed composition, density and molar volume of SnO - SiO_2 glasses*

Samples	*Analyzed Composition (mol%)*			*Density (ρ) g/cm^3*	*Molar Volume (V_m) cm^3/mole*
	SnO (Chemical ± 1.6%)	*SiO_2 (By difference)*	*Al_2O_3 (NMR ± 0.16%)*		
TS0	*0*	*100*	*-*	*2.20**	*27.31*
TS1	*16.8*	*83.0*	*0.2*	*2.681*	*27.12*
TS2	*28.2*	*71.2*	*0.6*	*3.090*	*26.33*
TS3	*29.6*	*70.13*	*0.27*	*3.120*	*26.37*
TS4	*32.6*	*67.09*	*0.31*	*3.323*	*25.44*
TS5	*39.7*	*60.0*	*0.3*	*3.584*	*25.06*
TS6	*40.9*	*58.7*	*0.4*	*3.744*	*24.24*
TS7	*49.4*	*50.4*	*0.2*	*3.867*	*25.09*
TS8	*53.5*	*46.4*	*0.1*	*3.873*	*25.83*
TS9	*55.4*	*43.3*	*1.3*	*3.973*	*25.66*
TS10	*64.0*	*35.4*	*0.6*	*4.282*	*25.24*
TS11	*71.5*	*27.4*	*1.1*	*4.435*	*25.68*

**Taken from reference [37] pg. 19*

5.9.3 THERMAL EXPANSION

The thermal expansion of glass is sensitive to changes in composition and structure of the glass, e.g. degree of polymerization, type of structural units and the role played by different cations, i.e. whether they occupy network modifying or network forming positions in the network [39]. The thermal expansion coefficient reflects the strength of the cross-linking of the network and in turn the strength and directionality of the cation-oxygen bonds. If the binding force is strong, the cation-oxygen separation will be increased by only a small extent due to a given increase in the vibrational energy. A measure of the closeness of the packing and therefore 'the binding forces' can be expressed in terms of the volume of glass which contains one mole of oxygen or the molar volume of oxygen (V_O) [40]. A high value

of V_O gives a high coefficient of thermal expansion and vice versa. Table 5.18, gives the coefficient of linear thermal expansion (α), oxygen molar volume, transformation temperature (Tg) and the dilatometric softening point (Mg) for the glasses studied. Figure 5.23 shows the variation of thermal expansion and oxygen molar volume as a function of SnO content. The thermal expansion and oxygen molar volume show the same trend with increase of SnO, with an inflexion in the 30-40 mol% SnO region. In the inflexion region there is some sort of rearrangement to a more compact structure which reflects the changing role of Sn^{2+} from modifier to glass former.

The variation of Tg and Mg as a function of SnO content (Figure 5.24) show the same overall trend. Tg and Mg decrease sharply when the SnO content increases from 16.8 to 30 mol%. For this composition range the SnO operates as a modifier, creating non-bridging oxygens, weakening the glass structure and thus decreasing Tg [41-42] and Mg. For SnO contents greater than 30 mol% the change in Tg and Mg is very slow indicating that SnO is now playing a different role in the glass structure. We suggest that SnO_n groups or chains are taking part in a more covalent cross-linking with SiO_4 groups [41].

Table 5.18: *Coefficient of linear thermal expansion (α), oxygen molar volume (V_O), transformation temperature (Tg) and dilatometric softening point (Mg) of SnO-SiO_2 glasses.*

Samples	*Mol% SnO*	*α($10^{-7}K^{-1}$) [30 - 400 °C]*	*V_O (cm^3/ mole)*	*Tg (°C)*	*Mg (°C)*
TS0	*0*	*5.7**	*13.65*	-	-
TS1	*16.8*	*25.8*	*14.78*	*651*	*711*
TS3	*29.6*	*44.1*	*15.43*	*485*	*517*
TS4	*32.6*	*42.5*	*15.17*	*477*	*508*
TS6	*40.9*	*43.9*	*15.19*	*453*	*493*
TS7	*49.4*	*50.1*	*16.64*	*425*	*476*
TS8	*53.5*	*53.2*	*17.62*	*414*	*473*
TS9	*55.4*	*54.1*	*17.59*	*417*	*476*
TS10	*64.0*	*61.6*	*18.60*	*428*	*483*

**Taken from reference [37] pg. 19*

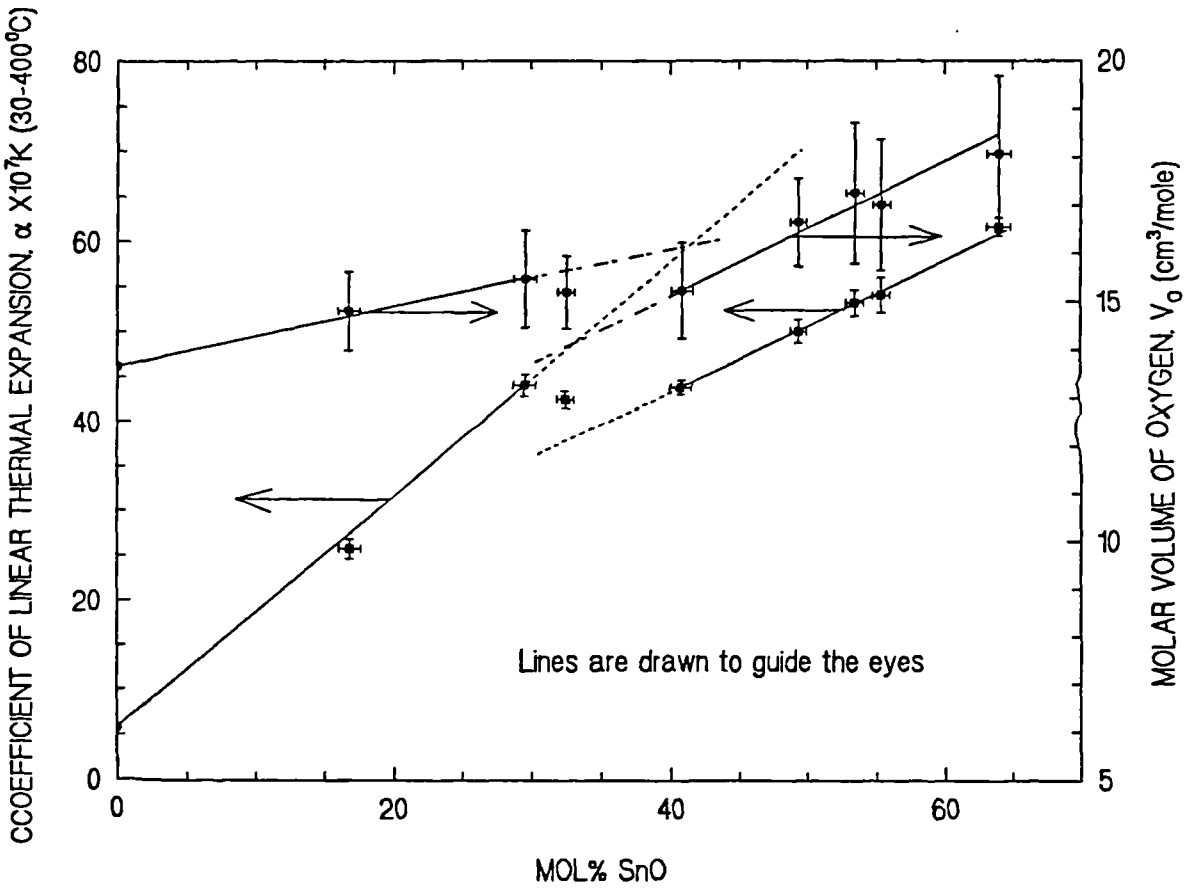

Figure 5.23: *Variation of coefficient of linear thermal expansion (α) and molar volume of oxygen (V_O) as a function of SnO content.*

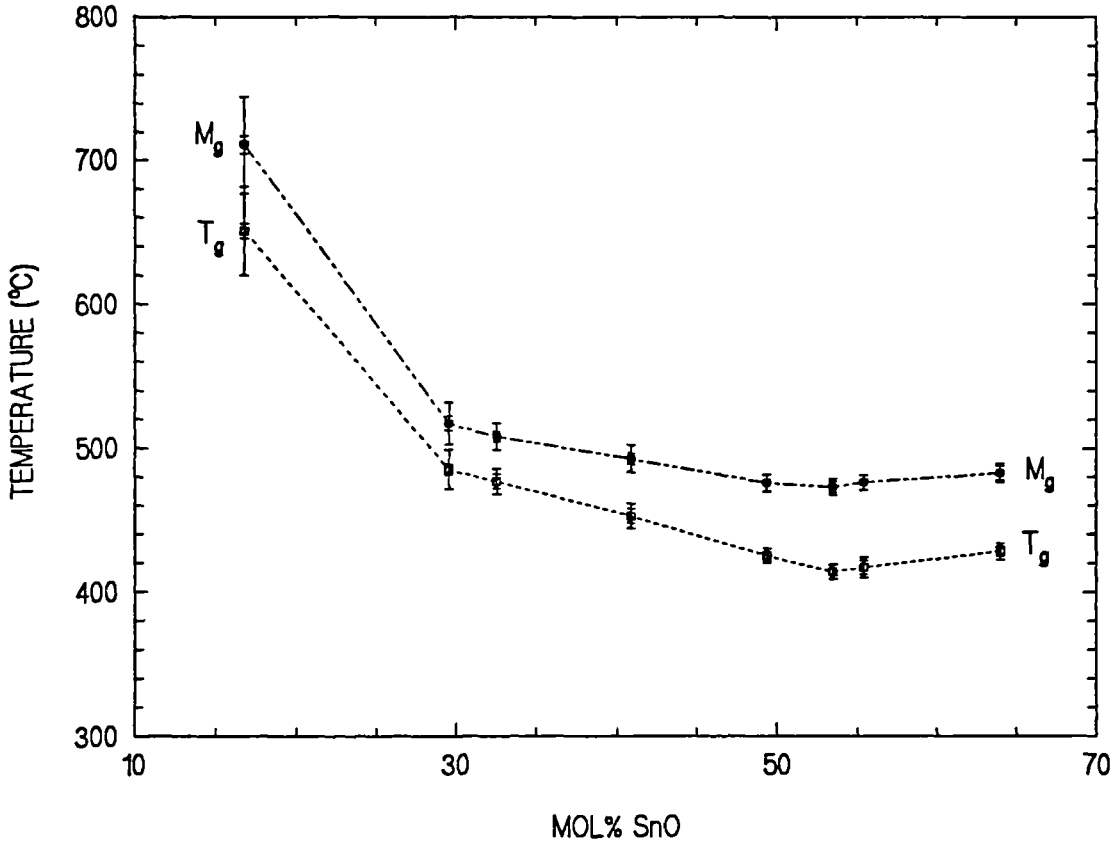

Figure 5.24 : *Glass transition temperature (T_g) and dilatometric softening point (M_g) versus SnO content.*

5.9.4 REFRACTIVE INDEX AND MOLAR REFRACTIVITY

Table 5.19 gives the refractive index and molar refractivity data for the glasses studied. The refractive indices are higher than alkali silicate and alkali earth silicate glasses [37], but are not as high as lead silicate [37] and stannous germanate [6] glasses. This is consistent with the molar masses involved. The variation of refractive index and molar refractivity as a function of SnO content are shown graphically in Figure 5.25. To explain the effect of composition of glass on its refractive index and indirectly upon its structure, we shall use the Lorenz & Lorentz formula for molar refractivity (R_m) which relates the molar volume (V_m) and the refractive index (η) by the equation,

$$R_m = \frac{V_m(\eta^2 - 1)}{(\eta^2 + 2)} \qquad 5.12$$

The molar refractivity is proportional to polarizability (σ) according to the relationship,

$$R_m = \frac{4\pi N\sigma}{3} \qquad 5.13$$

where N is the Avogadro number. R_m is a measure of electron polarization i.e. the displacement of the electron cloud under the effect of the visible electromagnetic wave and it also represents the actual volume of the polarisable particles i.e. the space in glass occupied by atoms [43-44]. Equation 5.12 can be written as

$$\eta^2 = \frac{1+2Y}{1-Y} \qquad 5.14$$

where $Y = \frac{R_m}{V_m}$.

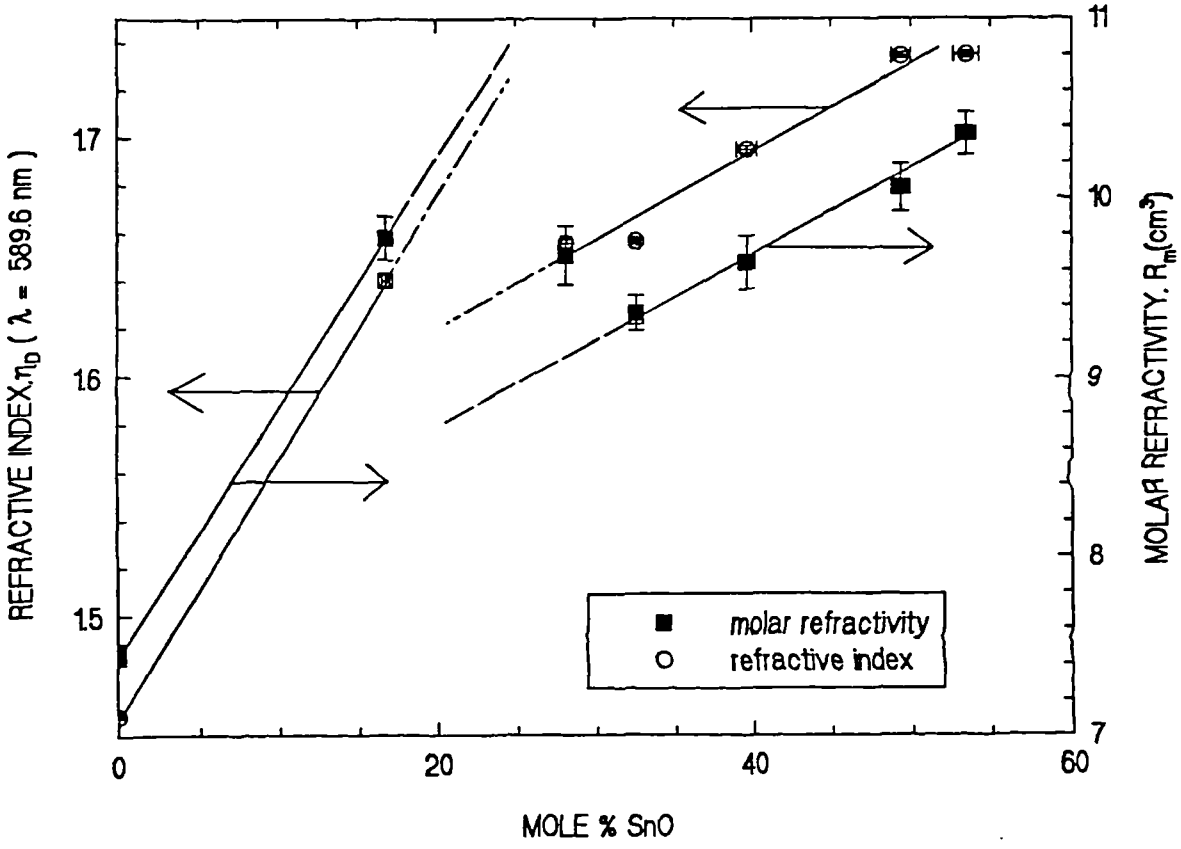

Figure 5.25 : *Refractive index (η_D) and molar refractivity (R_m) versus SnO content.*

Hence a low value of V_m (when the structure gets denser) and a high value of polarizability (σ) will result in a high refractive index. Turning to Figure 5.25 we see that the refractive index and the molar refractivity increase rapidly as SnO content increases from 0 to 20 mol%. The non-bridging oxygens introduced by SnO are more deformable giving higher polarizability and therefore higher values of refractive index. If the structural role of Sn^{2+} remained constant the trends in refractive index and molar refractivity would continue and there would be a continuous change of V_m and R_m on replacement of SiO_2 by SnO. However from 20 mol% SnO onwards the molar refractivity dips and has a minimum value at around 33 mol% SnO. The decrease in molar refractivity in this composition range (20-33 mol% SnO) retards the increase in refractive index as shown by the plateau in the graph. The observed positive deviation from linearity of V_m will produce some contribution to the negative deviation from linearity of η and σ and the minimum in the molar refractivity versus composition plot is an indication of structural change in the glass structure [44-45].

Table 5.19: *Refractive index (η_D) and molar refractivity (R_m) of SnO - SiO_2 glasses*

Samples	*Mol% SnO*	η_D *(λ = 589.6 nm)*	R_m *(cm^3 / mole)*
TS0	*0*	*1.4584*	*7.46*
TS1	*16.8*	*1.6406*	*9.78*
TS2	*28.2*	*1.6561*	*9.68*
TS4	*32.6*	*1.6571*	*9.36*
TS5	*39.7*	*1.6954*	*9.64*
TS7	*49.4*	*1.7347*	*10.06*
TS8	*53.5*	*1.7351*	*10.36*

5.10 CONCLUSIONS

The process of making a SnO-SiO_2 glass is complicated by the disproportionation of SnO to SnO_2 and Sn metal. Thus, the presence of SnO_2 and Sn metal together with SnO in the melt make it impossible to pour the melt into any required shape and also impossible to control the final composition of the glass. Although, this is the case, glasses in this system can be made up to compositions past

the orthosilicate composition. A maximum of ~ 70 mol.% SnO has been successfully incorporated in the binary SnO-SiO_2 glass. Glass with less than 20 mol.% SnO has not been made successfully because of the requirement of high melting temperature (≥1600°C) that increased the contamination by Al_2O_3 from the alumina crucibles and thus increased the viscosity of the melt. (Silica crucibles are only suitable for low temperature melting (< 1300°C) and platinum crucibles are not suitable because of the tendency of Sn metal to attack the crucibles). At high SnO contents where the melting temperatures are comparatively low, Al_2O_3 contamination was minimised by melting the charge in pellet form and melting for the minimum time. Thus apart from problems due to the disproportionation of SnO , the choice of suitable crucibles is also limiting. Attempts to make the glass with low SnO content (< 20 mol.%) by sol-gel method were hampered by limited availability of suitable precursors.

The first attempt to explain the ability of glass to form with high SnO contents is in terms of the polarizing power of Sn^{2+} and the structure of SnO. The glass system was compared to the PbO-SiO_2 system, which can form glass past the orthosilicate composition. The polarizing power of Sn^{2+} is slightly higher than Pb^{2+} and very much higher than Na^+. This means that the Sn—O bonds are more covalent and directional than Na—O bonds, thus the kinetic stability of the glass is enhanced because it is more difficult to rearrange SiO_4 groups linked together via strong, directed Sn—O bonds. In terms of structure, the deformability of the [SnO_4] polyhedron makes it easy to accommodate in the holes of the structural network of the glass.

The ^{29}Si MAS NMR results have shown that SnO does not depolymerise the silicate network to the same extent as Na_2O or even PbO. Computer simulations showed that, for SnO contents below ~30 mol.%, the disposition of Q^n species is consistent with the binary model, which means SnO acts like traditional modifier. For compositions greater than 30 mol.% SnO, the Q^n distribution follows the statistical model. This is compatible with the concept of Zachariasen's [46] random network theory, which implies that SnO is acting as an intermediate oxide in the glass. Hence,

at high SnO content, Sn^{2+} becomes bonded to non-bridging oxygens through the formation of Si—O—Sn linkages that restore the backbone of the glass structure. Although the ^{119}Sn NMR did not give much structural information due to the high chemical shift anisotropy of Sn^{2+} sites, it showed that the glass also contains very small amounts of Sn^{4+} species. The ^{119}Sn Mössbauer results showed that the decrease in isomer shift with increase of SnO is indicative of increasing covalent character of the Sn—O bonds while the larger quadrupole splitting suggests the distortion of the SnO polyhedral structure in the glass. A maximum in the isomer shift at ~30 mol.% SnO has been suggested as the point where the SnO changes role from modifier to an intermediate. The relation of the isomer shift and the quadrupole splitting shows that Sn^{2+} has significant *p* character which involves the p_z orbital. The results of the temperature dependent Mössbauer spectra of the glass showed that the increase of the electron density of the *p* orbital is not solely attributable to the changes to the molar volume alone. Other factors such as the change of hybridization due to the formation of Si—O—Sn linkages, could also contribute.

The viscosity measurement results showed that the decrease in the viscosity of the glass with increasing SnO is small when compared to the decrease of the viscosity in alkali metal and alkaline-earth metal silicates when the respective modifier oxide is increased in those glasses. From the fact that the stannous silicate glass can form glass past the orthosilicate composition, one can see that SnO has the characteristic of an intermediate or conditional network former at higher concentration of the oxide. The effect on some of the physical properties studied at low SnO concentration seems to follow the behavior of a modifier but at SnO contents around 30-40 mol% there is a discontinuity in the variation of the physical properties which may relate to a change in the structural role of SnO by which the network is strengthened again. This is supported by ^{29}Si NMR and ^{119}Sn Mössbauer studies of these glasses which have indicated a change in bonding at around 30-35 mol.% and formation of Si-O-Sn bonds of significant covalent character. These linkages help to restore the strength of the glass network.

REFERENCES

1. Carbo Nover, J. & William, J. (1967). *Physics Chem. Glasses* **8**(4), 164.
2. Itoh, H. & Mori, S. (1977). *Fukuoka Daigaku Kogaku Shuho* **19**, 13, Japan.
3. Ishikawa, T. & Akagi, S. (1978). *Physics Chem. Glasses* **19**(5), 108.
4. Keysselitz, B. & Kohlmeyer, E.J. (1933). *Metall Erz.* **30**, 185.
5. Levin, e.m., Robbins, C.R., & McMurdie, H.F. (1975). *Phase Diagrams for Ceranists 1975 Supplement, The American Ceramic Society, Inc. Columbus Ohio.* p.126.
6. Silver, J., White, E.A.D. & Donaldson, J.D. (1977). *J. Material Science* **12**, 828.
7. Paul, A., Donaldson, J.D., Donoghue, M.T., & Thomas, M.J.K. (1977). *Phys. Chem. Glasses* **18(6)**, 125.
8. Fajans, K. & Kreidl, N.J. (1948). *J. Am. Ceram. Soc.* **31**, 105.
9. Stanworth, J.E. (1948). *J. Soc. Glass Technol.* **32**, 154-172T.
10. Puddenphatt, R.J. & Monaghan, P.K. (1986). *The Periodic Table of the Elements,* Oxford Science Publications, p.48.
11. Cossement, C., Darville, J., Gilles, J-M., Nagy, J.B., Fernandez, C. & Amoureux, J-P. (1992). *Magnetic Resonance in Chemistry* **30**, 263.
12. Mortuza, M.G. PhD Thesis 1986.
13. Fujiu, T. & Ogino, M. (1984). *J. Non-Cryst. Solids* **64**, 287.
14. Eckert, H. (1992). *Progress in NMR Spectroscopy* **24**, \59.
15. Dupree, R., Holland, D., Mcmillan, P.W. & Pettifer, R.F. (1984). *J. Non-Cryst. Solids* **68**, 399.
16. Dupree, R., Holland, D., & Mortuza, M.G. (1990). *J. Non-Cryst. Solids* **116**, 148.
17. Dupree, R., Holland, D., & Williams, D.S. (1986). *J. Non-Cryst. Solids* **81**, 185.
18. Dupree, R., Ford, N., & Holland, D. (1987). *Physics Chem. Glasses* **28**(2), 78.
19. Lacy, E.D. (1965). *Physics Chem. Glasses* **6**(5), 171.
20. Lacy, E.D. (1967). *Physics Chem. Glasses* **8**(6), 238.
21. Schramm, C.M., de Jong, B.H.W.s. & Parziale, V.E. (1984). *J.Am. Chem. Soc.* **106**, 4396.
22. Greenwood, N.N., & Gibb, T.C. (1971). *Mössbauer Spectroscopy,* Chapman and Hall, London.
23. Hayes, M.C. (1968). in *Chemical Applications of Mössbauer Spectroscopy,* Edited by V.I. Goldanskii and R.H.Herber, Academic Press. London. Chapter 5.
24. Collins, G.S., Kachnowski, T., Benczer-Koller, N. & Pasternak, M. (1979). *Physical Review B* **19(3)**, 1369.
25. Donaldson, J.D. (1967). *Prog. inorg. Chem.* **8**, 287.
26.Donaldson, J.D., Filmore, E.J. & Tricker, M.J. (1971). *J.Chem. Soc. A*, 1109.
27. Donaldson, J.D., Puxley, D.C. & Tricker, M.J. (1975). *J. Inorg. Nucl. Chem.* **37**, 655.
28. Lees, J., & Flinn, P.A., (1965). *Phys. Letters* **19**, 186.
29.Eissa, N.A., Shaisha, E.E., & Hussiun, A.L. (1974). *J. Non-Cryst. Solids* **16**, 206.
30.Gibb. T.C. (1976). *Principles of Mössbauer Spectroscopy,* Chapman and Hall, London.
31. Kurkjian, C.R. (1970). *J. Non-Cryst. Solids* **3**, 157.
32. Parish, R.V. (1984). in *Mössbauer Spectroscopy Applied to Inorganic Chemistry Vol.1* Edited by Gary J. Long, Plenum Press, N.York. Chapter 16.

33. Mitrofanov, K.P. & Sidorov, T.A. (1967). *Soviet Physics - Solid State* **9(3)**, 693.
34. Mackenzie, J.D. (1956). *Chem. Rev.*, **56** , 455.
35. Mackenzie, J.D. (1960). *Modern Aspects of the Vitreous State,* Butterworth & Co. London.
36. Drake, C.F., Stephens, J.A. & Yates, B. (1978). *J. Non-Cryst. Solids* **28**, 61.
37. Bansal, N.P. & Doremus, R.H. (1986). *Handbook of Glass Properties,* Academic Press Inc., Orlando .
38. Weast, R. C. (Chief Editor). (1988). *Handbook of Chemistry & Physics, 68th edition,* CRC Press, Inc., Florida.
39. Ahmed, A.A., Abbas, A.F. & Salman, S.M. (1985). *Physics Chem. Glasses* **26**(1),17.
40. Moore, H. & McMillan, P.W. (1956). *J. Soc. Glass Technol.* **40**, 139.
41. Bridge, B. & Patel, N.D. (1986). *Physics Chem. Glasses* **27**(6), 235.
42. Pye, L.D., Stevens, H.J., & LaCourse, W.C., (1972). *Introduction to Glass Science,* Plenum Press, New York, p.51.
43. Fanderlik, I (1983), *Optical Properties of Glass,* Elsevier , Amsterdam. p.92.
44. Volf, M.B. (1988). *Mathematical Approach to Glass,* Elsevier, Amsterdam. p.244.
45. Rawson, H. (1980). *Properties and Application of Glass,* Elsevier, Amsterdam. p.166.
46. Zachariasen, W.H. (1932). *J. Am. Ceram. Soc.* **54**, 3841.

Chapter 6 - Differential Thermal Analysis and Devitrification of $SnO-SiO_2$ Glasses

This chapter presents the results and discussion of differential thermal analysis and the characterisation of some heat treated $SnO-SiO_2$ glasses. The techniques employed were Differential Thermal Analysis, X-Ray Diffraction, ^{119}Sn Mössbauer Spectroscopy, ^{29}Si MAS NMR and Scanning Electron Microscopy.

6.1 DIFFERENTIAL THERMAL ANALYSIS

Differential Thermal Analysis (DTA) traces of the glasses were obtained in air. Table 6.1 gives the values of T_g and the positions of the maxima of the exothermic peaks obtained from the DTA traces of the glasses. The variation of T_g as a function of SnO content is shown in Figure 6.1 using values obtained from both DTA and thermal expansion. Generally both methods give similar trends in T_g as SnO content is varied in the glass.

The DTA traces can be classified into three groups, as seen in Figure 6.2. The first group is for the composition range 17 to 33 mol.% SnO (TS1, TS2, TS3 and TS4), whose DTA traces featured a single, very broad exothermic peak spanning the temperature range 650°C to 1050°C. The second group is for the composition range 40 to 41 mol.% SnO (TS5 & TS6), showing three highly overlapping exothermic peaks that can be visually resolved into one broad and two narrow peaks. The third group is for the composition range 50 to 64 mol.% SnO (TS7, TS8, TS9 & TS10), showing three readily resolved overlapping exothermic peaks, one broad and two narrow. When it comes to assigning the exothermic peaks to particular events, Pope [1] has given some guidelines regarding this matter. According to him, for glass, narrow exotherms indicate decomposition or crystallization (ordering) or oxidation of a metastable state; broad exotherms denote chemical reaction and a very broad

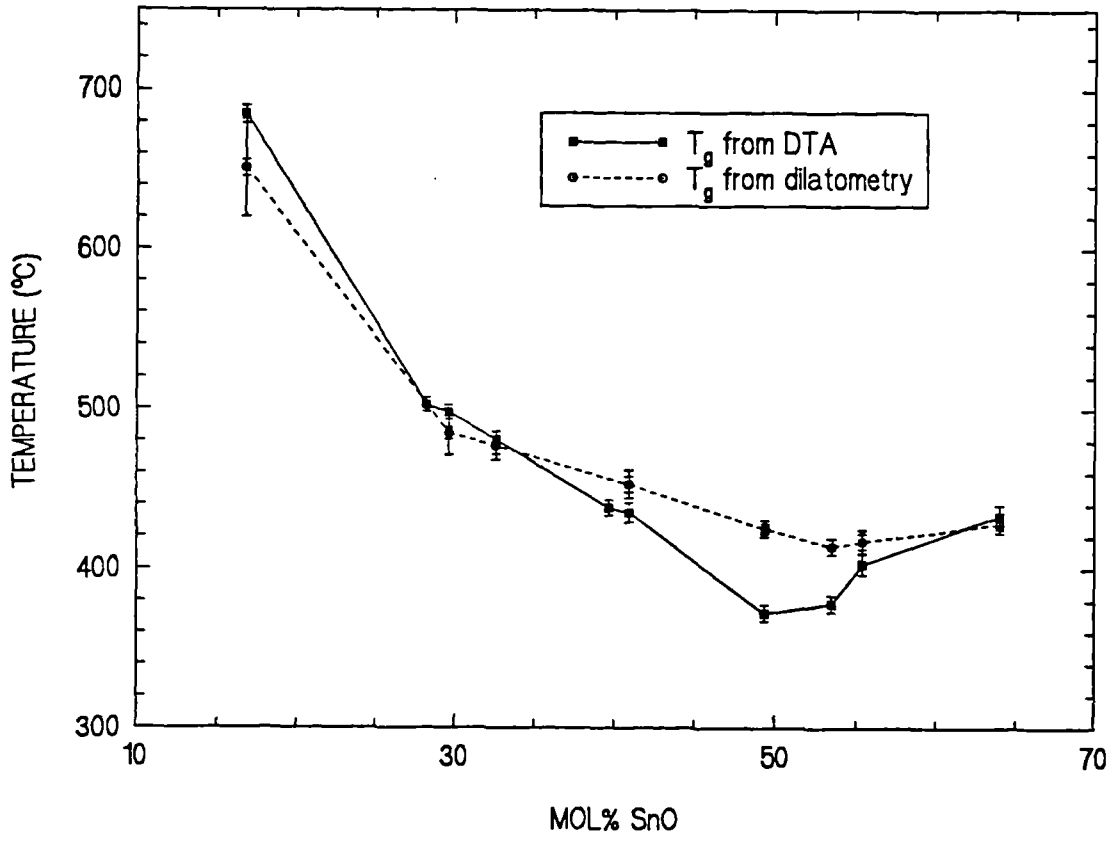

Figure 6.1 : *Glass transition temperatures of SnO-SiO_2 glasses obtained by DTA and Dilatometry experiments.*

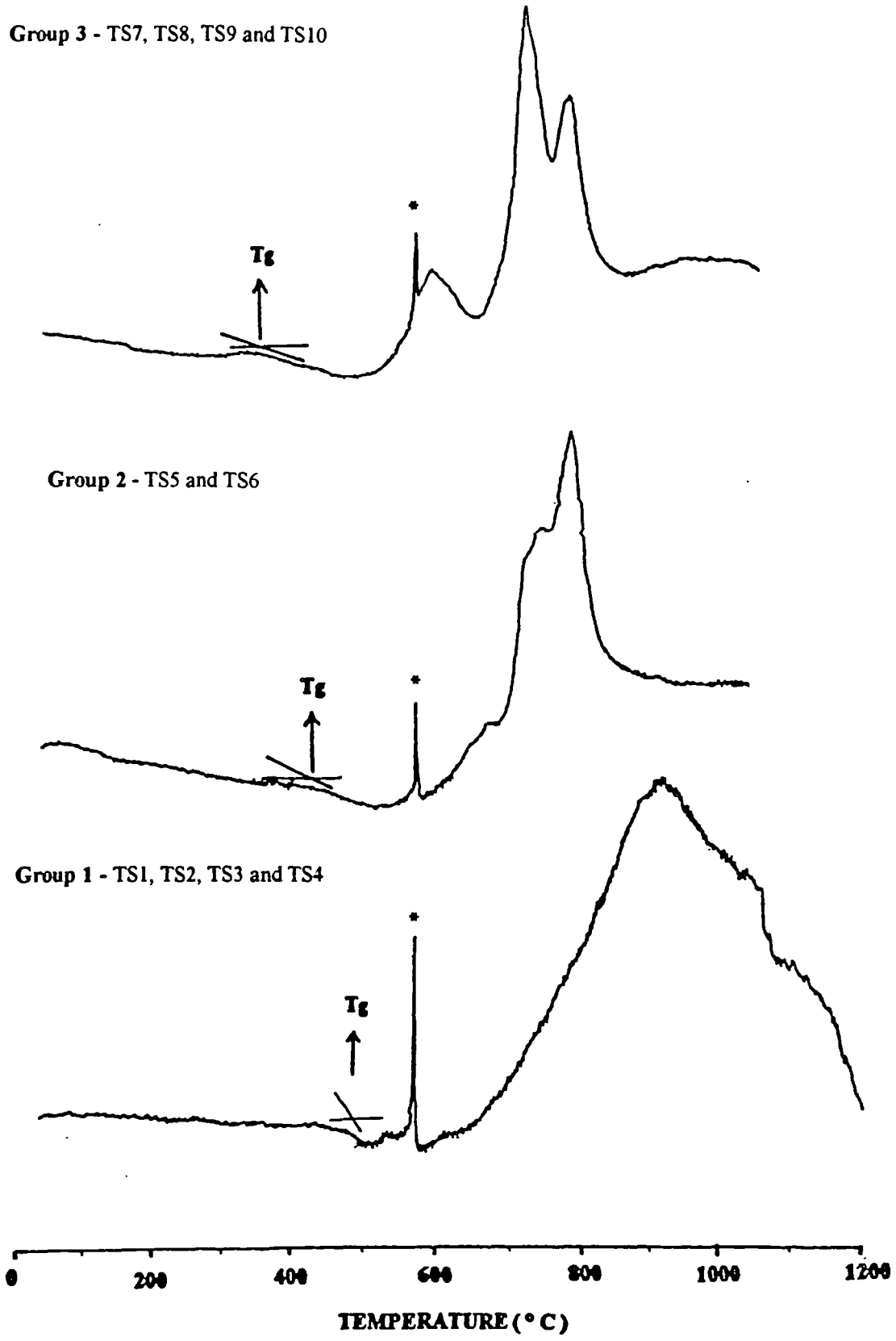

Figure 6.2 : *DTA traces of SnO-SiO_2 glasses. The symbol * is the reference peak of $\alpha \rightarrow \beta$ quartz transition.*

exotherm could indicate oxidative degradation of the material. As can be seen in Table 6.1, the three exothermic peaks (T_{x1}, T_{x2} and T_{x3}) occur at about the same temperatures for samples in the second and third group. This means that the exothermic peaks for these groups probably arise from the same thermal events.

Table 6.1: *Glass transition (T_g) and position of exothermic peak maximum obtained from the DTA experiment.*

Glass	*Mol.% SnO*	*T_g (± 10°C)*	*Positions of peak maximum of the exothermic events (±5°C)*		
			T_{x1}	*T_{x2}*	*T_{x3}*
Group 1					
TS1	*16.8*	*685*	*1067 (VB)*	-	-
TS2	*28.2*	*370*	*920 (VB)*	-	-
TS3	*29.6*	*356*	*915 (VB)*	-	-
**TS4*	*32.6*	*478*	*864 (VB)*	-	-
Group 2					
TS5	*39.7*	*438*	*660 (B)*	*741 (N)*	*783 (N)*
**TS6*	*40.9*	*400*	*660 (B)*	*738 (N)*	*780 (N)*
Group 3					
TS7	*49.4*	*368*	*586 (B)*	*714 (N)*	*776 (N)*
TS8	*53.5*	*378*	*591 (B)*	*718 (N)*	*783 (N)*
**TS9*	*55.4*	*403*	*595 (B)*	*720 (N)*	*782 (N)*
TS10	*64.0*	*433*	*605 (B)*	*713 (N)*	*773 (N)*

B - Very broad (FWHM ~ 300°C). B - Broad (FWHM ~ 100°C). N - Narrow (FWHM ~ 50°)

** Samples that were selected for heat treatment experiments.*

6.2 HEAT TREATED SnO-SiO_2 GLASSES

Because the glasses were very difficult to make, the availability of glass, from each composition, was limited for the heat treatment experiments. Thus only one composition from each group was selected for heat treatment experiment. Samples TS4, TS6, TS9, were selected from group one, two and three respectively.

6.2.1 HEAT TREATMENT IN AIR

Having determined the exothermic peaks from the DTA traces, fragments of glass from the three selected glass samples were heat treated in an electric furnace under ordinary atmosphere. Separate glass samples were inserted in the furnace at room temperature and heated in turn to the maximum temperatures corresponding to the exothermic peaks and maintained at the maximum temperatures for a specific time before being cooled to room temperature. The samples were then subjected to X-ray diffraction analysis for phase identification. The results of the heat treated glasses are discussed below.

Group 1

Glass TS4 with SnO content of 32.6 mol.% stayed glassy with some superficial oxidation after heat treatment at 700°C for 5 hours. Heat treatment of a sample at 900°C for 3 hours showed that the glass appearance was degraded. X-ray diffraction showed precipitated crystalline phases of SnO_2, SiO_2 (α-cristobalite) and traces of glass phase. These results showed that the very broad exothermic peak of the DTA trace corresponds to oxidative degradation or decomposition of the glass. It can be concluded that glasses with $\leq$ 33 mol.% SnO are very hard to devitrify i.e.

decomposition occurs before crystallisation can take place. This result is the same as that observed by Carbo Nover et al [1] and Ishikawa et al [2].

Group 2

Samples of glass TS6, with 40.9 mol.% SnO, underwent heat treatments corresponding to each of the three exothermic peaks. Heat treatment at 670°C for 3 hours produced the metastable crystalline $SnSiO_3$ [2-4] as the major phase + SnO as a minor phase + some SnO_2 + SiO_2 (cristobalite) phases and traces of glass estimated at about 8 %. The second heat treatment at 730°C for 4 hours produced SnO_2 + SiO_2 (cristobalite) as the major phases + minor phases of $SnSiO_3$ and SnO and about 3% of glass was left. The third heat treatment at 770°C for 5 hours produced SnO_2 + SiO_2 (cristobalite). From these results; we can assign the first small broad peak T_{x1} as the devitrification peak that produces the metastable $SnSiO_3$. The second peak T_{x2} corresponds to decomposition of metastable $SnSiO_3$ to SnO and SiO_2 and the third peak T_{x3} is the oxidation peak of SnO to SnO_2.

In addition to producing the $SnSiO_3$ crystal phase, the first heat treatment at 670°C also produced other phases. Two reasons can be suggested for this. The first reason is that peak T_{x1} is broad and overlaps with the decomposition peak; hence, as $SnSiO_3$ crystalline phase precipitated in the glass, some of it also started to decompose to SnO and SiO_2. The presence of some SnO_2 crystal phase can be attributed to the fact that these glasses also contain a very small amount of dissolved Sn^{4+} species (SnO_2). Because of its low solubility in glass, it is thought that the Sn^{4+} environment in glass differs little from its crystalline form (chapter 7); SnO_2 in the glass could thus easily be reverted back to its more stable SnO_2 crystal phase. In air this process is speeded up.

Group 3

Glass TS9 with 55.4 mol.% SnO underwent four separate heat treatments, each time carried out on fresh glass pieces. After heat treatment at 570°C for 2 hours, ~70% of the material stayed glassy with some precipitation of $SnSiO_3$, SnO_2 and SnO phases. Heat treatment at 620°C for 3 hours produced more $SnSiO_3$, making it the major phase, with minor phases of SnO , SnO_2 and SiO_2 (cristobalite) and ~ 40% of glass was left. These two heat treatment temperatures lie within the range of the first exothermic peak, Tx_1 , which can be identified as arising from formation of metastable $SnSiO_3$. The reasons for the presence of the other phases, apart from $SnSiO_3$, are the same as given before for group 2. Heat treatment, corresponding to the second peak Tx_2, was carried out at 720°C for 4 hours and produced SnO_2 and SiO_2 (cristobalite) phases with ~ 20% glass remaining. Heat treatment at 780°C for 5 hours produced SnO_2 and SiO_2 (cristobalite). This last heat treatment corresponds to Tx_3, which can therefore be assigned as the oxidation peak. The second peak of Tx_2 is thus identified as decomposition of $SnSiO_3$ into SnO and SiO_2 but, as the position of the heat treatment temperature overlapped with the tail of Tx_3, the SnO thus produced will readily oxidise to SnO_2. Figure 6.3 shows the XRD traces of the glass after each heat treatment.

6.2.2 HEAT TREATMENT IN ARGON

The results of the DTA and heat treatment experiments have shown that glasses with SnO contents ≥ 40 mol.% can be crystallised to form a metastable compound $SnSiO_3$ in the temperature range of 570°C to 680°C. According to Ishikawa et al [2], the structure of the $SnO\text{-}SiO_2$ glass appears to resemble the crystalline metastable stannous metasilicate, $SnSiO_3$. Therefore the crystalline phase $SnSiO_3$ is important. $SnSiO_3$ cannot be easily formed as a single phase by

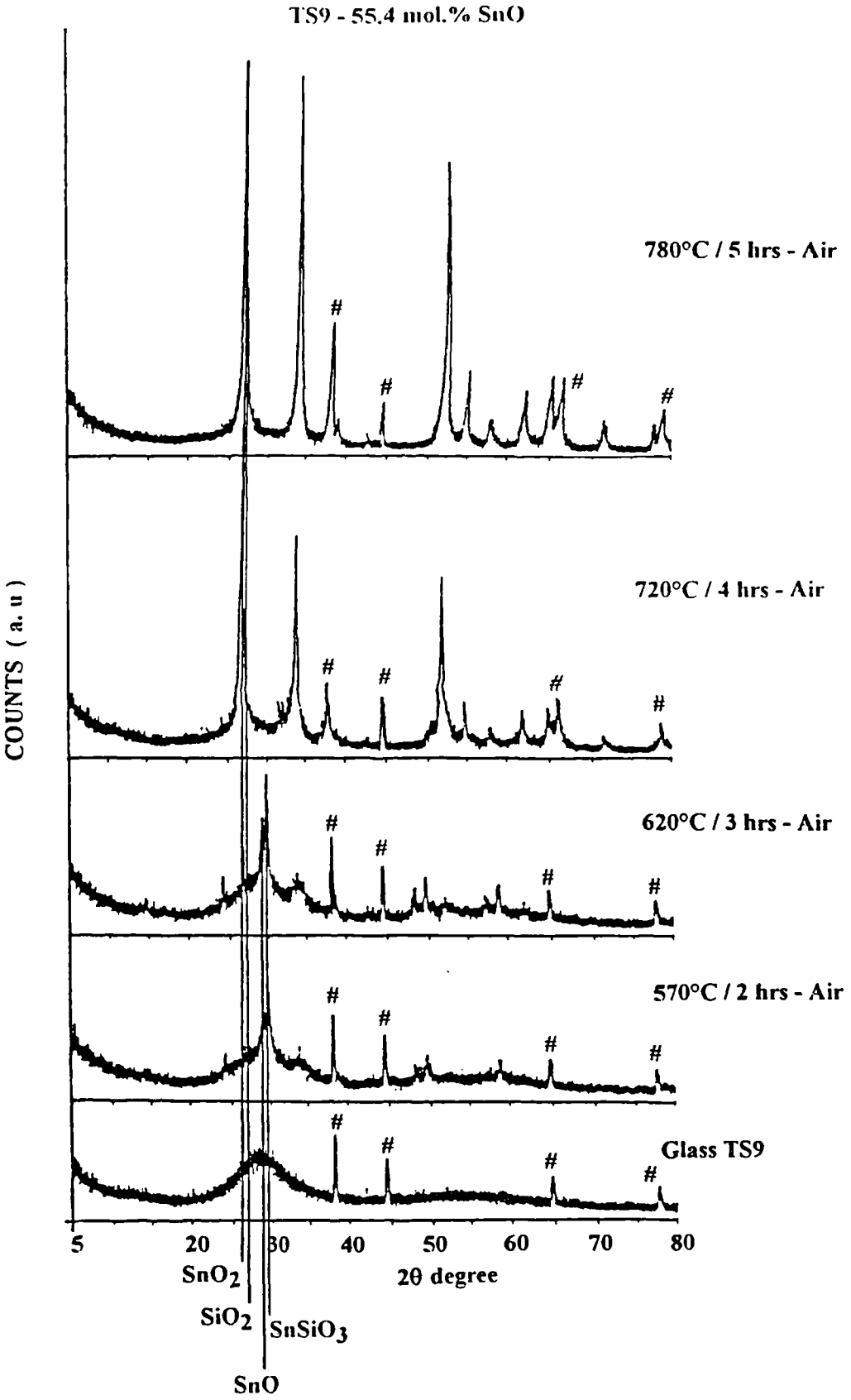

Figure 6.3 : X-ray powder diffraction patterns for heat treated TS9 glasses. Lines indicate the positions of the main peak of the various phases present. The symbol # indicates the peaks from aluminium sample holder.

devitrification. Decomposition and oxidation reactions simultaneously accompany the formation of the $SnSiO_3$ phase. Therefore, it was decided to try the heat treatment in an inert gas atmosphere, argon, using remaining samples of TS6 and TS9.

Glass TS6 (40.9 mol.% SnO)

This glass was heat treated in argon from cold and remained at 600°C for 4 hours before being slowly cooled to room temperature. Visually the glass appeared fully crystallised with a homogenous yellow colour. XRD showed that $SnSiO_3$ was the major phase with trace amounts of SnO and SiO_2 , and ~25% of glass left. Figure 6.4 shows the XRD traces for this glass when heat treated in Argon as compared to heat treated in air.

Glass TS9 (55.4 mol.% SnO)

This glass was heat treated in argon from cold and remained at 590°C for 4 hours and slowly cooled to room temperature. Visually the glass appeared fully crystallised, giving a block coloured in various shades of brown. XRD showed that $SnSiO_3$ was the major phase with a trace of SnO and ~30% of glass left.

This shows it is possible to crystallise the glass to get the metastable $SnSiO_3$ crystal phase by heating in an inert atmosphere but again, traces of other crystal phases and some glass pose difficulties in analysing the results properly.

6.2.3 SUMMARY OF THE RESULTS OF BOTH HEAT TREATMENTS

It is instructive to look at the results of these heat treatments as a whole and they are summarised in Table 6.2. It should be borne in mind that samples heat treated at a particular temperature will in fact pass through the preceeding transformation ranges as they come to equilibrium.

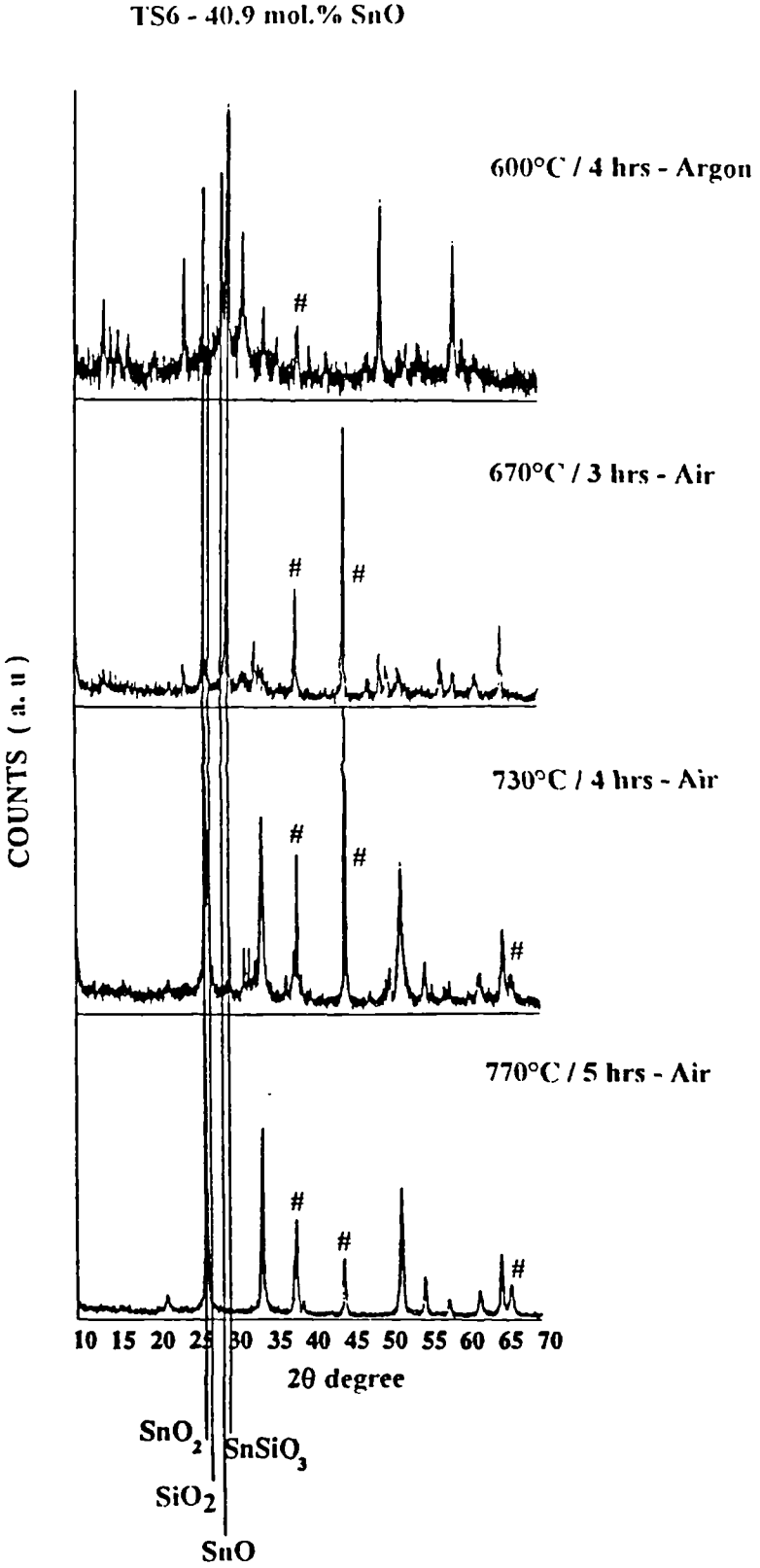

Figure 6.4 : X-ray powder diffraction patterns for heat treated TS6 glasses. Lines indicate the positions of the main peak of the various phases present. The symbol # indicates the peaks from aluminium sample holder.

Table 6.2 : *Summary of the results of heat treatment of some SnO-SiO_2 glasses*

Sample and heat treatment	*$SnSiO_3$*	*SnO*	*SnO_2*	*SiO_2*	*Glass*
TS4 - Air 700°C/ 5 h	-	-	-	-	*M (superficial oxidation)*
TS4 - Air 900°C/ 3 h	-	-	*M*	*M*	*t*
TS6 - Air 670°C/ 3 h	*M*	*m*	*m*	*m*	*~ 8 %*
TS6 - Air 730°C/ 4 h	*m*	*m*	*M*	*M(c)*	*~ 3 %*
TS6 - Air 770°C/ 5 h	-	-	*M*	*M(c)*	-
TS6 - Argon 600°C / 4 h	*M*	*t*	-	*t(c)*	*~ 25 %*
TS9 - Air 570°C/ 2 h	*m*	*m*	*m*	-	*~ 70 %*
TS9 - Air 620°C/ 3 h	*M*	*m*	*m*	-	*~ 45 %*
TS9 - Air 720°C/ 4 h	-	-	*M*	*M(c)*	*~ 18 %*
TS9 - Air 780°C/ 5 h	-	-	*M*	*M(c)*	-
TS9 - Argon 590°C / 5 h	*M*	*t*	-	-	*~ 30 %*

M - Major phase . m - minor phase . t - trace phase. c - cristobalite

Scanning Electron Microscope observations of the heat treated glasses were carried out on some of the samples. Some micrographs are shown in Figure 6.5 and 6.6. The morphology of the crystals grown by heat treatment both in air and argon for glass TS6 is lamellar. For glass TS9 the morphology of the crystals is spherulitic, both grown in air and argon.

6.3 ^{119}Sn MÖSSBAUER SPECTRA OF HEAT TREATED GLASSES

^{119}Sn Mössbauer spectra of heat treated glasses were taken at 77K. Typical spectra of the heat treated glasses in air are shown in Figure 6.7. They show a doublet (Sn^{2+}) and singlet (Sn^{4+}) with the Sn^{2+} species being oxidised to Sn^{4+} as the heat treatment temperature gets higher. The spectra (Figure 6.8) from glasses heat treated in argon show only doublets indicating that tin is still in the Sn^{2+} state. As can be seen

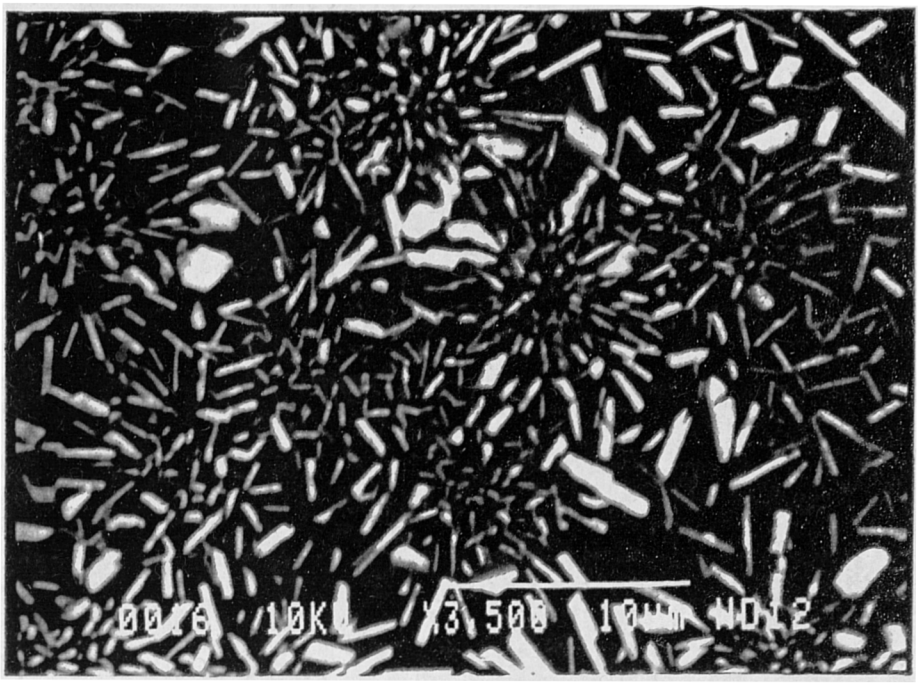

(a)

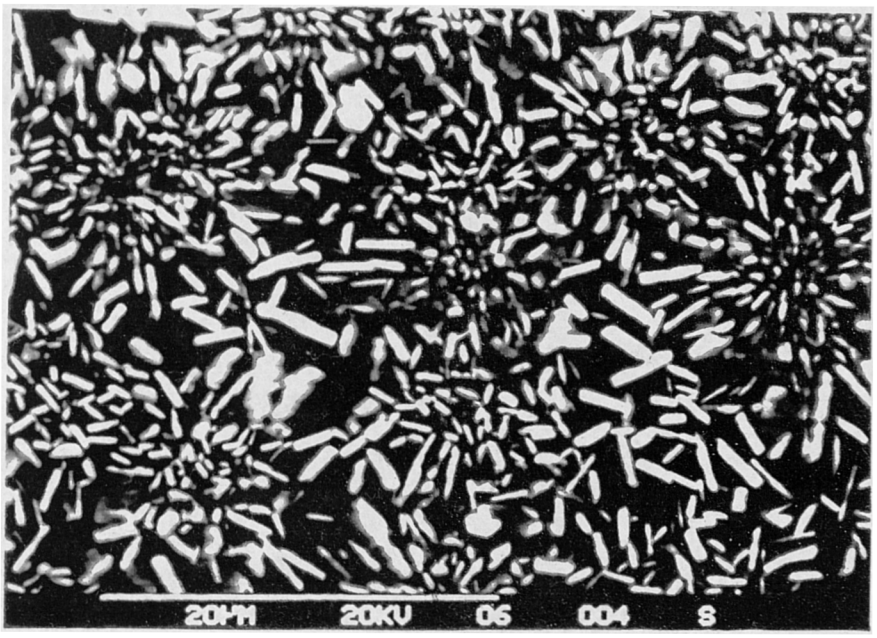

(b)

Figure 6.5 : *SEM micrographs of heat treated TS6 glasses. (a) Heat treated at 600°C for 5 hours in air. (b) Heat treated at 600°C for 4 hours in argon. The morphology of the crystal is lamellar for both grown in air and argon.*

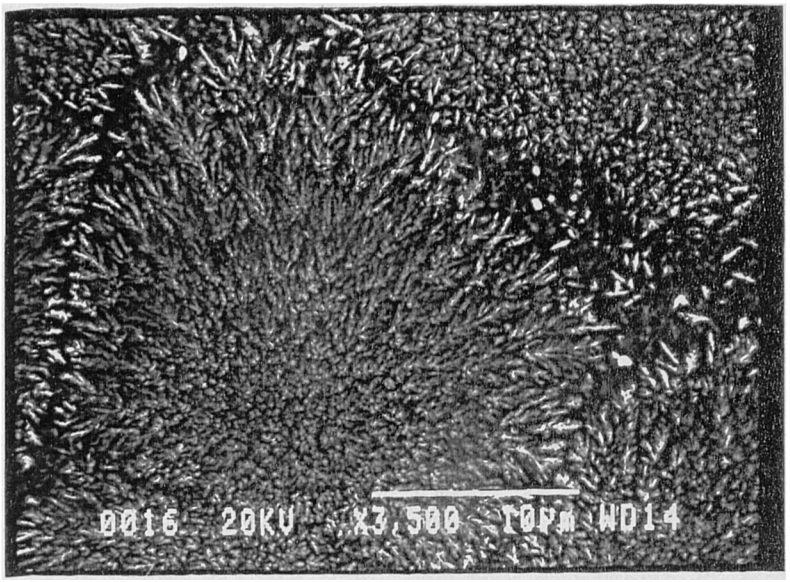

(a)

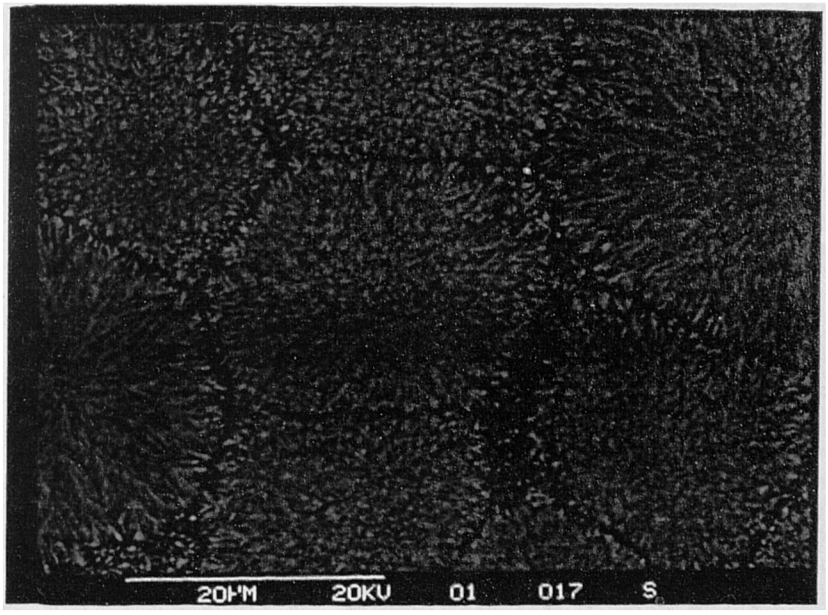

(b)

***Figure 6.6** : SEM micrographs of heat treated TS9 glasses. (a) Heat treated at 590°C for 5 hours in air. (b) Heat treated at 590°C for 5 hours in argon. The morphology of the crystal is spherulitic for both grown in air and argon.*

in both Figures 6.7 and 6.8, the singlet was fitted with one component and the doublet fitted to two components. In this way the doublet belonging to the Sn^{2+} site in $SnSiO_3$ phase has been identified. The Mössbauer parameters of Sn^{2+} in $SnSiO_3$ phase are compared to the parent glass and also to crystalline SnO, as shown in Table 6.3.

Table 6.3 : *Mössbauer parameters of the Sn^{2+} site in $SnSiO_3$, in the parent glass and in crystalline SnO.*

TS6 - 40.9 mol.% SnO	*Glass*	*$SnSiO_3$ from heat treatment at 670°C/3 hours in air*	*$SnSiO_3$ from heat treatment at 600°C/4 hours in Argon*	*SnO (crystalline)*
**Isomer shift, δ (±0.005 mm/s)*	*3.001*	*2.885*	*2.897*	*2.685*
Quad. splitting, Δ (±0.005 mm/s)	*2.070*	*2.277*	*2.112*	*1.36*
Linewidth, Γ (±0.005 mm/s)	*1.153*	*0.981*	*0.993*	*0.917*
TS9 - 55.4 mol.% SnO	*Glass*	*$SnSiO_3$ from heat treatment at 620°C/3 hours in air*	*$SnSiO_3$ from heat treatment at 590°C/4 hours in Argon*	*SnO (crystalline)*
**Isomer shift, δ (±0.005 mm/s)*	*2.964*	*2.918*	*2.893*	*2.685*
Quad. splitting, Δ (±0.005 mm/s)	*2.044*	*2.082*	*2.082*	*1.36*
Linewidth, Γ (±0.005 mm/s)	*1.152*	*1.017*	*0.997*	*0.917*

**Relative to $CaSnO_3$ source.*

One would expect the parameters of Sn^{2+} in $SnSiO_3$ to be the same whatever the glass composition or heat treatment. The difference presented in Table 6.3 illustrates the problems associated with the fitting of the Mössbauer lineshapes. The

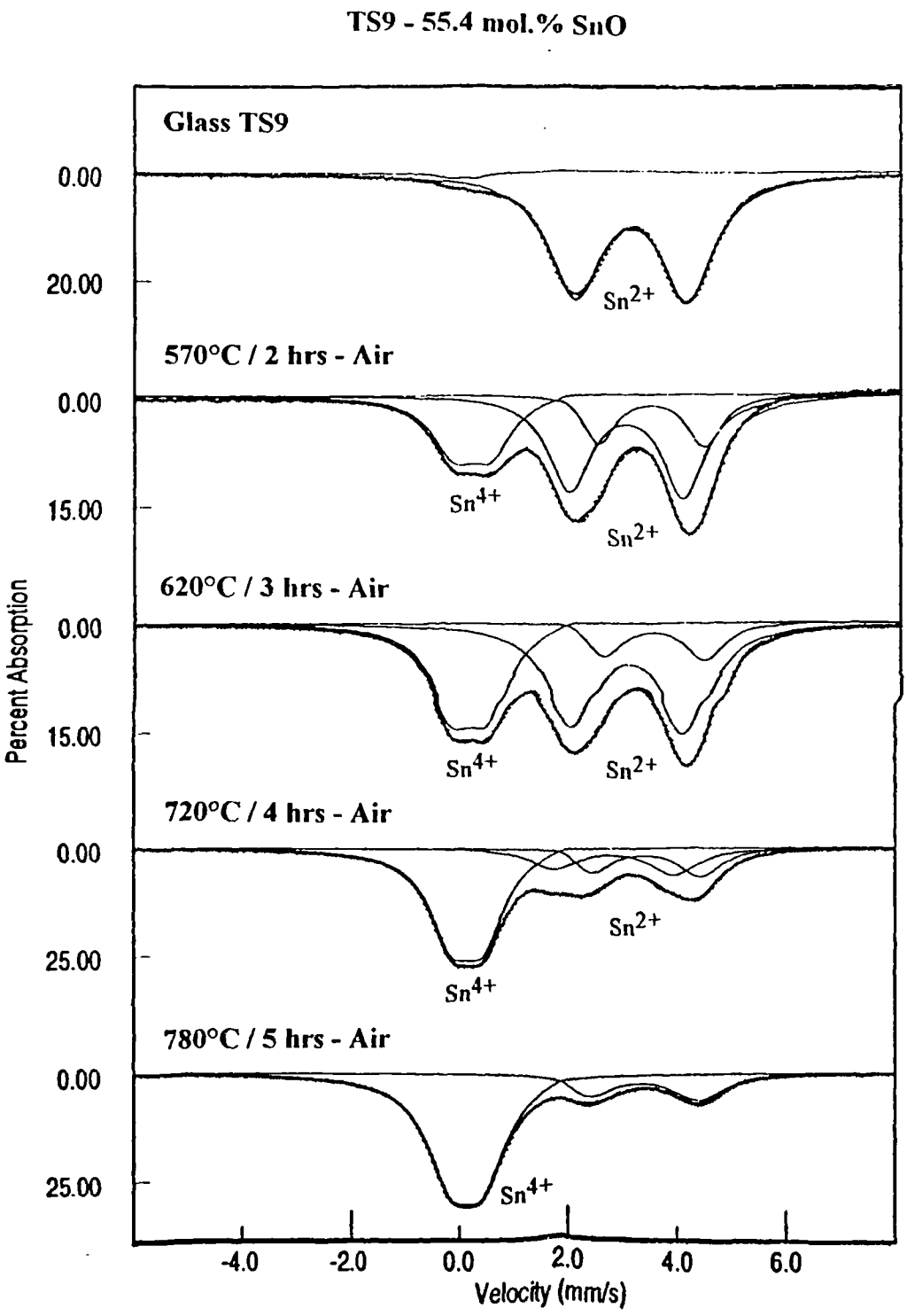

Figure 6.7 : ^{119}*Sn Mössbauer spectra of TS9 glass and air heat treated TS9 glasses.*

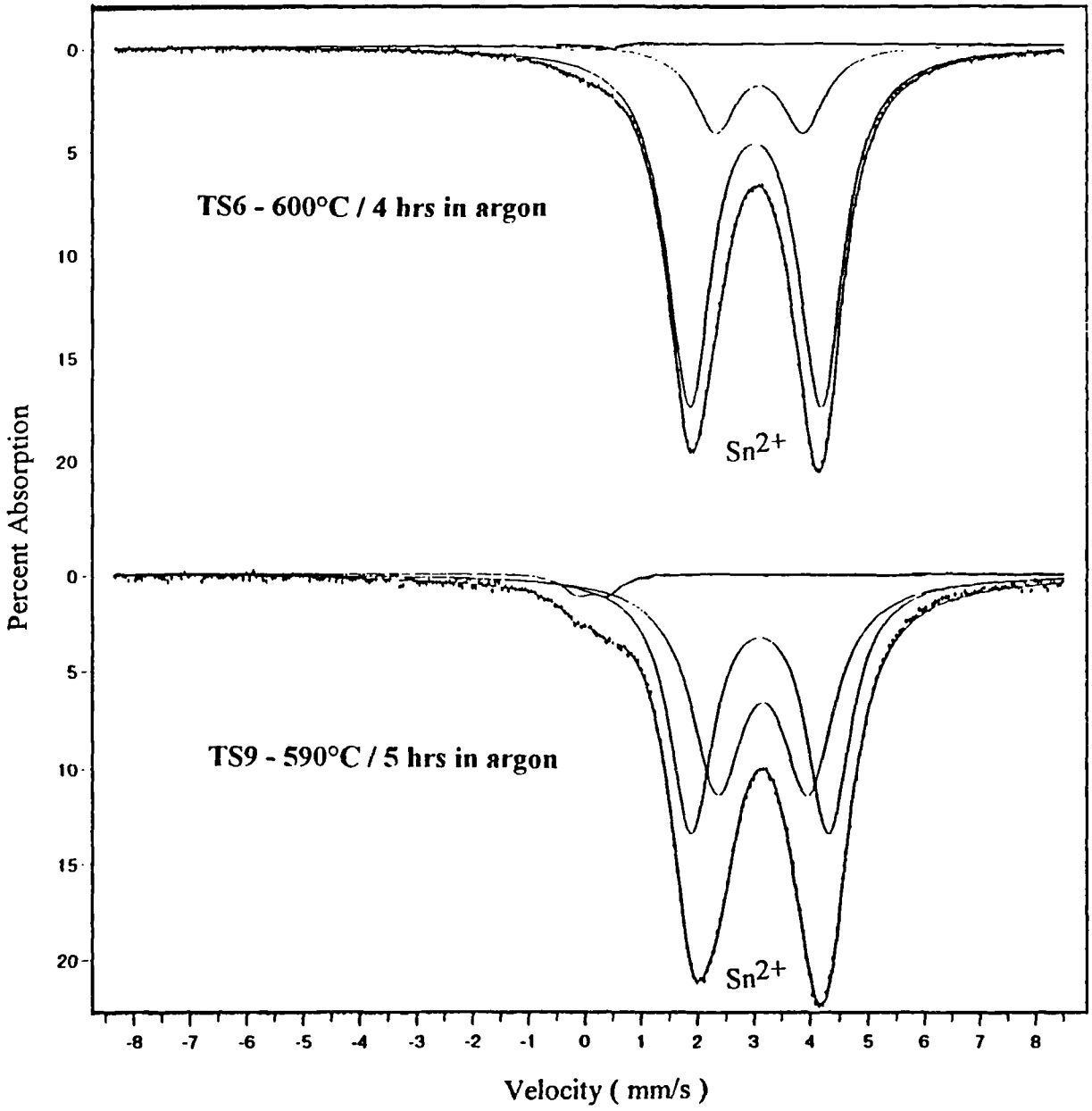

Figure 6.8 : ^{119}Sn Mössbauer spectra of glass TS6 and TS9 after heat treatment in argon.

species which could be contributing to the Sn^{2+} doublet are ; Sn^{2+} in $SnSiO_3$, Sn^{2+} in SnO and Sn^{2+} in any residual glass. It was feasible only to fit the doublet to two gaussians. The species with the smaller quadrupole splitting, (1.2 - 1.4 mm/s) corresponds to crystalline SnO (1.36 mm/s). Therefore the doublet with the larger quadrupole splitting must incorporate Sn^{2+} in $SnSiO_3$ and any Sn^{2+} remaining in the glass phase. The quadrupole splitting associated with the Sn^{2+} site in $SnSiO_3$ is higher than in glass. This shows that the Sn^{2+} site is experiencing a greater electric field gradient due to the influence of, probably the neighbouring ions. Formation of the $SnSiO_3$ crystal phase necessitates the formation of Si—O—Sn bonds and the nonequivalence of these bonds is manisfested in the greater values of the quadrupole splitting. The isomer shift of the Sn^{2+} site in $SnSiO_3$ is slightly lower than in the corresponding glass and the linewidth is narrower. This narrowing is to be expected because Sn^{2+} species are now in a more ordered lattice arrangement as compared to the low order in glass.

6.4 ^{29}Si MAS NMR OF HEAT TREATED GLASSES

Due to the small amounts of heat treated samples at our disposal , only a few samples of glass TS6 were used for ^{29}Si MAS NMR experiments. Generally the chemical shifts of ^{29}Si in the heat treated samples are shifted considerably towards higher field as compared to glass. Table 6.4 gives the summary of the ^{29}Si MAS NMR spectra for the devitrified glasses as compared to the parent glass.

Table 6.4: *Summary of ^{29}Si MAS NMR spectra for glass TS6 (40.9 mol.% SnO)*

	Glass	*Heat treated in Argon 600°C / 4 hours*	*Heat treated in air 670°C / 3 hours*	*Heat treated in air 770°C / 5 hours*
Peak position of chemical shift for the main peak (±0.1 ppm)	*-100.6*	*-109.5*	*-110.1*	*-111.2*
FWHM (± 0.1 ppm)	*23.2*	*14.2*	*13.8*	*11.6*
Descriptions of the spectra	*Asymmetric broad peak*	*The main peak is from Si site in $SnSiO_3$ and there is a broader peak at less negative shift identified as belonging to the residual glass*	*The main peak is from Si site in $SnSiO_3$ and there is a broader peak at less negative shift identified as belonging to the residual glass*	*The main peak is from Si site in cristobalite plus a broader peak at less negative shift identified as belonging to the residual glass*

6.5 CONCLUSIONS

The experiments have shown that glass containing ≥ 40 mol.% SnO can be heat treated in the temperature range of 570°C to 680°C to produce a metastable crystalline phase called stannous metasilicate ($SnSiO_3$). This is consistent with the observations of Carbo Nover et al [2] and Ishikawa et al [3]. At temperatures above ~700°C this phase decomposed to SnO + SiO_2 and at temperatures greater than 720°C oxidation of SnO + SiO_2 to SnO_2 and SiO_2 (cristobalite) took place. Sn metal was not observed to be one of the products of the devitrification process, contrary to the reports of Carbo Nover et al [2] and Ishikawa et al [3]. The crystallisation,

decomposition and oxidation of the $SnO\text{-}SiO_2$ glasses can be summarised schematically in Figure 6.9 below.

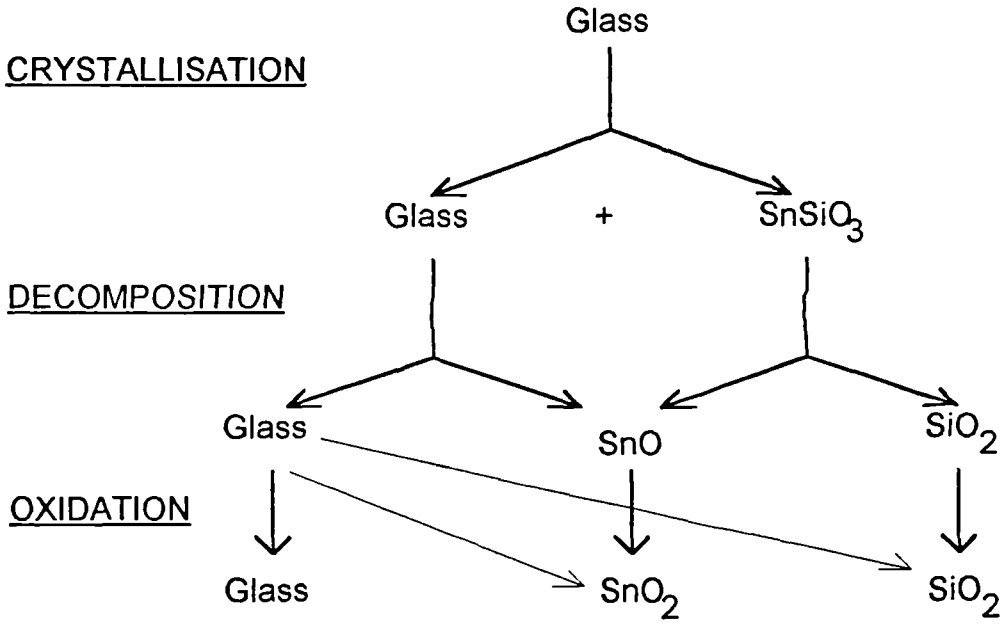

Figure 6.9 : *Schematic diagram of the mechanism of devitrification of $SnO\text{-}SiO_2$ glasses.*

It was generally found that the decomposition and oxidation events overlapped and the overlapping is much more pronounced if the heat treatment is carried out in air. The $SnSiO_3$ crystal phase can be grown by heat treatment in argon but XRD analysis showed that the product was not single phase under the conditions used.

REFERENCES

1. Pope,M.I. (1977). *Differential Thermal Analysis*, Heyden.
2. Carbo Nover, J. & William, J. (1967). *Physics Chem. Glasses* **8**(4), 164.
3. Ishikawa, T. & Akagi, S. (1978). *Physics Chem. Glasses* **19**(5), 108.
4. JCPDS file no. 20 - 1295

Chapter 7 - Tin-Doped Float Glass

7.1 INTRODUCTION

The general process of making the float glass has been outlined in chapter 1, which shows how molten tin in the float chamber modifies the physiochemical characteristics of the glass surfaces as compared to the bulk of the glass. Chapter 2 briefly reviewed some of the few past studies that have concentrated on the determination of tin oxidation states and profiling the tin concentration as a function of depth. A high concentration of tin is found in the first ~ 10 nm thickness of the surface and the concentration decreases rapidly with increasing depth. Only about one tenth of the float side concentration is found in the upper surface. Those studies also saw differences in the depth of tin diffusion, the type of tin oxidation states (Sn^{2+} or Sn^{4+} or Sn^{0}) and their relative amounts. These differences are due to variations in the production conditions, such as the thickness of the glass produced, the time the glass spends in the float chamber and the cleanliness of the float chamber. Depending on the glass thickness, hence the diffusion time, the maximum depth of tin diffusion reported is ~ 40 μm (diffusion time of ~ 60 min.) into the lower surface [1].

Table 7.1 gives a summary of some of the previous studies of tin in float glass. Generally most of the studies found that only Sn^{2+} and Sn^{4+} are present in the glass and Sn^{2+} predominates over Sn^{4+} but the ratio of Sn^{2+}/Sn^{4+} decreases with depth. Figure 7.1 shows a typical tin diffusion profile in the lower side of float glass specimens produced by Pilkington Glass Plc. For glass that had undergone heat treatment for tempering or to produce articles such as curved car windscreens, some Sn^{2+} oxidized to Sn^{4+} , and Sn^{2+} was no longer the predominant species. As for the effect of tin on float glass, the studies of Sieger [2] concluded that the chemical effects of tin on float glass very seldom lead to problems and in some cases are beneficial. For example, his cyclic humidity tests have shown that tin improved the glass

Table 7.1 : *Summary of some of the previous studies of tin in float glass*

	Samples thickness (mm)	*Maximum depth of penetration into the lower surface*	*Tin species found*	*Dominant species*	*Other remarks*	*Method*
Sieger [2]	*3, 6 and 12*	*30 μm for 6 mm thick*	Sn^{2+} *and* Sn^{4+}	Sn^{2+} *by Mössbauer* Sn^{4+} *by XPS*	*Tin profile exhibits an anomalous 'hump' at ~ ½ effective tin penetration*	*EPMA, Mössbauer XPS*
Colombin et al [3]	*5.3*	*~ 10 nm by XPS 6 nm by photoluminiscence*	Sn^{2+} *and* Sn^{4+} *by XPS*	*The ratio of* Sn^{2+}/Sn^{4+} *decreases with depth*	*High concentration mainly in first 6 nm from the surface*	*XPS, Photoluminisence*
Jie & Chao [4]	*1*	*170 nm*	Sn^{2+}, Sn^{4+} *and* Sn^{0}	Sn^{4+}	*The only studies that detect* Sn^{0}	*XPS*
Principi et al [5]	*N/A*	*N/A*	Sn^{2+} *and* Sn^{4+}	Sn^{2+} *in the 10 nm outer layer.*	Sn^{4+} *dominating after heat treatment*	*CEMS*
Pantano et al [6]	*2.1, 4, 6, 8 , 12*	*10 μm for 2.1 mm 12 μm for 4 mm 20 μm for 6 mm 31 μm for 8 mm 40 μm for 12 mm*	Sn^{2+} *and* Sn^{4+}	Sn^{2+}*dominating. The ratio of* Sn^{2+}/Sn^{4+} *decreases with depth*	Sn^{4+}*dominating after heat treatment. Steep concentration gradient in the outer 100 nm. Anomolous hump as observed by Sieger [2]*	*SIMS, EPMA and Mössbauer*
Chappell & Stoddart [7]	*Unweathered glass of unknown thickness*	*N/A*	*Two undetermined species*	*N/A*	*Concentration of tin in the underside is 10 times greater than the upper and mainly concentrated in first 3 nm*	*Auger electron spectroscopy*

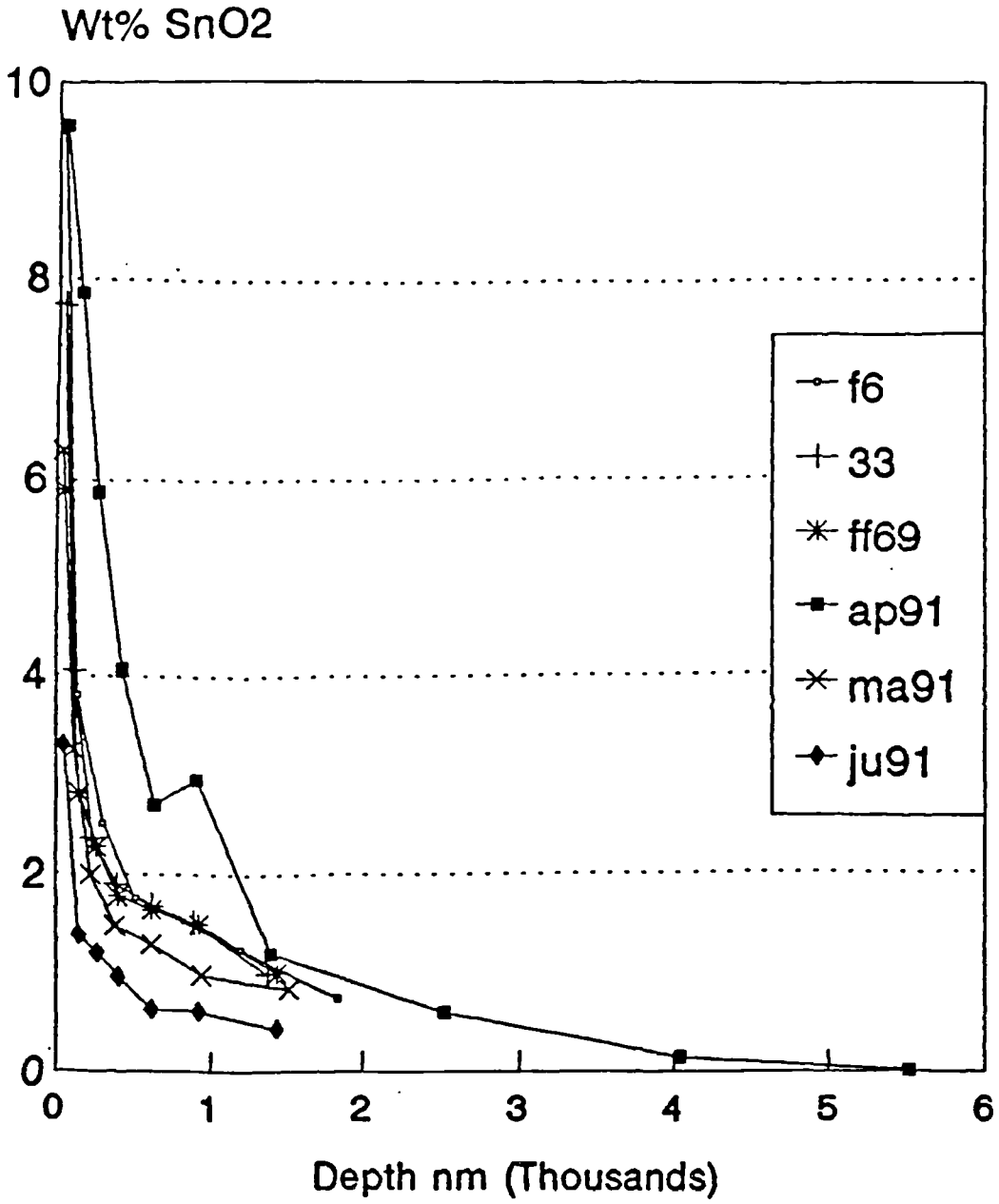

Figure 7.1 : *Typical tin diffusion profiles in the underside of float glass produced by Pilkington Glass Plc. For simplicity the tin oxide concentration is expressed in wt.% SnO_2, even though it has been shown that tin in both valence states of +2 and +4 coexist in the glass. It shows that the depth of tin penetration is to about 6μm and the tin oxide concentration at the surface is about 10 wt% (~3mol%). Specimens ap91 and ju91 exhibit what Sieger [2] described as an anomalous 'hump' or satellite peak at about 1μm depth. The graph is obtained by the courtesy of Pilkington Technology Management, Lathom, Ormskirk.*

weatherability. He also added that too much reduced tin (Sn^{2+}) can lead to a "bloom" problem in subsequent oxidizing bending and tempering applications.

The main objective of doping float glass with tin is to study the effect of tin on the structure and physical properties of float glass. The tin-doped float glass will contain varying amounts of tin, in different oxidation states, and thus we attempted to mimic the tin concentration found in the tin-diffused region of commercial float glass. This chapter present the results and discussion of the studies.

Table 7.2 : *Analyzed composition of float glass and tin-doped float glass.*

Samples	***PK0***	***PK2.5S***	***PK5S***	***PK7.5S***	***PK10S***	***PK12.5S***	***PK15S***
Wt.% of SnO added (nominal)	*0*	*2.5*	*5*	*7.5*	*10*	*12.5*	*15*
SiO_2 (mol.%)	*72.91*	*72.33*	*72.79*	*73.07*	*72.78*	*73.16*	*73.28*
Na_2O (mol.%)	*11.61*	*11.84*	*11.69*	*11.56*	*11.66*	*11.40*	*11.51*
CaO (mol.%)	*8.56*	*8.72*	*8.54*	*8.52*	*8.60*	*8.48*	*8.51*
MgO (mol.%)	*5.81*	*5.91*	*5.79*	*5.76*	*5.82*	*5.90*	*5.67*
Al_2O_3 (mol.%)	*0.63*	*0.66*	*0.66*	*0.63*	*0.67*	*0.60*	*0.54*
K_2O (mol.%)	*0.34*	*0.33*	*0.33*	*0.34*	*0.35*	*0.36*	*0.36*
SO_3 (mol.%)	*0.07*	*0.13*	*0.12*	*0.06*	*0.05*	*0.04*	*0.05*
Fe_2O_3 (mol.%)	*0.04*	*0.05*	*0.05*	*0.04*	*0.04*	*0.04*	*0.04*
TiO_2 (mol.%)	*0.03*	*0.03*	*0.03*	*0.02*	*0.03*	*0.02*	*0.04*
ZrO_2 (mol.%)	*<0.01*	*<0.01*	*<0.01*	*<0.01*	*<0.01*	*<0.01*	*<0.01*
As_2O_3 (mol.%)	*<0.01*	*<0.01*	*<0.01*	*<0.01*	*<0.01*	*<0.01*	*<0.01*
Total tin oxide $SnO+SnO_2$ (mol.%)	*0*	*1.19*	*1.39*	*3.64*	*5.26*	*6.00*	*6.97*
% Sn^{2+} tin of total tin (chemical)	*0*	*5*	*5*	*33*	*28*	*37*	*48*

The errors in the analysis is ± 3%

7.2 GLASS COMPOSITION

In terms of composition, float glass is a complex material but it is normally referred to as soda-lime-silica glass. The float glass sample obtained from Pilkington contains SiO_2, Na_2O, CaO and MgO as the major components which make up 98.9 mol.% plus 1.1 mol.% of seven minor components. Table 7.2 gives the detailed analyzed compositions of undoped (PK0) and the tin-doped float glasses studied. The tin oxide percentage contents were calculated as additional to the 100% of the undoped float glass (PK0). Compositional analysis of all samples showed that the mol.% of the major constituents do not change by more than 2 mol.% between the samples and the undoped float glass. Therefore; except for tin oxide, the tin-doped float glasses had the usual composition of float glass constituents.

Table 7.3 : *Tin contents of tin-doped float glasses*

Samples	***PK2.5S***	***PK5S***	***PK7.5S***	***PK10S***	***PK12.5S***	***PK15S***
Wt.% of SnO added (nominal)	*2.5*	*5*	*7.5*	*10*	*12.5*	*15*
Total tin oxide (analysed) $SnO+SnO_2$ (wt.%)	*2.99*	*3.52*	*8.93*	*12.99*	*14.68*	*16.83*
SnO (mol.%)	*0.06*	*0.07*	*1.20*	*1.47*	*2.22*	*3.35*
SnO_2 (mol.%)	*1.13*	*1.32*	*2.44*	*3.79*	*3.78*	*3.62*
Total tin oxide $SnO+SnO_2$ (mol.%)	*1.19*	*1.39*	*3.64*	*5.26*	*6.00*	*6.97*
mol% SnO_2 / mol% SnO	*18.83*	*18.86*	*2.03*	*2.58*	*1.70*	*1.08*

Errors in the analysis is ± 3 %

The analysis also shows that tin in the glass samples are in the Sn^{2+} and Sn^{4+} states. The percentage amounts of Sn^{2+} out of the total tin species were obtained by chemical analysis and Mössbauer spectroscopy. The chemical techniques show that samples PK2.5S and PK5S, contain a very small amount of SnO (Sn^{2+}). Such small amounts were not detected by the Mössbauer technique. So, for calculation of the mol.% of SnO and SnO_2 contents the chemical technique results were used. Table 7.3 details the tin oxide contents of the tin-doped float glass samples.

The source of the tin oxide in the tin-doped float glass comes from stannous oxalate, which decomposes to SnO and CO + CO_2 gases. These gases help to maintain a slightly reducing atmosphere during melting. However, some oxidation of SnO to SnO_2 does occur. Thus the concentrations of tin oxide mimic points along the diffusion profile of tin in float glass, in terms of tin content, but the distribution of oxidation states may differ.

We have said earlier that SnO is readily soluble in the glass but the solubility of SnO_2 in pure silicate glass is very small but increases in the presence of alkali oxides. In samples PK12.5S and PK15S, traces of crystalline SnO_2 were observed in some regions of the samples, suggesting that the solubility (saturation) limit of SnO_2 had been reached. These regions were removed before any measurements were made. The saturation of SnO_2 in the glass is better seen in the plot of the variation of tin oxidation state with total tin content in Figure 7.2. As the tin oxide content of the glass increases, SnO and SnO_2 increase but, at compositions greater than ~ 5 mol.% total tin oxides, SnO_2 reached its maximum content of ~ 3.8 mol.% SnO_2 and remains constant, whereas SnO increases more rapidly with the increase of tin content. At compositions ≥6 mol.% SnO, the glass shows traces of the undissolved cassiterite SnO_2. The results showed that ratio of Sn^{2+}/Sn^{4+} thus tends to increase with the total tin content of the glass. Min'ko [8] also observed that there is a solubility limit of SnO_2 in a glass system similar, in terms of the major constituents, to the float glass studied. The glass composition studied by Min'ko had 15 wt.% Na_2O + 10 wt.% CaO + 74 wt.% SiO_2 + small quantities of MgO and Al_2O_3. For SnO contents

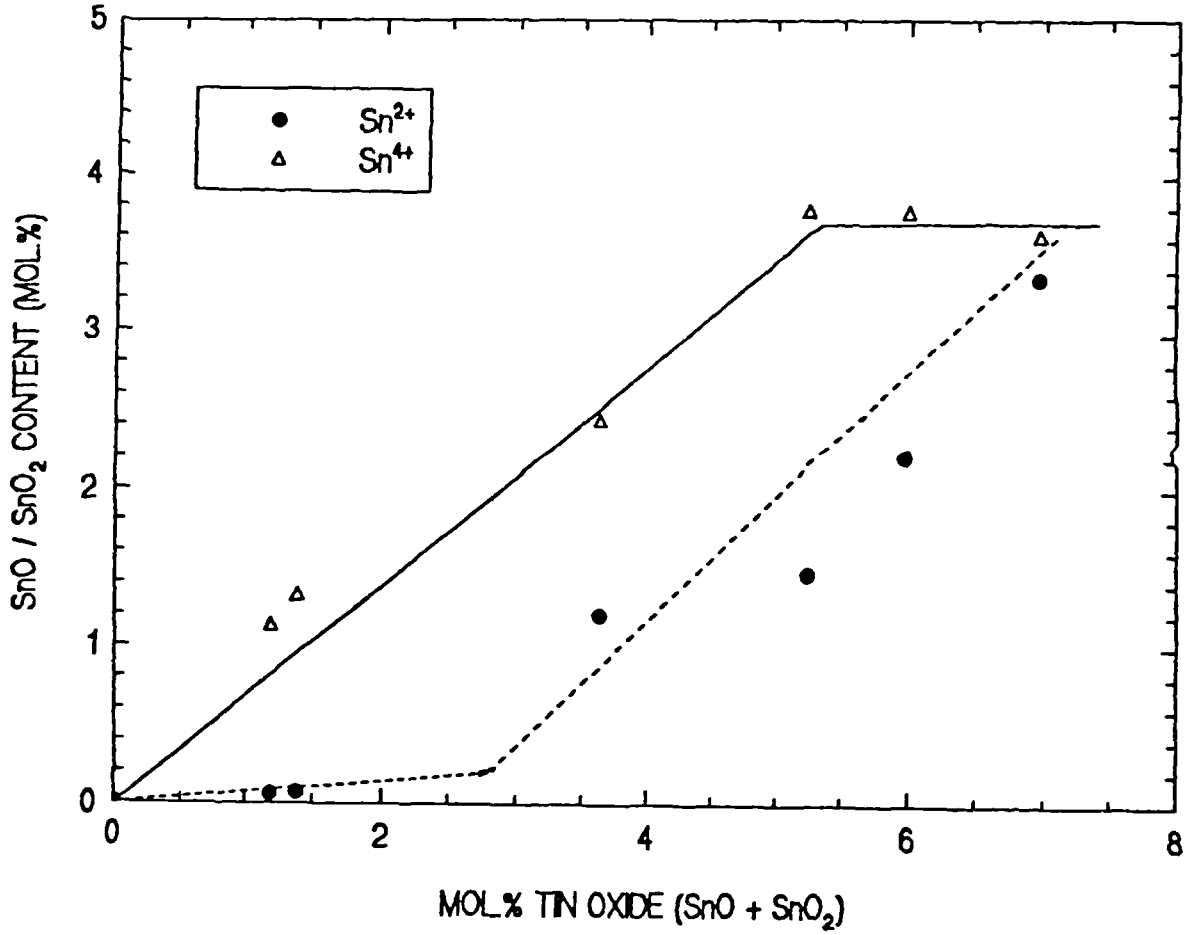

Figure 7.2 : *Variation of tin oxidation state with total tin content (Errors are within the dimension of the symbol used).*

of ≥ 15 wt.%, the glass melted in reducing conditions always contained undissolved cassiterite SnO_2.

7.3 ^{119}Sn MÖSSBAUER SPECTRA

The Mössbauer spectra of tin-doped float glasses taken at 77K are shown in Figure 7.3. The spectra show that the glasses contain Sn^{4+} and Sn^{2+}, with the exception that the lower tin oxide content (PK2.5S and PK5S) samples appear to contain only Sn^{4+}. Chemical analysis on PK2.5S and PK5S showed that both samples contain ~ 0.06 mol.% SnO (Sn^{2+}) but this could not be detected by Mössbauer at 77K.

Table 7.4: *The parameters of ^{119}Sn Mössbauer spectra of tin-doped float glasses*

Glass Samples	*Tin oxide (mol.%)*	*Temp. (±1K)*	*Tin state*	*Isomer shift, δ (±mms^{1})*	*Quad. splitting, Δ (mms^{-1})*	*Linewidth, I (mms-1)*	*Area*	*% Area*	χ^2
PK2.5S	*1.13*	*77*	*Sn^{4+}*	*-0.201*	*0.438*	*0.849*	*1.00*	*100*	*0.584*
	0.06		*Sn^{2+}*	-	-	-	-	*0*	
PK5S	*1.32*	*77*	*Sn^{4+}*	*-0.207*	*0.424*	*0.882*	*1.00*	*100*	*0.572*
	0.07		*Sn^{2+}*	-	-	-	-	*0*	
PK7.5S	*2.44*	*77*	*Sn^{4+}*	*-0.202*	*0.461*	*0.910*	*1.00*	*68.8*	*0.671*
	1.20		*Sn^{2+}*	*2.874*	*1.959*	*0.965*	*0.454*	*31.2*	
PK10S	*3.79*	*77*	*Sn^{4+}*	*-0.197*	*0.483*	*0.935*	*1.00*	*70.2*	*0.767*
	1.47		*Sn^{2+}*	*2.884*	*1.955*	*0.977*	*0.425*	*29.8*	
PK12.5S	*3.78*	*77*	*Sn^{4+}*	*-0.197*	*0.472*	*0.941*	*1.00*	*65.0*	*0.792*
	2.22		*Sn^{2+}*	*2.876*	*1.962*	*0.970*	*0.539*	*35.0*	
PK15S	*3.62*	*77*	*Sn^{4+}*	*-0.198*	*0.478*	*0.945*	*1.00*	*48.8*	*1.04*
	3.35		*Sn^{2+}*	*2.871*	*1.964*	*1.028*	*1.051*	*51.2*	

Errors in δ, Δ and I are ± 0.005 mm/s

This could indicate that Sn^{2+} has a lower value of recoil free fraction (f), compared to Sn^{4+} in the glass, and measurement at a temperature lower than 77K is needed in order to detect such a small quantity of Sn^{2+} species. The spectra were computer fitted and Table 7.4 gives the parameters of the spectra.

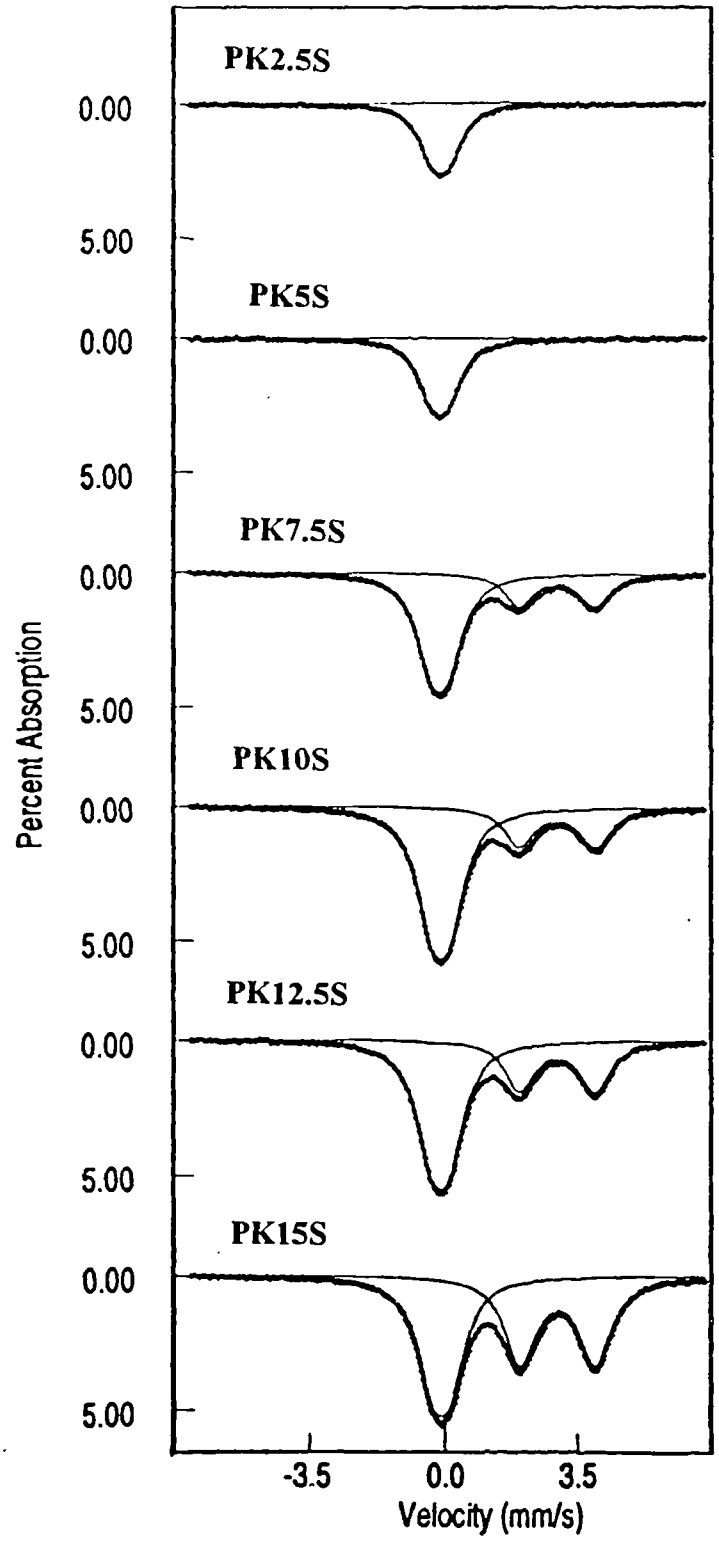

Figure 7.3 : *Mössbauer spectra of tin-doped float glass taken at 77 K. Samples PK2.5S and PK5S appear to contain only* Sn^{4+}.

7.3.1 ISOMER SHIFT, QUADRUPOLE SPLITTING AND LINEWIDTH

The isomer shifts are quoted relative to the room-temperature $CaSnO_3$ source, whose shift is identical to that of SnO_2 and $BaSnO_3$ [9]. For reasons given in section 5.7.1 (Chapter 5), the isomer shifts will be quoted relative to α-Sn. Table 7.5, now gives the isomer shifts relative to α-Sn, together with the Mössbauer parameters of crystalline and amorphous SnO and SnO_2.

Table 7.5: *Composition and Mössbauer parameters of tin-doped float glasses as compared to Mössbauer parameters of SnO and SnO_2 (crystalline and amorphous).*

Sn^{2+}				Sn^{4+}			
SnO (mol.%)	**Isomer Shift, δ (mm/s)*	*Quad. Splitting, Δ(mm/s)*	*Linewidth, Γ (mm/s)*	*SnO_2 (mol.%)*	**Isomer Shift, δ (mm/s)*	*Quad. Splitting, Δ(mm/s)*	*Linewidth , Γ (mm/s)*
0.06	-	-	-	*1.13*	*-2.216*	*0.438*	*0.849*
0.07	-	-	-	*1.32*	*-2.222*	*0.424*	*0.882*
1.20	*0.859*	*1.959*	*0.965*	*2.44*	*-2.217*	*0.461*	*0.910*
1.47	*0.869*	*1.955*	*0.977*	*3.79*	*-2.212*	*0.483*	*0.935*
2.22	*0.861*	*1.962*	*0.970*	*3.78*	*-2.212*	*0.472*	*0.941*
3.35	*0.856*	*1.964*	*1.028*	*3.62*	*-2.213*	*0.478*	*0.945*
SnO + (crystalline)	++ *0.67*	+ *1.36*	+ *0.917*	*SnO_2 (crystalline)*	++ *-2.10*	+ *0.45*	+ *0.965*
SnO + (amorphous)	*0.857*	*1.71*	*1.23*	*SnO_2 + (amorphous)*	*-1.886*	*0.702*	*1.041*

Errors in δ , Δ and Γ are ± 0.005 mm/s.

** Relative to α-Sn whose chemical shift from a CaSnO3 source is 2.015 mm/s*

+ Taken from reference [10] and ++ from reference [11].

7.3.1.1 THE ISOMER SHIFT AND QUADRUPOLE SPLITTING OF Sn^{2+}

Figure 7.4 shows the variation of the isomer shift and quadrupole splitting of Sn^{2+} with tin content as compared to crystalline and amorphous SnO. The isomer shift and quadrupole splitting values for the Sn^{2+} state are larger than those for crystalline tetragonal SnO but are very close to those for amorphous SnO and do not vary very much over the range of SnO contents. This means that the Sn^{2+} environment in the glass is the same as in amorphous SnO. Compared to the binary SnO-SiO_2 glasses, the isomer shift and quadrupole splitting values are lower in these glasses. The larger values of the isomer shift compared to crystalline SnO reflects the fact that there is a larger s electron density at the tin nucleus and thus an increase in the ionic character of Sn^{2+} (i.e charge separation in the Sn—O bonds). The crystal structure of SnO is tetragonal and Sn^{2+} sits at the top of a square pyramid of oxygens (see Figure 2.11). Here the major contribution to the electric field gradient arises from the unbalanced *p* electron population. The larger value of the quadrupole splitting as compared to SnO, could mean that there is an increase in the difference between the the *p*-electron population in the z direction and the population in the x-y plane. Therefore there is an axial elongation of the Sn^{2+} pyramid and longer Sn-O bond length in the glasses.

7.3.1.2 THE ISOMER SHIFT AND QUADRUPOLE SPLITTING OF Sn^{4+}

Figure 7.5 shows the variation of the isomer shift and quadrupole splitting of Sn^{4+} with tin content as compared to crystalline and amorphous SnO_2. There is very little change in the values of isomer shift and quadrupole splitting of Sn^{4+} within this range of SnO_2 contents. The average value of the isomer shift is -2.215 mm/s as compared to -2.10 mm/s for crystalline SnO_2 and -1.886 mm/s for amorphous SnO_2. This suggests that there is a small decrease in the *s* electron density at the tin nucleus in the glass. As for the quadrupole splitting, the average value for the glass is 0.46 mm/s,

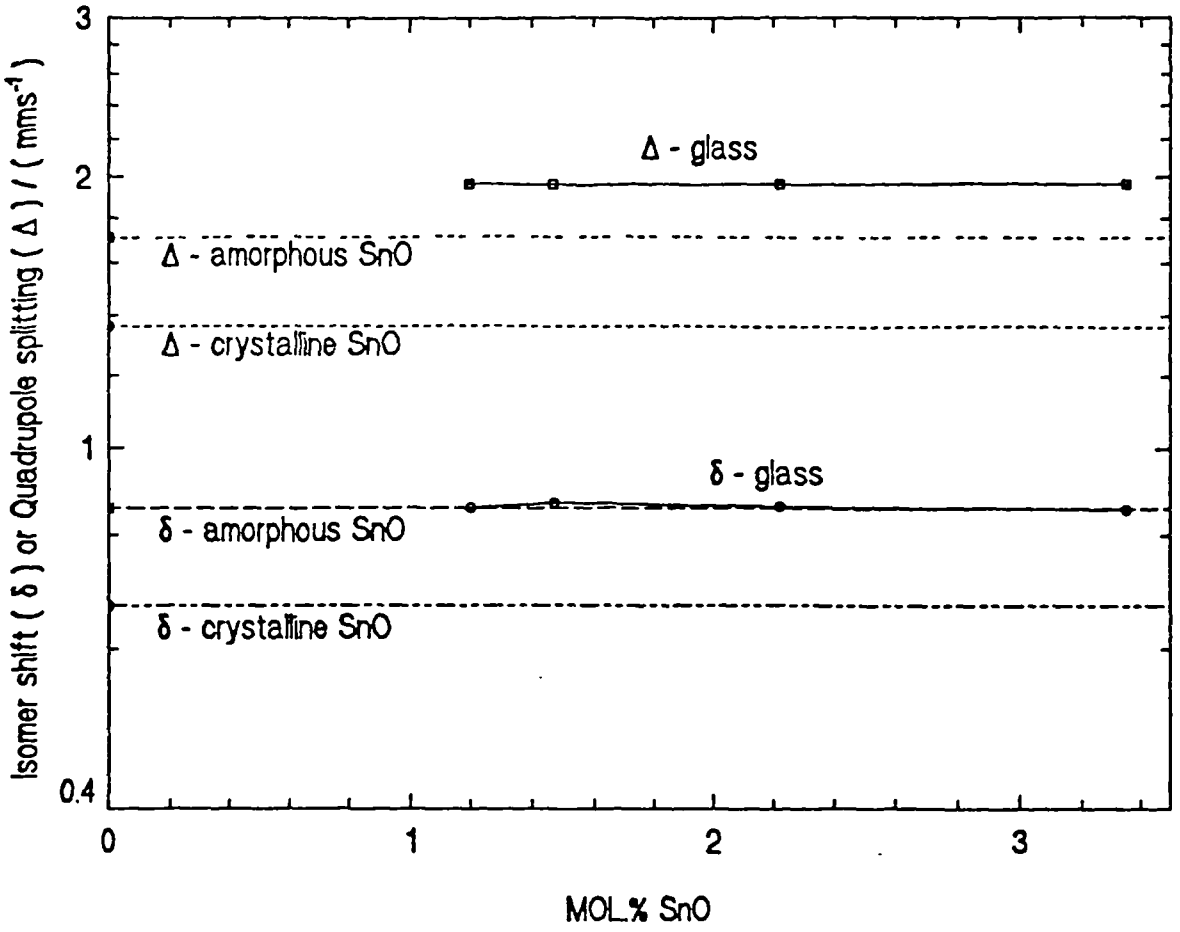

Figure 7.4 : *Variation of isomer shift and quadrupole splitting of Sn^{2+} in tin-doped float glasses, as a function of SnO content, compared to the isomer shift and quadrupole splitting of Sn^{2+} in crystalline and amorphous SnO . The shifts are relative to α-tin. (Errors are within the dimension of the symbol used).*

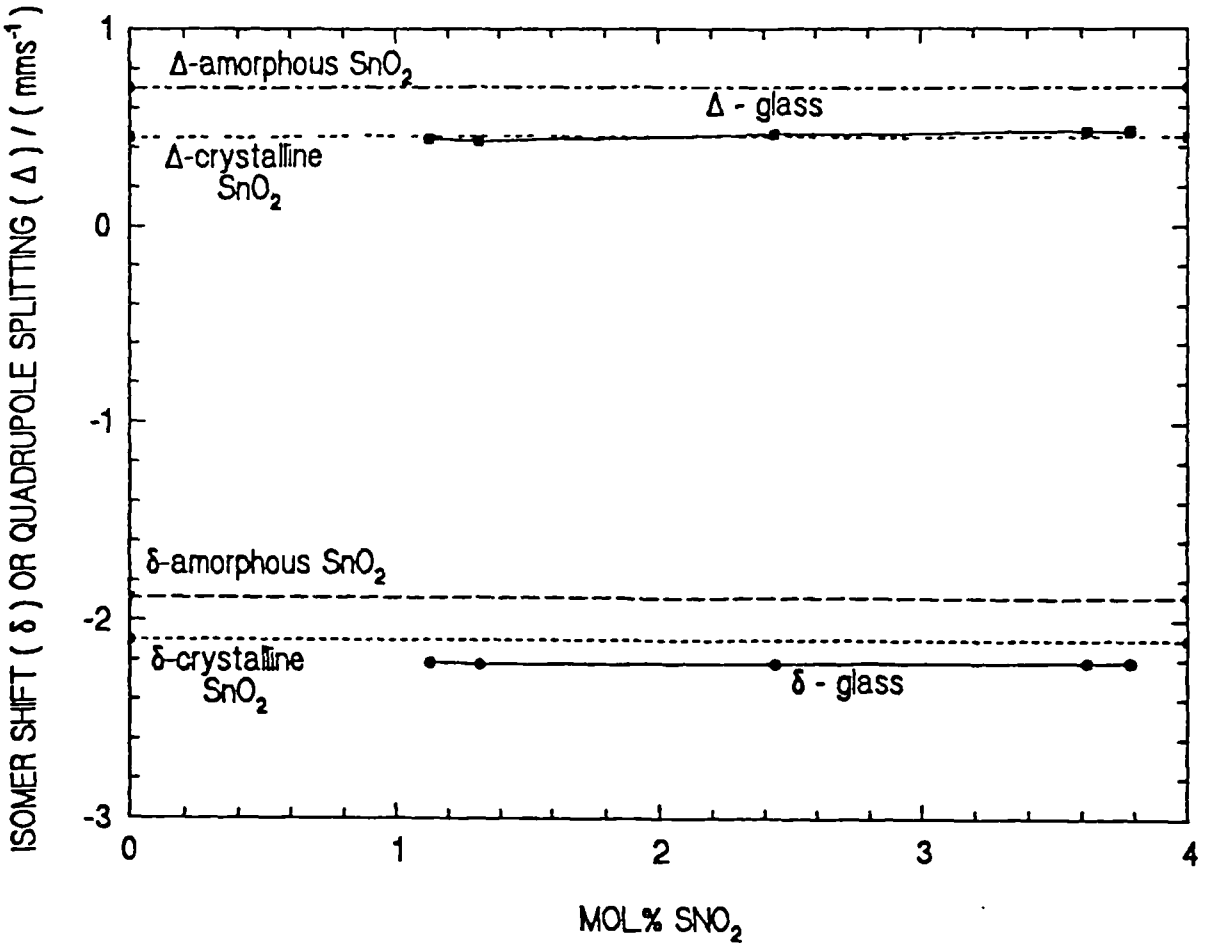

Figure 7.5 : *Variation of isomer shift and quadrupole splitting of Sn^{4+} in tin-doped float glasses, as a function of SnO_2 content, compared to the isomer shift and quadrupole splitting of Sn^{4+} in crystalline and amorphous SnO_2. The shifts are relative to α-tin. (Errors are within the dimension of the symbol used).*

which is close to the 0.45 mm/s for crystalline SnO_2 but very different from the 0.702 mm/s for amorphous SnO_2. Crystalline SnO_2 is of the rutile type (Figure 2.10). The Sn^{4+} is situated in a distorted octahedron of oxygens, with all Sn-O distances equal in the basal plane, but the O-Sn-O angles are not 90° but 78° and 102° respectively [12]. Therefore the Sn^{4+} environment is approximately symmetric and the electronic density close to the tin nucleus is fairly spherical. According to Collins et al [10] the Sn^{4+} environment in amorphous SnO_2 is distorted when compared to its crystalline form. In the glass the Sn^{4+} environment must be little different from crystalline SnO_2. This is compatible with the limited solubility of SnO_2 in silicate glass.

7.3.1.3 LINEWIDTH

The Sn^{2+} site in the glass exhibits narrow lines and an average broadening of

$$\frac{\Gamma_{glass}-\Gamma_{crystalline}}{\Delta} \approx 0.03 \pm 0.01$$

whereas the Sn^{4+} site exhibits a similar linewidth to crystalline SnO_2. This suggests a narrow distribution of electric field gradients for both sites. In amorphous SnO and SnO_2, the broadening found by Collins et al [10] is the same for both sites having a value of 0.16. Therefore anisotropy of the electric field gradient in this glass is smaller than in the corresponding amorphous oxides.

7.4 VARIABLE TEMPERATURE MÖSSBAUER SPECTRA

The last sections have shown that Sn^{2+} and Sn^{4+} play different structural roles in the tin-doped float glass. Accordingly both must have different Debye-Waller factors or recoiless free fractions (*f*). As seen in Section 3.2.1.2 the *f* factor is a temperature-dependent function of the nuclear recoil energy. The recoil energy is inversely proportional to the effective mass of the recoiling nucleus. In a solid, the motion of the nucleus is strongly coupled to its atom or ion in the lattice. A strongly coupled nucleus must have a larger effective mass. Thus the effective mass depends on the tightness of the binding of the solid lattice. Furthermore the intensity of absorption of a nucleus observed in a Mössbauer spectrum is proportional to the *f* factor [13]. Therefore the study of the spectrum intensity (*f* factor) as a function of temperature can yield information on the tightness of the chemical binding of Sn^{2+} and Sn^{4+} in the glass.

7.4.1 MEASUREMENT OF THE *f* FACTOR

A series of spectra was taken between 17.5K and 900K on sample PK15S. This sample was chosen because it has the maximum amount of tin oxide and the relative amounts of Sn^{2+} and Sn^{4+} (determined by chemical analysis) in the glass are about the same. Figure 7.6 shows the Mössbauer spectra of PK15S as a function of temperature. A noticeable feature of the spectra is the strong dependence of the absorption intensity (i.e the *f* factor) upon temperature, especially for Sn^{2+}. At 900K the Sn^{2+} doublet has practically disappeared. Table 7.6 gives the Mössbauer parameters of PK15S at temperatures between 17.5K and 900K.

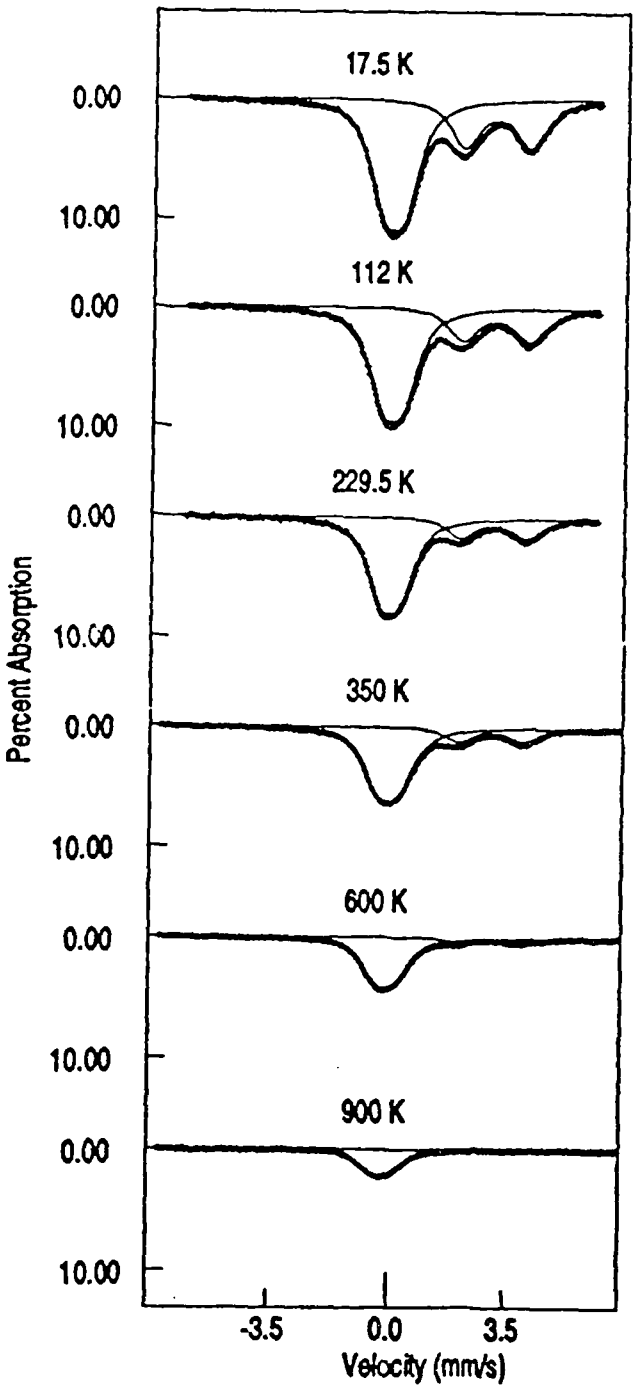

Figure 7.6: *Mössbauer spectra of glass PK15S as a function of temperature. At 900K the* Sn^{2+} *doublet has practically disappeared.*

From the spectrum, the area A of the Sn^{2+} and Sn^{4+} contributions to the spectrum at each temperature were measured. Section 5.8.1 (Chapter 5) has shown that the area A under any one peak is proportional to the *f* factor. Thus, following Section 5.8.1, the Debye temperature (θ_D) of Sn^{2+} and Sn^{4+} can be calculated from equation 5.3,

$$\theta_D = \sqrt{\frac{6E_R}{\kappa m}} \qquad 5.3$$

where m is the slope of graph *lnA versus T and* $E_R = 2.572\ X\ 10^{-3}$ *eV is the recoil* energy of the γ-ray for ^{119}Sn. Hence when θ_D is known, the recoil free fraction , *f* , at a given temperature can be calculated from equations given in chapter 3 i.e equation 3.26 for $T << \theta_D$, equation 3.27 for T = 0 and equation 3.28 for $T > \frac{\theta_D}{2}$. The relative concentration of Sn^{2+} and Sn^{4+} can be found from the intercepts $\ln A^0_{2+}$ and $\ln A^0_{4+}$ on the lnA axis, since

$$\frac{c_{2+}}{c_{4+}} = \frac{A^0_{2+}}{A^0_{4+}} \qquad 7.1$$

Table 7.6: *Mössbauer parameters of PK15S at temperatures between 17.5K and 900K*

	Sn^{2+}				Sn^{4+}			
T / K	*δ mm/s*	*Δ mm/s*	*Γ mm/s*	*Relative area*	*δ mm/s*	*Δ mm/s*	*Γ mm/s*	*Relative area*
14.2	*0.856*	*1.950*	*1.020*	*1.232*	*-2.204*	*0.508*	*0.941*	*1.00*
52.4	*0.855*	*1.947*	*0.995*	*1.171*	*-2.205*	*0.508*	*0.925*	*1.00*
101.5	*0.845*	*1.941*	*0.977*	*1.053*	*-2.212*	*0.508*	*0.906*	*1.00*
128.7	*0.838*	*1.936*	*0.961*	*0.988*	*-2.216*	*0.504*	*0.896*	*1.00*
152.9	*0.833*	*1.929*	*0.963*	*0.928*	*-2.220*	*0.500*	*0.898*	*1.00*
177.2	*0.827*	*1.932*	*0.958*	*0.876*	*-2.226*	*0.492*	*0.894*	*1.00*
205.7	*0.819*	*1.926*	*0.951*	*0.823*	*-2.234*	*0.491*	*0.878*	*1.00*
228.4	*0.815*	*1.924*	*0.942*	*0.770*	*-2.238*	*0.489*	*0.873*	*1.00*
255.2	*0.812*	*1.913*	*0.939*	*0.716*	*-2.244*	*0.485*	*0.875*	*1.00*
281.1	*0.802*	*1.907*	*0.934*	*0.664*	*-2.248*	*0.484*	*0.868*	*1.00*
298	*0.802*	*1.909*	*1.053*	*0.618*	*-2.255*	*0.505*	*0.935*	*1.00*
298.5	*0.801*	*1.896*	*0.943*	*0.628*	*-2.255*	*0.484*	*0.886*	*1.00*
298.8	*0.799*	*1.908*	*0.917*	*0.632*	*-2.256*	*0.476*	*0.854*	*1.00*
306.7	*0.794*	*1.906*	*0.907*	*0.618*	*-2.256*	*0.476*	*0.847*	*1.00*
345	*0.792*	*1.905*	*1.053*	*0.561*	*-2.265*	*0.504*	*0.938*	*1.00*
395	*0.787*	*1.887*	*1.172*	*0.496*	*-2.276*	*0.513*	*0.993*	*1.00*
495	*0.764*	*1.861*	*1.135*	*0.376*	*-2.301*	*0.516*	*0.973*	*1.00*
595	*0.753*	*1.858*	*1.049*	*0.288*	*-2.327*	*0.490*	*0.911*	*1.00*
695	*0.706*	*1.838*	*1.022*	*0.217*	*-2.352*	*0.463*	*0.871*	*1.00*
795	*0.672*	*1.835*	*1.719*	*0.149*	*-2.387*	*0.626*	*1.107*	*1.00*
845	*0.652*	*2.021*	*2.202*	*0.128*	*-2.408*	*0.622*	*1.115*	*1.00*

Errors in δ, Δ and Γ are ± 0.005 mm/s.

7.4.1.1 DEBYE TEMPERATURE

The isomer shift and quadrupole splitting are better measures of the nearest neighbour distortion and the Debye temperature reflects rather the bulk properties of the glass. The Debye temperatures of Sn^{2+} and Sn^{4+} for the tin-doped glass as compared to crystalline and amorphous SnO and SnO_2 , are given in Table 7.7.

Table 7.7: Debye temperatures of Sn^{2+} and Sn^{4+} in tin-doped float glass and corresponding tin oxides.

Compound	*Debye temperature (K)*
Sn^{2+} tin doped float	*206 ± 4*
Sn^{4+} tin doped float	*364 ± 8*
+SnO amorphous	*181 ± 2*
+SnO crystalline	*203 ± 1*
+SnO_2 amorphous	*243 ± 3*
+SnO_2 crystalline	*313 ± 6*

+ Taken from reference [10].

The Debye temperature of Sn^{2+} for the glass is higher than for amorphous SnO, having a value very close to crystalline SnO. For Sn^{4+} the Debye temperature is higher than in either the amorphous or crystalline SnO_2. The results imply that both Sn^{2+} and Sn^{4+} are more tightly bound in the glass than in their crystalline forms. According to Nishida et al [14] the value of θ_D could indicate the site of the tin species in the glass. When θ_D is higher than 270 K, the tin ion is covalently bonded to oxygen at network former (NWF) sites. Conversely, a lower value indicates that it is ionically and loosely bonded to oxygen at network modifier (NWM) sites. Based on this, the nature of the Sn(2+)—O bonding in the glass is mostly ionic and occupying NWM sites, whereas Sn^{4+} is covalently bonded to oxygen at NWF sites.

7.4.1.2 RECOIL FREE FRACTION OF Sn^{2+} and Sn^{4+}.

The recoil free fractions for both Sn^{2+} and Sn^{4+} , between 14.2K and 900K are given in Table 7.8.

Table 7.8: *The f factors of Sn^{2+} and Sn^{4+} in tin-doped float glass*

Temperature (±1 K)	*f (Sn^{2+})*	*f (Sn^{4+})*
14.2	*0.799 ± 0.004*	*0.883 ± 0.003*
50	*0.739 ± 0.007*	*0.871 ± 0.003*
100	*0.656 ± 0.009*	*0.858 ± 0.006*
150	*0.531 ± 0.012*	*0.816 ± 0.009*
200	*0.429 ± 0.012*	*0.763 ± 0.009*
250	*0.348 ± 0.013*	*0.713 ± 0.011*
300	*0.282 ± 0.012*	*0.667 ± 0.012*
350	*0.228 ± 0.011*	*0.623 ± 0.013*
400	*0.185 ± 0.011*	*0.582 ± 0.015*
450	*0.149 ± 0.011*	*0.544 ± 0.015*
500	*0.121 ± 0.011*	*0.509 ± 0.015*
550	*0.098 ± 0.008*	*0.476 ± 0.016*
600	*0.079 ± 0.007*	*0.444 ± 0.016*
650	*0.064 ± 0.006*	*0.415 ± 0.017*
700	*0.052 ± 0.005*	*0.388 ± 0.017*
750	*0.042 ± 0.004*	*0.363 ± 0.016*
800	*0.034 ± 0.004*	*0.339 ± 0.017*
850	*0.028 ± 0.003*	*0.317 ± 0.017*
900	*0.022 ± 0.003*	*0.296 ± 0.016*

Figure 7.7 shows a plot of the *f* factors of Sn^{2+} and Sn^{4+} as a function of temperature between 14.2K and 900K. The decrease of *f* factor with increase of temperature for Sn^{2+} is very much faster than for Sn^{4+}. The decrease in the *f* factors for Sn^{2+} and Sn^{4+} are -100 x $10^{-4}K^{-1}$ and 7.9 x $10^{-4}K^{-1}$ respectively. This shows that Sn^{4+} is more tightly bound in the network than Sn^{2+}. Extrapolation to 0 K gives the experimental values of the *f* factor of Sn^{2+} and Sn^{4+} at zero-point motion. These values are compared to the theoretical values calculated using the Debye model (equation 3.26) in Table 7.9.

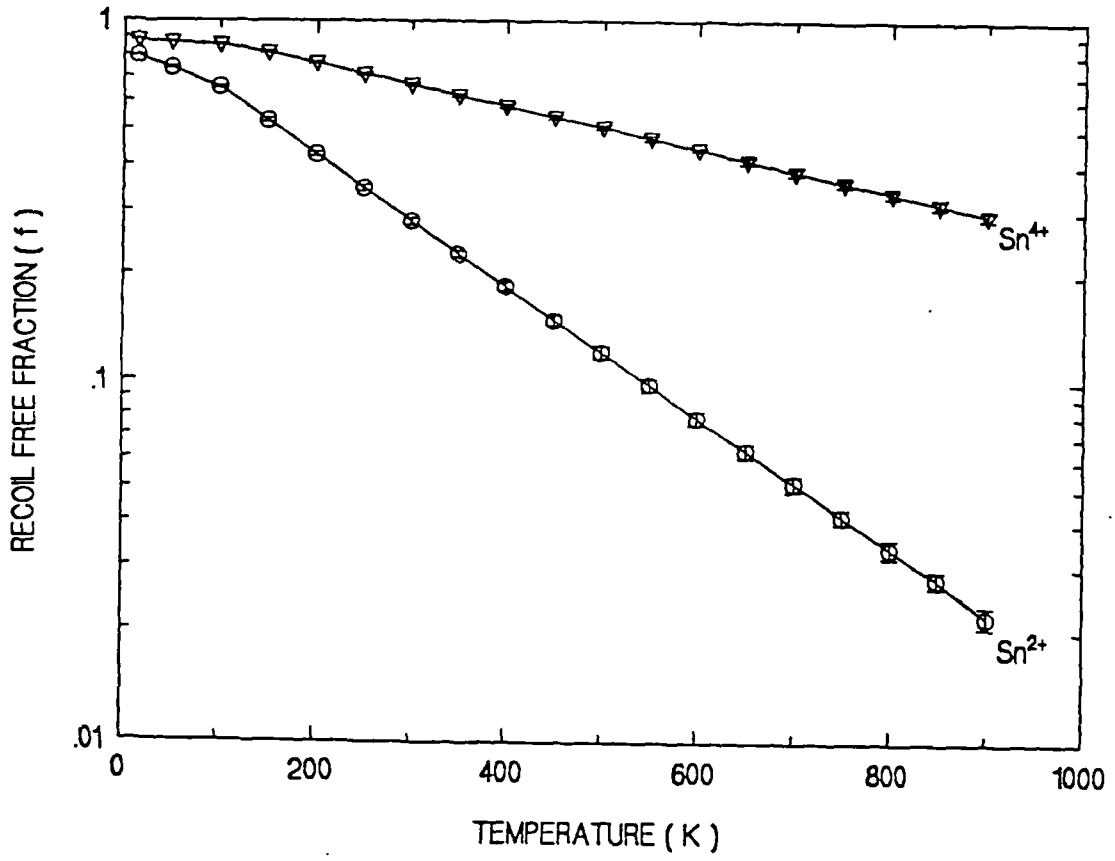

Figure 7.7 : *Variation of the f factors of* Sn^{2+} *and* Sn^{4+} *in tin-doped float glass as a function of temperature between 14.2K and 900K.*

Table 7.9: *The f factor at absolute 0 K*

Recoil free fraction at zero Kelvin	*Experimental*	*Theoretical*
f - Sn^{2+}	*0.819 ± 0.004*	*0.805 ± 0.004*
f - Sn^{4+}	*0.889 ± 0.002*	*0.884 ± 0.003*

As pointed out in Section 5.8.1 (Chapter 5), the temperature dependence of the *f* factor could be used to determine the coordination of an atom in a material. Thus, according to Kurkjian [15], Parish [9] and Mitrofanov & Sidorov [16]; the ratio of the *f* factor at liquid-nitrogen temperature and at room temperatures ($R = f_{77}/ f_{300}$) can determine the coordination of an atom by comparison with the known value of R of an established crystalline compound. Accordingly, for silicate glasses [16], $R \approx 1.3$ when Sn^{4+} is coordinated to 6 oxygens whereas $R \approx 2.5$ when Sn^{2+} is coordinated to 4 oxygen. Using this as a yardstick, Sn^{2+} in the glass is coordinated by 4 oxygens and Sn^{4+} coordinated to 6 oxygen. This summarized in Table 7.10 below.

Table 7.10 *The* $R = f_{77}/ f_{300}$ *factor.*

Compound	*R*	*Coordination number of Sn*	*Known or proposed structure*
**SnO*	*2.3*	*4*	*ionic + covalent*
***SnO_2*	*1.25*	*6*	*covalent*
SnO in tin doped float glass	*2.34*	*4*	*ionic + covalent*
SnO_2 in tin doped float glass	*1.28*	*6*	*polymeric covalent*

* *Taken from reference [17].* ***Taken from reference [16].*

The relative percentage of tin oxidation states in the glass is found using equation 7.1. Table 7.11 gives the percentage of Sn^{2+} obtained both by chemical and Mössbauer techniques. With the exception of very low tin contents, both techniques agree within about 3%.

Table 7.11 : *Composition of tin oxidation states in tin-doped float glass*

Samples	***PK0***	***PK2.5S***	***PK5S***	***PK7.5S***	***PK10S***	***PK12.5S***	***PK15S***
Total tin oxide $SnO+SnO_2$ (mol.%)	*0*	*1.19*	*1.39*	*3.64*	*5.26*	*6.00*	*6.97*
% Sn^{2+} tin of total tin (chemical)	*0*	*5*	*5*	*33*	*28*	*37*	*48*
% Sn^{2+} tin of total tin (Mössbauer)	*0*	*0*	*0*	*31.2*	*29.8*	*35.0*	*51.3*

7.5 VISCOSITY MEASUREMENT

The viscosities of the glass samples were measured between 550°C and 800°C which gave a viscosity range from 10^7 to 10^{12} Pa s with ± 1.5% error in the value of $\log_{10} \eta$. Figure 7.8 shows a graph of $\log_{10} \eta$ versus the reciprocal of absolute temperature (1/T). For each glass, a straight line can be fitted with the general equation

$$\log_{10} \eta = \frac{E_\eta}{2.3RT} + A \qquad 7.2$$

The slope of the line gives the activation energy of viscous flow E_η in the temperature range 550°C to 800°C. Table 7.12 gives the values of E_η as compared to the typical values of soda-lime-silica glass at low and high temperatures.

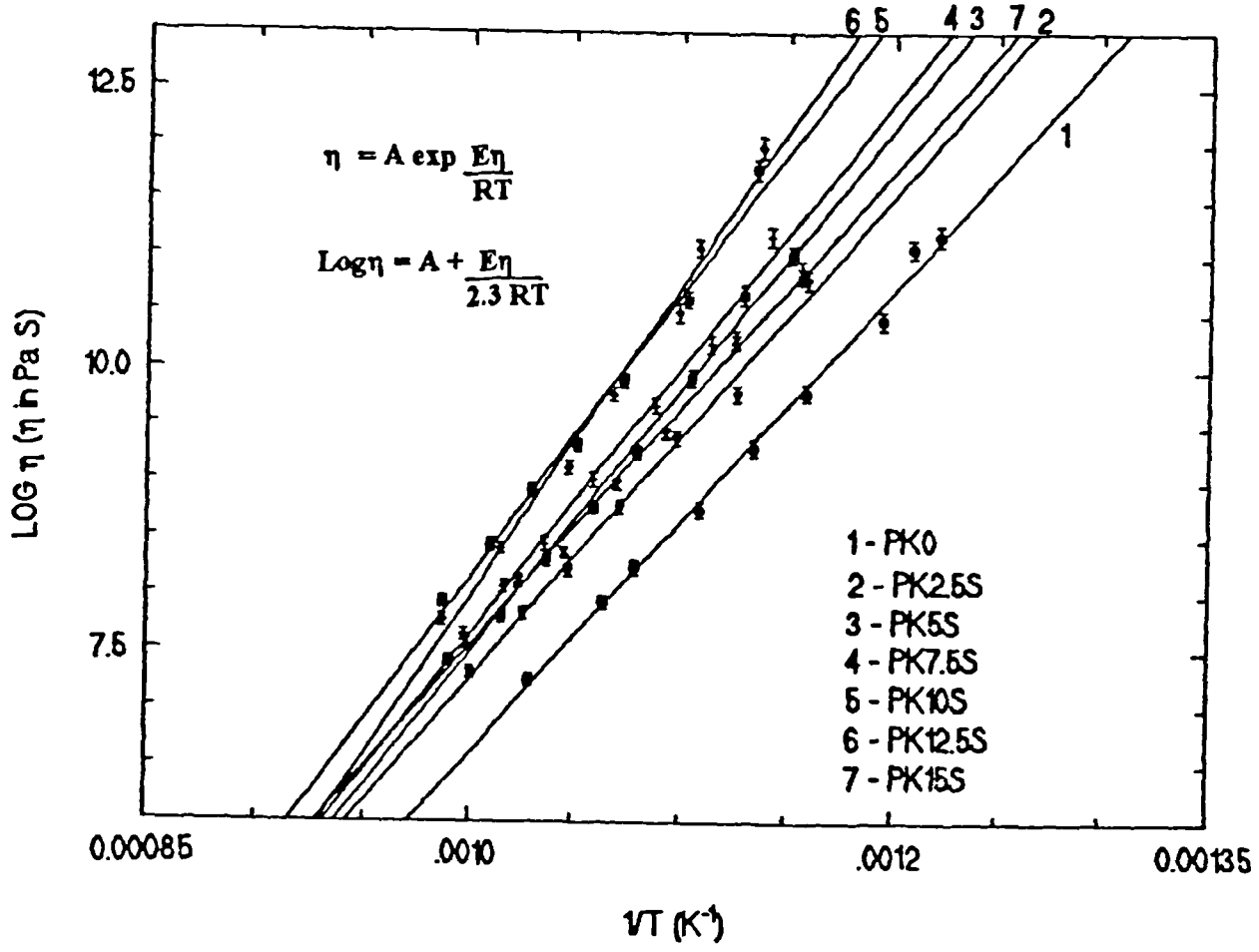

Figure 7.8 : *$Log_{10}\eta$ versus reciprocal temperature of tin-doped float glasses, fitted by a 1st order polynomial.*

Table 7.12: *Activation energy of viscous flow of tin-doped float glass (550°- 800°C)*

Samples	*Total tin (mol.%)*	*Mol.% SnO_2 / Mol.% SnO*	*E_η (KJ/ mole)*
PK0	*0*	*0*	*394.4 ± 37.9*
PK2.5S	*1.19*	*18.83*	*411.6 ± 37.0*
PK5S	*1.39*	*18.86*	*447.9 ± 36.5*
PK7.5S	*3.64*	*2.03*	*455.6 ± 36.2*
PK10S	*5.26*	*2.58*	*482.4 ± 48.2*
PK12.5S	*6.00*	*1.70*	*530.3 ± 54.6*
PK15S	*6.97*	*1.08*	*403.9 ± 26.9*
** Typical value for soda-lime-silica glass at low temperature (500°-700°C)*			*420*
**Typical value for soda-lime-silica glass at high temperature (800°- 1500°C)*			*207*

**Taken from reference [18].*

Figure 7.9 shows how E_η increases with tin content. The trend observed needs to be considered in the context of the oxidation states of the tin species present. Up to ~5 mol.% tin oxide, the dominant oxidation state is Sn^{4+} and this would be expected to strengthen the glass network. Beyond ~5 mol.% tin oxide, the fraction of the Sn^{2+} species increases such that the ratio of the oxidation states is approximately 1 at 6.97 mol.% tin content. The Sn^{2+} species has been shown, by Mössbauer to be less tightly bonded (Sn-O bonds more ionic in glass) to the network, and does not give the same rigid, 3D bonding as Sn^{4+} species. Thus the increase in relative amount of Sn^{2+} species weakens the glass network , hence the lowering of E_η.

In an attempt to understand more of the viscosity - composition - relationship of the glass; plots of logη versus reciprocal of absolute temperature (1/T) were fitted to a 2nd order polynomial equation of the form

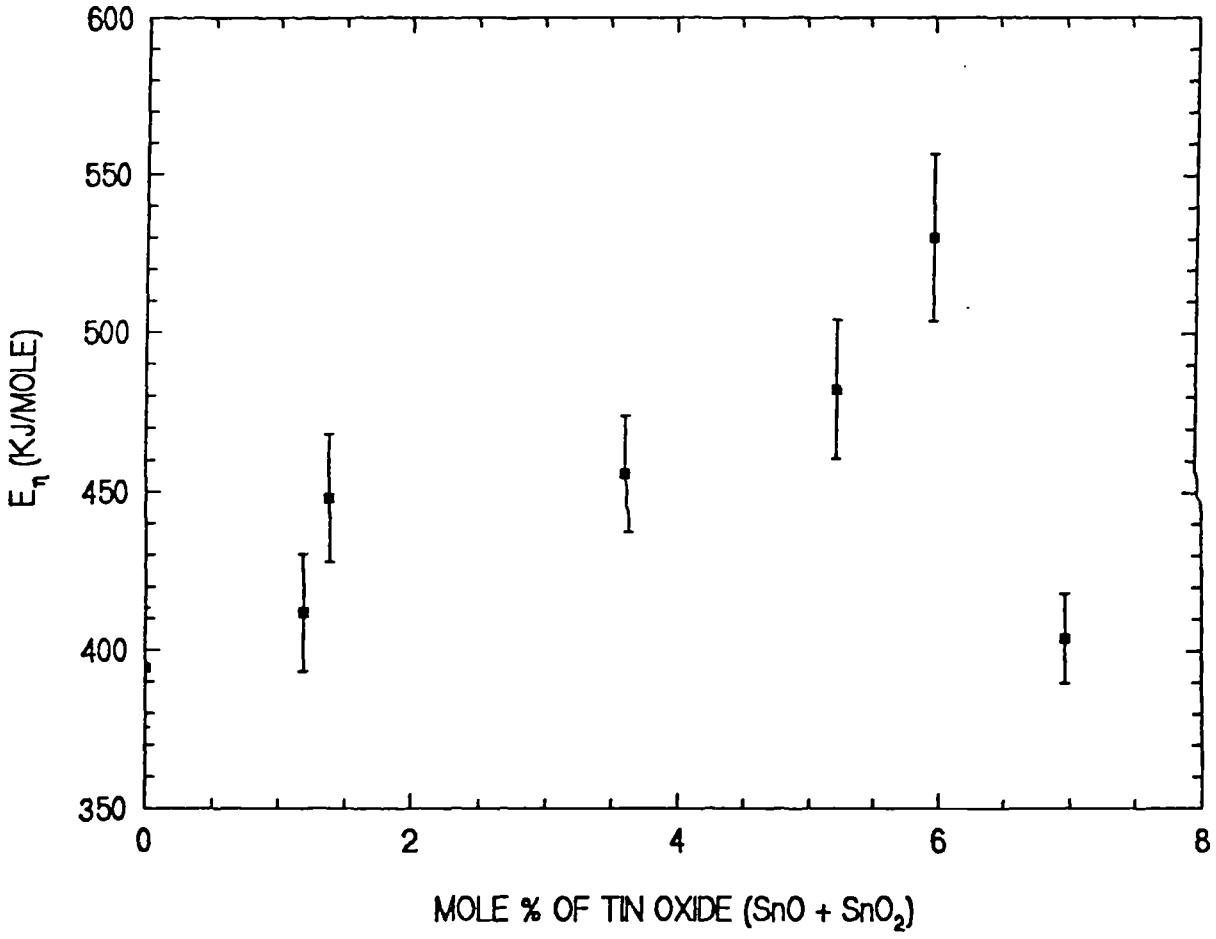

Figure 7.9 : *Activation energy for viscous flow (E_η) versus tin content.*

$$\log_{10}\eta = A + \frac{B}{T} + \frac{C}{T^2} \qquad 7.3$$

For all the samples, better fits were obtained. The parameters of the equations are presented in Table 7.13.

Table 7.13: *Parameters of the equation* $\log_{10}\eta = A + \frac{B}{T} + \frac{C}{T^2}$ *for the viscosity of tin-doped float glasses, valid for temperature range between 500° to 850°C.*

Samples	*Total tin (mol.%)*	*Mol.% SnO_2 / Mol.% SnO*	*A*	*B X 10^4 (K^{-1})*	*C X 10^7 (K^{-2})*
PK0	*0*	*0*	*4.31*	*-1.19*	*1.44*
PK2.5S	*1.19*	*18.83*	*10.9*	*-2.52*	*2.16*
PK5S	*1.39*	*18.86*	*15.4*	*-3.51*	*2.73*
PK7.5S	*3.64*	*2.03*	*25.5*	*-5.42*	*3.65*
PK10S	*5.26*	*2.58*	*18.5*	*-4.24*	*3.20*
PK12.5S	*6.00*	*1.70*	*44.8*	*-9.42*	*5.74*
PK15S	*6.97*	*1.08*	*14.6*	*-3.13*	*2.43*

The equations of fitting were used to calculate $\log_{10}\eta$ for each sample in the temperature range between 500°C to 850°C. The results are presented in the graph shown in Figure 7.10. The graph shows that the annealing and softening temperatures of the glass increase with tin contents, reaching the maximum value of 596°C and 827°C respectively, before decreasing at the tin content with oxidation ratio (Mol.% SnO_2 / Mol.% SnO) of approximately 1. The annealing and softening temperatures of the glasses are shown in Table 7.14.

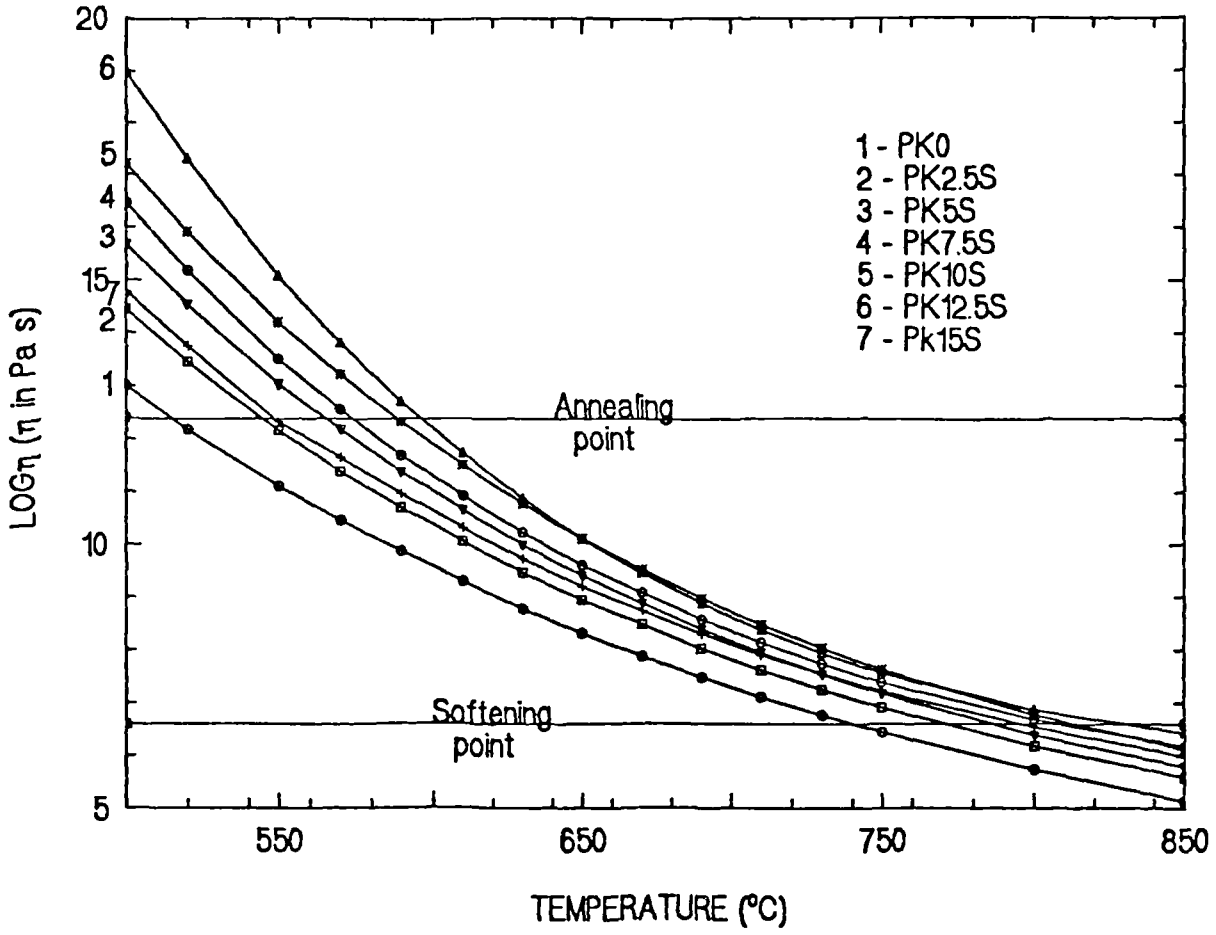

Figure 7.10 : *Variation of $Log_{10}\eta$ versus temperature for undoped and tin-doped float glasses. The annealing and softening points correspond to $Log_{10}\eta$ values of 12.4 and 6.6 respectively.*

Table 7.14: *Annealing and softening temperatures determined by viscosity measurements of tin-doped float glasses compared to some soda-lime-silica glasses*

Samples	*Total tin (mol.%)*	*Mol.% SnO_2 / Mol.% SnO*	*Annealing temp. ±5 °C { log η= 12.4 }*	*Softening temp. ±5 °C { log η= 6.6 }*
PK0	*0*	*0*	*515*	*740*
PK2.5S	*1.19*	*18.83*	*544*	*770*
PK5S	*1.39*	*18.86*	*565*	*788*
PK7.5S	*3.64*	*2.03*	*574*	*808*
PK10S	*5.26*	*2.58*	*588*	*812*
PK12.5S	*6.00*	*1.70*	*596*	*827*
PK15S	*6.97*	*1.08*	*551*	*795*
**Soda-lime-silica sheet glass*			*548*	*730*
**Soda-lime-silica plate glass*			*553*	*735*
**Soda-lime-silica container glass*			*548*	*730*
**Soda-lime-silica bulb glass*			*510*	*696*

**Taken from reference [19]*

7.6 SOME OTHER PHYSICAL. PROPERTIES OF TIN-DOPED FLOAT GLASSES.

Apart from viscosity. the other physical properties studied were thermal expansion, density, refractive index and microhardness. These properties are summarised in Table 7.15.

Table 7.15: *Coefficient of linear thermal expansion (α), transition temperature (T_g), dilatometric softening temperature (M_g), density, refractive index (η_D) and Knoop microhardness (H_k) of tin-doped float glasses*

Samples	*Total tin (mol.%)*	*Mol.% SnO_2 / Mol.% SnO*	*α±1.5 ($10^{-7}K^{-1}$) [30°-550°C]*	*Tg ± 5°C*	*Mg ± 5°C*	*Density (g/cm3)*	*η_D λ=589.6nm*	*H_k±27 (50g/30s)*
PK0	*0*	*0*	*89.7*	*535*	*590*	*2.494*	*1.5175*	*456*
PK2.5S	*1.19*	*18.83*	*89.1*	*555*	*600*	*2.540*	*1.5233*	*523*
PK5S	*1.39*	*18.86*	*86.2*	*575*	*610*	*2.554*	*1.5239*	*589*
PK7.5S	*3.64*	*2.03*	*83.2*	*580*	*620*	*2.623*	*1.5374*	*626*
PK10S	*5.26*	*2.58*	*79.3*	*595*	*645*	*2.707*	*1.5442*	*661*
PK12.5S	*6.00*	*1.70*	*78.6*	*590*	*635*	*2.705*	*1.5488*	*689*
PK15S	*6.97*	*1.08*	*77.2*	*570*	*625*	*2.704*	*1.5536*	*594*

7.6.1 THERMAL EXPANSION

The thermal expansion coefficients for the glasses as a function of tin content are shown in Figure 7.11. Values of the glass transition temperature T_g and the dilatometric softening point M_g were also obtained from the thermal expansion curves and these values are depicted in Figure 7.12 as a function of tin content. The decrease in the thermal expansion coefficient and the increase in T_g with increasing tin content reflect the network/intermediate characteristics of both tin oxidation states. Hence, the thermal properties of the glasses improved with added tin.

7.6.2 DENSITY

Figure 7.13 shows the variation in the density of the glasses with increasing tin content. This seems to increase in a near linear fashion until the tin content exceeds ~5 mol.%, after which, the density appears to remain constant. Since this is the point beyond which Sn^{4+} remains constant and Sn^{2+} increases, it indicates that the structural roles of each ion are very different.

7.6.3 REFRACTIVE INDEX

Figure 7.14 shows that the refractive index increases linearly with tin content, irrespective of the relative amounts of tin oxidation states. This suggests that Sn^{2+} and Sn^{4+} have similar molar volumes and polarisabilities or that differences in one are compensated by changes in the opposite sense of the other as the relative amounts of the oxidation states vary. Generally the effect of tin is to improve the glass optical property.

7.6.4 KNOOP HARDNESS

Figure 7.15 shows the variation of Knoop hardness as a function of tin content. This property shows almost exactly the same behaviour as the activation energy for viscous flow, E_η. The microhardness of the glass increases with increase of tin content, reaching a maximum value at 6 mol % tin oxide. Beyond 6 mol.%, when the Sn^{4+} species began to saturate and Sn^{2+} species increases to about the same amount of Sn^{4+}, the hardness decreases a little but its value is still very much greater than the float glass with 0 mol.% tin oxide. This suggests that the effect of Sn^{2+} on the hardness of the glass is to soften the glass whereas the effect of Sn^{4+} species harden the glass.

7.7 CONCLUSIONS

Float glass is a complex material in terms of composition; and the small amount of tin that diffuses into the surface through the process of production can be detrimental to the quality of the glass. We have demonstrated that, by remelting the float glass with tin(II) oxalate under ordinary conditions; we can mimic, in terms of tin content, the tin oxide distribution found along the tin diffusion region of float glass. Synthesis of the glass has shown that both Sn^{2+} and Sn^{4+} can be assimilated simultaneously in the glass but there is a solubility limit for Sn^{4+}.

We have shown that the Mössbauer effect is a valuable tool in studying the structural roles of tin in tin-doped float glass. The isomer shift and quadrupole splitting gave a measure of the nearest neighbour distortion of Sn^{2+} and Sn^{4+} ions and the Debye temperature and the recoil free fraction reflect the bulk properties of both ions in the glass. The environment of Sn^{2+} in the glass is similar to that in amorphous SnO, in which there is an axial elongation of the Sn—O bond length as compared to its crystalline form. This reflects a greater ionic character of the bond. The structure of

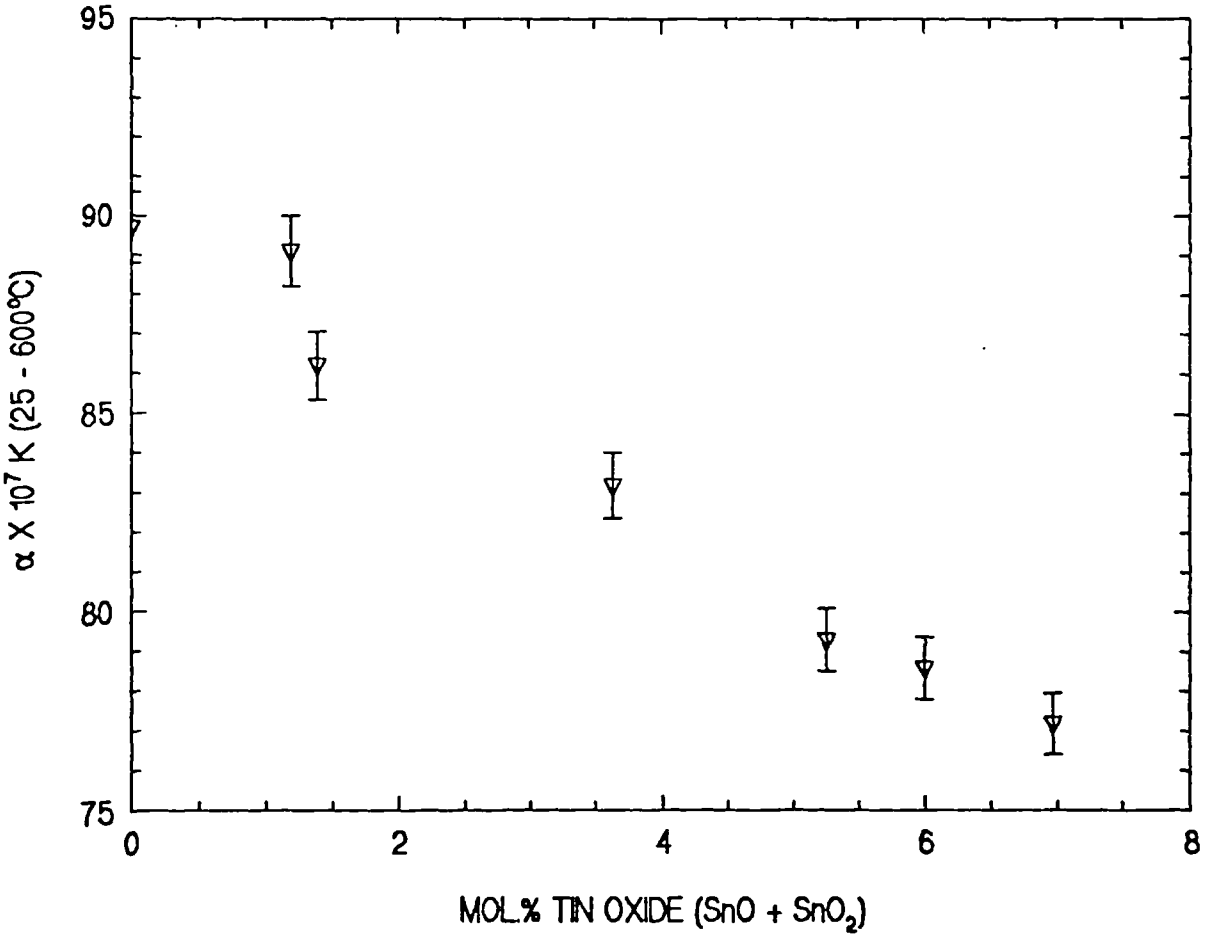

Figure 7.11 : *Coefficient of linear thermal expansion versus tin content of tin-doped float glasses.*

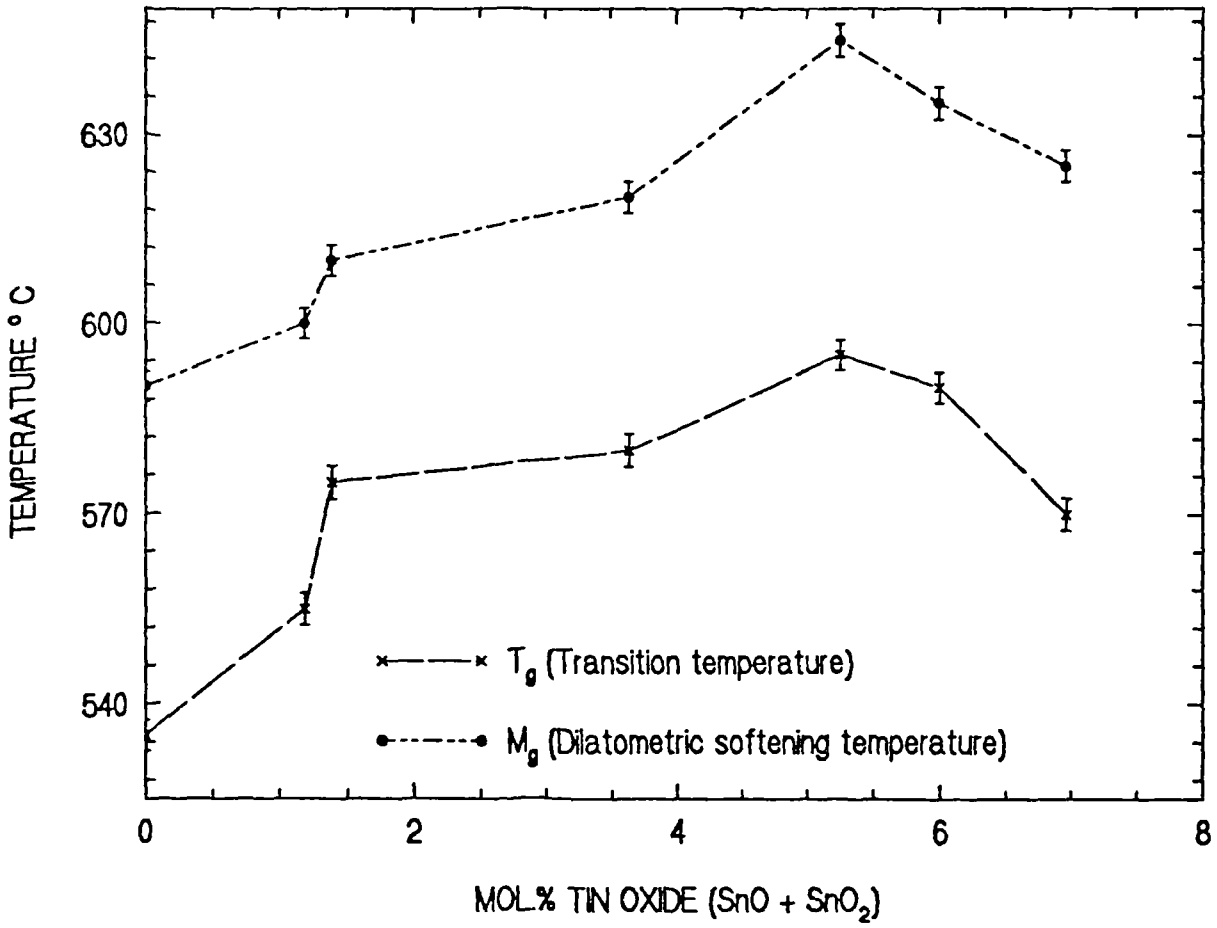

Figure 7.12 : *Transition temperature (T_g) and dilatometric softening temperature (M_g) versus tin content of tin-doped float glasses.*

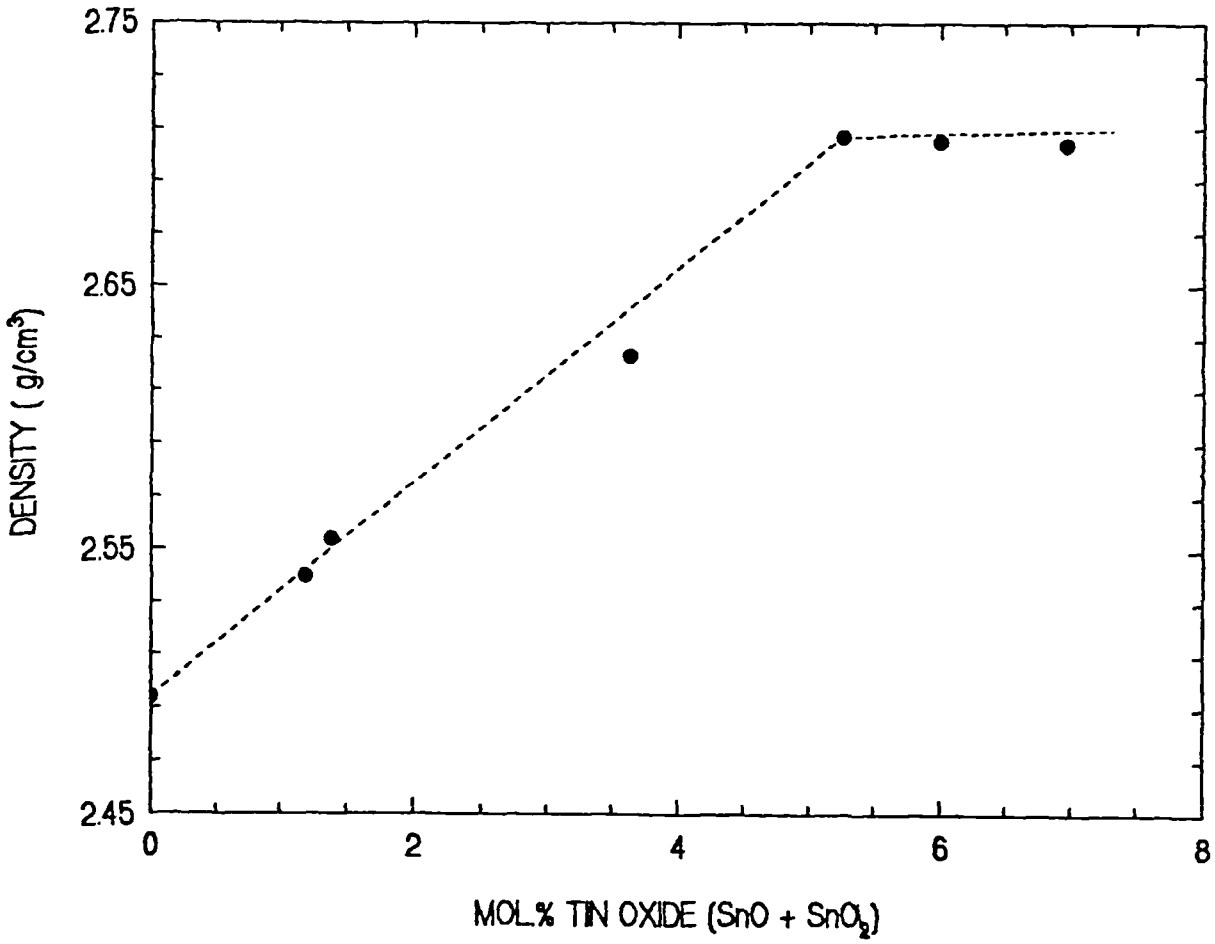

Figure 7.13 : *Density variation with tin content of tin-doped float glasses. (Errors are within the dimension of the symbol used).*

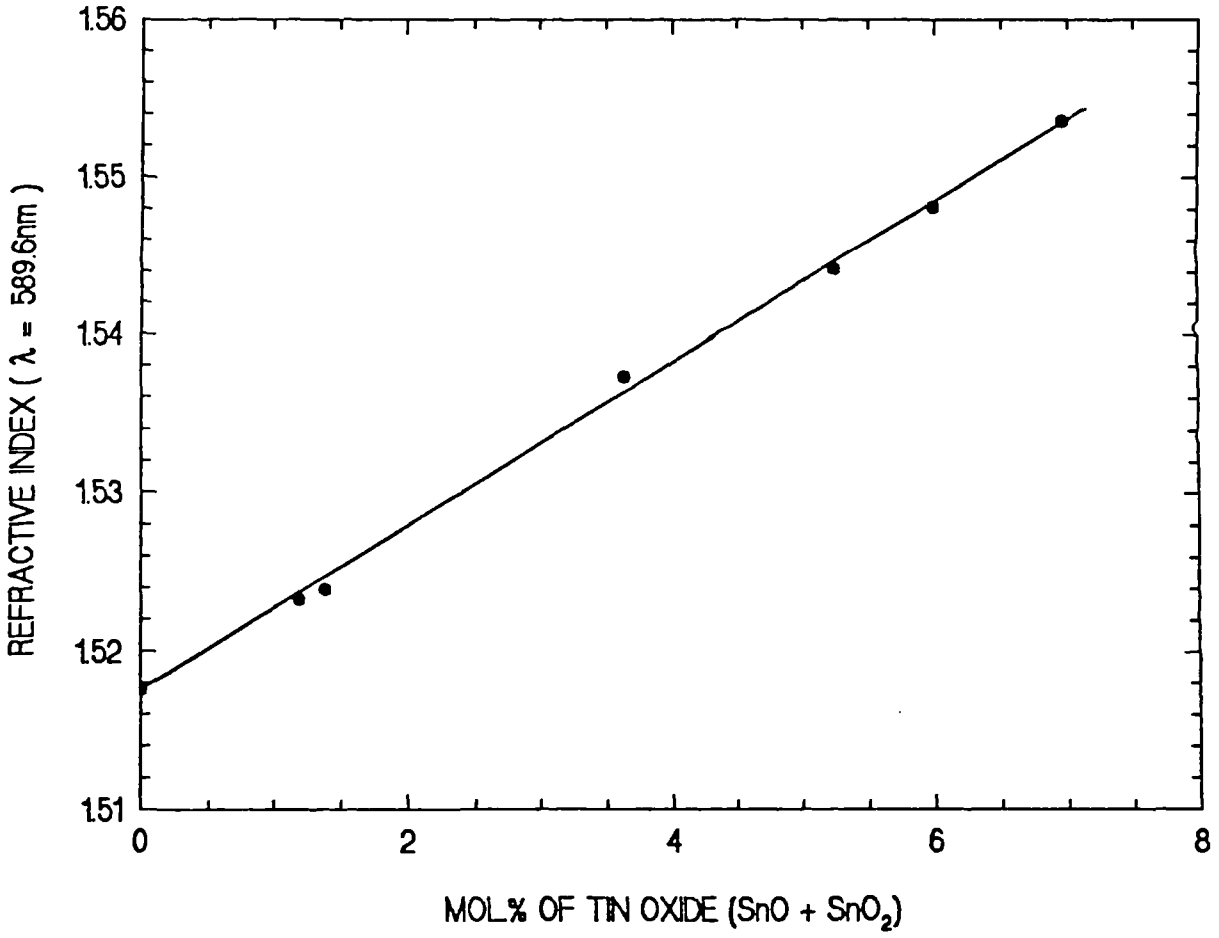

Figure 7.14 : *Refractive index as a function of tin content of tin-doped float glasses. (Errors are within the dimension of the symbol used).*

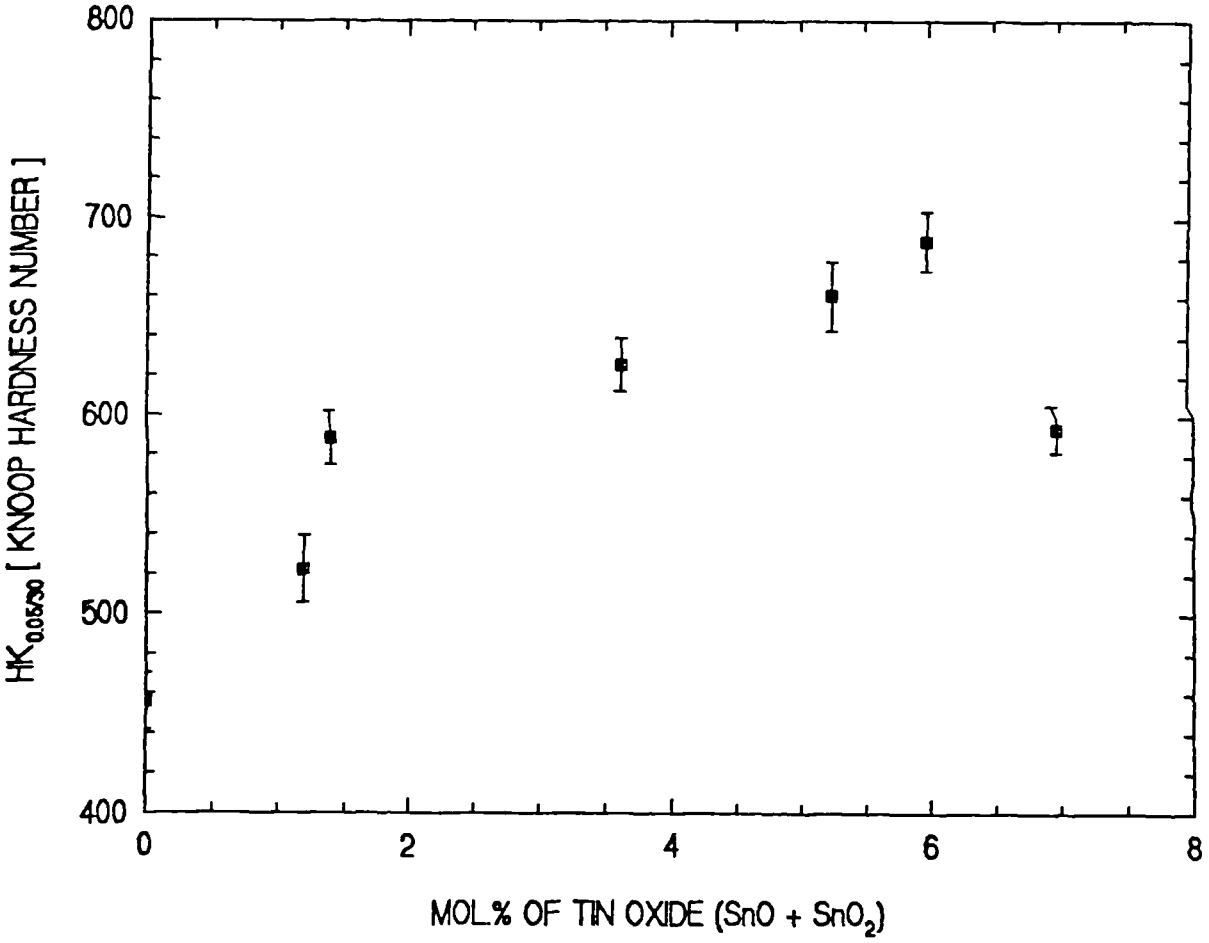

Figure 7.15 : *Knoop Hardness number as a function of tin content of tin-doped float glasses.*

Sn^{4+} in the glass does not change very much compared to crystalline SnO_2. The Debye temperature and the recoil free fraction show that Sn^{2+} is less rigidly bound to the network modifier sites while Sn^{4+} is rigidly bound at network former sites in the glass. Thus the two oxidation states will have different effects on the properties of the glass.

The thermal expansion and refractive index vary approximately linearly with total tin content while the activation energy of viscous flow, density and microhardness shows a discontinuity at tin contents above ~ 5 mol.%. This is the point at which Sn^{4+} content remains constant (saturation has probably occurred) and Sn^{2+} increases rapidly. These observations reflect several factors:

- Properties which reflect only the strength of the bonding are unaffected by the oxidation state, suggesting that the bond strengths are about similar for both oxidation states.

- Properties which depend also on the rigidity of bonding are affected by oxidation state suggesting that the local bonding symmetries of Sn^{2+} and Sn^{4+} are different. This is not unexpected. The Mössbauer results have shown that Sn^{4+} is rigidly bonded octahedrally into the network site, while Sn^{2+} adopts a local symmetry similar to that in crystalline SnO but with a slight distortion, i.e. it has a square pyramidal arrangement of 4 oxygens to one side and a lone-pair of electrons to the other. This arrangement may increase the deformability of the network which is of particular importance in viscous flow.

REFERENCES

1. Sanyal, A.S. & Mukerji, J. (1980). *J. Non-Cryst. Solids* **41**, 99-103.
2. Sieger, J.S. (1975). *J. Non-Cryst. Solids* **19**, 213-220.
3. Colombin, L., Jelli, A., Riga, J., Pireaux, J.J. & Verbist, J. (1977). *J. Non-Cryst. Solids* **24**, 253.
4.. Lie, L. & Chao, X. (1990). *J. Non-Cryst. Solids* **119**, 37.
5. Principi, G., Maddalena, A. & Gupta, A. (1993). *Nuclear. Instr. and Methods in Phys. Research* **B76**, 215.
6. Pantano, C.G., Bojan, V., Verita, M., Geotti-Bianchini, F. & Hreglich, S. (1993). *Rivista della Stazione Sperimentale del Vetro* **Vol. XX111**, 285.
7. Chappell, R.A. & Stoddart, C.T.H. (1974). *Physics Chem .Glasses* **15(5)**, 130.
8. Min'ko, N.I. (1973). Izv. Akad. Nauk SSSR, *Neorg. Mater.* **9(10)**, 1816.
9. Parish, R.V. (1984). in *Mössbauer Spectroscopy Applied to Inorganic Chemistry Vol.1* Edited by Gary J. Long, Plenum Press, N.York. Chapter 16.
10. Collins, G.S., Kachnowski, T., Benczer-Koller, N. & Pasternak, M. (1979). **Physical Review B 19(3)**, 1369.
11. Hayes, M.C. (1968). in *Chemical Applications of Mössbauer Spectroscopy*, Edited by V.I. Goldanskii and R.H.Herber, Academic Press. London. Chapter 5.
12. Baur, W.H. (1956). *Acta Crystallogr.* **9**, 515.
13. Gibb, T.C. (1976). *Principles of Mössbauer Spectroscopy,* Chapman and Hall, London.
14. Nishida, T., Katada, M. & Maeda, Y. (1994). *Fourth Seeheim Workshop on Mössbauer Spectroscopy*- Lufthansa Training Center, Seeheim Germany.
15. Kurkjian, C.R. (1970). *J. Non-Cryst. Solids* **3**, 157-194.
16. Mitrofanov, K.P. & Sidorov, T.A. (1967). *Soviet Physics - Solid State* **9(3)**, 693.
17. Harrison, P.G., Phillips, R.C. & Yhornton, E.W. (1977). *J. Chem. Soc. Commun.* **603.**
18. Askeland, D.R.(1990). *The Science and Engineering of Materials*, Chapman and Hall, London. pg. 480.
19. Paul, A. (1982). *Chemistry of Glasses*, Chapman and Hall, London. pg. 75.

Chapter 8 - Conclusions and Future Work

The study of tin oxides in silicate based glasses was motivated by the desire to understand the structural roles of tin in simple binary $SnO\text{-}SiO_2$ and in tin-doped float glasses. As tin can exists in both its oxidation states of Sn^{2+} and Sn^{4+} in both glasses, its synthesis and analysis poses many problems. Nevertheless, this work demonstrates for the first time that application of ^{29}Si NMR and ^{119}Sn Mössbauer spectroscopies to the study of the structure of binary $SnO\text{-}SiO_2$ glasses can prove fruitful. Both techniques complement each other in the effort to understand the role of tin in these glasses. For tin-doped float glass ^{119}Sn Mössbauer spectroscopy provided much information on the difference of the structural role of Sn^{2+} and Sn^{4+} in the glass. These techniques have been coupled with other physical measurements on the glasses which provide indirect evidence on structure. This chapter provides an overview of the preceding chapters and presents a proposal for future work.

8.1 $SnO\text{-}SiO_2$ GLASS SYSTEM

The making of a $SnO\text{-}SiO_2$ glass is complicated by the disproportionation of SnO to SnO_2 and Sn metal. The presence of SnO_2 and Sn metal together with SnO in the glass make it impossible to pour the melt into any required shape and also impossible to control the final composition of the glass. Although this is the case, glasses in this system have been made up a maximum of ~ 70 mol.% SnO. Glass with less than 20 mol.% SnO could not be made successfully because of the required high melting temperature (≥1600°C) that increased dissolution of Al_2O_3 from the alumina crucibles and increased the viscosity of the melt. Silica crucibles are only suitable for low temperature melting (< 1300°C) and platinum crucibles are not suitable because of the tendency of Sn metal to attack the crucibles. At high SnO contents where the

melting temperatures are comparatively low, Al_2O_3 contamination was minimised by melting the charge in pellet form and melting for the minimum time. Thus, the two main problems of making this glass are the disproportionation of SnO and the limited choice of suitable crucibles.

The ability of glass to form with high SnO contents in this system could be explained in terms of the polarizing power of Sn^{2+} and the structure of SnO. This glass was compared to the PbO-SiO_2 system which can form glass past the orthosilicate composition and Na_2O-SiO_2 system which cannot form glass past the metasilicate composition. The polarizing power of Sn^{2+} is slightly higher than Pb^{2+} and very much higher than Na^+. This indicates that the Sn—O bonds are more covalent and directional than Na—O bonds, thus the kinetic stability of the glass is enhanced because it is more difficult to rearrange SiO_4 groups linked together via strong, directed Sn—O bonds. In terms of structure, the deformability of the [$Sn^{II}O_4$] polyhedron, indicated by the Mössbauer *f* factor, makes it easy to accomodate in the holes of the structural network of the glass.

The ^{29}Si MAS NMR results have shown that SnO does not depolymerise the silicate network to the same extent as Na_2O or even PbO. Computer simulations showed that, for SnO contents below ~30 mol.%, the disposition of Q^n species is consistent with the binary model, which means SnO acts like traditional modifier. For compositions greater than 30 mol.% SnO, the Q^n distribution follows the statistical model which is compatible with the concept of Zachariasen's random network theory. This also implies that SnO is acting as an intermediate oxide at high SnO content in the glass. At these high SnO contents, Sn^{2+} becomes bonded to non-bridging oxygens through the formation of Si—O—Sn linkages that restore the 3D nature of the glass structure. The ^{119}Sn NMR did not give much structural information due to the high chemical shift anisotropy of Sn^{2+} sites, but it showed that the glass also contains negligible amounts of Sn^{4+} species. The ^{119}Sn Mössbauer results showed that the decrease in isomer shift with increase of SnO is indicative of the increasing covalent character of the Sn—O bonds. The larger quadrupole splitting indicates the greater

distortion of the SnO polyhedral structure in the glass. A maximum in the isomer shift at ~30 mol.% SnO has been suggested as the point where the SnO changes its role from modifier to an intermediate. The relation between the isomer shift and the quadrupole splitting shows that Sn^{2+} lone pair has a significant p_z character. The results of the temperature dependent Mössbauer spectra of the glass showed that the increase of electron density in the p orbital is not solely attributed to changes to the molar volume alone. Other factors such as the change of hybridization due to the formation of Si—O—Sn linkages, could also contribute.

The viscosity measurement results showed that the decrease in the viscosity of the glass with increasing SnO is not as large as that obtained with alkali metal and alkaline-earth metal oxides. Judging from the fact that stannous silicate glasses can be formed past the orthosilicate composition, one can envisage that SnO has the characteristic of an intermediate or conditional network former at higher concentrations of the oxide. The effect on some of the physical properties studied at low SnO concentration seems to follow the behavior of a modifier but at SnO contents around 30-40 mol% there is a discontinuity in the variation of the physical properties which may relate to a change in the structural role of SnO by which the network is strengthened again. This is supported by ^{29}Si NMR and ^{119}Sn Mössbauer studies of these glasses.

8.2 DEVITRIFICATION OF SnO-SiO_2 GLASSES

SnO-SiO_2 glasses with ≥ 40 mol.% SnO could be heat treated in the temperature range 570°C to 680°C to produce a metastable crystalline phase called stannous metasilicate ($SnSiO_3$). At temperatures around 700°C this phase decomposed to SnO + SiO_2. At temperatures greater than 720°C oxidation of SnO + SiO_2 to SnO_2 and SiO_2 (cristobalite) took place. Thus the effect of heat

treating these glasses is to induce crystallization, then decomposition and finally oxidation. It was also found that the decomposition and oxidation events overlapped and because of this overlapping, it was difficult to get a pure phase of $SnSiO_3$ crystal. Heat treatment in argon shows greater promise but, due to lack of glass the study of the $SnSiO_3$ crystal phase was limited.

8.3 TIN-DOPED FLOAT GLASS

Float glass is a complex material in terms of composition; and the small amount of tin that diffuses into the surface through the process of production can be detrimental to the quality of the glass. Synthesis of the tin-doped float glass has shown that both Sn^{2+} and Sn^{4+} can be assimilated simultaneously in the glass but there is a solubility limit for Sn^{4+}.

This study has shown that the Mössbauer effect is a valuable tool in studying the structural roles of tin in tin-doped float glass. The isomer shift and quadrupole splitting gave a measure of the nearest neighbour distortion of Sn^{2+} and Sn^{4+} ions whereas the Debye temperature and the recoil free fraction reflect the bulk properties of both ions in the glass. The environment of Sn^{2+} in the glass is similar to that in amorphous SnO, in which there is an axial elongation of the Sn—O bond length as compared to its crystalline form. This reflects a greater ionic character of the bond. The structure of Sn^{4+} in the glass does not change very much compared to crystalline SnO_2. The Debye temperature and the recoil free fraction show that Sn^{2+} is less rigidly bound to the network modifier sites while Sn^{4+} is rigidly bound at network former sites in the glass. Thus the two oxidation states will have different effects on the properties of the glass.

The thermal expansion and refractive index vary approximately linearly with total tin content while the activation energy of viscous flow, density and microhardness

show discontinuity at tin contents above ~ 5 mol.%. This is the point at which the Sn^{4+} content remains constant (saturation has probably occurred) and Sn^{2+} increases rapidly. These observations reflect the following factors:

(1) Properties which reflect only the strength of the bonding are unaffected by the oxidation state, suggesting that the Sn—O bond strengths are similar for both oxidation states.

(2) Properties which depend on the rigidity of bonding are affected by oxidation state. This suggests that the local symmetries of Sn^{2+} and Sn^{4+} are different.

The Mössbauer results have shown that Sn^{4+} is rigidly bonded octahedrally into the network site while Sn^{2+} is less rigidly bonded and structurally more deformable. The deformability of the [$Sn^{II}O_4$] unit may help to explain its tolerance in silicates glasses to high concentrations. The resistance of the [$Sn^{IV}O_6$] unit to deformation renders it unsuited to high concentration in the random structure of a glass.

8.4 SUGGESTIONS FOR FUTURE WORK

To find more evidence to support the conclusions of this work, it is pertinent to extend the study in the following ways,

- Since it is very difficult to make the $SnO\text{-}SiO_2$ glass with low tin content, ways should be explored to make the glass by routes other than melting. Although the sol-gel route has been tried once unsuccessfully, further attempts should be made.

- The study of the binary $SnO\text{-}SiO_2$ glass by ^{119}Sn NMR is hampered by the high chemical shift anisotropy of Sn^{2+} site in the glass but the relaxation time of Sn could be measured since the chemical shift anisotropy is not critical in this measurement.

- Other techniques such as XPS should be employed in the study of the $SnO\text{-}SiO_2$ glass, since this technique can provide information on the number of bridging and non-bridging oxygens in the glass.

- Neutron diffraction experiment could also be employed on the study of the structure of $SnO\text{-}SiO_2$ glasses.

- Other physical properties measurements such as dielectric measurement and heat capacity measurement at high and low temperature could probably provide more information as to the role of Sn^{2+} in the binary $SnO\text{-}SiO_2$ glass.

- The study of the devitrification of $SnO\text{-}SiO_2$ glasses should continued in order to understand the $SnSiO_3$ crystal phase that can be grown from this glass. Structure determination of $SnSiO_3$ will give further insight into the local environments of Sn and Si in the glasses.

- The devitrification of tin-doped float glass should be attempted to see if tin in the glass could behave as a nucleating agent to turn the glass to glass ceramic.

- The study should also be extended to new ternary systems such as $Na_2O\text{-}SnO\text{-}SiO_2$ and $CaO\text{-}SnO\text{-}SiO_2$. These systems should provide an interesting contrast as to the role of tin since Na_2O and CaO are known modifiers in silicate glasses. The conditions for increased solubility of Sn^{4+} could also be mapped.